Studies of Ionic Surfactant Systems Using Surface Rheology With a Focus on the Oscillating Bubble Technique

Dissertation zur Erlangung des
Doktorgrades der Naturwissenschaften (Dr. rer. nat.)

der Fakultät für Chemie und Pharmazie

der Universität Regensburg

vorgelegt von

Matthias Josef Hofmann

aus Waldmünchen

im Jahr 2018

Promotionsgesuch eingereicht am: Montag, 29. Januar 2018
Die Arbeit wurde angeleitet von: Prof. Dr. Hubert Motschmann

Die Belohnung für Geduld ist Geduld.

– *Augustinus Aurelius.* –

Danksagung

Ein herzliches Dankeschön möchte ich an dieser Stelle Herrn Prof. Dr. Hubert Motschmann für die anspruchsvolle und interessante Themenstellung aussprechen. Die gesetzten Rahmenbedingungen erlaubten ein angenehmes Arbeitsklima mit einer ausgewogenen Balance zwischen Betreuung und Freiraum zur Entwicklung neuer Lösungsansätze.

Zudem möchte ich mich bei den Mitarbeitern des Arbeitskreises für nützliche Hinweise und Anregungen bedanken. Ebenso möchte ich Prof. Dr. Werner Kunz sowie den weiteren Mitarbeitern des Lehrstuhls meinen Dank für das gute Miteinander aussprechen.

Ein weiterer Dank gilt Prof. Dr. Ramón González Rubio und Prof. Dr. Francisco Ortega. Im Rahmen meines Forschungsaufenthalts an der Universidad Complutense de Madrid konnte ich ihrer Arbeitsgruppe interessante neue Methoden kennenlernen.

Maßgebliche Beiträge zum Gelingen der Arbeit wurden ebenfalls von den Mitarbeitern der Elektronik-, Glasbläser- und Feinmechanik-Werkstätten der Fakultät für Chemie und Pharmazie geleistet. Insbesondere bedanken möchte ich mich bei Gerhard Armer, Andreas Graf und Markus Lindner für die Umsetzung zahlreicher Konstruktionen und Modifikationen der Apparatur, sowie bei Peter Fuchs, Andreas Gruber und Josef Bernhardt für die kompetente Hilfe bei Fragestellungen aus dem Bereich der Elektrotechnik.

Ein weiterer Dank gilt Alexander Ruhland für seine tatkräftige Unterstützung bei den Programmierungsaufgaben und die gute Zusammenarbeit im Verlauf des Projektes.

Besonders bedanken möchte ich mich bei Familie, Freunden und Katharina für die fortwährende Unterstützung und insbesondere die Geduld mit mir während der Versuche.

Der Studienstiftung des Deutschen Volkes e.V. möchte ich meinen Dank für die ideelle und finanzielle Unterstützung aussprechen.

Information

This work has been completed from October 2015 until December 2017 in the working group of Prof. Dr. Hubert Motschmann at the University of Regensburg in the Institute of Physical and Theoretical Chemistry directed by Prof. Dr. Werner Kunz. Furthermore, some measurements were carried out at the Grupo de Sistemas Complejos of the Universidad Complutense de Madrid guided by Prof. Dr. Ramón González Rubio and Prof. Dr. Francisco Ortega.

Further details on the thesis and the examination board are listed in the following.

Thesis:

Direct supervisor	Prof. Dr. Hubert Motschmann
Submitted	Monday 29th January, 2018
Day of colloquium	Friday 16th March, 2018

Examination board:

Head of board	Prof. Dr. Rainer Müller
1st referee	Prof. Dr. Hubert Motschmann
2nd referee	Prof. Dr. Georg Papastavrou
3rd referee	Prof. Dr. Joachim Wegener

Physical Constants

Constant	Value
R	$8.3145\ \mathrm{J \cdot K^{-1} \cdot mol^{-1}}$
k_B	$1.380\,658 \cdot 10^{-23}\ \mathrm{J \cdot K^{-1}}$
ϵ_0	$8.854\,187\,816 \cdot 10^{-12}\ \mathrm{C^2 \cdot J^{-1} \cdot m^{-1}}$
μ_0	$4\pi \cdot 10^{-7}\ \mathrm{J^2 \cdot s^2 \cdot C^{-2} \cdot m^{-1}}$
N_A	$6.022\,136\,7 \cdot 10^{23}\ \mathrm{mol^{-1}}$
h	$6.626\,075\,5 \cdot 10^{-34}\ \mathrm{J \cdot s}$
c	$2.997\,924\,58 \cdot 10^{8}\ \mathrm{m \cdot s^{-1}}$

List of Acronyms

ADSA	axis symmetric drop shape analysis
CCD	charge-coupled device
cmc	critical micellar concentration
CsDeS	cesium decyl sulfate
CTAB	cetyltrimethylammonium bromide
DeS	decyl sulfate
DH	Debye-Hückel
DLS	dynamic light scattering
DPC	*n*-dodecylphosphinecholine
DPPC	dipalmitoylphosphatidylcholine
DRS	dielectric relaxation spectroscopy
DS	dodecyl sulfate
ECW	electrocapillary wave
EDL	electric double layer
GAI	Gibbs adsorption isotherm
IR	infra-red
IRRAS	infrared reflection absorption spectroscopy
ITC	isothermal titration calorimetry
KDeS	potassium decyl sulfate
LED	light emitting diode
LiDeS	lithium decyl sulfate
LvdT	Lucassen-van den Tempel
MCT	mercury cadmium telluride
NaDeS	sodium decyl sulfate
NR	neutron reflectivity
OB	oscillating bubble
OPD	oscillating pendant drop
PC	personal computer
PMT	photo multiplier tube
PSD	position sensitive detector
RA	reflectance-absorbance
SDS	sodium dodecyl sulfate
SEOS	surface equation of state
SFG	sum frequency generation
SFGVS	sum frequency generation vibrational spectroscopy
USB	universal serial bus
UV	ultraviolet
UV-Vis	ultraviolet-visible

Vis	visible
VNA	vector network analyzer
XDeS	alkali decyl sulfate

Meinen Eltern.

Contents

Kurzzusammenfassung

Oberflächenaktive Substanzen, bzw. Tenside, verändern die Luft-Wasser-Grenzfläche in Bezug auf ihre Gleichgewichts- und dynamischen Eigenschaften. Auf makroskopischer Ebene ist die Bildung von Schäumen ein typisches Merkmal von Tensid-Lösungen. Sie wird bei mechanischer Deformation von wässrigen Lösungen beobachtet.

Die Hauptmotivation dieser Arbeit ist es, durch die erhaltenen Forschungsergebnisse ein besseres Verständnis von Luft-Wasser-Grenzflächen auf molekularen Ebene zu erlangen und dieses Wissen auf kolloidale Systeme zu beziehen. Letztere sind intrinsisch durch ein ungewöhnliches Verhältnis von Oberfläche zu Volumen bestimmt. Diese Arbeit zielt insbesondere auf ein Verständnis der Beziehung zwischen der mikroskopischen Struktur einer Adsorptionsschicht und der Molekülstruktur seiner Bestandteile ab. Darüber hinaus ist ein Hauptziel, die mikroskopischen Eigenschaften einer Grenzfläche mit dem makroskopischen Verhalten eines Systems in Beziehung zu setzen.

Der Oberflächen-Dilatationsmodul ist ein Schlüsselparameter für die Charakterisierung dynamischer Eigenschaften einer Grenzfläche. Eine wichtige Errungenschaft dieser Arbeit ist die Weiterentwicklung der Technik der „oszillierenden Blase“. Der Bereich zugänglicher Frequenzen wurde deutlich erweitert und erlaubt nun eine Domäne abzudecken, die mit der charakteristischen Zeitskala relevanter Relaxationsprozesse übereinstimmt. Die Technik hat das Potential, zu einem Standardverfahren in der Kolloid- und Grenzflächenforschung zu reifen. Eine zweite instrumentelle Errungenschaft ist ein neu entwickeltes Gerät, das die Lebensdauer einer einzelnen Schaumlamelle in feuchtigkeitsgesättigter Umgebung misst. Ziel ist die systematische Untersuchung der Stabilität von einzelnen Schaumlamellen mittels eines statistischen Ansatzes. Die reflexionsbasierte Messung der Lebensdauer von Lamellen ermöglicht die Bestimmung von Wahrscheinlichkeiten für deren Abreißen. Sie sind charakteristisch für eine gegebene Tensid-Lösung.

Diese eingeführten instrumentellen Entwicklungen sind die Grundlage für die folgenden Studien. Um die Anwendbarkeit der speziell angefertigten Apparaturen zu evaluieren, wurden im Rahmen dieser Dissertation insgesamt fünf Tensid-basierte Systeme untersucht.

i) Während die wichtigste Anwendung von Tensiden in ihrem Einsatz als Wasch- und Reinigungsmitteln besteht, wird hier ein unkonventionelles Phänomen aus der Biologie diskutiert, das ebenfalls auf der Wirkung von Amphiphilen beruht: der Fluchtmechanismus des Käfers *stenus comma* vor Fressfeinden durch Ausscheidung eines Sekrets, das oberflächenaktive Verbindungen enthält. Die Oberflächen-Rheologie einer Adsorptionsschicht bestehend aus den Hauptkomponenten des Sekrets wurde bestimmt

und der positive Effekt der Oberflächenviskosität erörtert.

ii) Die Vergleichbarkeit der Ergebnisse von Oberflächendilatationsexperimenten mittels der oszillierenden Blase und Studien von Elektrokapillarwellen, die einen ähnlichen Frequenzbereich abdecken, wurden bewertet. Dazu wurden Mischungen von Natriumdodecylsulfat und Natriumchlorid hinsichtlich ihrer Schäumungs- und Oberflächeneigenschaften in Abhängigkeit der Ionenstärke untersucht. Um die Ergebnisse zu interpretieren, wurde ein neuer Parameter eingeführt und gezeigt, dass dieser mit gemessenen Schaum- und Lamellen-Stabilitäten korreliert. Außerdem wird auf die Herausforderungen im Umgang mit den verwendeten rheologischen Methoden hingewiesen.

iii) Weiterhin wurden ionenspezifische Effekte in Lösungen von *n*-Alkylsulfaten mit variierenden monovalenten Alkali-Gegenionen untersucht. Neben den Abweichungen der Gleichgewichtseigenschaften ihrer Adsorptionsschichten werden die entsprechenden Schaumstabilitäten bezüglich der Nichtgleichgewichtseigenschaften diskutiert. Eine Ordnung entlang der von Hofmeister vorgeschlagenen Reihenfolge wurde gleichermaßen hinsichtlich der betrachteten Grenzflächeneigenschaften bestätigt.

iv) In konzeptionell verwandter Art und Weise wurde der charakteristische Einfluss hoch-geladener Lanthanoid-Ionen auf Adsorptionsschichten der Modellsubstanz *n*-Dodecylphosphocholin ausgewertet. Sie ist strukturell verwandt mit Phospholipiden, die zum Ausbau von Zellmembranen genutzt werden. Der räumliche Ursprung der Ionenspezifität wird geklärt und eine mögliche mechanistische Begründung vorgeschlagen, die auf abweichendem Solvatationsverhalten beruht.

v) Schließlich wurde die Leistungsfähigkeit und Empfindlichkeit der entwickelten oszillierenden Blasenapparatur durch Unterscheidung der geometrischen Isomere eines lichtempfindlichen Azotensids verdeutlicht. Messungen der Schaumstabilität bestätigen die von der oszillierenden Blase zu erwartenden Beobachtungen.

Die Ergebnisse der Punkte iii) bis v) wurden bisher nicht veröffentlicht. Die jeweiligen Manuskripte befinden sich jedoch derzeit in Vorbereitung zur Publikation. Eine vollständige Liste von Forschungsergebnissen, die im Zusammenhang dieser Dissertation und vorheriger Studienabschnitte entstanden sind, wird angegeben.

Rheologische Messungen mit Hilfe der speziell angefertigten oszillierenden Blase stellen den Hauptteil der Dissertation dar. Darüber hinaus wurde eine weitere Charakterisierung durch Techniken wie Analyse von Elektrokapillarwellen, Summenfrequenzspektroskopie, Infrarot-Reflexions-Absorptionsspektroskopie, dynamische Lichtstreuung, isotherme Titrationskalorimetrie und dielektrische Relaxationsspektroskopie durchgeführt, um die Ergebnisse rheologischer Messungen sinnvollen zu ergänzen.

Die vorgestellte oszillierende Blase ist schrittweise zu einer Apparatur herangewachsen, die zusätzliche Einblicke in die Eigenschaften von Grenzflächenschichten verspricht und erhebliche Vorteile gegenüber konkurrierenden Methoden bietet. In diesem Projekt konnte die Robustheit des Geräts und die Zuverlässigkeit der erhaltenen Daten signifikant erhöht werden. Weitere Entwicklungs-Bemühungen werden diese Methode zu einem Standard-Messverfahren für Oberflächen-Dilatationseigenschaften über einen erhöhten, erweiterten - und bisher schwer zugänglichen – Frequenzbereich reifen lassen.

Abstract

Surface active agents, shortly referred to as surfactants, tune the air-water interface with respect to both its equilibrium and dynamic properties. On a macroscopic scale, the formation of foam is the most prominent characteristic of a surfactant solution. It takes place when subjecting an aqueous solution to mechanical deformation.

Prime motivation of the research presented in this thesis is to obtain a better understanding of air-water interfaces on a molecular scale and to relate this knowledge to colloidal systems which are naturally determined by an unusual ratio of surface to volume. In particular, this thesis aims for an understanding of the relationship between the microscopic structure of an adsorption layer and the molecular structure of its constituent molecules. Moreover, relating the microscopic properties of an interface to the macroscopic behavior of a system is a major objective.

The surface dilatational modulus E is a key parameter for the characterization of dynamic properties of an interface. A major accomplishment of this thesis is that the oscillating bubble technique has been pushed to new limits by extending the accessible frequency range via thorough reengineering. It now allows covering the mid-frequency range matching the characteristic time scale of important relaxation processes. The technique has the potential to mature to a standard procedure in colloid and interface science. Recent advances and concepts for automatization are outlined in

D. Stadler, M. J. Hofmann, H. Motschmann and M. Shamonin. "Automated System for Measuring the Surface Dilational Modulus of Liquid–Air Interfaces." *In Meas. Sci. Technol.*, *27*(6) 65 301. **2016**.

A second instrumental achievement is a new device that measures the lifetime of an individual foam lamella in a humidity-saturated environment. It aims to systematically investigate the stability of individual foam lamellae relying on a statistical approach. The reflection-based measurement of lamella lifetimes allows for determining probabilities of rupture, which are characteristic of a surfactant solution as described in

M. J. Hofmann and H. Motschmann. "Measurement of the Lifetime of Individual Foam Lamellae." *In Rev. Sci. Instrum.*, *87* 94 101. **2016**.

These accomplished instrumental developments are the basis for the studies presented in the following. In order to evaluate the applicability of the custom-built apparatuses, a total of five surfactant-based

systems has been studied within this dissertation.

i) Whereas the probably most prominent application of surfactants is in washing and cleansing agents, a rather unconventional amphiphile-related phenomenon from biology is discussed: the escape mechanism of the beetle *stenus comma* from predatory insects via excretion of a mixture containing surface active compounds. The surface rheological characteristics of their main components' adsorption layers were determined and the beneficial effect of surface dilatational viscosity κ was pointed out in the peer-reviewed publication

> **A. A. Dietz, M. J. Hofmann and H. Motschmann**. "The Role of Surface Viscosity in the Escape Mechanism of the Stenus Beetle." *In J. Phys. Chem. B*, *120*(29) 7143–7147. **2016**.

ii) The comparability of surface dilatational results obtained from the oscillating bubble device and electrocapillary wave (ECW)-studies targeting a similar frequency range has been assessed. Mixtures of sodium dodecyl sulfate (SDS) and NaCl were studied with respect to their foaming properties and surface characteristics as a function of ionic strength. To interpret the results, a new parameter has been introduced in

> **M. J. Hofmann and H. Motschmann**. "A Parameter Predicting the Foam Stability of Mixtures of Aqueous Ionic Amphiphile Solutions With Indifferent Electrolyte." *In Colloids Surf. A*, *529* 1024–1029. **2017**.

and shown to be correlated with experimentally measured foam and lamella stabilities. Besides, the challenges associated with both the oscillating bubble and ECW-based methods are pointed out.

iii) Furthermore, effects of ion specificity in solutions of molecular *n*-alkyl sulfate surfactants with varying monovalent alkali-counterions have been studied. Besides the deviations in equilibrium characteristics evidenced for the adsorption layers, the corresponding foam stabilities are discussed with respect to the non-equilibrium properties. Trends along the established series proposed by Hofmeister have been equally recovered concerning interfacial properties.

iv) In a conceptually related manner, the characteristic influence of highly charged lanthanide ions on adsorption layers of the model substance *n*-dodecylphosphinecholine (DPC), which is structurally related to the phospholipids forming cell membranes, has been evaluated. The spatial origin of ion specificity is clarified and a possible mechanistic rationale based on deviating solvation behavior is suggested.

v) Finally, the capability and sensitivity of the developed oscillating bubble apparatus was showcased by distinguishing the geometrical isomers of a photosensitive azo-surfactant via its response to surface dilatational perturbation. Measurements of foam stability confirm the expectation suggested by the oscillating bubble results.

The results of points iii) to v) have not been published so far, but the respective manuscripts are currently under preparation. An exhaustive list of research results published in the course of this dissertation and previous stages of studies is given.

Rheological measurements by means of the custom-built oscillating bubble device represent the major part of the thesis. In addition, further characterization by techniques such as ECW-studies, sum frequency generation vibrational spectroscopy (SFGVS), infrared reflection absorption spectroscopy (IRRAS), dynamic light scattering (DLS), isothermal titration calorimetry (ITC) and dielectric relaxation spectroscopy (DRS) has been carried out to complement the rheological results in a sensible manner.

The presented oscillating bubble device has gradually grown to an apparatus providing additional insight into the characteristics of interfacial layers. It exhibits considerable advantages over competing methods such as accelerated data acquisition and the direct measurement of the system's response originating from its mechanical perturbation. Within this project, the robustness of the device and the reliability of the obtained data could be increased significantly. Some further efforts will allow this method to mature to a routine technique of measurement for surface dilatational characteristics over an elevated, extended – and so far not readily accessible – frequency range.

1 Introduction

Surface active agents are at the heart of numerous commodity products such as cleansing agents, shampoos and cosmetic products. These compounds, shortly referred to as *surfactants*, are amphiphilic molecules characterized by a structural asymmetry. A distinct partitioning between a hydrophilic, *i.e.,* water-seeking headgroup and a longer hydrophobic tail with a low affinity towards water causes this kind of substances to arrange in a defined manner at an air-water interface. This equally holds true for the adsorption at liquid-liquid interfaces.

A multitude of scientific questions arises from the presence of interfacially active molecules. How to prove the existence of a surface layer? How does it behave under equilibrium and dynamic conditions? What are the macroscopically observable consequences of surfactant adsorption? How can processes on the molecular level be bridged to „real world“ properties? And most importantly: How to rationally tune the composition of a mixture or a system in order to control its characteristics? The answer to the first question can be clarified by means of a very simple experiment. If a solution generates a foam subsequent to shaking or other mechanical agitation, this can be considered a strong indicator for the presence of surface active materials in both the bulk and especially at the interface. Foams can be formed by dissolved molecular amphiphiles, larger polymeric foaming agents, particles, biological molecules such as proteins and other compounds. Besides the colorful appearance of individual foam lamellae allowing for conclusions about film thickness, foams are applied as valuable materials in personal care products. Other types of foam are widely used in construction business and automotive industry.

After their formation, aqueous foams exhibit a remarkable structural transition, if they are left to decay. Besides foaming, there are other circumstances and applications in which non-equilibrium properties assessed in dynamic conditions are particularly relevant. For example, this is the case in enhanced oil recovery. The effect of an elevated surface viscosity is considered to be beneficial to separation speed and efficiency for the collection of oil from porous media. On the other hand, increased stiffness, *i.e.,* pronounced elastic behavior is frequently found to aggravate foam generation. Exemplarily, this can be induced by high contents of polymeric surfactants.

Within this thesis, a simplistic device allowing for the measurement of single foam lamella lifetimes has been developed. It allows for measuring the stability of individual foam lamellae based on the reflection of light. A statistical description yields a characteristic probability of rupture for a given surfactant solution, which is correlated with foam column stabilities.

Even though both rheological and surface characterization are deemed to play decisive roles for an understanding of the mechanisms governing foam stability, the literature on simultaneous investigations of the latter quantities is scarce. As discussed extensively in several contributions at the 6th International Workshop on Bubble and Drop Interfaces 2015 in Potsdam/Golm, this situation is due to the lack of appropriate instrumentation covering particularly the range of elevated frequencies. This especially holds true, when it comes to studies of *interfacial* rheology despite the detailed information obtainable from this class of experiments. For example, minor changes in lipid headgroup orientation were found to alter surface rheological characteristics in model systems of biological membranes. It is therefore apparent that interfacial rheology is able to serve as a valuable tool, if it is possible to relate the obtained *indirect* information to a comprehensible molecular picture. The present work intends to relate surface rheological data collected from the custom-built „oscillating bubble“ device, supplemented by additional measurement techniques, to molecular constitution, foaming behavior and the exchange processes occurring at and within the surface of the respective aqueous solutions as suggested in Figure I.1. Considerable advances concerning the instrumentation have been put forward recently. Among others, new hardware components, a refined image processing algorithm, improved automated control features and a state-of-the-art graphical user interface have been implemented.

In the following, the focus will be on both the equilibrium and dynamic interfacial properties of aqueous surfactant solutions studied at the air-water interface.

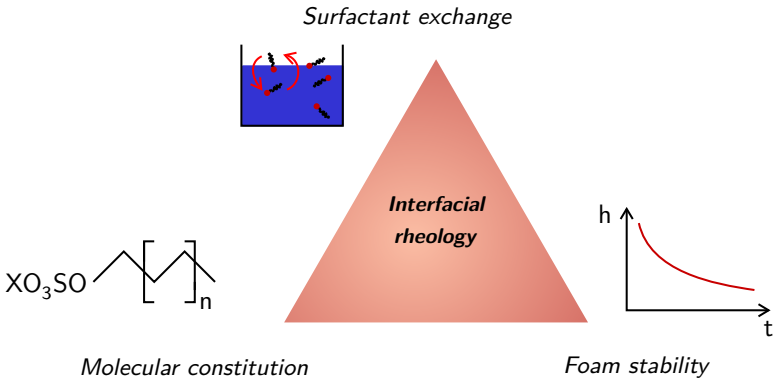

Figure I.1: Conceptual triangle of molecular constitution, surfactant exchange and foam stability.

Within this dissertation, a total of five systems has been examined.

i) Whereas amphiphiles are most commonly encountered in washing powder, they are found in biology as well. The beetle *stenus comma* is known to excrete surface active material under certain circumstances. The beneficial consequence of surface dilatational viscosity κ in the respective adsorption layer for this insect has been pointed out. Predators chasing the escaping beetle are required to spend additional energy for overcoming the dissipation of energy provided by the interfacial visco-elastic adsorption layer.

ii) Effects on foam stability and interfacial properties upon addition of NaCl to sodium dodecyl sulfate

(SDS) have been observed and interpreted in terms of a newly introduced parameter. It was shown to correlate with measured foam and lamella stabilities. Additionally, the challenges of assessing surface dilatational properties by different instrumental approaches are discussed.

Furthermore, the elucidation of relations between surfactant structure, ion specificity and foaming characteristics was one of the major points of interest.

iii) Effects of ion specificity in solutions of molecular *n*-decyl sulfate with varying monovalent alkali-counterions are studied with respect to dynamic interfacial properties and foam stability. An ordering of foam stabilities and interfacial characteristics according to the series proposed by Hofmeister could be confirmed.

iv) The characteristic influence of highly charged lanthanide ions on adsorption layers of the model substance *n*-dodecylphosphinecholine (DPC) is evaluated. It is structurally related to phospholipids, which are the main components of cell membranes and therefore potentially of interest to achieve a better understanding of processes at their interfaces. Deviations in bulk solvation behavior of the studied lanthanide ions were assumed to be the origin of ion specificity evidenced in surface dilatational rheology.

v) Capability and sensitivity of the developed oscillating bubble apparatus was showcased by distinguishing the geometrical isomers of a photosensitive azo-surfactant based on its response subject to surface dilatational perturbation. Observations of a previous study from literature not taking into account surface dilatational properties could be confirmed and rationalized in terms of a molecular picture.

Rheological measurements with the custom-built device constitute the major part of the presented work. Further characterization using a multitude of different surface specific, bulk and spectroscopic techniques has been carried out to complement the results in a sensible manner.

The thesis is structured as follows: A summary of the theoretical background of the applied experimental methods and behavior of surfactants at interfaces is given in Chapter II. Chapters IV and V show the results obtained in the course of the conducted separable projects i) to v) and the corresponding discussions, respectively. Whereas an introduction specific to the topic is given at the beginning of each section in the Results (Chapter IV), the appertaining conclusion is drawn at the end of the respective section in the Discussion (Chapter V). Furthermore, brief descriptions of the utilized experimental devices and materials are summarized in Chapter III. A unifying conclusion highlighting the most relevant findings and pointing towards successfully resolved challenges completes this thesis in Chapter VI. Published results emerging from the work of this thesis and previous stages of studies are listed exhaustively in Appendix A.

II Theoretical Framework

1 Surface Model

An adequate description of the air-water interface requires taking into account the „under-monolayer“ as an important part of the interfacial region. This is achieved by the use of the further developed Guggenheim rather than the older Gibbs-surface model. The latter ascribes deviations from the adjacent bulk phases to a mathematical plain and grounds on the fundamental Gibbs-Duhem-relation. Only recently, there have been contributions pointing out the importance of this understanding based on experiments using sum frequency generation vibrational spectroscopy (SFGVS).[5,6] An essential part in the analysis of surfactant properties is their characterization with respect to equilibrium surface tension. Typically, the results are represented as plots of equilibrium surface tension γ_e against the bulk concentration c of the surfactant solution in logarithmic scale. For classical surfactants, the plot assumes the generic form as shown in Figure II.1. It features three characteristic regions A, B and C with different concentration-dependencies. In region A, there is only a slight decrease in equilibrium surface tension γ_e, which turns into a very pronounced descent in region B. The onset of the range of constant equilibrium surface tension γ_e in region C is identified as the critical micellar concentration (cmc), which defines the lowest concentration at which micelles, *i.e.,* a certain type of aggregates are formed in a cooperative process.

Interestingly enough, this type of representation, or to be more precise, its accompanying interpretation has only recently led to vigorous discussions in the field of colloid and interface science. This is due to apparently contradicting results from long-standing equilibrium thermodynamic considerations and experimental evidence from evolved surface analysis techniques, which have been developed over the last decades. The main subject of discussion is the interpretation of region B and the information to be extracted from it. Around 50 papers trying to clarify and discussing the so called „Gibbs-paradox“ have been published over the last ten years.

According to Gibbs, the topmost monolayer is *fully* saturated upon the transition from region A to region B at a surfactant concentration where only a slight decrease in equilibrium surface tension γ_e is observable. At concentrations beyond, the surface tension will decrease more severely even though the number of molecules in the monolayer remains constant. This consideration implies, that in the concentration range of region B, a change in surfactant bulk concentration c will have a more pronounced impact on the monolayer properties in terms of equilibrium surface tension γ_e than a

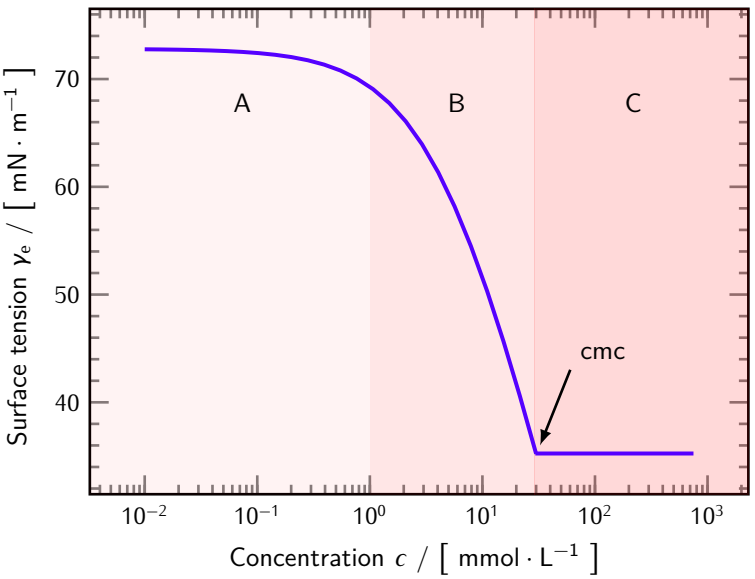

Figure II.1: Generic plot of equilibrium surface tension γ_e vs. bulk concentration c for a conventional surfactant with its three characteristic regions A, B and C. The sharp transition from a close to linear decrease to a constant value of equilibrium surface tension γ_e as a function of bulk concentration c is identified as the cmc.

modification of the surface layer itself, which is truly a paradox observation.

Menger *et al.* argue that an estimation of the area-per-molecule obtained from the negative slope of the equilibrium surface tension isotherm relying on the Gibbs adsorption isotherm (GAI) leads to „greatly overestimated“ values of molecular surface area.[7] Two major points of their work concern their call for a more cautious handling of surface tension data demanding to take into account results from highly surface specific techniques such as neutron reflectivity (NR) and the interpretation of declining equilibrium surface tension γ_e in region B in terms of a cooperative process.

The latter authors were criticized harshly for their disapproval of Gibbs-thermodynamics[8] by another research group, which stated, that the disagreement between their published data and the Gibbs-theory arises from a non-adequate application of the latter theory to the conducted experiments. Finally, they even concluded, that the data intended to challenge the Gibbs-analysis serve to prove the validity of the classical approach if used properly.

In a later work, Bermúdez-Salguero *et al.* showed that surface saturation is obtained only at the higher concentration end of region B and that micellation - if the surfactant is capable of this kind of aggregation - can occur only if the surface is saturated.[9] This will be shown in the following.

The surface chemical potential of a solute in a binary mixture obtained from coupling the GAI to the non-ideal surface equation of state (SEOS) according to Volmer is given by

$$\ln\left(\frac{\pi^*}{x}\right) = z_m\,(1-\pi^*) + \ln\gamma^\infty, \tag{II.1}$$

whereas π^* denotes the reduced surface pressure defined as

$$\pi^* = \frac{\pi}{\pi_{CMC}}. \tag{II.2}$$

The remaining quantities represent the molar fraction of the solute x and the bi-dimensional compressibility factor z_m. Approaching the molar fraction of the cmc, the reduced surface pressure assumes a value of 1 and the latter equation simplifies to

$$\ln\left(\frac{\pi^*}{x}\right)_{x\to x_{CMC}} = \ln\gamma^\infty = -\ln x_{CMC}. \tag{II.3}$$

Analysis of the limiting case for vanishing surfactant concentration leads to a relation between the standard energy of adsorption ΔG°_{ads} and the standard energy of micellation ΔG°_{mic}. Starting from

$$\ln\left(\frac{\pi^*}{x}\right)_{x\to 0} = z_m + \ln\left(\frac{\pi^*}{x}\right)_{x\to x_{CMC}} \tag{II.4}$$

with

$$\Delta G^\circ_{ads} = -RT\ln\left(\frac{\pi}{x}\right)_{x\to 0} \tag{II.5}$$

$$\Delta G^\circ_{mic} = RT\ln x_{CMC} \tag{II.6}$$

rearranging leads to

$$\Delta G^\circ_{mic} = \Delta G^\circ_{ads} + RT\,(z_m + \ln\pi_{CMC})\,. \tag{II.7}$$

The standard energy of micellation ΔG°_{mic} is smaller in amplitude than the standard energy of adsorption ΔG°_{ads} by the constant in the latter equation, meaning that adsorption is favored over micellation. It is the basis for the interpretation of adsorption as a cooperative process, which is a prerequisite for the second possible cooperative process, namely micellation. This implies, that micelle formation starts (only) after completion of monolayer adsorption.

Just as the interpretation of region B in Figure II.1, also the determination of the cmc and Gibbs surface excess is subjects of discussion.[10] Different methods are known to lead to slightly deviating values of the cmc and its interpretation as a concentration range rather than a sharp value. The

maximum surface coverage Γ_∞ can be obtained as the constant of a polynomial fit of the surface coverage Γ against the reciprocal bulk concentration c. Therein, the surface coverage Γ itself is determined from a second or third order polynomial fit of the plots of equilibrium surface tension γ_e against logarithmic bulk concentration c in combination with the GAI.

Recent experiments relying on surface specific techniques are indicative for a saturation of the monolayer only in region B. Next to the already mentioned SFGVS-results,[5,6] this equally holds for data obtained from NR,[11] and pyrene-fluorescence[12]. Radiotracer methods have been found to lead to the same quantities as measured by thermodynamic methods.[13]

But also the GAI itself has been subject to discussion due to rise of the mentioned surface specific techniques. It allows accessing the surface coverage Γ from experimental equilibrium surface tension isotherms via

$$\Gamma = -\frac{1}{mRT}\frac{\mathrm{d}\,\gamma}{\mathrm{d}\ln a}, \tag{II.8}$$

whereas a denotes the activity, R the natural gas constant, T the temperature and m a prefactor representing the number of surface active species emerging from the dissolved amphiphile. Equation II.8 allows determining the surface coverage Γ only *indirectly* from tensiometric data. „It is still unclear exactly, what is being measured in tensiometric experiments.“[11] From comparison with the complementary NR, which grants *direct* access to surface coverage Γ within an accuracy in a range of 5 % the following conclusion is to be drawn:[14] the prefactor m of the GAI assumes a value of 2 for aqueous solutions of 1:1 ionic surfactants. If ion condensation has to be considered, however, the value of the prefactor is lower than in the idealistic case of full dissociation.[15]

In contrast to the abstract concept of a Gibbs dividing surface for the selection of a separation plain between interface and bulk with the consequence of a mathematical surface with no volume, Guggenheim suggested to assign a volume with a defined mass to this plain.[16,17] The formalism for a theoretical description of this interfacial region characterized by a finite extension nevertheless remains similar to the procedure developed by Gibbs.[18] In short, the Guggenheim-concept favors the existence of an „interphase“ characterized by a smooth, but steep transition between bulk and interface, whereas the classical Gibbs-model describes a step-like progression.

Despite the ongoing discussion and (mis)interpretation of the GAI its foundations going back to the Gibbs-Duhem relation cannot be challenged. Also overinterpretation of the GAI should be given up on. The key point for the following considerations of dynamic processes at interfaces is the assumption of an interfacial region with a finite thickness. This allows for an interpretation of the experimental findings in terms of exchange processes between the bulk, this „subsurface“ and the interface.

2 Surface Equations of State

Surface equations of state (SEOSs) serve to relate the surface pressure π defined as difference in surface tension between the pure solvent γ_{solvent} and an adsorption layer covered interface by

$$\pi = \gamma_{\text{solvent}} - \gamma \tag{II.9}$$

to the area per molecule a through a mathematical expression. The area per molecule can be expressed equally well by means of the adsorption Γ, whereas this quantity defines the ratio of number of molecules adsorbed to the available area via

$$\Gamma = \frac{1}{a} = \frac{n \cdot N_{\text{A}}}{A}. \tag{II.10}$$

Therein, n represents the number of moles, N_{A} Avogadro's number and A the surface area available for the respective n surfactant molecules. In analogy to the ideal gas law, the SEOS for an ideal surface film is given by [19]

$$\pi a = k_{\text{B}} T \tag{II.11}$$

with the Boltzmann constant k_{B} and the temperature T. A connection between the adsorption Γ and the concentration of the respective surfactant is achieved via an adsorption isotherm. A combination of the Gibbs adsorption isotherm (GAI)

$$\Gamma = -\frac{1}{RT} \frac{\mathrm{d}\,\gamma}{\mathrm{d}\ln c} \tag{II.12}$$

with a SEOS allows for deriving a direct relation between the experimentally accessible surface pressure π and the adsorption Γ via the integrated form of the GAI. Deviations from the ideal behavior of the previously described non-interacting dimensionless adsorbed surfactant molecules are accounted for by using an appropriate SEOS based on physical or empirical models. [20] The non-ideal course of surface pressure π as a function of concentration is due to the finite volume of the molecules. Upon close mutual approach this property causes increasing values of surface pressure π. Furthermore, the interactions between the surfactants have to be taken into account. Depending on their nature, this leads to elevated or decreased surface pressure π for repulsive and attractive forces in between the molecules, respectively. The latter considerations are in analogy to the case of a three-dimensional gas.

The adsorption isotherms proposed by Langmuir [21] and Frumkin [22] are typically used for the description of adsorption at interfaces. Both models assume the build-up of a monomolecular adsorption layer upon increasing surfactant concentration to a maximum surface coverage Γ_{∞}. They differ, however,

in the actual mathematical expression representing the asymptotic approach of fractional surface coverage x given as

$$x = \frac{\Gamma}{\Gamma_\infty}. \tag{II.13}$$

From a mathematical point of view, the Langmuir adsorption isotherm is to be considered a special case of the Frumkin isotherm

$$x = \frac{c}{c + a_F \exp^{K_F \cdot x}} \tag{II.14}$$

with the parameters a_F and K_F. This leads to the associated SEOS

$$\pi = -\Gamma_\infty RT \left[\ln(1 - x) - \frac{K_F}{2} \cdot x^2 \right] \tag{II.15}$$

and simplifies to the corresponding Langmuir expression for $K_F = 0$. Beyond these classical approaches, also so called reorientation and interfacial aggregation models have been used for quantitative description of experimental surface tension data.[23] Also the adsorption processes occurring in mixed surfactant protein layers can be described systematically.[24]

3 Ionic Surfactants at Interfaces

The interaction of ionic species with charged interfaces has been subject to several modeling approaches. Descriptions of the „double layer“ have been put forward among others by Helmholtz, Gouy and Chapman, Stern and Grahame. A more recent concept to model the distribution of charged species in the electric double layer (EDL) of an interface was introduced by Warszyński and coworkers.[25] A schematic representation of the conceptual ion distribution assumed in this theory is given in Figure II.2.

Surfactant molecules adsorb at the interface with their headgroups in the Stern layer. But in the model presented in the following, also the counterions can adsorb specifically in the Stern layer at the Helmholtz plane. The Stern layer is considered a two-dimensional electrolyte which does *not* meet the condition of electroneutrality. The following relations constitute a set of equations, which has to be solved numerically in order to determine the adsorptions of both surfactant and counterions. The total charge in the Stern layer σ is given by the sum of charges of the adsorbed ions via

$$\sigma = z_S F \Gamma_S + z_C F \Gamma_C, \tag{II.16}$$

whereas F denotes Faraday's constant and z_i and Γ_i represent the charge and surface concentration

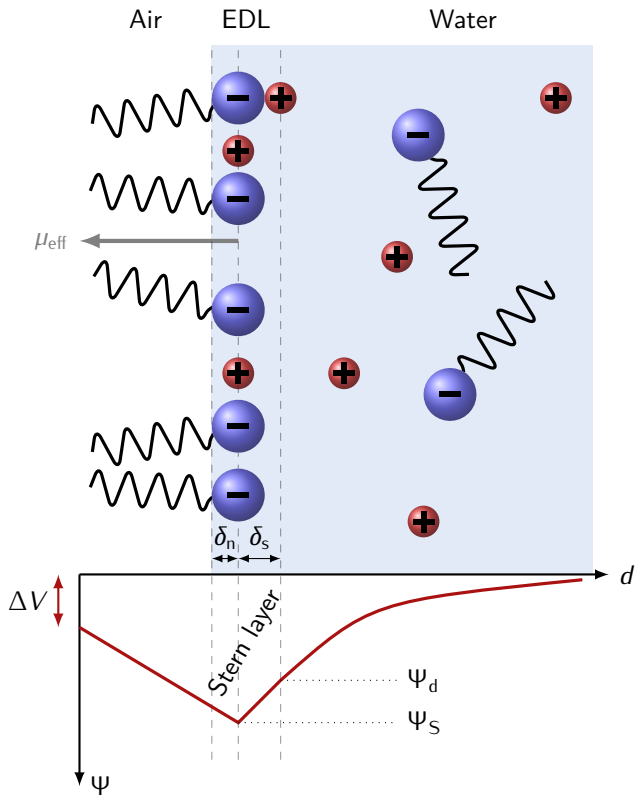

Figure II.2: Model of surfactant and counterion adsorption at the air-water interface according to Warszyński. [25]

of either the surfactant ($i = S$) or the counterion ($i = C$), respectively. The diffuse layer potential at the boundary between the Stern layer and the diffuse part Ψ_d of the EDL can be determined via

$$\Psi_d = \frac{2k_B T}{e} \sinh^{-1}\left(\frac{\sigma e}{2\epsilon_0 \epsilon_r k_B T \kappa}\right) \tag{II.17}$$

taking into account the Boltzmann constant k_B, temperature T, elementary charge of the electron e, vacuum dielectric permittivity ϵ_0, relative permittivity of the solution ϵ_r and Debye-Hückel (DH) reciprocal length κ. The Stern layer potential Ψ_S can be calculated from the potential at the boundary Ψ_d assuming a linear drop with the distance δ_s according to

$$\Psi_S = \Psi_d + \frac{\sigma \delta_s}{\epsilon_0 \epsilon_S} \tag{II.18}$$

taking into account a dielectric constant in the Stern layer ϵ_S. The adsorption isotherms can be derived from the equilibrium of electrochemical potentials for the bulk phase and the Stern layer and by application of the Flory-Huggins statistics for the concentrated two-dimensional electrolyte. For convenience, the adsorption of surfactant and counterions is expressed in terms of relative surface coverages

$$\theta_i = \frac{\Gamma_i}{\Gamma_{i\infty}}, \tag{II.19}$$

where $\Gamma_{i\infty}$ denotes the limiting surfactant concentration of the respective species. The adsorption of surfactant and counterions is related to the potentials and concentrations via equations

$$\frac{a_-}{\alpha_S} \exp\left(\frac{e\Psi_S}{k_B T}\right)(1 - \theta_S - \theta_C) = \theta_S \exp\left(-2H_S \theta_S\right) \exp\left(\frac{\Phi_S}{k_B T}\right) \quad \text{and} \tag{II.20}$$

$$\frac{a_+}{\alpha_S} \exp\left(-\frac{e\Psi_S}{k_B T}\right)(1 - \theta_S - \theta_C) = \theta_C \exp\left(\frac{\Phi_C}{k_B T}\right). \tag{II.21}$$

Within this system of equations, some additional parameters and variables are taken into account: the respective charge dependent activity of counterions and surfactant ions $a_\pm$, the „surface activity“ of the surfactant α_S, an interaction parameter H_S quantifying the latter attraction and correction factors Φ_C and Φ_S. The two parameters Φ_C and Φ_S serve to correct the activity for the lateral interactions between the ions of the two-dimensional electrolyte in the Stern layer. An approximation to the ionic activity coefficient $\gamma_{S\pm}$ for the quasi-two-dimensional electrolyte analogous to the DH-formulation valid for the bulk is given by

$$\ln \gamma_{S\pm} = \frac{\Phi_C}{k_B T} = \frac{\Phi_S}{k_B T} \approxeq -\frac{e^2}{8\pi\epsilon_0 \epsilon_S k_B T} \frac{\kappa_s}{1 + \kappa_S a_S} \tag{II.22}$$

with the two-dimensional equivalent of the DH screening length

$$\kappa_S = \frac{e^2 (\Gamma_S + \Gamma_C)}{\epsilon_0 \epsilon_S k_B T}. \tag{II.23}$$

The numerical solution of the latter set of equations using an iterative Newton-Rapshon scheme allows obtaining the adsorption of surfactant and counterions corresponding to a given set of fitting parameters.[25,26] The surface tension corresponding to the surface coverages is accessible from integration of the Gibbs adsorption equation

$$\mathrm{d}\,\gamma = -RT\,(\Gamma_S\ \mathrm{d}\ln a_S + \Gamma_C\ \mathrm{d}\ln a_C)\,. \tag{II.24}$$

4 Lamella and Foam Stability

Foams can be considered as dispersions of gas in a liquid or solid. They are characterized by thermodynamic instability due to their large surface area. Exclusively kinetic stabilization can lead to the formation of so called instable or metastable foams.[27,28] Throughout this thesis, only liquid foams will be studied. They are formed by externally induced mechanical perturbation of the disperse phase in presence of surface active components. Subsequent to its formation, a transition of the initially formed wet *kugelschaum* to the so called *polyederschaum* foam type is typically observed. This evolution is often referred to as *de-watering process* and schematically represented in Figure II.3.

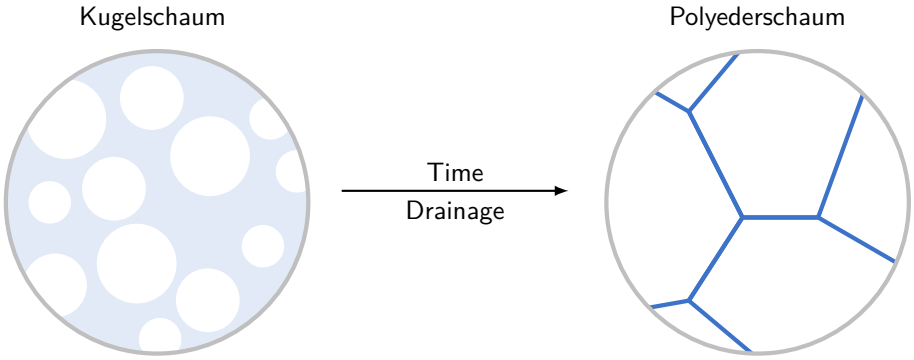

Figure II.3: Schematic representation of kugelschaum and polyederschaum phases of liquid foam. The transition is referred to as de-watering process and promoted by the destabilizing mechanisms of liquid drainage, coalescence and Ostwald-ripening. The polyederschaum cells are stabilized by Plateau-borders.

The eventual rupture of foam lamellae and three-dimensional foams, which can be thought of as a complex structure of lamellar building blocks, is to be interpreted as an interplay between forces and effects causing stabilization and destabilization of the lamellae. In the following, some of the most

relevant contributions will be explained.

The effect of gravity causes the bulk liquid to drain from the kugelschaum phase leading to the formation of polyhedral cells delimited by rather plain foam lamellae with adsorbed surface active material at their interfaces.[29] Within this phase, the lamellae are connected via so called Plateau-borders honoring the experimental work of Joseph Plateau on foam patterns.[30] The latter refer to the contact line of three - more or less - plain lamellae at an angle of 120° as schematically shown in Figure II.4.

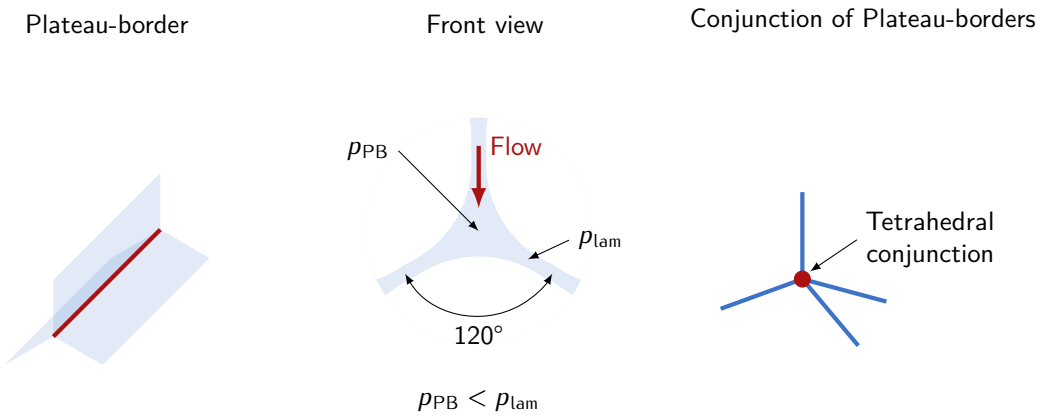

Figure II.4: Schematic representation of a Plateau-border formed by three adjoining lamellae at an angle of 120° and the conjunction of four of them at the tetrahedral angle of 109.47°.

Due to the curvature in close proximity to the Plateau-borders, the pressure p_{PB} inside is reduced with respect to the pressure in the flatter regions of the lamellae p_{lam} by the action of the Laplace-law describing an inverse relation between the pressure p and the radius of curvature r.[31] This gradient between the lamellae and its Plateau-borders leads to a flow of liquid from the lamella towards the Plateau-border resulting in a thinning until a critical thickness is reached. In literature, this effect has also been referred to as *capillary suction*.[32,33] Once this critical thickness is reached, the lamellae are susceptible to rupture by mechanical disturbances or fluctuations. An additional reason for foam destabilization based on the action of the Laplace pressure is well-known in colloidal chemistry: Ostwald-ripening. The initially randomly formed kugelschaum gas compartments feature different internal pressures according to size, shape and curvature. To relieve the pressure gradients between them, a disproportionation process described by expansion of lower pressure large cells at the expense of high pressure small cells takes place. This ultimately leads to the formation of low pressure gradient polyhedral foams according to the laws of Plateau, where eventually Plateau-borders meet in tetrahedral arrangements as indicated in Figure II.4.[34]

Despite the mentioned effects promoting the decay of foams, there is also a considerable number of processes favoring their existence. One of the most obvious and frequently used approaches is based on increasing the solutions' bulk viscosity thereby reducing drainage.[35] Whereas this concept

aims to hinder the transition from kugelschaum to polyederschaum, there are as well mechanisms stabilizing the then prevalent lamellae. The disjoining pressure π_d is an experimentally readily available parameter and describes the interaction between the surfactant layers adsorbed at both sides of a lamella.[36–42] It constitutes from electric, steric and van der Waals forces. Stable foams are observed for a compensation of disjoining pressure π_d and capillary pressure.[34] Another beneficial effect for maintaining a foam lamella subject to deformations is the Gibbs-Marangoni mechanism. It describes a „self-healing effect“ due to an emerging gradient in surface tension caused by its extension as illustrated in Figure II.5.

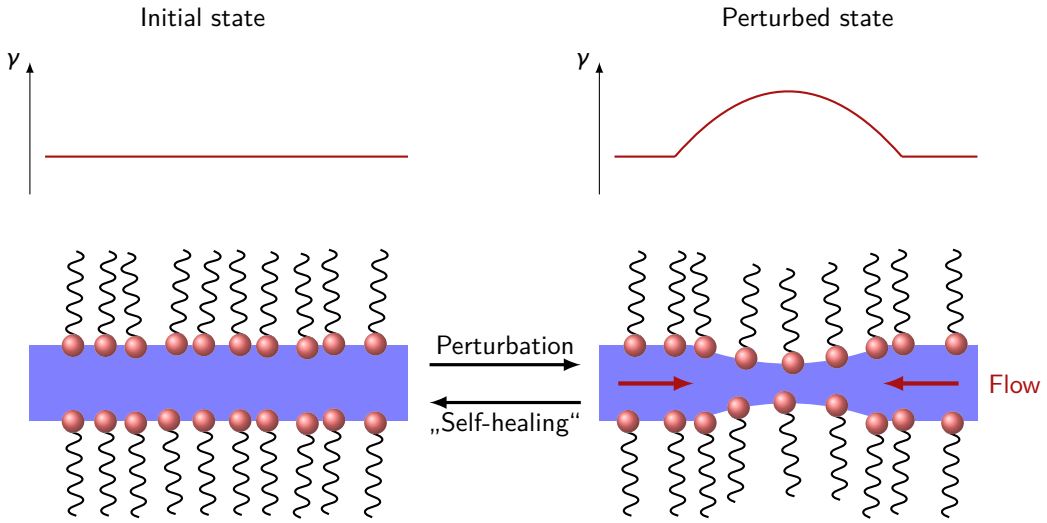

Figure II.5: Scheme of the Gibbs-Marangoni mechanism. A local lamella deformation causes a surface tension gradient. The tendency to relieve this non-equilibrium state by induction of a surfactant flow dragging along water molecules generates the „self-healing“ effect.

A local increase in surface area is associated with a decrease in surfactant concentration corresponding to a higher value of surface tension compared to the unperturbed parts of the lamella. To counteract this non-equilibrium state, a flow of surfactant molecules opposite to the deformation-induced surface tension gradient emerges. As water is dragged along with the flowing surface active compound, this process acts to restore the original state of the lamella.[43–46] These processes described in terms of a so called surface dilatational modulus E expressing the resilience against an induced deformation serves to quantify the Gibbs-Marangoni effect. It represents the ability of a system to restore its equilibrium surface tension γ_e upon deformation. However, it is to be noted that there is a certain medium concentration range in which this effect is most pronounced. In case of too low surfactant concentrations, the appearing surface tension gradient is too small to induce a flow. For too high concentrations, the gradient is mainly eliminated by surfactant diffusion processes from the bulk towards the interface without dragging along a sufficient number of water molecules to effectively counteract the thinning process. Therefore, foam systems have been reported to show maximum stability around the critical micellar concentration (cmc). A lamella can gain further stability, if its

adsorption layers feature surface viscoelastic behavior, *i.e.,* energy can be dissipated within the surface layer by the action of additional energy-consuming processes.

The relation between foam stability and drainage rate within the constituting liquid is well established.[47] However, several parameters intending to characterize foam stability judging from the respective aqueous solutions' interfacial properties have been proposed. In most of the cases they are traced back to elasticity and reduction of surface tension. Moreover, experimental evidence for a layering phenomenon manifested as film thickness transitions in solutions containing pure surfactants was observed.[48]

In their 2014 paper, Zell *et al.* point out the shear inviscidity of pure surfactant solutions for both high- and low-foaming solutions. According to their argumentation, pure shear rheological properties are of minor relevance for foam stabilization. Furthermore they claim to have proven all shear rheological measurements conducted up to this date as invalid and subject to errors on the order of factors from $1 \cdot 10^3$ to $1 \cdot 10^4$.[49] This exclusion of surface shear measurements is to be interpreted as a hint on the importance of *dilatational* characteristics, especially for interfaces stabilized by small molecular surfactants.

Stabilization in mixed surfactant-polymer layers is based on the two effects of retarding liquid drainage in bulk and providing enhanced adsorption, which might also be irreversible in some cases. Reduction of coalescence and increasing film strength go hand in hand.[47] Typically, the use of polymeric additives causes elevated viscoelasticity and viscosity of the aqueous phase, which as a consequence leads to slowed drainage accompanied by increased foam stability.[50] Synergistic adsorption effects in mixed polymer-surfactant adsorption have been found to lead to packed layers.[51] In this type of systems, viscosity at high shear rates ($200\,s^{-1}$) was found to be correlated to the rate of liquid drainage pointing out the importance of rheological data over a possible broad frequency range to identify potential mechanisms of stabilization.[47]

Another part of foam and emulsion stability research focuses on the use of particles as surface active material. The finely disperse solids have proven to cause pronounced modification in food and beverages as well as in combination with classical surfactants and other mixtures of interest in colloid and interface science.[52–57]

The investigation of non-aqueous and smart foams has recently been developing to a „hot topic".[58,59] Next to the goal of tuning foam stability on demand by application of external stimuli such as light, temperature, electric or magnetic fields targeting at certain molecular features, also „non-classical" stabilization processes such as crystallization within the interface are exploited. Of course, some of the new questions arising in this field cannot be addressed appropriately by the conventional methods targeting aqueous foams formed due to the presence of amphiphiles.

5 Debye-Hückel-Theory

The Debye-Hückel (DH)-theory provides a quantitative description of electrolyte solutions taking into account the interplay of randomizing thermal motion and ordering electrical attraction.[60] In more advanced models derived from DH as a starting point, also the dimension of ions and interaction between ion and solvent are considered. Key idea of the concept is to establish a distribution function, *i.e.,* probability to find a particle in a position relative to another. In case of electrolyte solutions, the distribution of ions is to be understood as a consequence of long range coulombic electrical forces and thermal motion. This means, that in electrolyte solutions the ion distribution is *not* random even at considerable distance, *i.e.,* in the dilution regime.

A known ion distribution allows for calculation of the corresponding arising electrical potential. The challenge of this approach is that the calculation of a distribution requires knowledge of the potential. The first accepted theory has been put forward by Debye and Hückel[61] and further extended by Bjerrum,[62] Onsager[63] and Falkenhagen.[64]

The DH-theory demands the calculation of a potential at a given point in the solution as a function of concentration and charge of ions as well as solvent properties. Therefore, a combination of the Poisson-equation, *i.e.,* the most general form of Coulombs law of force between charged bodies from electrostatics with a statistical mechanical distribution function according to Boltzmann is applied. The Poisson-equation relates the charge density ρ to the potential Ψ via the Laplace operator ∇^2 and the dielectric constant of the medium ϵ via

$$\nabla^2\Psi = -\frac{4\pi}{\epsilon}\rho. \tag{II.25}$$

For convenience and due to the symmetry of the mathematical problem assuming spherical ions, one particular ion is chosen as the origin of the coordinate system. It is to be noted, that the Poisson-equation of electro*statics* holds strictly only for a system of charges at rest. In order to apply this theory for the case of charges in solution, it is assumed, that time-averaging due to thermal motion makes it valid also for a real case. Electro-neutrality of the system specified as

$$\sum_{i=1}^{s} n_i z_i = 0 \tag{II.26}$$

with algebraic valences z_i (can take + and - values) and an average number of ions per unit volume n_i has to be met as a boundary condition. Assuming an ion j to be the center of the coordinate system, any shell around this central charge carrier will have opposite charge to fulfill this constraint. The total charge from the surface of the ion a to infinity is opposite to the charge of the central ion expressed by

$$\int_a^\infty 4\pi r^2 \rho_j \mathrm{d}\, r = -z_j e \tag{II.27}$$

to fulfill the requirement of electroneutrality. *The* assumption of DH-theory is to specify a Boltzmann-ansatz for the ion distribution with energy given as the product of potential and charge. Therefore, the local concentration $n_i^{'}$ of ion type i is given by

$$n_i^{'} = n_i \exp\left(-\frac{z_i e \Psi_j}{k_\mathrm{B} T}\right), \tag{II.28}$$

whereas the subscript j represents the orientation with respect to the (moving) coordinate system centered at ion j. The remaining quantities denote the Boltzmann constant k_B, elementary charge e and temperature T. Accordingly, the charge density is obtained by summing up the latter local concentrations multiplied with the respective charge. The Boltzmann-relation demands an exponential relation between charge density ρ and the potential Ψ_j leading to an intrinsic problem: the principle of linear superposition of fields does not hold due to the exponential relation. This means that doubling of charge density does not lead to a double potential.

A remedy is to use a linearized version of the Boltzmann equation, which is valid at low potentials compared to thermal energy, *i.e.,* when the ions are able to move freely. In this linearized form, the superposition principle with a proportionality between charge density ρ and potential Ψ_j holds. But even for very low electrolyte concentrations, strong deviations from ideal behavior due to noticeable interaction between ions are possible. In the course of the linearization, the Boltzmann distribution is replaced by

$$n_i^{'} = n_i \left(1 - \frac{z_i e \Psi_j}{k_\mathrm{B} T}\right). \tag{II.29}$$

In comparison to other types of salt, univalent electrolytes are best described by these approximations, as in this case the linear approximation appears to be a more realistic description of the ion distribution. The expression for the charge density of the linearized Boltzmann is introduced into the Poisson-equation. It is referred to as the Poisson-Boltzmann equation. In order to arrive at a simplified form for solution of this differential equation, a new constant is defined. It is related to the inverse Debye-length κ^{-1}, has dimensions of a reciprocal length and is defined by compressing the coefficient of the Poisson-Boltzmann equation according to

$$\kappa^2 = \frac{4\pi e^2 \sum_{i=1}^{2} n_i z_i^2}{\epsilon k_\mathrm{B} T}, \tag{II.30}$$

whereas the so called ionic strength I for a binary electrolyte in units of $\mathrm{mol} \cdot \mathrm{L}^{-1}$ is given by

$$I = \frac{1}{2} c \left(\nu_1 z_1^2 + \nu_2 z_2^2 \right) \tag{II.31}$$

with the number of ions emerging from dissociation of the electrolyte ν_i and charge of the respective ion z_i.

Abandoning the exponential form of the Boltzmann-equation in favor of the linearized relation in the case of low potential, a linear second order differential equation with general solution can be obtained. From the condition of electroneutrality and integration, an expression for the time averaged DH-potential imposed by a selected j-ion at a point at distance r from it in absence of external forces is given by

$$\Psi_j = \frac{z_j e}{\epsilon} \frac{\epsilon^{\kappa a}}{1 + \kappa a} \frac{\exp^{-\kappa r}}{r}. \tag{II.32}$$

The closest possible approach of any other charge to the central ion is the distance a. This implicitly demands the same size of all ions taken as spheres of diameter a. In order to arrive at a full description of the forces operating in electrolyte solutions, long-range ionic forces and short-range interactions between ions and solvent have to be considered. These opposing effects are of comparable magnitude in typical electrolyte solutions, but characterized by different scaling as a function of concentration. Whereas the short-range forces are linear in c, the proportionality is less pronounced for the $\sqrt{c}$-relationship of interionic interaction. For purely mathematical considerations, short-range interactions can therefore be neglected with respect to the long-range forces due to their diverging scaling behavior at high dilutions. There are different scaling laws for the potential imposed by the presence of an ion in case of

- an individual ion
$$\Psi \propto \frac{z_j e}{\epsilon r} \tag{II.33}$$
- and an ion in electrolyte solution
$$\Psi \propto \frac{z_j e \exp^{-\kappa r}}{\epsilon r}. \tag{II.34}$$

This means a slower decay of the potential in electrolyte solutions compared to an individual ion. Due to the principle of linear superposition, the DH-potential can be rewritten as the sum of the potential of a central ion and the potential caused by the presence of the surrounding ions. Subtracting the potential of the isolated ion from the DH-potential of a central ion within an electrolyte gives

$$\Psi_j' = \frac{z_j e}{\epsilon r} \left[\frac{\exp^{\kappa a}}{1 + \kappa a} \exp^{-\kappa r} - 1 \right] \qquad \text{only for } r > a \tag{II.35}$$

and represents the potential due to the *remaining* charges. At the surface of the central ion, *i.e.*, $r = a$ the potential assumes the value

$$\Psi_j' = -\frac{z_j e}{\epsilon}\frac{\kappa}{1+\kappa a} = -\frac{z_j e}{\epsilon}\frac{1}{a+\frac{1}{\kappa}} \tag{II.36}$$

This expression describes the effect of the surrounding electrolyte on the potential of the central ion caused by the resulting field. The structure of this relation matches the previously shown potential of an individual ion. Therefore, the central ion contained in a cloud of surrounding counterions is described by the same potential as if all of the surrounding ions were distributed over a spherical surface at a distance of

$$a + \kappa^{-1}. \tag{II.37}$$

The net charge on this hypothetic surface is equal and opposite to the charge of the central ion and the quantity κ^{-1} is the Debye length measured from the surface of the ion.

A DH activity coefficient is used in order to describe the change in interaction strength between ions surrounded by counterion shells as discussed previously. The rationally obtainable expression is typically modified by a linear empirical summand in order to achieve better agreement between experimentally accessible values of mean rational activity coefficients $f_\pm$ and the theoretical expression

$$\ln f_\pm = -\frac{A|z_1 z_2|\sqrt{I}}{1+Ba\sqrt{I}} + bI. \tag{II.38}$$

Therein, the constants A and B serve to introduce the influence of solvent type and temperature. The values of a (ion size parameter, values of around 4 Å are typically used) and b are obtained as fitting parameters to suit experimental results. From the evaluation of activity coefficients for NaCl at 25 °C, sound agreement between theory and experiment was found for $a = 4\,\text{Å}$ and $b = 0.055\,\text{mol}\cdot\text{L}^{-1}$ for concentrations up to $2\,\text{mol}\cdot\text{L}^{-1}$

It is to be noted, however, that changes in the value of a depend on the fitted concentration range and are not necessarily to be interpreted as real changes of ion size. For reasons of plausibility, values of a can be checked based on an estimate gained from the sum of crystallographic radii or radii of ionic hydration. Access to activity coefficients is granted by measuring transport numbers.

6 Adsorption at Interfaces

The analysis of equilibrium surface tension γ_e is essential for the characterization of interfaces, both the gas-liquid interface and the liquid-liquid interface. In the following, ring tensiometry and pendant drop/bubble tensiometry will be presented. Also, some general principles related to the measurement of surface dilatational properties are highlighted.

6.1 Ring Tensiometry

The de Noüy ring method is a classical method for determining the equilibrium surface tension γ_e.[65] During the experimental procedure, a ring consisting of a platinum-iridium alloy is immersed into a container holding the sample to be studied and the force upon retraction is measured. The maximum force F_{max} is related to the contact angle θ of 0°. Given a circumference U, the static equilibrium surface tension γ_e of the solution is given by the relation

$$\gamma_e = \frac{F_{max}}{U \cdot \cos\theta}. \tag{II.39}$$

On a molecular level, surface tension is a measure for the net force pulling interfacial molecules from the surface towards the bulk. In terms of a thermodynamic formalism, it describes the change in Gibbs energy G upon changing the surface area A as

$$\gamma_e = \left(\frac{\partial G}{\partial A}\right)_{T,p,n} \tag{II.40}$$

at constant temperature T, pressure p and composition of the system as represented by the number of moles n. In order to arrive at a minimum of the Gibbs energy G, the system seeks to decrease its overall surface area A. This leaves the interpretation of surface tension as a quantity proportional to the urge of the system to reduce its surface area. A schematic representation of the measuring procedure and the characteristic force curve measured upon retraction of the probe is given in Figure II.6.

6.2 Pendant Drop Tensiometry

Pendant drop tensiometry has matured to an established technique for measuring surface tension at both gas-liquid and liquid-liquid interfaces exploiting the shape of a drop in order to obtain a corresponding surface tension value. The principle of image analysis is shown in Figure II.7. A schematic representation of the experimental setup is given in Figure II.8. The personal computer (PC)-controlled setup consists of a light emitting diode (LED) light source, a capillary connected to a motorized pump and a charge-coupled device (CCD)-camera.

Devices working on the axis symmetric drop shape analysis (ADSA)-principle used for pendant drop tensiometry allow accessing several interfacial properties such as equilibrium and dynamic surface tension and the elasticity parameters of the respective adsorbed layers. In all of these cases, the key principle for determining an instantaneous surface tension value is the interplay between the counteracting effects of surface tension and gravity. The shape of the droplet is described by the Gauss-Laplace equation. It serves to establish a connection between the curvature of a liquid meniscus and surface tension γ via

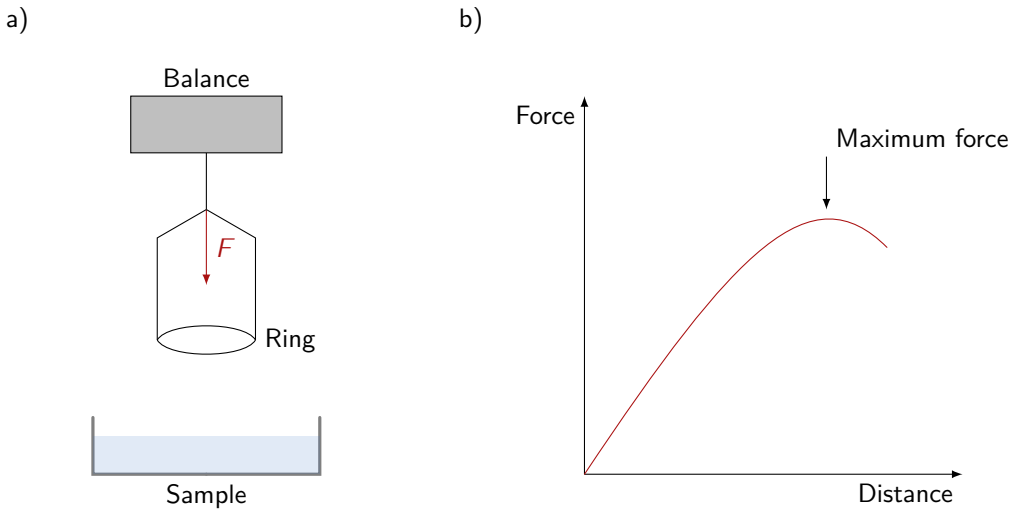

Figure II.6: Scheme of ring tensiometry. a) A ring is immersed into the aqueous sample solution and the force upon retraction is measured by means of a high precision balance. b) Schematic force distance curve upon retraction. The maximum force corresponds to the surface tension of the solution. Increasing the distance any further will cause a rupture of the lamella.

$$\gamma \left(\frac{1}{R_1} + \frac{1}{R_2} \right) = \Delta P_0 + \Delta \rho g z. \tag{II.41}$$

Therein, R_1 and R_2 denote the main radii of curvature, ΔP_0 the pressure difference in a reference plane, $\Delta\rho$ the density difference between the two studied media, g the gravitational acceleration and z the vertical height of the drop measured from the reference plane. The CCD-camera captures images of the droplet, from which, after an appropriate contour-tracing and fitting of the Gauss-Laplace equation, a surface tension value is obtained. For this purpose, the radii of curvature as indicated in Figure II.7 are used.

Depending on the type of interface to be studied and the density of the adjoining bulk media, variable measuring geometries are applied in different types of ADSA-experiments: sessile drop, emerging bubble and buoyant bubble.[66] Furthermore, most available devices additionally allow for measurements of contact angles.

Next to determining equilibrium surface tension γ_e, it is possible to access surface rheological properties of the respective adsorption layers by periodic perturbation of the surface area via action of the syringe pump as indicated in Figure II.8. It is to be noted, that the accessible frequency range of perturbation with this setup is limited to a maximum frequency of about 1 Hz for the typically studied droplets of bubbles formed at capillaries with diameter ranging from 2 to 4 mm. Furthermore, the type of deformation induced in the course of the experiment typically is not purely of dilatational nature and

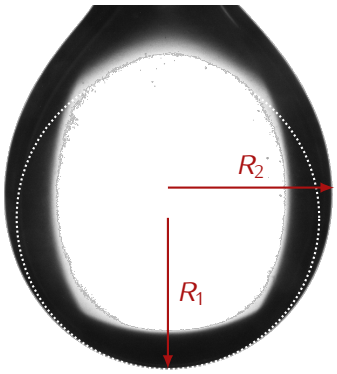

Figure II.7: Schematic representation of the parameters used in pendant drop tensiometry to obtain the surface tension value corresponding to the shape of the droplet. The axis symmetric shape of the drop identified by contour tracing is mathematically defined by the radii of curvature R_1 and R_2. It results from a competition between the forces of curvature and gravity. The dotted line serves to visualize the circle corresponding to R_1.

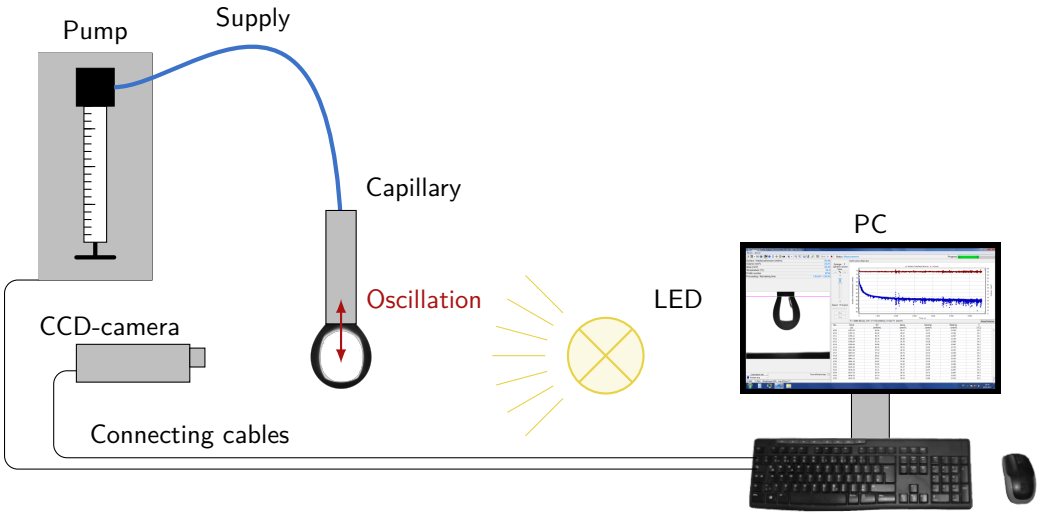

Figure II.8: Scheme of pendant drop tensiometry operating on the ADSA-principle. A mm-sized drop hanging from a capillary is formed automatically by a PC-controlled syringe pump. Images captured of the LED-illuminated droplet are fed to the on-line image processing of the control program.

comprises additional contributions of shear. However, the influence of shear on the overall response to an induced strain is generally negligible.[49] Determination of the relevant parameters and the information to be obtained from them will be discussed in subsection 9.1, where the custom-built oscillating bubble device for measurements of surface dilatational rheology is described in more detail.

6.3 Measuring Dynamic Interfacial Properties

Dynamic interfacial properties such as dynamic surface tension can be assessed by a multitude of tools over wide ranges of timescales. Relying on a combination of data collected from different techniques, typically the range of characteristic deformation frequencies from $1 \cdot 10^{-2}$ to $1 \cdot 10^{6}$ Hz can be covered as schematically shown in Figure II.9. An extensive review on available techniques was given by Noskov in 2010.[67] Some of the most relevant methods will be shortly outlined in the following.

As described in more detail in section 8, capillary wave techniques infer the dilatational viscoelasticity from applying a dispersion equation to the profile of surface waves.[68] Takajo *et al.* used this approach to study the formation of aggregates in binary mixtures of short chain phosphatidylcholine-based lipids.[69] A major drawback of capillary wave techniques is their strong dependence on the chosen model. Furthermore, they are complicated to operate and the measurement procedure is relatively time-consuming.

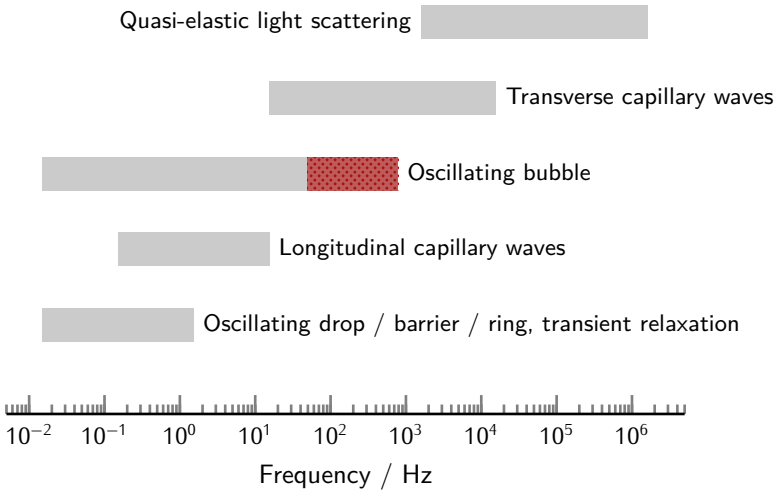

Figure II.9: Frequency ranges of techniques used to assess dynamic interfacial properties. Established oscillating bubble techniques allow for measurements up to the range of tens of Hz. The presented device has the potential to extend the upper accessible frequency range to about 1000 Hz as indicated by the red bar. Measurable frequency ranges are completed to the lower side by longitudinal capillary wave, oscillating drop, barrier and ring methods. Transverse capillary wave and quasi-elastic light scattering techniques grant access to these properties at higher frequencies. The figure has been adapted from a review by Noskov from 2010.[67]

A class of instruments closely related to the oscillating bubble device are based on the drop volume technique and are also commercially available. The volume of a drop attached to the tip of a capillary is increased by pumping further solution into it. Depending on the experimental geometry, the droplet detaches from the tip of a capillary once the restoring force of surface minimization is compensated by buoyancy or gravity in case of analyzing oil in water or water in oil emulsions respectively.[70–73] Measuring the volumes required for detachment as a function of flow rate delivers information on the prevailing adsorption kinetics. Relying on this principle, knowledge on the surface tension at the moment of detachment, *i.e.,* surface tension as a function of surface age can be attained. An alternative realization of this working principle is given by the stalagmometer arrangement. Therein, the number of droplets into which a given total volume disintegrates is captured.[74]

In a recent contribution by Javadi *et al.*, capillary pressure experiments at the water-hexane liquid-liquid interface considering diffusion and mass exchange between the two phases were carried out. An overall mass transfer coefficient accounting for both diffusive and convective effects was defined.[75]

Oscillating bubbles have been used among others to study biomedical interfaces[76–81] and surfactant dynamics[82–90] mainly at aqueous liquid-vapor interfaces. An extended discussion of other methods was given by Johnson *et al.* in 1996.[91] The Franses group referred to the oscillating bubble device as pulsating bubble surfactometer.[80–82] They focused on a theoretical analysis of the parameters governing dynamic surface tension. Bulk shear viscosity, gas flow, inertia and convection were considered to be decisive. Furthermore, coupled non-linear flow fields created by the motion of the bubble interface and surfactant mass transfer were modeled.

Also Kotula *et al.* used a device for accessing purely dilatational properties of air-water interfaces pinned to the tip of a µm-sized capillary introduced previously by Alvarez and coworkers.[92,93] Their presented solvent exchange procedure allows adjusting the concentration of the surface active model substances. The obtained surface pressure results were found to agree with experiments from the compression isotherms from a macroscopic Langmuir trough. However, this device is also limited to a frequency range from 0.1 to 1 Hz.

Raudino *et al.* made use of an oscillating bubble as a model for a fluctuating cell. In their setup, oscillations were induced by applying a periodic electric field acting on the effective net charge at the air-water interface.[94,95]. The induced surface motions were monitored via an interferometric setup. Due to the finiteness of the bubble surface, only a discrete spectrum of stationary modes could be excited. Typically the bubble is excited at its lowest resonance frequency, which appears in the range from 100 to 200 Hz depending on the system. This application of induced perturbations in a resonance-like manner limited this approach to a rather narrow region around the resonance phenomenon.

A device based on the principle of an oscillating droplet in confined geometry at the tip of a capillary was used by Zou and coworkers. The main focus of recent contributions of this group was on the study of lung surfactants and the influence of contaminants, *e.g.,* nano-particles, on the dilatational

properties of their adsorption layers.[96–98] Some aspects of their analysis are based on plots of change of surface tension $\Delta\gamma$ against the relative change of surface area $\Delta A/A$ upon applying periodic expansion-compression cycles to the volume of the bubble. This is not possible in the presented version of the oscillating bubble technique in the range of elevated frequencies due to limitations in the imaging components such as lacking contrast in case of short illumination times. These shortcomings can potentially be overcome using a high-speed camera.

The elasticity properties for frequencies up to around 0.5 Hz can be determined via commercially available ADSA tensiometers (see subsection 6.2). Karakashev *et al.* correlated the modulus at a fixed frequency of 0.1 Hz as a function of concentration of nonionic surfactant tetraethylene glycol octyl ether with foam stability.[99]

7 Optical Characterization of Aqueous Interfaces

Vibrational spectroscopic techniques allow accessing detailed molecular characteristics of interfacial films such as chain conformation, hydrogen bonding or the extent of ionic interactions.[100] In the following, the most relevant aspects of sum frequency generation vibrational spectroscopy (SFGVS) (shortly also referred to as sum frequency generation (SFG)-spectroscopy) and infrared reflection absorption spectroscopy (IRRAS) will be introduced.

7.1 Sum Frequency Generation Spectroscopy

SFG-spectroscopy (more precisely SFGVS) is a non-linear optical technique to study interfaces. Its most prominent characteristic is surface specificity down to sub-monolayer surface coverages.[101,102] The overall result of an SFG-experiment can be understood as a vibrational spectrum recorded specifically from the interfacial region.

Figure II.10 shows a scheme of the non-linear processes involved and the experimental setup. Two Laser beams, *i.e.,* a visible (Vis) and an infra-red (IR)-beam tunable in frequency are brought to overlap both spatial and temporally on the sample. Due to the high intensities of the incident beams, a signal is generated at the sum frequency

$$\omega_{\mathrm{SFG}} = \omega_{\mathrm{VIS}} + \omega_{\mathrm{IR}} \tag{II.42}$$

according to the principles of non-linear optics. After separating the signal from the reflected incident beams by means of mirrors, it is directed into a monochromator and a photo multiplier tube (PMT). In an energy diagram, the generation of light pulses at the sum frequency is interpreted as a vibronic excitation by the IR-beam followed by an up-conversion initiated by the Vis-beam. This process is described in terms of a coherent anti-Stokes Raman transition.

To ensure sufficiently high intensities to cause non-linear effects, either ps or fs-pulsed lasers are used as sources for the IR- and Vis-beams.

The surface specificity of SFG-spectroscopy is due to the fact that non-linear optical processes are forbidden within the electric dipole approximation in both molecular arrangements possessing inversion symmetry and isotropic ensembles. Therefore, the bulk phases adjacent to the interfacial region are „silent“ in this technique. Only ordered molecular structures arranged in non-centrosymmetric environments lead to the emergence of a SFG-signal. All types of accessible interfaces are intrinsically non-centrosymmetric making this type of spectroscopy a highly valuable tool for the analysis of surfaces and interfaces.

Incident light represented by the electric fields $\vec{E}_i$ of IR and Vis-light induces a second order polarization $\vec{P}^{(2)}$ within the sample. The second-order nonlinear susceptibility $\chi^{(2)}$ is to be understood as a proportionality constant between these quantities and defined via

$$\vec{P}^{(2)} = \epsilon_0 \chi^{(2)} \vec{E}_{IR} \vec{E}_{VIS} \tag{II.43}$$

with the absolute electrical permittivity of vacuum ϵ_0. It is formally represented by a third-rank tensor $\chi^{(2)}_{ijk}$ acting as a material constant and serves to characterize the sample. Information on the properties of the specimen can be interpreted in terms of determining tensor elements of the second-order nonlinear susceptibility $\chi^{(2)}_{:}$ Making use of experiments with polarized incident and emitted beams some of them can be accessed. This knowledge can be used to infer the orientation of SFG-active molecular fragments. From their orientation, information on the overall arrangement of interfacial species can be obtained.

In conventional SFG-experiments, only the intensity of the signal can be measured. It is proportional to the absolute square of the second-order nonlinear susceptibility $\chi^{(2)}$. In recent years, techniques have been developed to experimentally determine both the real and imaginary part of the tensor elements by means of interference experiments with a known reference material. [103–106]

But also the mere measured signal-intensity allows obtaining additional information from SFG-spectroscopy in terms of both surfactant adsorption and orientation of the alkyl chains within the adsorbed amphiphile. Here, an adapted version of the procedure outlined by Shahir *et al.* will be discussed. [5] The SFG-intensity is known to be proportional to the intensities of the incident Vis and IR-beams I_{VIS} and I_{IR}, respectively. Furthermore, the squared sum of the resonant and non-resonant second order effective susceptibilities $\chi^{(2)}_{eff,NR}$ and $\chi^{(2)}_{eff,R}$ serve as proportionality constants. This leads to the overall expression

$$I_{SFG} \propto \left| \chi^{(2)}_{eff,NR} + \chi^{(2)}_{eff,R} \right|^2 I_{IR} \cdot I_{VIS}. \tag{II.44}$$

Therein, the resonant second order susceptibility $\chi^{(2)}_{eff,R}$ is given by the sum of all SFG-active resonant

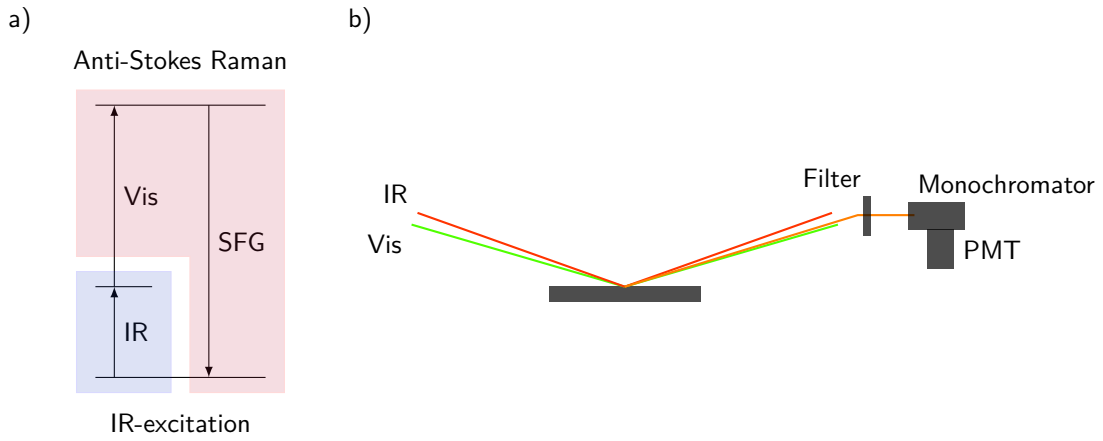

Figure II.10: Scheme of SFG-Spectroscopy. a) Energy diagram of the SFG-process. b) Probing scheme for ps-SFG including a representation of the involved beams.

vibrational modes q of the molecules probed within the SFG-accessible interfacial region. These modes can be represented by Lorentz-oscillators characterized by an amplitude A_q, a resonant frequency ω_q and a damping coefficient Γ_q as

$$\chi^{(2)}_{\text{eff,R}} = \sum_q \frac{A_q}{\omega_{\text{IR}} - \omega_q + i\Gamma_q}, \tag{II.45}$$

whereas i represents the imaginary unit defined as $i^2 = -1$. In their work, Shahir *et al.* chose to fit their experimentally acquired spectra under *ssp*-polarization and *ppp*-polarization using Equations II.44 and II.45 to obtain „quantitative" information. It is, however, a difficult task to retrieve valid data from this kind of Lorentzian peak fitting due to experimental error and the influence of the non-resonant background. Instead of performing the tedious fitting procedure and calculating the Fresnel-coefficients in order to obtain values of the effective second order resonant susceptibilities $\chi^{(2)}_{\text{eff,R}}$ for the studied solutions, a simplified and therefore only semi-quantitative approach based on the following assumptions as approximations was used.

- The Fresnel-coefficients for the studied solutions at the given experimental conditions (influenced by temperature and angles of incidence in the SFG-setup) are constant. All aqueous solutions under investigation were far below critical micellar concentration (cmc).
- As the Fresnel-coefficient for *ssp*-polarization is increased in comparison to studies using *ppp*-polarization, only the experiments using the more sensitive polarization combination are performed. [5]

A quantity proportional to $\chi^{(2)}_{\text{eff,R}}$ can be extracted from Equation II.44 by rearrangement as

$$\tilde{\chi}^{(2)}_{\mathrm{eff,R}} \propto \sqrt{\frac{I_{\mathrm{SFG}}}{I_{\mathrm{VIS}} \cdot I_{\mathrm{IR}}}}. \tag{II.46}$$

The value of $\tilde{\chi}^{(2)}_{\mathrm{eff,R}}$ is calculated for each frequency in an experimentally measured SFG-spectrum. In order to arrive at a comparison of the studied solutions, they are normalized with respect to a reference solution by

$$R = \frac{\left(\tilde{\chi}^{(2)}_{\mathrm{eff,R}}\right)_{\mathrm{sample}}}{\left(\tilde{\chi}^{(2)}_{\mathrm{eff,R}}\right)_{\mathrm{reference}}}. \tag{II.47}$$

Similarly to the acquired SFG-spectra, also the derived values of $\tilde{\chi}^{(2)}_{\mathrm{eff,R}}$ feature a rather strong scatter due to fluctuations in laser intensity and noise of the amplifiers moving from one probed frequency to another. Instead of rectifying this issue by obtaining a smooth curve from the experimental SFG-spectra by Lorentzian fitting, an integration over the frequency range of interest with respect to $\tilde{\chi}^{(2)}_{\mathrm{eff,R}}$ is conducted. This procedure is favored since conventional fitting itself is prone to intrinsic errors and often leads to unphysical values of the parameters, if a good fit is intended.

7.2 Infrared Reflection Absorption Spectroscopy

IRRAS is to be understood as another powerful variant of IR-spectroscopy based on the detection of vibrations upon the excitation of dipoles.[100] In combination with appropriate theoretical models, molecular information in terms of tilt angles can be obtained similar to the results of SFGVS with the benefit of lower experimental complexity. Besides the experimentally rather challenging polarization modulation IRRAS introduced by Blaudez *et al.*,[107] the more straightforward sample shuttle approach is mostly used.[108] A schematic view of the experimental setup is given in Figure II.11.

A spectrometer and a corresponding MCT-detector are at the heart of the IRRAS-setup. In the course of the experiment, the IR-beam passes an IR-filter and several mirrors. A polarizer positioned right behind the first mirror ensures a defined state of either *s*-polarized or *p*-polarized light impinging at the interface of a sample provided in a Langmuir trough. It is to be noted that the point of incidence is at the focal length of the adjoining mirrors. The angle of incidence of the IR-beam is another adjustable parameter in the setup. In order to overcome the major issue of interference from water vapor in proximity to the focal point, a shuttling of the tandem trough is applied. Due to a connection between the individual troughs with movable barriers, the same water level and vapor atmosphere immediately above the interface is ensured. Another small barrier between the troughs avoids mixing of the surfactant-laden interface with the pure reference solvent. A personal computer (PC)-controlled table is used to alternately move either the reference or sampling trough in the beam-line.

The quantity of interest from this kind of experiments is the so-called reflectance-absorbance (RA). It

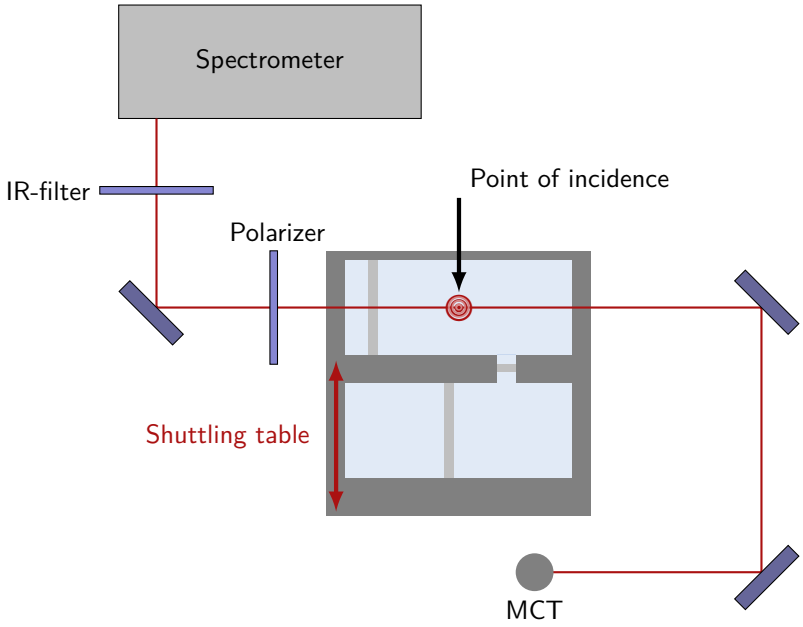

Figure II.11: Schematic view of an IRRAS-setup. The IR-beam is directed from the spectrometer to the mercury cadmium telluride (MCT)-detector via filter, polarizer, several mirrors and the sample. A shuttling table allows measuring the reflectivity from the interfaces of the inter-connected sampling and reference troughs in an alternate fashion.

serves to relate the reflectivity of the film-covered interface R to the reflectivity collected from the pure solvent phase R_0 (typically water for most of the conducted studies) via

$$\mathrm{RA} = -\log_{10}\frac{R}{R_0}. \tag{II.48}$$

For convenience, most of the IRRAS-results are reported in mRA („milli-RA“). This definition implies that a negative RA is associated with a higher reflectivity of the surfactant-laden film in comparison to the pure solvent. Consequently, the presence of an adsorption layer will manifest in several „dips“ in the IRRAS-data within the spectral region corresponding to the vibrational excitation of interfacially adsorbed species, *e.g.*, the alkyl-stretching region. Vice versa, positive values of the RA are indicative for a lower concentration of the respective interfacial species causing the IR-response in the layer compared to the reference.

8 Optomechanical Characterization of Aqueous Interfaces

Excitation and observation of electrocapillary waves (ECWs) is a technique to characterize rheological properties of adsorption layers in a frequency range comparable to that of the oscillating bubble device

(see subsection 9.1), *i.e.*, roughly from 10 to 1000 Hz.[69] Owing to this method, surface rheology has grown to an established probe of interfacial dynamics.[68] A schematic view of the setup used for studying ECWs is shown in Figure II.12.

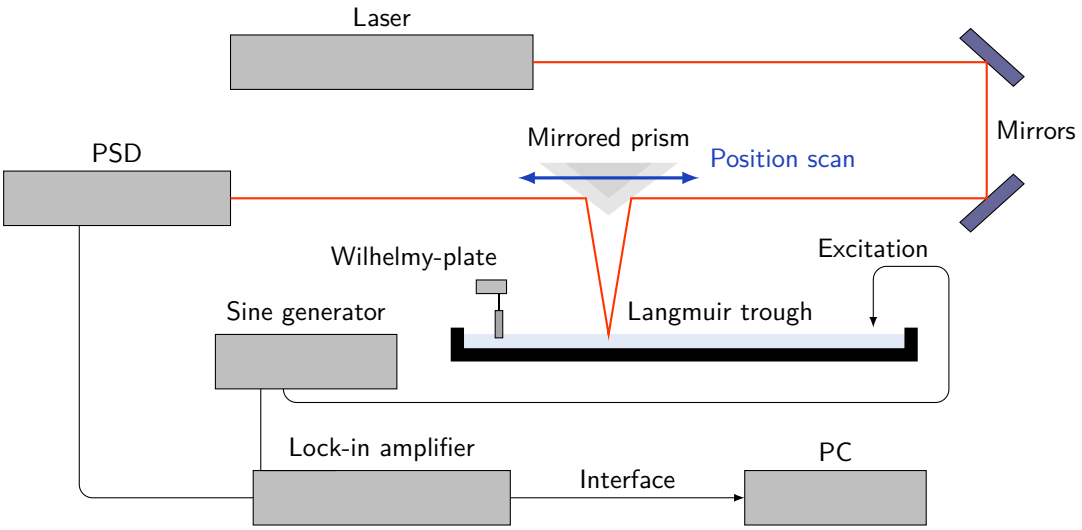

Figure II.12: Schematic experimental setup used for the excitation and observation of ECWs. The sample is contained within a Langmuir-trough equipped with a Wilhelmy-plate for simultaneous measurement of the equilibrium surface tension γ_e. Periodic excitation of the air-water interface is achieved via a razor blade connected to an amplified sine voltage generator. Spatial profiles of the surface waves are monitored and analyzed by an analysis unit comprising a laser, a movable mirrored prism, a PSD and a Lock-in amplifier. The experiment is PC-controlled via an appropriate interface.

The basic principle for the generation of surfaces waves in the utilized ECW device dates back to the work of A. H. Pfund, who proposed a simple device to generate and visualize ripples at liquid surfaces to show analogies to optical waves for lecture-room demonstrations in 1911.[109] The current from a transformer operating at 2000 V and a frequency of 60 Hz passed through a helium vacuum tube and a wire just touching the surface of the liquid. Another wire closing the connection to the transformer penetrated deeply into the liquid.

Ripples are produced at the point, where the wire is about to touch the liquid surface. It is to be noted, that each pulsation of the applied current leads to the formation of a wave spreading rapidly to the edge of the container. As a consequence, the surface appears to be undisturbed under continuous illumination. Due to the illumination generated synchronously with the rate of ripple production by the helium vacuum tube, the arising waves *appear* as standing and are therefore observable. A processed version of the published photograph of the apparently standing wave generated from a round point source is shown in Figure II.13.

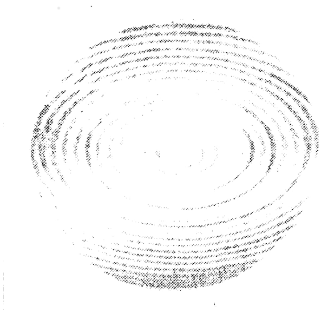

Figure II.13: Surface ripples generated by application of a periodic voltage to a point source observed relying on intermittent illumination synchronous to the wave generation. The photograph has been adapted from the original publication of Pfund.[109]

It is to be noted, that the surface waves generated by this method are not standing waves; using the appropriate observation conditions however, they can be made to *appear as standing waves*, which also is the principle of detection for the spatial profile of capillary waves in the ECW device used.

The mechanical properties of the adsorbed film are accessible by studying the propagation properties of ECWs at the respective interfaces. Dilatational viscosity is directly influenced by molecular interactions in the surface layer as well as molecular relaxation processes such as surface-bulk exchange and reorientation. The complex quantity describing the response of an adsorption layer subject to a deformation is referred to as dilatational viscoelasticity ϵ^*. In the scope of this technique, it is determined from applying the dispersion equation of surface waves generated by the ECW method and given as

$$\epsilon^* = \epsilon + i\omega\kappa \tag{II.49}$$

with dilatational elasticity ϵ, dilatational viscosity κ and the angular frequency ω.

For exciting the ECWs, an alternating current electric field at a frequency ω_0 is applied between an electrode just above the solution and a needle in contact with the aqueous solution (not shown in Figure II.12 for clarity of the scheme). This leads to the generation of an ECW with frequency

$$\omega \overset{!}{=} 2\omega_0 \tag{II.50}$$

due to the difference in dielectric constants between the delimiting water and air bulk phases. A laser beam reflected from the liquid surface is monitored as a function of the distance from the excitation electrode via a PSD. The obtained spatial profiles of the ECW can be expressed formally as an exponentially decaying sine wave with a maximum amplitude A, a wavelength λ, a spatial damping coefficient α and a phase angle ϕ (see Equation III.4).

Next to the dependence of the latter parameters on the nature of the interfacial layer, they are also dependent on the frequency of the applied electric field. The relation between the ECW-frequency ω and excitation frequency ω_0 is due to the observation that the dielectric ponderomotive deformation u_z is proportional to the square of the applied field E. The oscillation is induced due to a difference of the dielectric constants between both sides of the interface and can be described by

$$u_z \propto E^2(\omega_0) \propto (\cos \omega_0)^2 \propto \cos 2\omega_0 \propto \cos \omega. \tag{II.51}$$

From a comparison of the arguments in the cosine-terms in the latter relation, it is obvious that the excited ECW has a frequency twice as high as the applied field according to Equation II.50. The relation between the cosines of different frequencies is based on the trigonometric identity

$$\cos^2 x = 0.5 + 0.5 \cos(2x). \tag{II.52}$$

Once the characteristic parameters of the excited ECW are known, the complex surface dilatational modulus is evaluated by solution of the dispersion equation of the excited ECW. For a quantitative evaluation, the following quantities have to be known under the experimental conditions of interest: density of water ρ, viscosity of water η, complex wave vector

$$q = \frac{2\pi}{\lambda} - i\alpha \tag{II.53}$$

and the reciprocal penetration depth of the surface velocity field μ, which is related to other system parameters by

$$\mu^2 = k^2 + i\frac{\omega\rho}{\eta}. \tag{II.54}$$

The quantity i in the latter equations represents the imaginary unit with $i^2 = -1$. In the theoretical treatment of surface waves it is to be noted that liquid interfaces are continuously perturbed by random thermal fluctuations considered as dynamic roughness.[110] As the surface deformation caused by thermal excitation is not efficient to produce scattering of light at low values of the wave vector q ($q < 100\,\mathrm{cm}^{-1}$, $\lambda > 1\,\mathrm{mm}$), an external excitation of larger amplitude has to be applied in order to arrive at reasonably large displacements for measurements at low wave vectors q. Typically, the magnitude of these deformations is on the order of 1 µm. Due to its non-invasive nature, the ECW-method is highly appreciated. In the limiting case, the fluid interface is treated as a viscoelastic continuum medium with a characteristic experimental wavelength

$$\lambda = \frac{2\pi}{q}, \tag{II.55}$$

which is large compared to the molecular dimensions. The hydrodynamic motion within a film can be decomposed into several contributions: Capillary waves (= out of plane deformation), longitudinal waves (= in plane deformation) and further decoupled modes such as splay or bending.

The out of plane capillary mode produces strong fluctuations in the dielectric constant at the surface and is therefore responsible for the light scattered by the surface of a liquid. It can be interpreted as a shear mode determined by the counteracting forces of gravity and surface tension. The longitudinal mode is further decomposable into a compression and a shear motion quantified by the two corresponding elastic moduli. Dissipative effects within the film are not assumed. The Navier-Stokes-equation at the air-water interface takes into account a coupling between dilatational and capillary motions, which is at the heart of applicability of ECW for the study of dilatational characteristics. Due to this coupling, dilatational properties can be inferred using capillary wave devices.

As the common concept of rheological experiments, the appearance of a stress in response to an applied strain is measured.[68] The proportionality constant is a material function bearing information on both dilatational and shear components, whereas in fluid systems the shear component is negligible.[49]

In surface wave experiments, the propagation of small-amplitude surface waves excited by thermal agitation or an external drive (electrical or mechanical) are studied. The intrinsic drawback of this class of methods is the requirement of a mathematical model and the indirect determination of the response functions. Surface hydrodynamics is required to obtain the viscoelastic parameters from the dispersion curve of the surface modes. Displacement of the fluid interface can be conceived as a surface motion driven by an external force and can be restored through the viscoelastic response of the adjacent phases and the interface.

In case of random motion, the interfacial shape can be built up as a Fourier-series of independent waves propagating in the xy-surface plane. Also slight penetration into the bulk phase is possible. The equilibrium position of the interface is chosen to be at $z = 0$. A wave is characterized by its complex wave vector q. The relation between the wave vector q and the frequency ω is referred to as dispersion relation. There are also a forces counteracting the appearance of surface ripples. Any curvature of the interface causes a surface tension-governed Laplace stress which tends to restore the planar equilibrium shape of the interface. Therefore, surface tension γ is the main restoring force for surface transverse motions. The same holds for the effect of gravity favoring plain interfaces.

The longitudinal restoring force f_x is proportional to the dilatational modulus $\tilde{\epsilon}$ through

$$f_x = \tilde{\epsilon}(\omega)\frac{\partial^2 u_x}{\partial x^2}, \tag{II.56}$$

where u_x is the displacement of the surface along the x-direction within the surface plain. Accounting for the boundary conditions in the description of surface motion, a solution of the hydrodynamic equations for oscillatory motion leads to the dispersion equation. The transversal (= perpendicular) and longitudinal (= parallel) deformations are governed by different effects. Whereas the transversal

component depends only on surface tension, the main influencing factor for the longitudinal part is related to the dilatational modulus. The extent of coupling between transversal and longitudinal displacement is determined by the type of interfaces in the considered system and assumes a maximum at the air-water interface due to the so called kinematic asymmetry of these bulk phases.

In case of viscoelastic films at the air-liquid interface, the dispersion relations of transversal $T(\gamma)$ and longitudinal $L(\epsilon)$ deformation are given by

$$L(\tilde{\epsilon}; q, \omega) = \tilde{\epsilon}(\omega)q^2 + i\omega\eta(q + m) \qquad \text{and} \tag{II.57}$$

$$T(\gamma; q, \omega) = \gamma q^2 + i\omega\eta(q + m) - \omega^2\rho/q, \tag{II.58}$$

respectively. Due to this coupling between transversal and longitudinal modes at the free surface of a liquid, dilatational parameters are accessible from the analysis of the propagation characteristics of capillary waves probed by transverse wave devices. For the limiting case of bare interfaces characterized by $\epsilon = \kappa = 0$, well-known solutions can be obtained: Kelvin's law for the frequency of the capillary waves and Stoke's law for damping due to viscous friction.

9 Mechanical Characterization of Aqueous Interfaces

Next to the characterization of aqueous interfaces relying on non-invasive perturbation, there are several methods at hand, where a mechanical deformation is introduced via direct contact of the sample and the measurement device. The following section briefly describes the principles of the custom-built oscillating bubble device and further equipment used for the determination of foam column and lamella stabilities.

9.1 Oscillating Bubble

Devices operating on the principle of the oscillating bubble technique can be used to measure surface dilatational properties of aqueous surfactant, protein or polymer solutions and their mixtures.[111] Thereby, the bulk volume phase is considered to be an incompressible three-dimensional fluid. Its influence and all hydrodynamic contributions are eliminated by means of calibration measurements. The surface is assumed to be a two-dimensional compressible phase of finite extension and variable composition.[112] The flowing properties of adsorption layers present at these interfaces are assumed to be decisive for the stability of emulsions and foams.[41,113–115] Dilatational properties can be subdivided into the effects of dilatational elasticity and dilatational viscosity. In conjunction with knowledge on the typically negligible surface shear properties and transport effects, *i.e.,* adsorption kinetics

at the liquid-vapor interface and the liquid-liquid interface, compressible adsorption layers can be characterized extensively. It is to be noted that for radially oscillating hemispherical bubbles an almost purely dilatational deformation is carried out and other types of deformation are vastly absent. [116]

A schematic view of the setup used for the periodic perturbation of a hemispherical air bubble and the observation of its response behavior is given in Figure II.14.

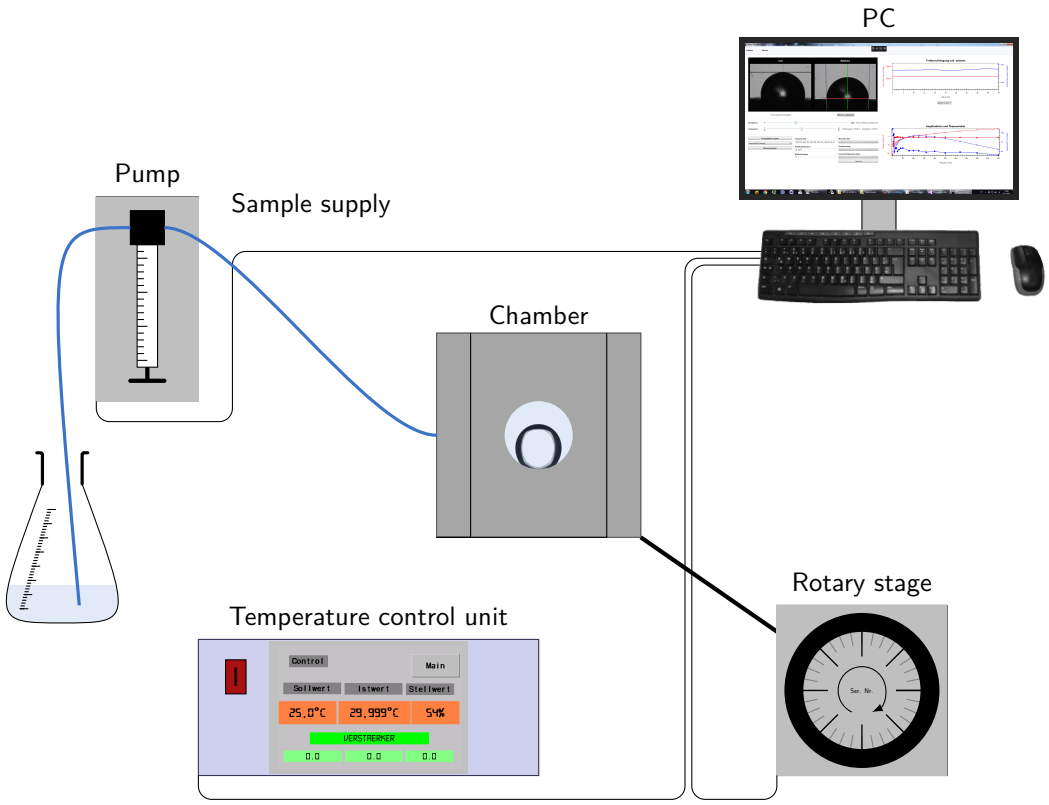

Figure II.14: Scheme of the oscillating bubble device. The bubble is formed inside the stainless steel chamber at the tip of a glass capillary by concerted action of a syringe pump and a rotary stage. A PC controls the experiment and processes the collected data. The temperature is regulated by a custom-built control unit based on Peltier-elements.

The theoretical treatment of this experiment is based on the description of oscillatory flow of viscoelastic fluids in circular tubes such as the used capillaries. The measured pressure difference across the crossed bubble interface is associated with changes in radius r and surface tension γ. Measurements are carried out as a function of applied perturbation frequency ω. The amplitude of the oscillation is considered as a parameter, which can be varied in series experiments. Definition of the surface dilatational modulus E as the ratio between a change in surface pressure $\Delta\pi$ and the *relative* change in surface area $\Delta A/A \approx \Delta \ln A$ serves to relate the experimentally accessible properties via [117]

$$E = -A\frac{\Delta\pi}{\Delta A} \qquad \text{with} \qquad \pi = \gamma_0 - \gamma \tag{II.59}$$

$$= \frac{\Delta\gamma}{\Delta \ln A}. \tag{II.60}$$

It is a measure for the system response to exerted harmonic perturbations. Typically, periodic disturbances in the linear regime, *i.e.*, relative changes of surface area below 10 %, are applied. The surface dilatational modulus E is a complex quantity. This property of the modulus is apparent from its equivalent definition as

$$E = E_0 \exp^{i\phi}, \tag{II.61}$$

whereas it is described in terms of an amplitude E_0 and a phase angle ϕ between surface area perturbation and resulting pressure response. From an analysis of the frequency dependent surface dilatational modulus E, information on elastic, viscous and transport properties can be obtained.

Relative surface area perturbations $\Delta A/A$ induced at a defined amplitude and frequency will cause changes in adsorption layer density, which will in turn lead to harmonic changes of pressure p across the interface. Oscillations around a hemispherical reference state of the bubble are found to be ideal for the assessment of changes in surface tension $\Delta\gamma$ due to the maximum pressure occurring at this geometry. So called maximum bubble pressure methods[118,119] are based on this observation. The resulting pressure is affected by both a change in radius Δr and a change in surface tension $\Delta\gamma$ of the bubble. Dilatational properties are affected only by changes in surface tension and lead to pressure signals proportional to $\Delta\gamma$, given that oscillations are carried out close to the half-sphere geometry of the bubble. This is obvious from the relation describing the change in pressure across the interface according to[111]

$$\Delta p = \frac{2\Delta\gamma}{R_\mathrm{K}} \tag{II.62}$$

for oscillations around the hemispherical reference state with radius r_0, the pressure difference Δp can be related to the capillary radius R_K.

At higher frequencies, effects of inertia have to be taken into account.[120,121] Their influence is referred to as the reason for the limitation of oscillation bubble devices to a relatively low frequency range, especially for the case of studies at liquid-liquid interfaces.[122–126] In order to determine surface dilatational and transport properties, the macroscopically observable dynamic surface tension has to be considered. It is closely related to the adsorbed amount of surfactant and the respective adsorption kinetics. Surface tension is interpreted as a function of the surface excess concentration Γ_i

of component i. In a formal way, the change in surface tension as a function of surface concentration is given by

$$\Delta\gamma = \Delta\gamma(\Gamma_i) = \sum_i \frac{\partial\gamma}{\partial\Gamma_i}\Delta\Gamma_i = \sum_i \frac{\partial\gamma}{\partial\Gamma_i}\left(\frac{\Delta N_i}{A} + \Gamma_i\frac{\Delta A}{A}\right), \tag{II.63}$$

whereas N_i represents the number of molecules of the i-th component. The corresponding change in number of molecules present at the surface is given by Fick's first law acting both as a boundary condition and definition of the flux $j(t)$, which is given as

$$j(t) = D\cdot\frac{\partial c_i}{\partial r} = \frac{1}{A}\frac{\mathrm{d}\,N_i}{\mathrm{d}\,t} = \frac{1}{A}\frac{\mathrm{d}\,\Gamma_i(t)A(t)}{\mathrm{d}\,t}. \tag{II.64}$$

At spherical surfaces, the flux has only a radial component r, as surface tension is laterally homogeneous within the surface. Solving the diffusion equation

$$\frac{\partial c_i}{\partial t} = D\frac{\partial^2 c_i}{\partial x^2} \tag{II.65}$$

yields an expression for the time and space dependent concentration $c_i(x,t)$ of component i. A relation between the change in surface tension $\Delta\gamma$ and relative change of surface area $\Delta A/A$ is given by the Lucassen-van den Tempel (LvdT)-model according to[86]

$$\Delta\gamma = \epsilon_0\frac{1+\xi+i\xi}{1+2\xi+2\xi^2}\left|\frac{\Delta A}{A}\right|\exp^{i\omega t}, \tag{II.66}$$

whereas ω and t denote perturbation frequency and time respectively. The parameters ϵ_0 and ξ will be addressed in the following. The LvdT-relation serves as a model to describe the surface dilatational modulus E at lower frequencies and surfactant concentrations. In this model, an instantaneous equilibrium between surfactant monolayer and a subsurface layer is assumed. The value of dynamic surface γ tension is taken to be exclusively dependent on the current surface concentration Γ. The magnitude of the complex surface dilatational modulus E is given by

$$|E| = \frac{\epsilon_0}{\sqrt{1+2\xi+2\xi^2}} \qquad \text{with} \qquad \epsilon_0 = -\frac{\partial\gamma}{\partial\ln\Gamma} = -\Gamma\frac{\partial\gamma}{\partial\Gamma}, \tag{II.67}$$

whereas ϵ_0 denotes the Gibbs-elasticity and ξ represents an isotherm parameter. The Gibbs-elasticity ϵ_0 is defined via fitting parameters obtained from the equilibrium surface tension isotherm of the respective surfactant. This implies that equilibrium parameters have to be known in order to determine dynamic properties of an adsorption layer. The molecular exchange parameter ξ is associated to isotherm parameters via the derivative of the subsurface concentration c_s with respect to the surface concentration $\mathrm{d}\,c_s/\mathrm{d}\,\Gamma$, applied frequency of perturbation ω and the diffusion coefficient D by

$$\xi = \sqrt{\frac{D}{2\omega}} \frac{\mathrm{d}\, c_s}{\mathrm{d}\, \Gamma}. \tag{II.68}$$

The differential in this relation is defined by an appropriate adsorption isotherm and a surface equation of state (SEOS), *i.e.,* a relation between surface tension γ and surface concentration Γ. The value of the surface dilatational modulus E as obtained from fitting model adsorption isotherms to the corresponding experimentally measured values tend to differ at high frequencies. [127]

The isotherm parameter ξ is inversely proportional to the square root of the applied perturbation frequency and proportional to the exchange of surfactant. This is represented by the square root of the diffusion coefficient D. Furthermore, ξ is related to the change in surfactant concentration inside the subsurface with surface concentration. Both of the latter parameters depend on derivatives and model constants obtained from fitting an adsorption isotherm. In general, higher derivatives are more susceptible to errors than the actual fit function. [112]

Assuming that the dynamic surface tension is dependent not only on the surface concentration of surfactants, but also an additional arbitrarily defined variable M, the change in surface tension can be written formally as

$$\Delta\gamma = \frac{\partial\gamma}{\partial\Gamma}\Delta\Gamma + \frac{\partial\gamma}{\partial M}\Delta M. \tag{II.69}$$

Therein, the partial derivatives represent material constants and the associated Δ-terms are referred to as working coordinates of the respective variable. In analogy to the definition of viscous effects, an intrinsic surface dilatational viscosity κ is defined to be the partial derivative associated to the variable of relative temporal change (denoted by a dot) of surface area, *i.e.,* the rate of change of relative surface area. Taking into account the dependence of surface tension on both the surface concentration Γ and relative temporal change of surface area, the change of surface tension can be expressed as

$$\Delta\gamma\left(\Gamma, \frac{\Delta\dot{A}}{A}\right) = \frac{\partial\gamma}{\partial\Gamma}\left(\frac{\Delta N}{A} + \Gamma\frac{\Delta A}{A}\right) + \frac{\partial\gamma}{\partial\frac{\Delta\dot{A}}{A}}\frac{\Delta\dot{A}}{A} \qquad \text{with} \qquad \kappa = \frac{\partial\gamma}{\partial\frac{\Delta\dot{A}}{A}} \tag{II.70}$$

$$= \frac{\partial\gamma}{\partial\Gamma}\left(\frac{\Delta N}{A} + \Gamma\frac{\Delta A}{A}\right) + \kappa\frac{\Delta\dot{A}}{A}. \tag{II.71}$$

Using the latter equation instead of Equation II.63, the change in surface tension and surface area are related by

$$\Delta\gamma = \left(\epsilon_0 \frac{1 + \xi + i\xi}{1 + 2\xi + 2\xi^2} + i\omega\kappa\right)\left|\frac{\Delta A}{A}\right| \exp^{i\omega t}. \tag{II.72}$$

Therein, also the contribution of an intrinsic surface dilatational viscosity κ in surface dilatational processes is accounted for. It leads to very pronounced effects in case of polymer solutions. Fruhner *et al.* used a sample of clean water without the presence of an adsorption layer as a reference system.[111] The complex frequency dependent surface dilatational modulus

$$E(\omega, c) = \frac{\epsilon_0}{\sqrt{1 + 2\xi + 2\xi^2}} \cdot \left(1 + \xi + i\left(\xi + \frac{\omega\kappa}{\epsilon_0}(1 + 2\xi + 2\xi^2)\right)\right) \tag{II.73}$$

could be obtained from measured pressure amplitude, relative change of surface area and phase shift between the latter quantities. For $\kappa = 0$, the expression simplifies to the classical Lucassen-van den Tempel elasticity modulus $E(\omega, c)$.[128,129] It serves as a theoretical model in case of diffusion controlled exchange between bulk and subsurface layer. The term of diffusion control refers to the fact that diffusion is the slowest and therefore rate determining step in the overall process of adsorption. Kinetically occurring processes are in equilibrium with respect to diffusional transport of surfactants towards the surface. This corresponds to an instantaneous establishment of equilibrium between subsurface layer and surfactant monolayer.

The influence of diffusional exchange is determined by the adsorption isotherm via its influence on the isotherm parameter ξ. This is the only occasion, in which the adsorption isotherm appears in the formalism. For small values of this parameter, the effect of diffusion can be neglected and the effective elasticity asymptotically approaches towards the Gibbs-elasticity ϵ_0. This so called insoluble surfactant behavior is apparent for ordinary small molecular surfactants at high frequencies. The higher the surface activity of the respective surfactant, the lower is the frequency at which insoluble characteristics can be observed. For frequencies approaching zero, the elasticity is controlled purely by diffusion. Upon increasing the isotherm parameter ξ, the effective elasticity deviates stronger from the value of Gibbs-elasticity ϵ_0. This is accounted for in a more extended version of the theory presented by Wantke, where also an intrinsic surface dilatational viscosity κ has been incorporated as given in Equation II.73.[130]

9.2 Analysis of Foam Column Stability

Foaming is known to depend on many parameters and therefore challenges associated with foam property characterization (such as foaming stability vs. foaming ability, *i.e.,* foamability) are faced. To allow for a standardized comparison of foam characteristics, several methods have been proposed. An established method for the estimation of foamability is the Ross-Miles test, where a surfactant solution falls onto the same mixture from a defined height.[131,132] As a result of the turbulence in this mixing process, a foam is formed and its height in the cylindrical column is measured as a function of time. Several devices utilize this working principle in air bubbling[133] or foam column stability[134] devices. A foam column is generated by passing a gas through a porous frit at the bottom of a cylindrical foam column. Typically, the height of the foam column and the drained liquid volume is

monitored during the course of foam decay. These kinds of devices have been used in the study of both classical surfactant and protein solutions. Lunkenheimer *et al.* introduced several characteristic parameters derived from the temporal dependence of foam height such as the R5-value [135] specifying the relative foam height remaining five minutes after foam generation has ceased or the times of deviation and transition from simultaneously measuring foam and drained liquid volume. [136] A further frequently studied property of single foam lamellae is the disjoining pressure upon thinning. [37,137] In practice, there are several difficulties associated with the nonuniform decay of the foam column, thinning behavior of the foams and reduced reproducibility of the experiments. One attempt to tackle this issue is the use of enhanced image processing routines allowing for an analysis of foam texture, pore size and pore size distribution from additional evaluation of drainage rates. [134]

A schematic view of a foam column stability device is given in Figure II.15

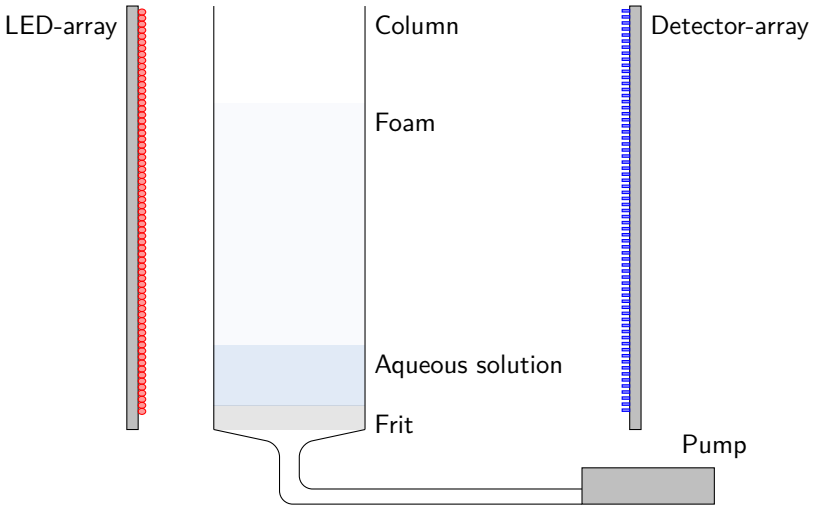

Figure II.15: Scheme of a foam column stability analyzer. The sample solution is placed in a glass column having a porous frit at its bottom. A foam column is formed by passing a defined volume of ambient air at a specified flow rate through the sample from below. The height of the foam column and remaining sample liquid are determined from opposing LED- and detector-arrays.

9.3 Analysis of Foam Lamella Stability

Another approach for the quantitative estimation of foam stability is to reduce the complexity of studied foam columns (see subsection 9.2) to a single foam lamella formed in a rectangular frame. The information gained on foamability from this experiment is limited to whether or not a lamella is formed. Data on stability is obtained from measuring the time until rupture of this foam lamella by visual observation. This simplistic device has been used in a number of studies on cationic, anionic and non-ionic model surfactants for correlating a parameter of foam stability to surface rheological

or other characteristics.[120,138–140] For this purpose, an improved and fully automated version of the latter method along with a statistical analysis of the experiments has been set up.

An individual foam lamella is formed at a glass frame attached to the bottom of a sample cell by its rotation around 90° according to the sketch in Figure II.16. The presence of the lamella is detected by a non-zero intensity of visible light reflected from the surface of the lamella as detected by a photo-diode. Control of the overall experiment is system-internally enabled by an universal serial bus (USB)-device. An overview of the overall experimental setup is given in Figure II.17.

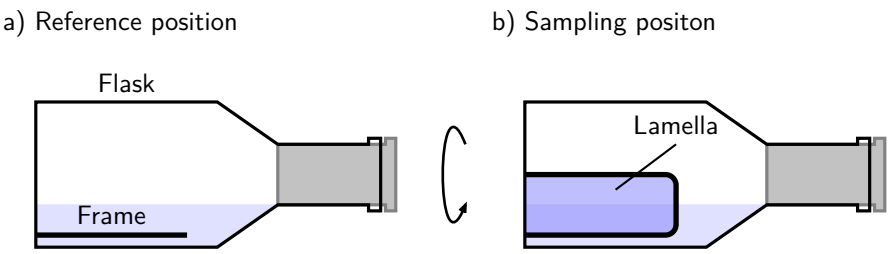

Figure II.16: Glass frame mounted in a rotatable flask for the determination of foam lamella stability in its a) reference position and b) sampling position.

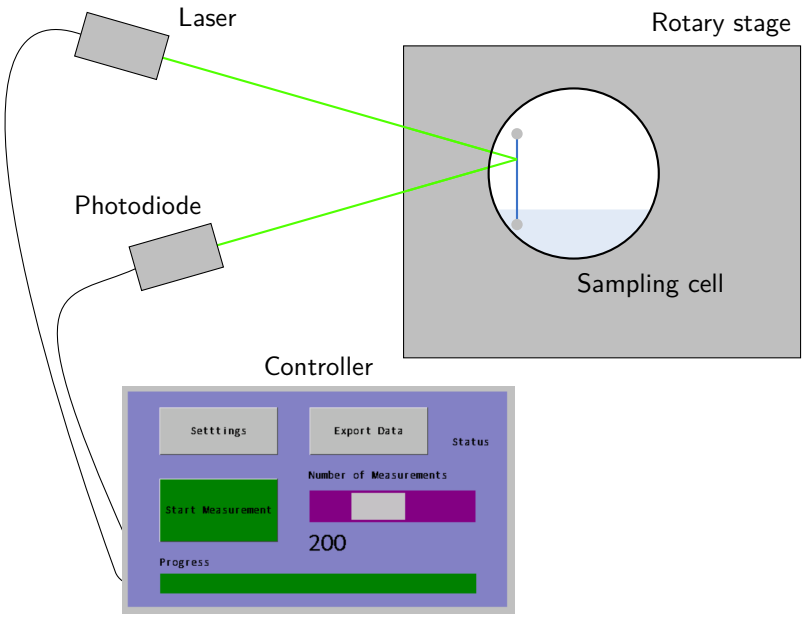

Figure II.17: Scheme of the experimental setup comprising the rotatable sample cell, lasing and detection unit, a PC for operating the rotary stage, and a monitor for on line visualization of the sampled lifetimes.

Foam lamella lifetimes are obtained from the difference of two timers started upon reaching the

reference position. The first timer captures the dead time t_d between lamella formation and reaching the sampling position. The second timer t' is stopped as soon as the intensity detected by the photo-diode is below a threshold indicating the rupture event. The dead time corrected lifetimes $t = t' - t_d$ are used for further evaluation. This procedure is repeated for a specified number of cycles.

Typically, lifetime measurements of several tens to hundreds individual lamellae are carried out and the raw data show a broad scatter.[2] Therefore, they are re-plotted in terms of lifetime probability p_i within a time t_i. It is defined as

$$p_i = 1 - \frac{N_i(t \leq t_i)}{N_{tot}}, \tag{II.74}$$

whereas N_{tot} represents the total number of studied lamellae and N_i is the number of individual lamellae having a lifetime below a chosen time t_i. A related measure is the probability of rupture, which is given by the fractional term in the latter expression. The lifetime probabilities according to this relation can be calculated for each time up to the maximum individual lifetime in the repeated experiments.

The single foam lamella device is to be understood as an alternative or complementary method for characterization of foam stability parameters based on a statistical approach. However, the *absolute* values of lamella lifetimes should not be over-interpreted and are rather to be considered as an apparatus function.[141] Comparison of the relative values of foam column and lamella stability have been found to show good agreement.

10 Bulk Characterization of Samples

The aqueous solutions studied within this thesis have also been subject to several experiments targeting at their bulk properties. Next to quantitative studies of dielectric characteristics using dielectric relaxation spectroscopy (DRS), density, viscosity and electrical conductivity, the aggregation and interaction behavior was evaluated based on isothermal titration calorimetry (ITC) and dynamic light scattering (DLS).

10.1 Dielectric Relaxation Spectroscopy

DRS serves as a highly valuable tool for the analysis of dynamics of both homogeneous and multi-component liquid systems.[142] Its key feature is the high sensitivity with respect to changes within the cooperative dynamics of hydrogen bonding networks, which is hardly accessible with other methods.

Electromagnetic phenomena can in principle be calculated relying on the Maxwell-equations relating the magnetic flux density $\vec{B}$ and the dielectric displacement $\vec{D}$. In order to simplify, only homogeneous, non-dispersive, isotropic materials at low fields in the linear regime are considered and a set of

conservation equations given by

$$\vec{D} = \epsilon\epsilon_0\vec{E}, \tag{II.75}$$

$$\vec{j} = \kappa\vec{E} \qquad \text{and} \tag{II.76}$$

$$\vec{B} = \mu\mu_0\vec{H} \tag{II.77}$$

is introduced. Therein, $\vec{D}$ and $\vec{H}$ fields are related to $\vec{E}$ and $\vec{B}$ by time- and field-strength-independent scalars, *i.e.,* they are to be considered as material constants. The remaining parameters denote the relative electrical permittivity ϵ, relative magnetic permeability μ, absolute magnetic permeability of free space μ_0 and absolute electrical permittivity of vacuum ϵ_0. These constitutive equations are valid only for the special case of time-independent field response. In case of an electric field $\vec{E}$ oscillating with an amplitude $\vec{E}_0$ and an angular frequency ω, the electric field $\vec{E}$ is described by

$$\vec{E} = \vec{E}_0 \cos(\omega t). \tag{II.78}$$

In DRS, frequencies ranging from the MHz to the GHz-regime are typically applied in order to investigate dynamics in condensed systems. Upon increasing the experimental frequency, a significant phase delay between the electric field $\vec{E}$ and the dielectric displacement $\vec{D}$ characterized by means of a loss angle δ becomes apparent. The amplitude of the corresponding dielectric displacement $\vec{D}$ is given by

$$\vec{D}(t) = \vec{D}_0 \cos(\omega t - \delta(\omega)). \tag{II.79}$$

Making use of the addition theorems, this phase-shifted response can be rewritten as

$$\vec{D}(t) = \vec{D}_0 \cos(\delta)\cos(\omega t) + \vec{D}_0 \sin(\delta)\sin(\omega t), \tag{II.80}$$

whereas the loss angle δ has to be specified by the frequency dependent loss angle $\delta(\omega)$, to be more precise. From this equation, the storage and loss modulus are defined as the in and out of phase components of the relation specified in Equation II.75 via

$$\vec{D}_0 \cos(\delta(\omega)) = \epsilon'(\omega)\epsilon_0\vec{E}_0 \tag{II.81}$$

$$\vec{D}_0 \sin(\delta(\omega)) = \epsilon''(\omega)\epsilon_0\vec{E}_0. \tag{II.82}$$

This allows expressing the dielectric displacement $\vec{D}$ given in Equation II.80 as

$$\vec{D}(t) = \epsilon'(\omega)\epsilon_0\vec{E}_0\cos(\omega t) + \epsilon''(\omega)\epsilon_0\vec{E}_0\sin(\omega t). \tag{II.83}$$

The phase shift can be expressed in terms of the tangent of the completely out of phase loss modulus and the completely in phase storage modulus as

$$\tan(\delta(\omega)) = \frac{\epsilon''(\omega)}{\epsilon'(\omega)}. \tag{II.84}$$

Accordingly, the relation between the electric field $\vec{E}$ and dielectric displacement $\vec{D}$ can be expressed as a real and an imaginary part rather than by a phase shift and amplitude. The complex permittivity $\hat{\epsilon}(\omega)$ is given by

$$\hat{\epsilon}(\omega) = \epsilon'(\omega) + i\epsilon''(\omega), \tag{II.85}$$

whereas the real part describes the dispersive in phase part of the electric displacement field and the imaginary part represents the dissipative out of phase contribution. For a simplified mathematical treatment, complex field vectors describing electric field $\vec{E}$ and dielectric displacement $\vec{D}$ are introduced by

$$\hat{\vec{E}}(t) = \vec{E}_0\exp^{i\omega t} \qquad \text{and} \tag{II.86}$$

$$\hat{\vec{D}}(t) = \vec{D}_0\exp^{i(\omega t-\delta)}. \tag{II.87}$$

$$\tag{II.88}$$

These definitions allow describing the constitutive equations also for the non-static case if the corresponding complex quantities are used. They are able to describe the frequency-dependent linear dielectric response of dissipative systems by

$$\hat{\vec{D}}(t) = \hat{\epsilon}(\omega)\epsilon_0\hat{\vec{E}}(t), \tag{II.89}$$

$$\hat{\vec{j}}(t) = \hat{\kappa}(\omega)\hat{\vec{E}}(t) \qquad \text{and} \tag{II.90}$$

$$\hat{\vec{B}}(t) = \hat{\mu}(\omega)\mu_0\hat{\vec{H}}(t) \tag{II.91}$$

with definition of complex conductivity $\hat{\kappa}(\omega)$ and complex relative magnetic permeability $\hat{\mu}(\omega)$. Making use of the latter expressions, the Maxwell-equations can be rewritten to arrive at the reduced form of the wave equation of the magnetic field

$$\Delta\vec{H}_0 + \hat{k}^2\vec{H}_0 = 0 \tag{II.92}$$

with the propagation constant being given as

$$\hat{k}^2 = k_0^2\left(\hat{\nu}(\omega)\hat{\epsilon}(\omega) + \frac{\hat{\nu}(\omega)\hat{\kappa}(\omega)}{i\omega\epsilon_0}\right). \tag{II.93}$$

The propagation constant of a wave in vacuum is defined as

$$k_0 = \omega\sqrt{\epsilon_0\nu_0} = \frac{2\pi}{\lambda_0} \qquad \text{with} \qquad c_0 = \frac{1}{\sqrt{\epsilon_0\nu_0}}. \tag{II.94}$$

In case of a source-free medium, division by the electric field vector $\vec{E}$ leads to the reduced wave equation

$$\Delta\vec{E}_0 + \hat{k}^2\vec{E}_0 = 0. \tag{II.95}$$

Even further simplification is achieved for non-magnetizable substances characterized by $\hat{\nu} = 1$, which leads to

$$\hat{k}^2 = k_0^2\left(\hat{\epsilon}(\omega) + \frac{\hat{\kappa}(\omega)}{i\omega\epsilon_0}\right) = k_0^2\hat{\eta}(\omega) \tag{II.96}$$

with definition of the generalized complex permittivity $\hat{\eta}(\omega) = \eta' - i\eta''$. It is to be noted, that the individual parts contain mixed contributions from the complex permittivity $\hat{\epsilon}(\omega)$ and the complex conductivity $\hat{\kappa}(\omega)$

$$\eta'(\omega) = \epsilon'(\omega) - \frac{\kappa''(\omega)}{\omega\epsilon_0} \qquad \text{and} \qquad \eta''(\omega) = \epsilon''(\omega) + \frac{\kappa'(\omega)}{\omega\epsilon_0}. \tag{II.97}$$

This implies, that in principle dielectric and conductivity properties of a system cannot be measured separately or independently of one another. Usually, the dispersion, *i.e.*, the frequency-dependence of the complex conductivity $\hat{\kappa}(\omega)$ can be neglected.[143] This holds true especially for low electrolyte concentrations, which leads to the fairly reasonable assumptions of neglecting the imaginary part of the complex conductivity $\hat{\kappa}(\omega)$, *i.e.*,

$$\kappa'(\omega) = \kappa \qquad \text{and} \qquad \kappa''(\omega) = 0. \tag{II.98}$$

Finally, the complex permittivity $\hat{\epsilon}(\omega)$ is calculated from the measured generalized complex permittivity $\hat{\eta}(\omega)$ and the measurable conductivity by

$$\epsilon'(\omega) = \eta'(\omega) \qquad \text{and} \qquad \epsilon''(\omega) = \eta''(\omega) - \frac{\kappa}{\omega\epsilon_0}. \tag{II.99}$$

The dielectric displacement $\vec{D}$ can be split into two contributions according to

$$\hat{\vec{D}} = \hat{\epsilon}\epsilon_0\hat{\vec{E}} \tag{II.100}$$

$$= \epsilon_0\hat{\vec{E}} + \hat{\vec{P}} \qquad \text{with} \qquad \hat{\vec{P}} = (\hat{\epsilon} - 1)\epsilon_0\hat{\vec{E}} \tag{II.101}$$

by introducing the polarization $\hat{\vec{P}}$ according to the latter equation. It serves to describe the effect of an electric field $\vec{E}$ on a medium. The macroscopic definition of the polarization $\hat{\vec{P}}$ can be rewritten in terms of microscopic quantities as the sum of the orientational and induced polarizations $\hat{\vec{P}}_\mu$ and $\hat{\vec{P}}_\alpha$, respectively [144]

$$\hat{\vec{P}} = \hat{\vec{P}}_\mu + \hat{\vec{P}}_\alpha. \tag{II.102}$$

Whereas the orientational polarization describes the reorientation of molecular dipoles with a dipole moment $\vec{\mu}_k$ and number density ρ_k when an external field is applied, the molecular polarization arises due to a polarizability caused by an inner field leading to the formation of induced dipole moments. The characteristic timescale of the processes covers the ns to ps-range corresponding to microwave frequencies. Based on these matching timescales of perturbation and relaxation processes, the key concept of DRS is the measurement of the frequency dependent complex permittivity $\hat{\epsilon}(\omega)$ to get insight in liquid dynamics. It is to be noted that the value of $\hat{\vec{P}}_\alpha$ bears information on intra-molecular dynamics of the system and is *not* observable in the microwave range. These contributions can be separated by the introduction of an infinite frequency permittivity ϵ_∞.

Various equations have been put forward to describe relaxation phenomena. The practical procedure for the description of spectra in terms of a sum of several relaxation modes is described in more detail in subsection 11.2. The background for modeling of relaxation in the Debye-formalism is based on the simple idea that the decrease of dielectric polarization in the absence of an outer electric field is proportional to the polarization itself, *i.e.,* a first order law is assumed [145]

$$\frac{\partial}{\partial t}\vec{P}_\mu(t) = -\frac{1}{\tau}\vec{P}_\mu(t). \tag{II.103}$$

Introducing the relaxation time τ as a constant, the differential equation is solved by

$$\vec{P}_\mu(t) = \vec{P}_\mu(0)\exp\left(\frac{-t}{\tau}\right). \tag{II.104}$$

Making use of the concept of step and pulse response functions, finally the Debye-equation can be written as a complex permittivity $\hat{\epsilon}(\omega)$ with

$$\hat{\epsilon}(\omega) = \epsilon_\infty + \frac{\epsilon - \epsilon_\infty}{1 + i\omega\tau}. \tag{II.105}$$

Depending on the actual shape of a relaxation mode in a spectrum, the latter expression is modified by additional peak shape parameters α and β to achieve a higher quality in the description of experimental spectra. The most general description is given by the expression

$$\hat{\epsilon}(\omega) = \epsilon_\infty + \frac{\epsilon - \epsilon_\infty}{(1 + (i\omega\tau)^{1-\alpha})^\beta}, \tag{II.106}$$

which simplifies to the previously described Debye-equation for $\alpha = 0$ and $\beta = 1$. For $\alpha \in [0, 1]$ and $\beta = 1$ the relaxation is referred to as Cole-Cole relaxation. It describes a flatter dispersion curve and broadened absorption. Peaks of the Cole-Davidson-type are characterized by asymmetric time relaxation distribution with $\alpha = 0$ and $\beta \in [0..1]$. Both asymmetric dispersion and absorption curves are obtained from the most general Havriliak-Negami-type peaks, where both peak-shape parameters are allowed to vary from 0 to 1.

A relation between the amplitude of a relaxation peak and its concentration is established by the Cavell-equation.[146] The dispersion amplitude $S_j = \epsilon_j - \epsilon_{j+1}$ of a relaxation process j can be obtained from the concentration c_j of the species, its effective dipole moment $\mu_{\text{eff},j}$ and polarizability α_j by

$$\frac{2\epsilon + 1}{\epsilon} \cdot (\epsilon_j - \epsilon_{\infty,j}) = \frac{N_A c_j}{k_B T \epsilon_0} \cdot \frac{\mu_{\text{eff},j}}{(1 - f_j \alpha_j)^2}, \tag{II.107}$$

whereas f_j represents the so called reaction field factor accounting for the shape and size of cavity in the dielectric medium due to the presence of a dipolar species. The further quantities in the latter equation represent the Boltzmann constant k_B, Avogadro constant N_A, temperature T and static permittivity ϵ with

$$\epsilon = \epsilon_\infty + \sum_j S_j. \tag{II.108}$$

10.2 Isothermal Titration Calorimetry

A quantitative study of molecular interactions in the bulk phases of aqueous solutions at defined temperature can be achieved by measuring recalescences upon the occurrence of binding processes. Whereas the more abundantly used differential scanning calorimetry relies on measuring the temperature difference between two cells when applying a defined temperature sweep, the related ITC technique operates isothermally.

The benefits of ITC are highly appreciated in biochemistry and biology. In these disciplines, it is used to access thermodynamic parameters of binding processes such as stoichiometry, binding constant, entropy and enthalpy in a label-free approach, *i.e.,* without the use of marker substances having potential influence on the interaction process to be studied. ITC provides valuable contributions for clarifying reaction mechanisms.[147]

Assuming a reversible binding process between a molecule at concentration $[M]$ and a ligand at concentration $[L]$ at a 1:1 stoichiometry leading to formation of an associate at concentration $[ML]$, the equilibrium association and dissociation constants K_a and K_d are defined as[148]

$$K_\mathrm{a} = \frac{[ML]}{[M]\cdot[L]} = \frac{1}{K_\mathrm{d}}. \tag{II.109}$$

The latter constants are related to the Gibbs binding energy ΔG by

$$\Delta G = -RT \ln K_\mathrm{a} = RT \ln K_\mathrm{d} \tag{II.110}$$

with the usual meaning of R and T.

Figure II.18 shows a schematic of the experimental ITC setup. Within an adiabatic jacket, the microcalorimeter comprises two cells, whereas one acts as a reference cell and the other one holds the sample with one of the interaction partners of the process to be studied. The other is provided via an automated syringe. During the measurement process, aliquots are injected into the sample cell. A precise feedback control system ensures equal temperature of the cells by compensating for temperature differences that occur due to binding processes in the sample cell associated with a heat of reaction which is dependent on the interaction strength.

In order to get quantitative information from injecting aliquots, a rescaling of the experimental raw data has to be carried out. Therefore, the heat of reaction upon the respective aliquot addition is obtained from integrating the corresponding heat-flow peak and plotting against the molar ratio of the reactants. The resulting isotherm grants access to the thermodynamic parameters of interest. Information on heat of reaction, stoichiometry and entropy of the process are accessible by means of ITC.

10.3 Density

The density ρ of aqueous solutions can be inferred from the shift in resonant behavior of a container filled with the respective solution. In practice, the period of vibration τ of an U-shaped borosilicate glass tube filled with the sample is measured, whereas ρ and τ are related by

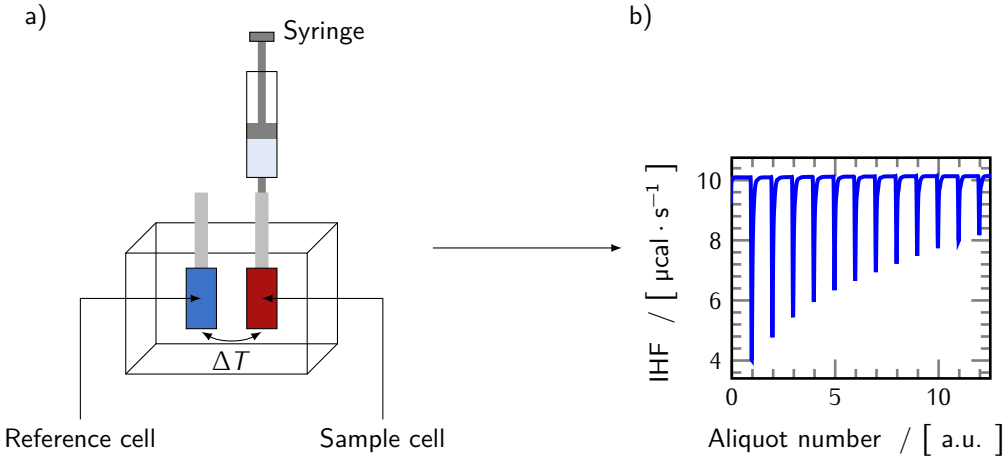

Figure II.18: Scheme of the microcalorimeter used for ITC. a) The setup comprises a reference cell and a sample cell enclosed within an adiabatic jacket. The heat of reaction released upon injecting aliquots of a reactant is compensated by a precise feedback control systems to maintain the preset temperature. b) Characteristic course of instantaneous heat flow (IHF) to maintain the preset temperature.

$$\rho = A \cdot \left(\frac{\tau}{\tau_0} \right)^2 \cdot (f_1 - B) \cdot f_2. \tag{II.111}$$

The parameters A and B denote calibration constants and τ_0 represents the period of a reference oscillator. Correction for effects of non-linearity, viscosity and temperature is accounted for by f_1 and f_2.

10.4 Dynamic Light Scattering

DLS is an optical method based on the gradient in refractive indices between a solvent and the solute dissolved within. It relies on the evaluation of the fluctuation in time dependent scattered light as a consequence of aggregate motion. A strict mathematical treatment allows for extraction of size and shape information from DLS-experiments. [149,150]

A monochromatic coherent light source of wavelength λ serves to illuminate an optically transparent solution contained in a sampling vial. The scattered light intensity is measured at a scattering angle θ. From the wave vectors of the incident light $\vec{k}_\mathrm{i}$ and scattered light $\vec{k}_\mathrm{s}$, the scattering vector $\vec{q}$ is defined as the vector conveying the wave vector of the incident light $\vec{k}_\mathrm{i}$ to the wave vector of scattered light $\vec{k}_\mathrm{s}$. In mathematical terms, this reads

$$\vec{q} = \vec{k}_\mathrm{s} - \vec{k}_\mathrm{i}. \tag{II.112}$$

A graphical representation of this definition and the relation of the scattering vector $\vec{q}$ to the scattering angle θ is given in Figure II.19.

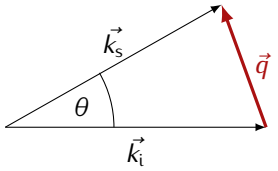

Figure II.19: Relation between scattering vector $\vec{q}$ and the scattering angle θ in DLS-experiments.

Brownian motion of aggregates due to thermal agitation causes the overall detected scattered light intensity to fluctuate as a consequence of constructive and destructive interference phenomena from light that is scattered by individual particles. A digital auto-correlator is at the heart of any DLS-equipment and compares the similarity of a scattered light intensity to the intensity detected a defined time interval τ later. This procedure is carried out for a multitude of varying time intervals $n \cdot \tau$ with $n \in \mathbb{N}$ and allows for the extraction of the correlation function $G^1(\tau)$ at a defined scattering vector $\vec{q}$ from the time dependent intensity $I(t)$ as

$$G^1(\tau) = \langle I(t) \cdot I(t+\tau) \rangle \tag{II.113}$$

It is to be noted, that no quantitative evaluation of DLS-data is shown in the presented work. Therefore, the corresponding theory allowing for an extraction of aggregate sizes from the auto-correlation function is omitted.

10.5 Viscosity

Rolling ball viscometers are typical devices for the determination of viscosities. In this type of experiments, the rolling time t for a steel ball to fall down a specified distance within a tilted capillary of uniform diameter is measured.

With known calibration constant K, density of the steel ball ρ_{ball} and density of the sample ρ, the viscosity η of the sample solution is obtained via

$$\eta = K \cdot (\rho_{\text{ball}} - \rho) \cdot t. \tag{II.114}$$

The calibration constant K of the device retrieved from measuring the falling time for a sample of known viscosity.

10.6 Electrical Conductivity

The measurement of electrical conductivities is based on the principle of a Wheatstone bridge. In this electrical circuit, an unknown resistance is measured by balancing the two legs of a bridge circuit. The corresponding conductivity is given by the inverse resistance. The circuit diagram is given in Figure II.20

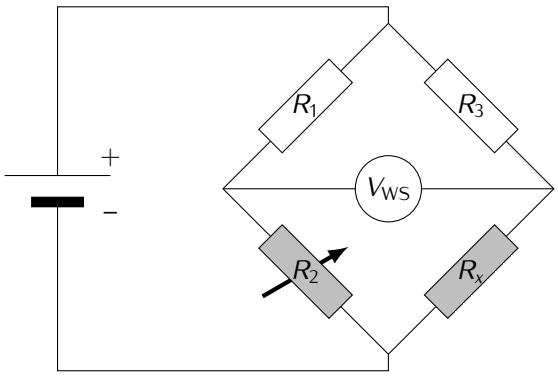

Figure II.20: Circuit diagram of the Wheatstone bridge.

Whereas the precisely known resistances R_1 and R_3 are fixed, R_2 is additionally adjustable. If the measured voltage V_{WS} equals zero, for the ratios between the resistances, the ratio

$$\frac{R_2}{R_1} = \frac{R_x}{R_3} \tag{II.115}$$

holds. Rearranging the latter equation then yields the unknown resistance R_x.[151]

11 Data Processing

The relevant data processing schemes for raw data obtained from oscillating bubble and dielectric relaxation spectroscopy (DRS)-experiments will be briefly introduced in the following.

11.1 Oscillating Bubble

Extended Lucassen-van den Tempel (LvdT)-Model

A formal description of the experimental data obtained from oscillating bubble experiments to yield quantitative surface dilatational properties can be achieved by an extended LvdT model. As compared to the original theory, the expression accounts for an additional intrinsic surface dilatational viscosity κ.

Within the original LvdT-model, relaxation processes at the interface are assumed to be of pure diffusional origin and the modulus is given by [152]

$$|E| = \frac{\epsilon^{\mathrm{m}}}{\sqrt{1 + 2\xi + 2\xi^2}}, \tag{II.116}$$

whereas the diffusional parameter ξ is related to the surfactant's diffusion coefficient D, applied perturbation frequency f and concentration dependent adsorption $\Gamma(c)$ by

$$\xi = \sqrt{\frac{D}{2f}} \left(\frac{\mathrm{d}\, c}{\mathrm{d}\, \Gamma} \right) = \sqrt{\frac{f_{\mathrm{diff}}}{2f}}. \tag{II.117}$$

Therein, f_{diff} denotes a characteristic diffusion frequency and ϵ^{m} the high frequency limiting elasticity. The additional intrinsic surface dilatational viscosity κ transforming the classical LvdT-model to its corresponding extended version is achieved by adding a the intrinsic surface dilatational viscosity κ via a complex-valued constant to the modulus leading to the frequency dependent expression

$$E(f) = \epsilon^{\mathrm{m}} \frac{1 + \xi + i\xi}{1 + 2\xi + 2\xi^2} + i \cdot \kappa \cdot 2\pi f, \tag{II.118}$$

which is used to fit the experimentally obtained data with the high frequency limiting elasticity ϵ^{m}, characteristic diffusion frequency f_{diff} and intrinsic surface dilatational viscosity κ as fitting parameters. Least-squares minimizers provided by Matlab [153] and Python [154] were applied to get hold of the best model constants.

The classical LvdT-parameters high frequency limiting elasticity ϵ^{m} and characteristic diffusion frequency f_{diff} describe the maximum resistance against increasing the interfacial area and the inverse of a characteristic time describing the diffusional relaxation processes at the interface. It is conceivable, that the characteristic diffusion frequency f_{diff} of a system has to be related to the externally induced perturbation frequency in order to relate diffusional processes to the timescale of the experiment. Frequently, experimental observations of increasing magnitude of the classical LvdT elasticity modulus $E(f, c)$ at elevated perturbation frequencies cannot be described in terms of the classical modulus but rather only taking into account the frequency-proportional summand leading to Equation II.118. Due to its proportionality to the rate of perturbation, *i.e.*, the perturbation frequency f it is interpreted as a viscosity and serves to capture dissipative processes occurring within the interfacial region.

Two Process Model

Consideration of a broader frequency range by combination of oscillating pendant drop and oscillating bubble surface rheological data can provide a deeper understanding of the prevailing mechanical properties and kinetic processes of adsorbed layers. Ravera *et al.* suggested a model accounting for

both surfactant relaxation due to diffusion and additional processes internal to the adsorption layers such as reorientation, aggregation, phase transitions and interfacial chemical reactions. [155]

Within this model, a relaxation process at a certain frequency manifests as a maximum in the imaginary and an inflection point in the real part of the frequency dependent surface dilatational property curve. [156] This principle – as similarly known from spectroscopic techniques – is generally valid, as it is a consequence of relaxation phenomena assumed to obey linear kinetics. In particular, the case of an adsorption layer characterized by changing average molecular area is considered here. [157] Taking into account the required boundary conditions and rearranging eventually leads to the expression

$$E(f) = \frac{\epsilon_{0\Gamma}(1 - i\lambda) + \epsilon_{0\Omega} G_1 i\lambda}{\frac{1 - G_2 + \xi - i\xi}{1 - G_2} - (1 + \xi - i\xi)} \tag{II.119}$$

for the surface dilatational modulus E of adsorbed layers with changing molecular area.

In Equation II.119, ξ follows the definition of Equation II.117, G_1, G_2, $\epsilon_{0\Gamma}$ and $\epsilon_{0\Omega}$ depend on the thermodynamic properties of the system and the reference state. Just as in the previous paragraph, the diffusion based LvdT-model fails to predict the increasing surface dilatational modulus E at elevated frequencies. Therefore, Equation II.119 was complemented by the intrinsic surface dilatational viscosity κ to yield

$$E(f) = \frac{\epsilon_{0\Gamma}(1 - i\lambda) + \epsilon_{0\Omega} G_1 i\lambda}{\frac{1 - G_2 + \xi - i\xi}{1 - G_2} - (1 + \xi - i\xi)} + i \cdot \kappa \cdot 2\pi f \tag{II.120}$$

taking into account a frequency-proportional summand. The corresponding multi-parameter non-linear least-squares minimization has been implemented into a Matlab-script and applied to combined surface rheological data obtained from oscillating pendant drop and oscillating bubble experiments. [153]

11.2 Dielectric Relaxation Spectroscopy

The importance of a valid and robust fitting procedure of DRS-data is crucial for the extraction of meaningful parameters and thus an appropriate interpretation of the extractable physical information. As the dielectric response of solutions – other than pure compounds – typically comprises two or more overlapping relaxation processes over a frequency range covering several orders of magnitude and the measurement of dielectric properties is subject to technological limitations, a decomposition into the individual constituting processes remains challenging. [158]

Methods granting access to these relaxation contributions are based on non-linear fitting algorithms. In order to apply these in a reasonable manner, good practice guidelines for selecting sound fitting models have been discussed by Stoppa and coworkers. [159] Rational criteria for a formal description

in terms of number and types of relaxation modes present in the dielectric relaxation spectra have been suggested. As a „golden rule of fitting“ in experimental DRS-spectra described with empirical relaxation models, the number of parameters should be as low as possible. Furthermore, the overall relaxation model of a spectrum, *i.e.*, number and types of peaks should not vary as a function of concentration except for good physical reasons such as, *e.g.*, phase transitions or association processes.

In the previously described fitting procedures,[160–163] the experimentally accessible total loss $\eta^{''}(\nu)$ was corrected for the conductivity contribution to yield the dielectric loss $\epsilon^{''}(\nu)$. It is to be noted that the latter quantity is related to the total loss $\eta^{''}(\nu)$ via the vacuum permittivity ϵ_0, frequency ν and electrical conductivity κ_{el} by

$$\eta^{''}(\nu) = \epsilon^{''}(\nu) + \frac{\kappa_{el}}{2\pi\nu\epsilon_0}. \tag{II.121}$$

As „one“ overall experimental DRS-spectrum in practice contains information from three independent experiments, this preprocessing step needs to be carried out for each of the individual data sets. The corresponding values of the electrical conductivity κ_{el} can be obtained as fitting parameters and are generally found to deviate slightly from independent experimental measurements of electrical conductivity $\kappa_{el}^{(exp)}$. Deviations between the latter values can be rationalized.[164] This preprocessing correction step, yields complex permittivity spectra described by

$$\hat{\epsilon}(\nu) = \epsilon^{'}(\nu) - i\epsilon^{''}(\nu). \tag{II.122}$$

They comprise only the relative permittivity $\epsilon^{'}(\nu)$ and the dielectric loss $\epsilon^{''}(\nu)$ and will then summarize selectively the contributions depending explicitly on frequency, whereas the latter reflect the cooperative dynamics within the bulk phase of the respective sample. The complex permittivity $\hat{\epsilon}(\nu)$ according to Equation II.122 is then fitted to relaxation models of the type

$$\hat{\epsilon}(\nu) = \epsilon_\infty + \sum_{j=1}^{n} \frac{S_j}{\left[1 + (i2\pi\nu\tau_j)^{1-\alpha_j}\right]^{\beta_j}} \tag{II.123}$$

with n independent modes of relaxation j characterized by specific amplitudes S_j, relaxation times τ_j and peak shape parameters α_j and β_j. In this model, ϵ_∞ defines the high-frequency limit of the relative permittivity $\epsilon^{'}(\nu)$. The so called static relative permittivity ϵ is given by the sum of the high frequency limiting permittivity ϵ_∞ and the amplitude of all emerging relaxation modes $\epsilon = \epsilon_\infty + \sum_{j=1}^{n} S_j$.

As this procedure requires knowledge of the peak characteristics in order to determine an appropriate *fitting* value of the electrical conductivity κ_{el}, an iterative procedure might be suitable. Shortcomings of the approach described to this point are documented especially for the empirical description of small-amplitude modes peaking at the edges of the covered frequency range, as they tend to be over-estimated in terms of their amplitudes.[165]

To overcome this drawback, an alternative procedure allowing for simultaneous direct fitting of the experimental data obtained from the three probes, *i.e.*, three independent experiments without the need for any further preprocessing and fitting steps is suggested. Therefore, only a slight modification in the previously used model function (Equation II.123) is required. The experimentally accessible values of frequency dependent relative permittivity $\epsilon^{'}(\nu)$ and total loss $\eta^{''}(\nu)$ are fitted to

$$\epsilon^{'}(\nu) - i\eta^{''}(\nu) = \epsilon_{\infty} + \sum_{j=1}^{n} \frac{S_j}{\left[1 + (i2\pi\nu\tau_j)^{1-\alpha_j}\right]^{\beta_j}} + i\frac{\dot{\kappa}_{\mathrm{el}}}{2\pi\nu\epsilon_0}, \tag{II.124}$$

whereas the parameters in Equation II.124 are identical to the ones used in Equation II.123 with exception of $\dot{\kappa}_{\mathrm{el}}$. This value is allowed to vary for data points determined via the two vector network analyzer (VNA) probes and fixed to zero for the interferometrically gathered points. As schematically shown in Figure II.21, this means that each of the three experimental spectra „has a common knowledge“ on the relaxation processes covering the overall frequency range by referring to the same set of peak parameters, but uses „its own“ fitting parameter for the electrical conductivity $\kappa_{\mathrm{el}}^{\mathrm{i}}$.

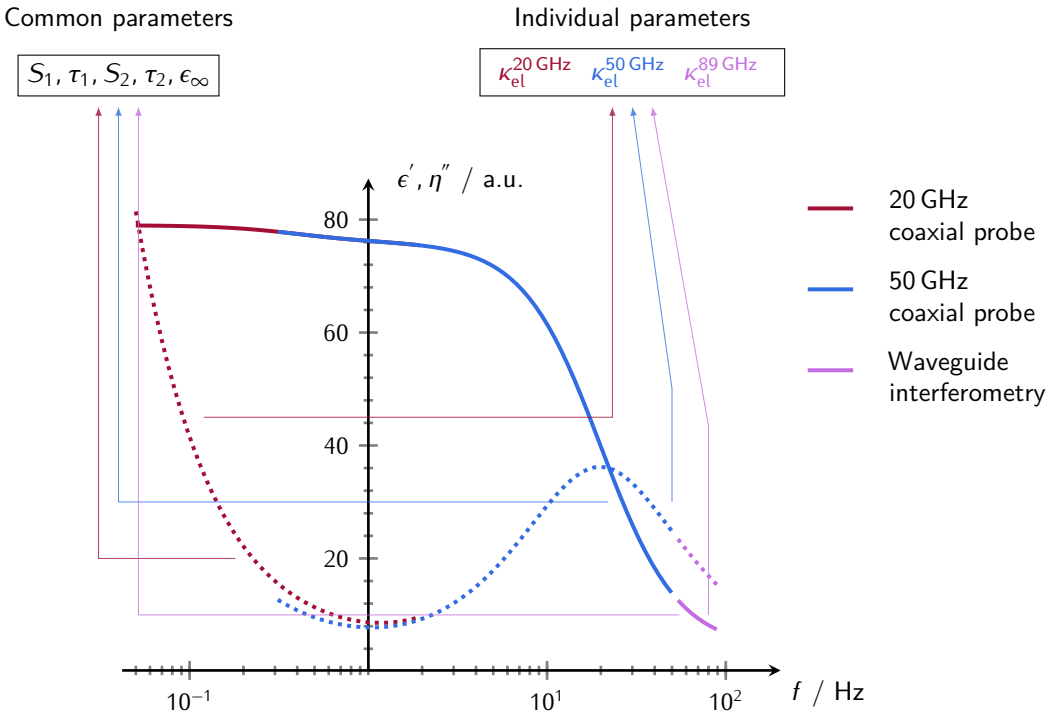

Figure II.21: Scheme of the procedure and parameters used in the proposed simultaneous direct fitting approach for DRS-spectra obtained from three independent experiments. The dielectric responses of sampled relative permittivities (solid) and total losses (dotted) are characterized by the common relaxation parameters of the peaks S_1, τ_1, S_2, τ_2 and an individual conductivity value $\kappa_{\mathrm{el}}^{\mathrm{i}}$ for each of the data sets is represented by different colors. The real and imaginary parts are fitted simultaneously.

The non-linear optimization is carried out relying on a custom-built program implemented in Python based on the lmfit-package.[154] Furthermore, no restriction of any of the model constants is required to reach stable solutions of the minimization problem. Just as in the previously applied fitting procedure, the square root of the diagonal elements of the covariance matrix is used as a measure of uncertainty of the resulting parameters.[166]

By virtue of this strategy, the overall number of effective parameters used in the course of the overall fitting procedure could be reduced dramatically. In a – so far only very limited number of experimental data sets – the amplitudes of weakly pronounced edge modes of the covered frequency range tend to be lower as compared to the previously used procedure relying on the preprocessing conductivity correction. This encouraging result will have to be validated by further experiments and compared to the results of the conventional routine. As another preliminary result based on a rather small set of data, the results of the routines were found to converge within experimental and fitting error if the modes are roughly on the same order of magnitude and the respective dielectric loss $\epsilon''(\nu)$ peaks farther from the spectral edges. The DRS-spectra in the present work are analyzed based on the simultaneous direct fitting approach.

III Experimental

1 Materials

1.1 Surface Effects in the Escape Mechanism of the Stenus Beetle

The spreading alkaloids stenusine and norstenusine were synthesized in a two-step procedure starting from the pyridine derivative 3-picoline according to a synthetic route published by Gedig *et al.* in 2007.[167] After alkylation with 2-bromobutane and 2-bromopropane, respectively, the intermediate products were *N*-ethylated and hydrogenated simultaneously with acetaldehyde under acidic conditions and 20 bar of hydrogen pressure. Distillation yielded stenusine and norstenusine, as verified by means of ^{1}H- and ^{13}C-NMR-spectroscopy. The corresponding molecular structures of both compounds are shown in Figure III.1.

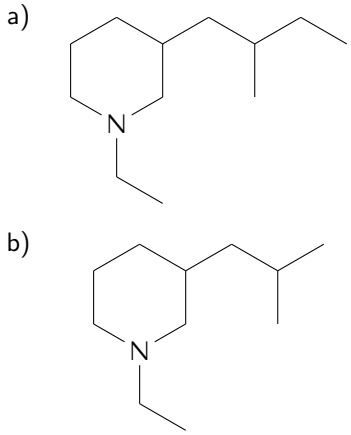

Figure III.1: Molecular structures of the spreading alkaloids a) stenusine and b) norstenusine in their neutral forms.

Both oily compounds were diluted with Millipore water (resistivity above 18 MΩ · cm at 25 °C) to stock solutions having concentrations of 20.6 mmol · L^{-1}, which is marginally lower than the visually observable solubility limit. An aqueous phosphate buffer containing KH_2PO_4 (26 mmol · L^{-1}) and Na_2HPO_4 (41 mmol · L^{-1}) was used to constantly maintain the pH at 7. Since alkali phosphates act as bulk electrolytes, no noteworthy difference in the equilibrium surface tension of the buffer solutions

compared to pure Millipore water was observed.

Residual trace impurities originating from the synthesis were removed from the stock solutions using a protocol and an apparatus developed by Lunkenheimer *et al.* to achieve the state of surface chemical purity (300 cycles, adsorption time of 600 s).[168] The underlying operating principle of the purification device is given in more detail in Subsection 1.6.

Solutions of lower alkaloid concentrations were produced by successive dilution of the purified stock solutions with untreated buffer solution by a dilution factor of 2. All of the glassware used in the course of the experiments was cleaned by soaking in KOH and subsequently HCl for at least 24 h followed by exhaustive rinsing with Millipore water. Prior to the oscillating bubble experiments, the aqueous solutions were degassed by sonication with ultrasound for 10 min.

1.2 Mixed Surfactant-Electrolyte System

The mixed surfactant-electrolyte solutions studied in the course of this project consisted of the anionic model surfactant sodium dodecyl sulfate (SDS) and the electrolyte NaCl.

A stock solution of SDS ($\geq$ 99.0 %, Merck) at a concentration of 6 mmol $\cdot$ L^{-1} was prepared using Millipore water with a resistivity above 18 MΩ $\cdot$ cm at 25 °C. The solution was brought to the state of surface chemical purity using the apparatus introduced by Lunkenheimer *et al.* as described in subsection 1.6 (here: 300 cycles with an adsorption time of 1000 s respectively).[169] Thereby, the dominating contaminant *n*-dodecanol, which has shown to have a more than 350-fold higher surface activity compared to SDS could be removed successfully.[170]

The mixed solutions of purified SDS and sodium chloride (99.999 %, Sigma-Aldrich) were prepared to have an equal mean ionic activity I_{mean} of 1 mmol $\cdot$ L^{-1}. Therefore, the required amounts of the SDS stock solution and solid NaCl were placed in a flask and filled to the calibration mark with Millipore water. In terms of the Debye-Hückel (DH)-theory (more details in section 5) the mean ionic activity I_{mean} is related to the concentrations of the salt and the ionic surfactant via the mean activity coefficient $f_{\pm}$ by

$$I_{\text{mean}} = f_{\pm}\sqrt{c_{\text{SDS+NaCl}} \cdot c_{\text{SDS}}}, \tag{III.1}$$

whereas the activity coefficient can be calculated by the DH-equation using the numerical parameters adequate for a temperature of 25 °C according to[60]

$$\log f_{\pm} = -\frac{0.5115 \cdot \sqrt{I}}{1 + 1.316 \cdot \sqrt{I}} + 0.055 \cdot I. \tag{III.2}$$

It is to be noted, that the values of ionic strength I in the latter equation have to be provided in units of mol $\cdot$ L^{-1}. The concentrations of SDS, c_{SDS}, sodium chloride, c_{NaCl}, ionic strength I and mean

ionic activity I_{mean} required for the preparation of the studied solutions are summarized Table III.1.

Table III.1: Specifications of the Studied Mixtures of SDS and NaCl.

No.	Name	c_{SDS} [mmol · L^{-1}]	c_{NaCl} [mmol · L^{-1}]	I [mmol · L^{-1}]	I_{mean} [mmol · L^{-1}]
1	SDS-NaCl-1	1.00	0.00	1.00	1.00
2	SDS-NaCl-2	0.66	1.00	1.66	1.00
3	SDS-NaCl-3	0.45	2.00	2.45	1.00
4	SDS-NaCl-4	0.22	5.00	5.22	1.00
5	SDS-NaCl-5	0.12	10.00	10.12	1.00
6	SDS-NaCl-6	0.07	20.00	20.07	1.00

The errors in mean ionic activity I_{mean} were estimated to be below 0.01 mmol · L^{-1} for the investigated solutions. All the used glassware was soaked in nitric acid (35 %) for at least 48 h and thoroughly rinsed with deionized water before use.

1.3 Ion Specific Effects in Alkali Decyl Sulfates

Several alkali decyl sulfates (XDeSs) were available in laboratories of the Institute of Physical and Theoretical Chemistry II of the University of Regensburg from previous work. They have been synthesized by Dr. Haage from the Max Planck Institute of Colloids and Interfaces. Stock solutions of lithium decyl sulfate (LiDeS), sodium decyl sulfate (NaDeS), potassium decyl sulfate (KDeS) and cesium decyl sulfate (CsDeS) at concentrations of 35, 30, 27 and 20 mmol · L^{-1}, *i.e.,* below their respective critical micellar concentration (cmc)-values were prepared by dissolving the white solids in Millipore water characterized by a resistivity above 18 MΩ · cm at 25 °C. The surfactants, differing only in their counterion as shown in Figure III.2 were subject to a purification procedure as described in subsection 1.6 with more than 300 compression-expansion cycles and an adsorption time of 300 s.

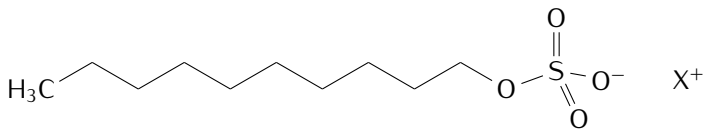

with X = Li, Na, K, Cs.

Figure III.2: Molecular structure of XDeSs with counterions Li, Na, K and Cs.

The absence of any major decomposition products due to prolonged storage time has been checked by means of ^{1}H-NMR-spectroscopy via comparison with recently acquired NaDeS.

1.4 Ion Specificity in Adsorption Layers of *n*-Dodecylphosphinecholine

The surfactant *n*-dodecylphosphinecholine (DPC) was obtained from Avanti Polar Lipids and used as received. The molecular structure of the zwitter-ionic compound is shown in Figure III.3. Hydrates of the lanthanide nitrates were purchased as the respective hydrates ($Yb(NO_3)_3$, 99.9 % and $Ce(NO_3)_3$, REacton, 99.99 %) from Alfa Aesar and used without further processing.

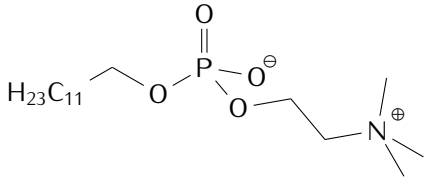

Figure III.3: Molecular structure of DPC.

Stock solutions of DPC, $Ce(NO_3)_3$ and $Yb(NO_3)_3$ were prepared at concentrations of 10, 45 and 45 mmol $\cdot$ L^{-1} using Millipore water, respectively. For the dielectric relaxation spectroscopy (DRS)-study, aqueous salt solutions of $Ce(NO_3)_3$ and $Yb(NO_3)_3$ at concentrations of 10, 20, 30 and 40 mmol $\cdot$ L^{-1} *without* DPC were obtained from the stock solutions by dilution with Millipore water. These samples were referred to with the ending „-DRS“. In order to study the influence of lanthanide nitrates on the surface rheological characteristics of DPC layers, 1 mmol $\cdot$ L^{-1} solutions of the zwitter-ionic compound with and without the presence of the corresponding salt solution were prepared as described above. An overview of the sample composition is given in Table III.2.

Table III.2: Composition of the samples comprising DPC, $Ce(NO_3)_3$ and $Yb(NO_3)_3$ used for the different sets of experiments.

Sample	$c_{Ce(NO_3)_3}$ [mmol $\cdot$ L^{-1}]	$c_{Yb(NO_3)_3}$ [mmol $\cdot$ L^{-1}]	c_{DPC} [mmol $\cdot$ L^{-1}]
DPC	0	0	1
Ce2-Bubble	30	0	1
Yb2-Bubble	0	30	1
Ce1-DRS	40	0	0
Ce2-DRS	30	0	0
Ce3-DRS	20	0	0
Ce4-DRS	10	0	0
Yb1-DRS	0	40	0
Yb2-DRS	0	30	0
Yb3-DRS	0	20	0
Yb4-DRS	0	10	0

1.5 Photo-Responsive Azo-surfactant

A stock solution of the photo-responsive azo-surfactant T226 at a concentration of $1\,g \cdot L^{-1}$ was prepared using Millipore water with a resistivity above $18\,M\Omega \cdot cm$ at 25 °C. The molecular structure of the azo-surfactant in its *cis*- and *trans*-states is shown in Figure III.4. Dr. Prescher (IDM Teltow) is gratefully acknowledged for the synthesis of this compound. The solubility in water is introduced via the hydrophilic ethylene-oxide units.

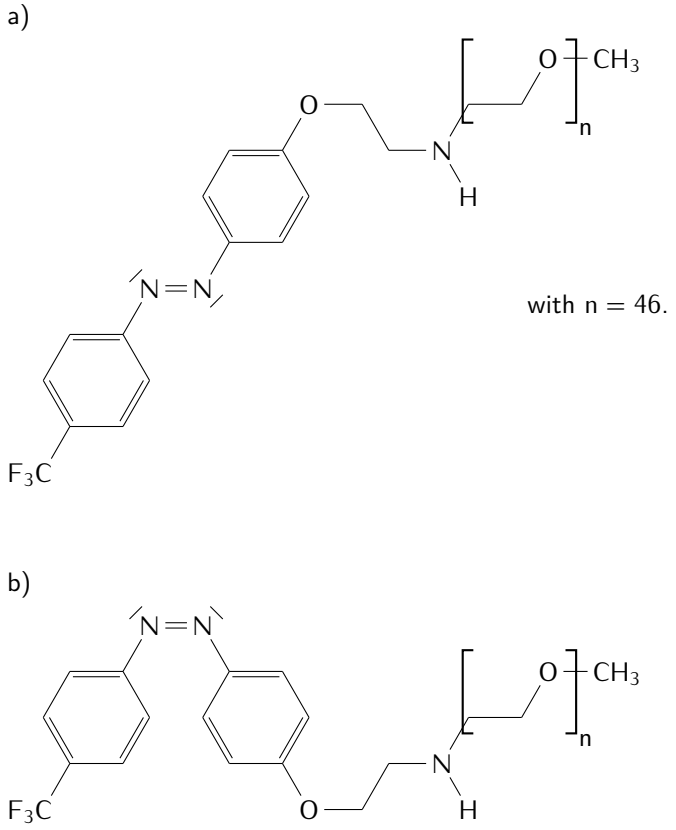

Figure III.4: Molecular structure of the photo-sensitive surfactant T226 in its a) *trans*- and b) *cis*-state.

In order to induce the *cis*-*trans* geometrical isomerization, the container holding the sample to be studied was irradiated with an ultraviolet (UV)-lamp (Konrad Benda, Type NU-4KL) at main intensity wavelengths of 254 and 366 nm for 3 h before conducting the surface tension and rheology experiments described in the following. The modifications of the respective devices required to study the solutions with a prevailing geometrical isomer will be detailed on in the corresponding result sections.

1.6 Sample Purification

A purification of surfactant solutions to reach the state of surface chemical purity was achieved by an apparatus developed and commercialized by Lunkenheimer and coworkers.[169] The apparatus is based on the principle of competitive adsorption of surfactant and surface active impurities towards an interface. A specially designed glass container as schematically shown in Figure III.5 is allowed to equilibrate for a defined time. In a next step, the reservoir is tilted, which leads to a compression of the surface area. Subsequently, a defined volume of the solution is removed from the compressed surface region enriched with active trace impurities by means of a capillary. An appropriate positioning of the suction capillary is achieved by an adequate filling volume and adjusting the tilting angle.

The applied purification scheme ensures a complete removal of any surface active impurities of high surface activity by repeated cycles of a) compression of the surface layer, b) its removal with the aid of a capillary and c) dilation to an increased surface area. These cycles are repeated until the equilibrium surface tension between subsequent cycles remains constant.

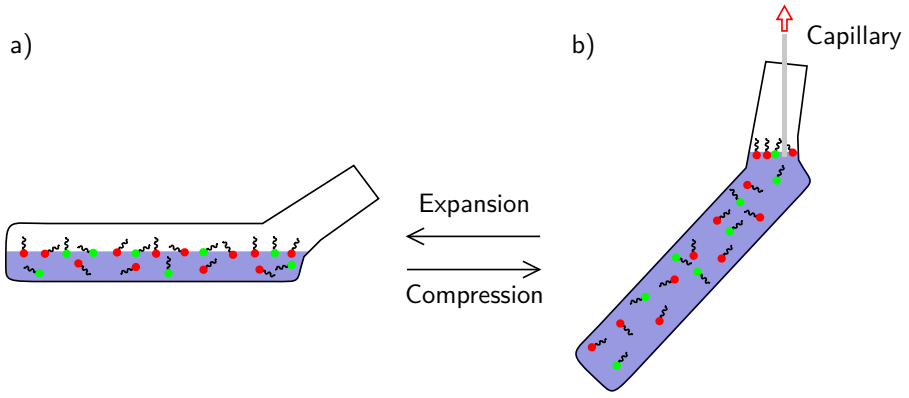

Figure III.5: Scheme of the Lunkenheimer apparatus for purification of surfaces. Both surfactant molecules (green head group) and surface active impurities (red head group) adsorb at the interface. Long times of expanded surfaces as shown in a) are followed by a compression of surface area as in b) by tilting the glass container. In this state, a capillary is approached to the surface to suck a small volume from the surface.[168]

For an efficient purification, the solutions have to meet certain prerequisites. The contaminants have to feature much lower concentration but at the same time a considerably higher surface affinity as compared to the main compound. Furthermore, the surfactant concentration of the solution to be „cleaned“ is limited to the sub-cmc-range as surface active impurities tend to be solubilized within the hydrophobic core of surfactant micelles.[171]

Criteria to check the success of a performed purification process have been proposed.[172,173] As a first estimation of purity, the equilibrium surface tension γ_e should not change upon performing further cycles. Additionally, the equilibrium surface tension of pure solutions is reached faster as if it was the case in the presence of impurities, *i.e.*, the temporal dependence of surface tension of pure solutions is

remarkably lower. Surface chemically pure surfactant solutions exhibit kinetics accelerated by a factor in the range of two orders of magnitude, as there is no other surface active agent to compete against. Also the higher equilibrium surface tension γ_e of purified solutions is to be considered an indicator of purity.

An alternative procedure to remove *n*-dodecanol from SDS relies on repeated crystallization of the surfactant from ethanol.[174]

2 Optical Methods

2.1 Sum Frequency Generation Spectroscopy

The experimental setup to carry out sum frequency generation (SFG)-measurements operates in the co-propagating geometry.[175] The spectrometer (EKSPLA PL 2143A/SS and PG 401/DFG2-10P) produces 27 ps pulses at a repetition rate of 10 Hz. The 532 nm visible (Vis) and tunable infra-red (IR) pulses at angles of incidence of 59° and 54°, respectively, were made to overlap both spatially and temporally at the sample. The energy of the Vis pulses was about 300 µJ and roughly 200 µJ for the IR pulses at 3000 cm^{-1}.

Spectra were acquired in the range from 2800 to 3800 cm^{-1} at a mesh size of 2 cm^{-1} by tuning the IR-beam to the respective target frequency. Each spectrum was normalized by the intensity of the incident IR and Vis beams.

2.2 Infrared Reflection Absorption Spectroscopy

A spectrometer (Vertex 70 FT-IR spectrometer, Bruker) equipped with a liquid-nitrogen-cooled mercury cadmium telluride (MCT)-detector attached to an external air/water reflection unit (XA-511, Bruker) was used for acquisition of the infrared reflection absorption spectroscopy (IRRAS) data. An angle of incidence of 40 °C was chosen for both *s*-polarized and *p*-polarized light obtained from a wire grid polarizer (KRS-5). The trough-position was adjusted by a personal computer (PC)-controlled shuttle system to consecutively focus the beam either on the sample or the reference part. A correction for the water signal arising from the presence of vapor immediately above the interface is achieved by calculation of the reflectance-absorbance (RA) according to Equation II.48. In order to maintain a constant water vapor content, the whole system was placed into a hermetically sealed box. Sampling was performed at a rate of 20 kHz at a grid of 4 cm^{-1} in the spectral range from 800 to 4000 cm^{-1}. Experiments were carried out at 25 °C in the thermostatically controlled tandem shuttle Langmuir trough. Sample and reference were provided in glass dishes placed inside the individual troughs and filled to the same level.

2.3 UV-Vis-Spectroscopy

Absorption spectra in the ultraviolet-visible (UV-Vis) range from 190 and 800 nm were obtained by a spectrophotometer (CARY3E, varian) using a quartz cuvette. Between changing the samples, the cuvette was rinsed multiple times with water, ethanol and acetone and subsequently dried in a stream of N_2.

3 Surface Tension Analysis

3.1 Ring Tensiometry

A ring tensiometer (KRÜSS K100) was used for measuring both equilibrium surface tension isotherms relying on the automated dosing system and time dependent surface tension (at lower temporal resolution as compared to the used pendant drop device).

Depending on the solution to be studied, either a ring or a plate was used as measuring object. To ensure uncontaminated sampling, the respective object was heated in the flame of a Bunsen burner and the glassware used in the course of the experiment was thoroughly rinsed with water and acetone (p.A.) subsequent to longer storing periods in KOH and HCl solutions.

3.2 Pendant Drop Tensiometry

Time dependent values of surface tension were captured using a drop profile analysis tensiometer (PAT1M, Sinterface). Due to its operating principle based on the evaluation of the Gauss-Laplace equation, temporal resolution well below 1 s could be achieved.

In order to build up equilibrium surface tension isotherms from these individual time dependent surface tension values at fixed surfactant concentration, an „equilibrium“ surface tension corresponding to the respective solution had to be extracted from the data. Depending on the purity and concentration of the solution, this could be achieved by pure averaging or an appropriate extrapolation.[176] The Ward-Tordai model achieves a quantitative description of adsorption kinetics assuming a diffusion-controlled adsorption model characterized by a fast transfer between subsurface and interface compared to a slower process exchanging surfactant between bulk and subsurface.[177–179] It can therefore be applied to the assumed surface model comprising a topmost surface layer and an adjacent transition layer towards the bulk provided that the interface is initially devoid of surfactant. Typically, the asymptotic long time solution of the Ward-Tordai-equation given by

$$\gamma(t) \cong \gamma_{eq} + \frac{n_{tpye} R T \Gamma^2}{c} \sqrt{\frac{\pi}{4Dt}} \qquad \text{for} \qquad t \to \infty \tag{III.3}$$

is used for the estimation of equilibrium surface tension γ_e from time dependent surface tension values as obtained from the pendant drop device operating on the axis symmetric drop shape analysis (ADSA) principle. In the latter equation, the parameter n_{tpye} assumes a value of 1 for non-ionic surfactants and $n_{tpye} = 2$ holds for ionic surfactants. Next to the diffusion coefficient D, gas constant R, temperature T concentration c and surface coverage Γ are required. A value of equilibrium surface tension γ_e is obtained as the intercept of linear fit of surface tension γ plotted against the inverse square root of time, *i.e.*, $t^{-1/2}$.

The surface tension of water was measured over the time scale of the respective experiment and checked for the absence of dynamics and agreement with the literature value to ensure purity of the capillary, tubing and syringe of the device.

4 Foam Characterization

4.1 Foam Column Analysis

A dynamic foam analyzer (KRÜSS, DFA100) was used to characterize aqueous solutions with respect to the foam columns formed by them. If not stated otherwise, an air flow at a rate of $0.3\,\mathrm{L}\cdot\mathrm{min}^{-1}$ was applied for 15 s via the bottom frit of the sample container holding 40 ml to produce a foam column.

The apparatus was ensured to be free of contaminants before analyzing the next sample by testing the foaming properties of pure Millipore water subsequent to flushing the bottom frit and glass column with acetone and water.

4.2 Single Lamella Analysis

The key idea for the instrumental design was inspired from previous work dealing with the analysis of single foam lamella stability.[120,139,140] A custom made, wide necked flask (volume of approximately 120 ml) containing a rectangular glass frame (2.5 x 1.5 cm) mounted at the bottom of the flask served as the measurement cell. By means of appropriate positioning and the use of an adjusted liquid volume, an individual foam lamella is generated by rotation around 90° to a vertical sampling position. Also after its formation, the lamella is still in contact with its parent solution and the humidity-saturated gas atmosphere.

A laser diode (1 mW, 532 nm) is positioned to be incident on the lamella surface at an angle of 20 to 30° with respect to the surface normal. In case of presence of a lamella, the reflected light is collected by a photo-diode (PIN-10D,OSI Optoelectronics). As soon as the lamella ruptures, the voltage trace of the photo-diode drops from 5 V to below 0.01 V. The electrical signal of the photo-diode is amplified and processed by an analogue to digital / digital to analogue-converter. The measurement cell is

mounted onto a rotary stage (Physik Instrumente) equipped with an optical encoder (HEDS 5500, HP), which is controlled by the universal serial bus (USB)-connected ADwin-card (ADwin-light-16, Jäger Messtechnik GmbH). A MATLAB-programmed graphical user interface allows for setting experimental parameters and on-line visualization of the collected data.

The original choice of components was essentially motivated by the availability in the laboratory. At a later stage, the device has been rebuilt based on a microprocessor unit. An extension of the device to simultaneously measure the thinning of foam lamellae by using a second laser operating at different wavelength is intended. [29,36]

5 Dynamic Surface Tension Analysis

5.1 Oscillating Pendant Drop

In order to gather surface rheological data in a frequency range from the mHz to the Hz-regime, the device described in subsection 3.2 was used in a different operation mode. Frequencies and amplitudes of the induced surface area changes could be adjusted in a customized fashion via the supplied control program. The cleaning and rinsing procedure was conducted as described previously.

5.2 Electro Capillary Waves

A schematic overview of the setup used for the excitation and observation of electrocapillary waves (ECWs) is given in Figure II.12. The deformation is achieved by application of an amplified alternating current-voltage (amplifier Model 601C amplifier, TREK) (100 to 500 V) via a cutter-shaped electrode positioned at a distance of approximately 1 mm above the interface. As difference of the dielectric constants of the phases forming the interface, leads to the formation of a surface wave oscillating at twice the applied frequency.

The spatial profile of the wave is scanned by laser reflectometry, whereas the reflected beam oscillates as the surface does. These oscillations are monitored using a position sensitive detector (PSD) placed at a sufficiently large distance from the point of excitation (ca. 4 m). [69] A Lock-In amplifier (Model SR830 DSP Lock-In Amplifier, Stanford Research Systems) locked to the excitation signal allows gaining both amplitude and phase information of the measured intensity signal with respect to the frequency-doubled excitation voltage. The reflected signal is scanned as a function of distance from the excitation point (= position of the electrode). The spatial profile of the capillary wave, also referred to as transverse or perpendicular wave, can be parametrized by

$$u_{z(x)} = A\cos\left(\frac{2\pi}{\lambda}x + \phi\right)\exp(-\alpha x). \tag{III.4}$$

Therein, the wavelength λ and damping coefficient α can be obtained as fitting parameters from a least squares fitting process. Information on the surface dilatational characteristics can be extracted from the solution of the dispersion equation for given values of surface tension γ, wavelength λ and damping coefficient α as described in section 8.

In order to allow for a sensitive detection of surface waves of wavelength λ, the diameter of the laser beam has to be small compared to the object of observation, *i.e.,* the wave. This is achieved by an appropriate focusing lens. The principle of intermittent (or synchronous) detection described above has been suggested by Sohl.[180] The spatial profile of the apparently standing waves, as if observed at a fixed rate of synchronized illumination is obtained by measuring the deflection of a focused HeNe laser beam (JDSU) reflected from the fluid surface acting as a rocking mirror. The shape of the wave leads to a corresponding angular deflection of the reflected beam. The beam reflected at a certain distance from the excitation spot carries information on the surface wave amplitude. Combining the amplitude information from scanning the lateral position, the profile of the apparently standing wave can be obtained in terms of the characteristic parameters amplitude at zero distance to the place of excitation, wavelength and attenuation, whereas only the two latter parameters are of interest to the evaluation of the complex surface dilatational modulus.

5.3 Oscillating Bubble

The presented oscillating bubble device was fully designed and constructed at the University of Regensburg by a joint effort of with the machine and electronic shops of the faculty, to whom I would like to express my gratitude for their persistent work. It is subject to ongoing adjustments and modifications. The main task of this instrument development was to extend the frequency range of surface dilatational data acquisition compared to commercially available equipment. Therefore, a thorough reengineering of the apparatus' previous evolution steps[181] in terms of both hardware and software was required. Besides the redesign of the chamber allowing for a reduction of the sample volume to roughly 4 ml, a discrete Fourier transform analysis of the raw data was implemented. Most recent technical advances are the use of a combined filling and tilting algorithm allowing for a reproducible and facile preparation of a measurement. For this purpose, a personal computer (PC)-controlled syringe Pump (Hamilton PSD6) has been introduced. This suppresses the formation of disturbing air bubbles inside the sampling cell. Furthermore, a protocol allowing for sample exchange without opening the assembled chamber has been put forward.

Formation of the bubble is achieved by concerted action of the pump and one of the piezo-controllers (PI Ceramic). Sinusoidal perturbations of the bubble are applied via another piezo-element capable of oscillating at higher frequencies. A highly sensitive pressure transducer (Kistler, Typ 7261) connected to a customized voltage amplifier enabled detection of the periodic pressure signal across the curved air-water interface.

A recently improved image processing scheme allowed determining the surface area of the bubble from

the frames collected by a stroboscopically triggered universal serial bus (USB)-camera (UK1117, ehd imaging).[182] Analysis of the pressure-signal with respect to the voltage signal applied to the piezo-driver is ensured by real-time processing via an USB-card (ADwin-light-16, Jäger Messtechnik).[183] A more detailed, yet not fully up-to date description of the apparatus is given elsewhere.[116]

Furthermore, a user-friendly graphical user interface has been implemented in close collaboration with the Informatics department of the University of Regensburg.[182] The improvements in both the instrumentation hardware and the control program enable a user to perform reliable measurements of surface dilatational characteristics conveniently and within an acceptable time frame similar to other standard devices.

6 Dielectric Relaxation Spectroscopy

6.1 Coaxial Probes

Vector network analyzers (VNAs) allow for measurement of dielectric properties of electrical networks. The large benefits of this kind of devices lie in the possibility to simultaneously measure amplitude and phase information of the generalized complex permittivity $\hat{\eta}(\omega)$ over a broad frequency range within a short time-frame. Coaxial lines serve as a valuable manner for the signal transmission of electro-magnetic waves in the spectrum from MHz to GHz. The reflected and transmitted electrical signals determine an electrical network. In two-port setups, the relation between incident waves $\hat{a}_j$ and reflected waves $\hat{b}_j$ of port j, is described by the scattering matrix S via[184,185]

$$\begin{pmatrix} \hat{b}_1 \\ \hat{b}_2 \end{pmatrix} = \begin{pmatrix} \hat{S}_{11} & \hat{S}_{12} \\ \hat{S}_{21} & \hat{S}_{22} \end{pmatrix} \begin{pmatrix} \hat{a}_1 \\ \hat{a}_2 \end{pmatrix}. \tag{III.5}$$

For a simplified one-port setup, an electrical network is characterized by an impedance step from $\hat{Z}_1$ to $\hat{Z}_2$. The normalized aperture admittance $\hat{Y}$ is related to the only remaining constant of the scattering matrix S by

$$\hat{S}_{11} = \frac{1-\hat{Y}}{1+\hat{Y}} \qquad \text{with} \qquad \hat{Y} = \frac{\hat{Z}_2}{\hat{Z}_1}. \tag{III.6}$$

It is to be noted, that these types of one-port reflection measurements require calibration. The actual scattering coefficient is determined from three calibration standards, *i.e.,* an open, short and a load reference with air, purified mercury and the standard liquid, respectively. The latter should be comparable to the samples to be studied with respect to the dielectric properties. Otherwise, a complex Padé-approximation is to be applied to the raw data sets.[186]

Experimentally, a dielectric probe kit (Agilent 85070E) was used to assess the dielectric properties in

the frequency range from 0.2 to 50 GHz in conjunction with an electronic calibration module (Agilent ECal N4693) to cope with conductive samples connected to a VNA (Agilent E8364B). Two different probes (Agilent 85070E-020 for 0.2 to 20 GHz and Agilent 85070E-050 for 1 to 50 GHz) mounted in a thermostatically controlled cell were used to cover the specified frequency ranges.[142] Precise temperature control was achieved by a thermostat (Huber CC505) with a precision of $\pm 0.02\,^{\circ}\mathrm{C}$ and continuously monitored with a platinum thermometer (PRT, Pt-100) via a data logger (Agilent 34970A). The implemented software calculates dielectric properties from the normalized aperture admittance $\hat{Y}$ via a numerical scheme.

6.2 Waveguide Probes

Waveguides are the appropriate tool for studies of wave propagation in the E-band range from 60 to 90 GHz. The experimentally used transmission setup relies on measuring the absorption coefficient α_a as a function of the path length of the electromagnetic wave through the sample by means of a high precision receiver (Mirco-Tel 1259). Information on the phase coefficient β of the beams obtained from splitting the originally generated one into a reference and a sampling portion is obtained according to the operation principle of a Mach-Zehnder interferometer.[187,188] Making use of the medium wavelength λ_M from this experiment grants access to the complex wave propagation coefficient $\hat{\gamma}$ in a rectangular waveguide via

$$\hat{\gamma}^2 = \left(\alpha_\mathrm{a} + i\frac{2\pi}{\lambda_\mathrm{M}}\right)^2 = k_\mathrm{c}^2 + \hat{k}^2. \tag{III.7}$$

Therein, k_c represents the cut-off wavenumber determined by the geometrical confinement of the propagating wave. This is due to the profile of the rectangular waveguide characterized by its edge lengths a and b with $a > b$.[189] For the TE_{10} mode, the cut-off wavelength equals πa^{-1}. Experimentally, the attenuation of the electromagnetic waves subsequent to coupling the reference and sampling beams is measured as a function of path length through the sample. It is varied by personal computer (PC)-controlled retraction of the waveguide from the sample cell. A thermostat (Lauda RKS 20-D) served to define the temperature of the sampling cell at a accuracy of $\pm 0.02\,^{\circ}\mathrm{C}$. Further details on the experimental setup and the procedure of tuning the beams to destructive interference allowing for an assessment of the medium wavelength λ_M are given elsewhere.[163]

Extraction of the absorption coefficient α_a and medium wavelength λ_M from a four-parameter fit of the experimentally determined path length dependent relative attenuation of the coupled electromagnetic waves yields the real and imaginary parts of the generalized complex permittivity $\hat{\eta}(\omega)$ as

$$\eta' = \left(\frac{c_0}{\nu}\right)^2 \left[\left(\frac{1}{\lambda_M}\right)^2 - \left(\frac{\alpha_a}{2\pi}\right)^2 + \left(\frac{k_c}{2\pi}\right)^2\right] \qquad \text{and} \tag{III.8}$$

$$\eta'' = \left(\frac{\alpha_a}{\pi\lambda_M}\right)^2. \tag{III.9}$$

In these expressions, c_0 represent the speed of light in vacuum and ν the frequency of the propagating electromagnetic wave. With the experimental setup available, interferometric measurements at 60, 66, 72 and 89 GHz were carried out.

7 Further Physical Characterization Methods

7.1 Isothermal Titration Calorimetry

A partially automated micro-calorimeter (MicroCal PEAQ-ITC, Malvern) was used for isothermal titration calorimetry (ITC) measurements. The experiments were carried out at a constant temperature of 25 °C and conducted with degassed Millipore water contained within the reference cell. Sample volumes of 3 ml were prepared immediately before performing a sufficient number of repeats.

7.2 Dynamic Light Scattering

Dynamic light scattering (DLS)-data were acquired by means of a system (CGS-3, ALV) comprising a digital correlator (LSE 5004, ALV) and a p-polarized 22 mW laser (HeNe, JDSU) operating at a wavelength of 632.8 nm as its main components. Precise temperature control to ensure 25 °C constantly was achieved by a high precision thermostat (K6-cc-NR, Huber). Prior to sampling, the solutions were filtered through polytetrafluoroethylene membrane filters (0.2 µm, Carl Roth) into dust-free thoroughly acetone-rinsed cylindrical DLS-vials with an outer diameter of 10 mm. Auto-correlation functions were recorded exclusively at a scattering angle θ of 90° and for a duration of 300 s.

7.3 Density

A vibrating tube density meter (DMA 5000 M, Anton Paar, Graz, Austria) with an uncertainty of $\pm 5 \cdot 10^{-6}\,\mathrm{g \cdot ml^{-1}}$ was used for determining the densities ρ of aqueous solutions.

It is to be noted that the correction parameters f_1 and f_2 described in subsection 10.3 are relevant only at elevated temperatures as the instrument is solely calibrated with water at 20 °C. A temperature range from 0 to 90 °C is accessible with this device, whereas the sample temperature is measured and controlled by a Pt-100 resistance thermometer and Peltier-elements, respectively.

7.4 Viscosity

Dynamic viscosities η of aqueous solutions were determined using an automated rolling ball viscometer (AMVn, Anton Paar, Graz, Austria). The experimental setup comprises a temperature controlled glass capillary of uniform diameter attached to a rotary stage for setting a specified tilting angle.

Selecting a suitable combination of capillary and ball, viscosities in the range from 0.3 to 2500 mPa · s can be assessed. According to the manufacturer, repeatability and reproducibility are specified to be below 0.1 % and 0.5 %, respectively. The full temperature range from 5 to 135 °C was not utilized in the present work. In the following, viscosities will be given as averaged values of repeated runs at inclination angles of 30° and 70°.

7.5 Electrical Conductivity

Electrical conductivities of the aqueous solutions were obtained using a personal computer (PC)-controlled Wheatstone-bridge based setup.[190–193] Two-electrode capillary cells with cell constants C in the range from 12 to 46 cm^{-1} were thermostatically set to a temperature of 25.0 ± 0.5 °C using a custom-built precision thermostat.[194] The cell resistance in frequency range from 0.1 to 10 kHz was measured by means of a high-precision LCR-bridge (HAMEG HM8118) with a relative uncertainty below 0.0005. Aqueous solutions of KCl were used for calibration of the cells.[195] The experimental resistances were extrapolated to a resistance at infinite frequency R_∞ by

$$R(\nu) = R_\infty + a \cdot \nu^b \tag{III.10}$$

with cell-specific fitting parameters a and b. This empirical equation served to eliminate effects of electrode polarization. Parasitic impedances were accounted for by an open/short calibration of the LCR-bridge and the PC-controlled switchboard addressing the individual sample cells before running a measurement. Specific conductivities κ could be related to the extrapolated resistance at infinite frequency R_∞ via the respective cell constant by

$$\kappa = \frac{C}{R_\infty}. \tag{III.11}$$

The uncertainty was estimated to be below 0.5 %.

IV Results

In the following sections of the present chapter, the experimental results of several conducted projects will be shown. The respective discussions will be given in chapter V.

The material presented in this chapter has been (partially) published or is currently under revision for publication in peer reviewed journals. A list of respective publications is given in Appendix A.

1 Surface Effects in the Escape Mechanism of the Stenus Beetle

Nature and wildlife are abundant in exceptional effects and phenomena. One of them can be observed for some species of the rove beetles utilizing an unconventional manner of locomotion on water surfaces, referred to as „skimming“.[196] Beetles of the genus *stenus comma* inhabit banks of ponds and slow-flowing streams. During their hunt for springtails, they are prone to fall onto the water surface.[197] Due to their limited ability to walk on water surfaces, these terrestrial bugs would usually be doomed in such situations. They may drown or – reversely – themselves be an easy prey for other predators such as water striders.[198] The latter feed to a large extent from non-aquatic insects unintentionally trapped at the water surface.[199]

In order to escape from such situations, the *stenus comma* is pointing its pygidial glands located at the tip of its abdomen towards the water surface and releases a multi component secretion propelling the animal to the safety of the shore.[197] Relying on the Marangoni effect, the beetle can reach maximum velocities of 0.4 to 0.75 $\mathrm{m \cdot s^{-1}}$ and distances up to 15 m.[200,201] By excretion of surface active substances, a gradient in surface tension along the contact line between the animal's body and the fluid is established. This provides a force pushing the beetle forward. The active ingredients in the *stenus comma* secretion are two piperidine alkaloids. Schildknecht *et al.* found the principal component to be *N*-ethyl-3-(2-methylbutyl)piperidine, also referred to as stenusine.[202] A structurally similar molecule, norstenusine, was detected in the biological excretion later on in smaller relative amounts.[203] Further constituents, such as 1,8-cineole, appear only in low quantities and are therefore regarded to be of minor importance for the skimming activity. Nevertheless, they have been deemed to serve other purposes.[197] Presumably, the secretion of locomotion-supporting substances was not

the main function of pygidial glands in the first place. Instead, they are assumed to have evolved for protective reasons such as antimicrobial activity.[198]

Water walking arthropods usually exhibit a higher density than water but still they do not sink. Therefore, buoyancy must be supplemented by additional contributions, namely curvature forces arising from the displacement of a water volume by the formation of a meniscus at the contact area between the liquid and the hydrophobic legs of the animals.[201] Baudoin developed a parameter to estimate the physical boundaries for surface walking, referred to as Baudoin number Ba with

$$Ba = \frac{mg}{\gamma P}. \tag{IV.1}$$

It expresses the ratio between body weight mg and tensile force provided by the surface tension γ along the contact perimeter P.[201,204] In order to approach their prey, water walking predators employ their legs to strike the water surface analogous to the mode of operation of a paddle. Thereby, these beetles experience a drag proportional to the exposed leg area, which enables a net propulsion. Accordingly, surface locomotion requires deformation of the air-water interface.

In the aftermath of secretion by the *stenus comma*, a mono-molecular surfactant film is spread over the surface, which does not only reduce the equilibrium surface tension γ_e, but may also affect the properties of the air-water interface under dynamic conditions.[205] It is conceivable that the deposition of such an adsorption layer may influence the dilatational characteristics of the interfacial region. A viscoelastic behavior of the adsorbed layer would imply that for each propulsion stroke of a predator, an additional amount of energy is required for surface area perturbation due to dissipative losses within the adsorption layer. It would thus be tremendously more difficult for them to pursue the *stenus comma* beetle upon skimming.

To clarify the existence of this effect, the surface dilatational properties of interfacial layers formed from the spreading alkaloids stenusine and norstenusine were measured by means of joint oscillating pendant drop and oscillating bubble experiments over a frequency range covering several orders of magnitude. The described oscillating bubble setup operates in the frequency range from 2 to 500 Hz. This allows capturing the processes occurring on the biologically relevant time scale of rapid surface deformation caused by predatory water striders in the course of approaching their prey, the *stenus comma*.

1.1 Surface Tension

The equilibrium surface tension isotherms of stenusine and norstenusine presented in Figure IV.1 were obtained by the previously described drop profile tensiometer in a temperature controlled room at $23 \pm 1\,°C$. Therefore, drops of the indicated concentrations were formed at the tip of a steel capillary with 3 mm in diameter and an averaging of the individual surface tension values in the time range

from 200 to 300 s after drop formation was carried out.

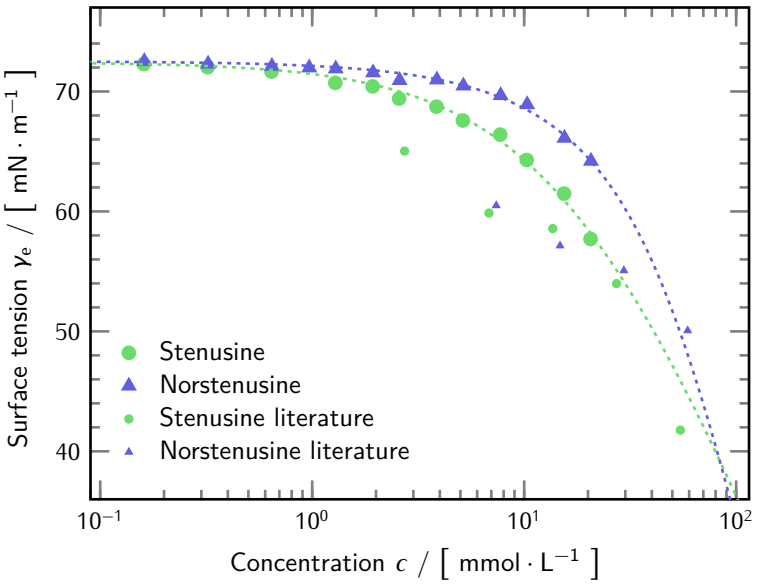

Figure IV.1: Experimental equilibrium surface tension isotherms of stenusine, norstenusine and the respective best fits (dotted lines) according to the Frumkin adsorption isotherm. Published literature data extracted from dynamic surface tension measurements are shown for comparison. [167]

Starting already from low alkaloid concentrations, a considerable reduction of the equilibrium surface tension of water begins at the 1 mmol · L^{-1} regime for stenusine and roughly at about the tenfold molar concentration for norstenusine. Increasing the concentrations further induces a drop-off in equilibrium surface tension γ_e to values of 58 or 64 mN · m^{-1} for the respective 20.6 mmol · L^{-1} stock solutions. They were characterized further by surface dilatational rheology.

1.2 Oscillating Bubble and Pendant Drop Rheology

The frequency dependent values of the amplitude and phase shift of the surface dilatational modulus E for aqueous solutions of stenusine and norstenusine at concentrations of 20.6 mmol · L^{-1} in the frequency range accessible by the oscillating bubble technique are shown in Figures IV.2 and IV.3, respectively.

The amplitude of the surface dilatational modulus E featured a moderate increase for the studied solutions of stenusine and norstenusine. Furthermore, a rising phase angle between the induced surface area perturbation and the measured pressure response at frequencies exceeding 100 Hz was observable.

The experimental data was fitted appropriately to the extended Lucassen-van den Tempel (LvdT)-model by tuning the parameters to simultaneously match the amplitude and phase angle according

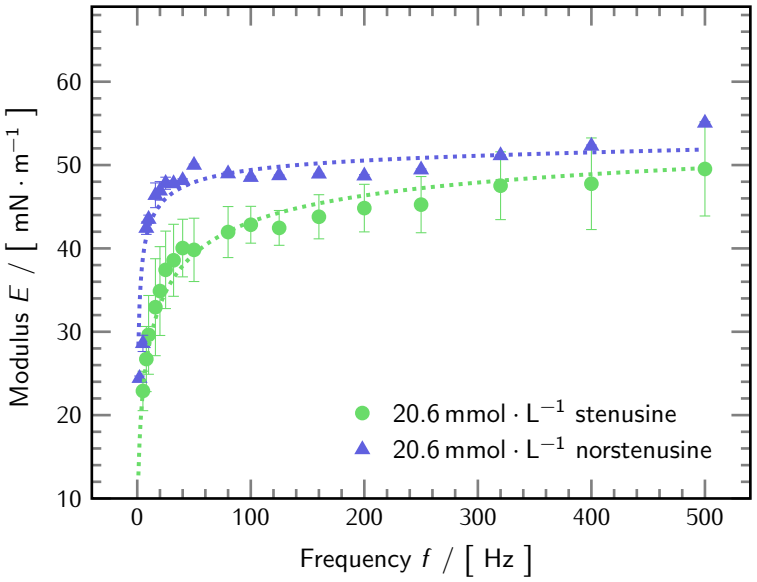

Figure IV.2: Amplitude of the frequency dependent surface dilatational modulus E of stenusine, norstenusine and the respective best fits (dotted lines).

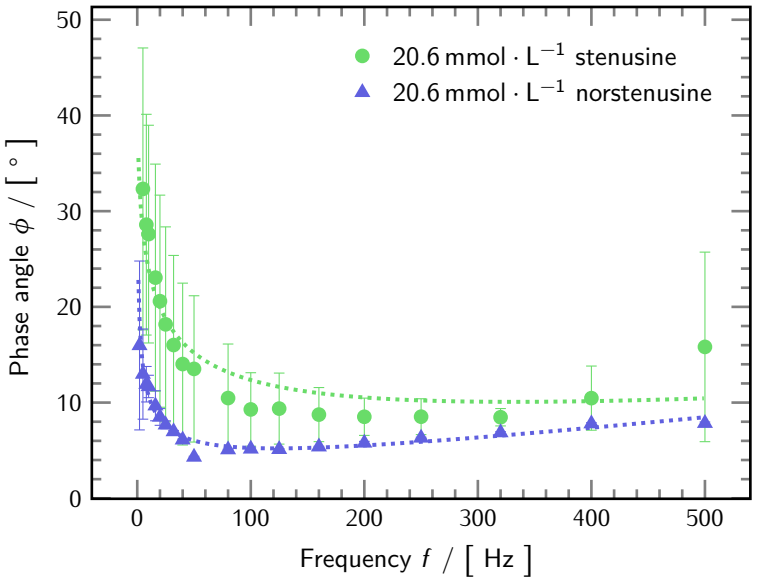

Figure IV.3: Frequency dependent phase angle ϕ of stenusine, norstenusine and the respective best fits (dotted lines).

to the previously described procedure. The best values of the model parameters are summarized in Table IV.1 and the corresponding theoretical curves of magnitude and phase angle are shown in Figures IV.2 and IV.3, respectively.

Table IV.1: Best values of parameters for matching the model described in Equation II.118 to the experimental data obtained from the oscillating bubble device.

Solution	c [$\mathrm{mmol \cdot L^{-1}}$]	ϵ^{m} [$\mathrm{mN \cdot m^{-1}}$]	f_{diff} [Hz]	κ [$\mathrm{N \cdot s \cdot m^{-1}}$]
Stenusine	20.6	54.8	1.245	$1.305 \cdot 10^{-6}$
Norstenusine	20.6	53.0	1.051	$1.919 \cdot 10^{-6}$

A joint overview of surface dilatational characteristics in terms of amplitude and phase angle in the accessible frequency range spanning around five orders of magnitude by combining data from oscillating pendant drop (OPD) and oscillating bubble (OB) rheological measurements is given in Figures IV.4 and IV.5, respectively. The additional data from oscillating pendant drop experiments were found to follow a rather monotonous trend for both the amplitude of the surface dilatational modulus E and the phase angle ϕ. Whereas the amplitude of the pendant drop data increased with frequency, the phase angle ϕ gradually approached lower values. Except for some outliers in the transition zone between the two sets of experiments approximately from 0.7 to 5 Hz, *i.e.,* the limiting operating range of the respective devices, a sound continuity was observable. This holds true especially for the amplitude of the surface dilatational modulus E.

The dotted and dashed lines in Figures IV.4 and IV.5 correspond to the best fit curves according to an extended version of the model suggested by Ravera *et al.* allowing for a formal description of the rheological characteristics of adsorption layers over a broad frequency range.[156] Details on the data processing are given in subsection 11.1.

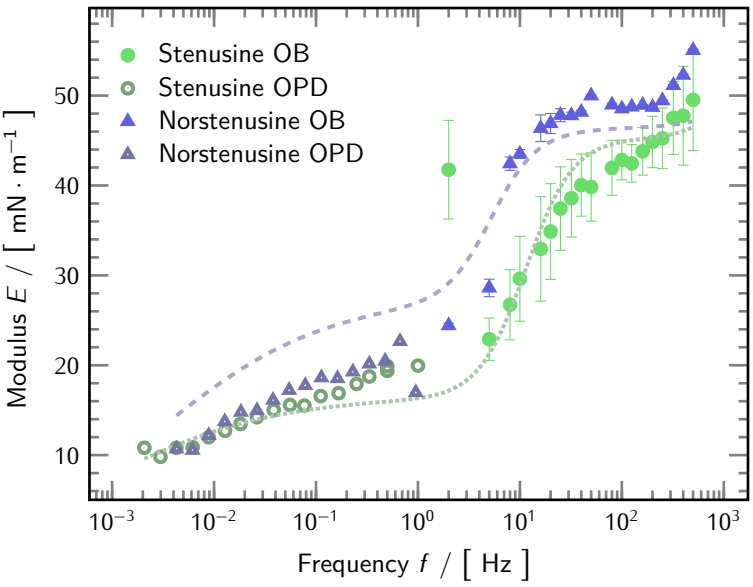

Figure IV.4: Frequency dependent surface dilatational modulus E of 20.6 mmol · L^{-1} aqueous solutions of stenusine and norstenusine as obtained from oscillating pendant drop experiments and oscillating bubble experiments. The lines correspond to the best respective fits of an extended model originally proposed by Ravera, Ferrari and Liggieri.[156]

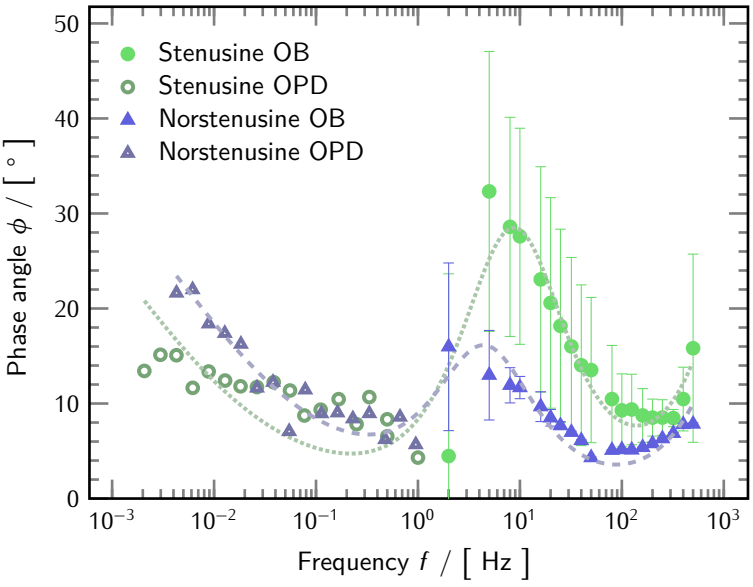

Figure IV.5: Frequency dependent phase angle ϕ of 20.6 mmol · L^{-1} aqueous solutions of stenusine and norstenusine as obtained from oscillating pendant drop experiments and oscillating bubble experiments. The lines correspond to the best respective fits of an extended model originally proposed by Ravera, Ferrari and Liggieri.[156]

2 Mixed Surfactant-Electrolyte System

The anionic surfactant sodium dodecyl sulfate (SDS) is probably one of the most well-known substances in colloid and interface science. A consultation of Web of Science® reveals that over 69 000 articles have been published where SDS either plays a key role in applications or is used as a model system to address fundamental questions. Besides its wide-spread applications in personal care and industrial cleansing products, it is used as a standard reagent in SDS polyacrylamide gel electrophoresis (SDS-PAGE) for separation purposes.[206,207] Furthermore, its action in boosting the antimicrobial activity of levulinic acid on pathogens in biofilms is known.[208]

There is an interesting approach illustrating the versatility of this water soluble anionic amphiphile: Combination of SDS with silica nanoparticles and the cationic surfactant cetyltrimethylammonium bromide (CTAB) to leads to the formation of stimuli responsive foams.[209] Alternating addition of equimolar quantities of CTAB and SDS was used to compensate the surface charge. Furthermore, mixtures of the salts NaCl and KCl with solutions of SDS were found to produce ultra-stable thermo-responsive foams.[210]

Only recently, a study on the influence of the electrolyte NaCl on the stability of foams generated from SDS has been published by Wang and coworkers.[211] Next to measuring dynamic surface tension and zeta-potential, the authors attempted to establish a correlation between decreasing foam stability upon increasing salt concentration and the surface rheological characteristics. Therefore, measurements using the oscillating pendant drop method at a fixed perturbation frequency of 0.05 Hz have been carried out. The influence of co-adsorption of the hydrolysis product corresponding to SDS, *n*-dodecanol, into adsorption layers of SDS in an extended frequency range has been studied in detail by Wantke *et al.* in 2003.[121]

In this section, similar issues have been taken up and studied in more detail. The dynamic properties of mixed adsorption layers formed from SDS and NaCl subject to dilatational deformation were considered in a wider frequency range from 5 to 400 Hz using the oscillating bubble method. Validation of these results was sought by both checking the connection to lower frequency oscillating pendant drop data and opto-mechanical electrocapillary wave (ECW)-experiments operating at comparable and higher perturbation rates as the oscillating bubble. This intends to further describe the system proposed by Wang *et al.* and gain additional insight into the processes governing the stability of the respective foams. A rheological characterization of the adsorption layers relying on only one relatively low perturbation frequency seems insufficient. This calls for an in-depth consideration of the frequency dependent surface dilatational modulus over a broad range probed independently by a spectrum of methods.

Aqueous mixtures of SDS in a surface chemically purified state and high purity NaCl were studied with respect to their equilibrium and dynamic surface tensions at a constant mean ionic activity I_{mean} of $1\,\text{mmol}\cdot\text{L}^{-1}$. All studied solutions characterized by roughly the same equilibrium surface tension, were analyzed with respect to their differences in foam column and foam lamella stability experiments.

Investigations by means of the oscillating bubble technique were conducted to determine the frequency dependence of the surface dilatational modulus E. The obtained results could be described by the extended Lucassen-van den Tempel (LvdT)-model, which allows capturing dissipative processes within the interfacial region via the intrinsic surface dilatational viscosity κ. A new dimensional parameter derived from the fitting parameters of the LvdT-model correlates reasonably with direct measurements of the solutions' foam stability. Further corroboration for this observation was obtained from oscillating pendant drop and ECW experiments complementing the frequency range accessible by the oscillating bubble method towards lower and higher frequencies, respectively. The data suggest the important role of surface dilatational rheology for the stability of foams. Spectroscopic investigations using infrared reflection absorption spectroscopy (IRRAS) and sum frequency generation vibrational spectroscopy (SFGVS) were used to shed further light on the interfacial arrangement on a molecular level.

2.1 Surface Tension

The equilibrium surface tension γ_e is plotted against the bulk concentration of SDS in Figure IV.6. Each experimental surface tension value represents the average value of 10 measurements performed within a time span on the order of three minutes by a ring tensiometer. Changes in surface tension were below $0.1\,\mathrm{mN \cdot m^{-1}}$, *i.e.*, an equilibration of SDS adsorption has been attained. For comparison, published literature equilibrium surface tension isotherms of SDS obtained at different degrees of surfactant purity are shown.[170,212]

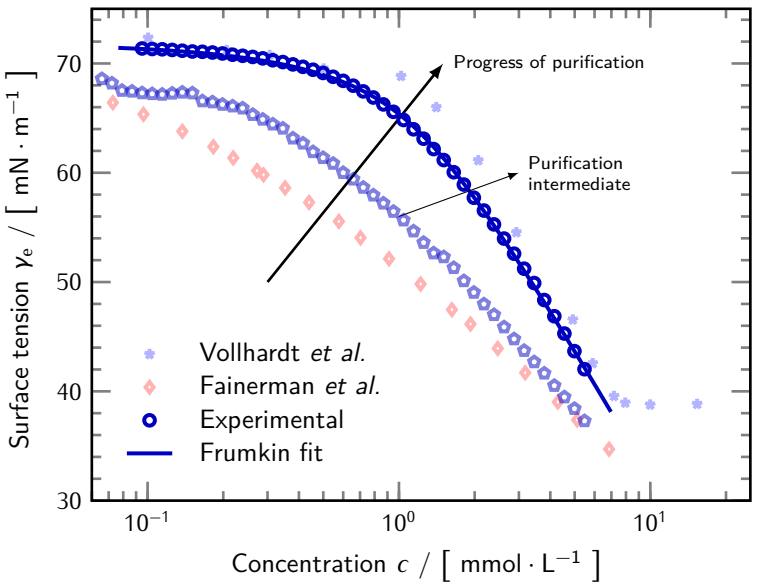

Figure IV.6: Equilibrium surface tension isotherms of SDS. Experimental results, comparison to literature data (Vollhardt *et al.*[170] and Fainerman *et al.*[212]) and best fit of experimental data according to the Frumkin isotherm.

Whereas the values measured by Vollhardt *et al.*[170] for surface chemically purified SDS agree with the experimental data from this study, a clear deviation with respect to the data shown by Fainerman *et al.* is apparent.[212] The latter values had been obtained using the commercially available SDS as received. Despite the similarity of measured surface tension at high concentrations, there were considerable deviations between purified and non-purified solutions in the concentration range below $5\,\mathrm{mmol \cdot L^{-1}}$ with a maximum difference at intermediate concentrations around $1\,\mathrm{mmol \cdot L^{-1}}$.

To ensure similar equilibrium properties of the solutions (see Table III.1) studied also with other experimental techniques, time dependent measurements of surface tension were carried out. The findings are compared in Figure IV.7. For all studied solutions, surface tension remained constant within $0.2\,\mathrm{mN \cdot m^{-1}}$ during the experimental time scale. Despite the fact that different concentrations of surfactant SDS were used, similar values around $65\,\mathrm{mN \cdot m^{-1}}$ were measured for solutions SDS-NaCl-1 to SDS-NaCl-5 (see Table III.1). Only solution SDS-NaCl-6 with the highest amount of NaCl and lowest amount of surfactant exhibited a surface tension around $2\,\mathrm{mN \cdot m^{-1}}$ higher as compared to the other solutions characterized by the same mean ionic activity I_{mean}.

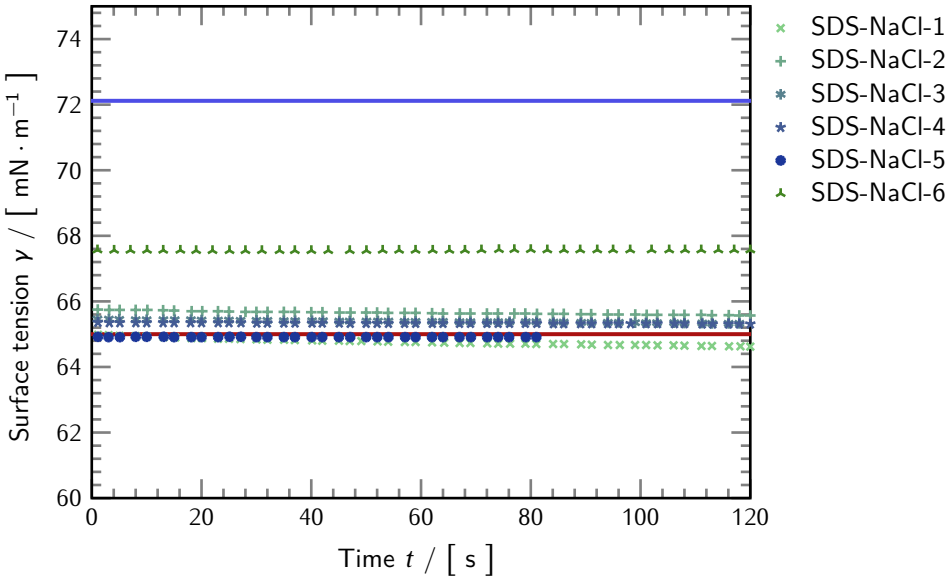

Figure IV.7: Dynamic surface tension of the studied solutions as specified in Table III.1. Values of water (solid blue line around $72\,\mathrm{mN \cdot m^{-1}}$) and $1\,\mathrm{mmol \cdot L^{-1}}$ SDS (solid red line around $65\,\mathrm{mN \cdot m^{-1}}$) for comparison.[169]

Additionally, the published equilibrium surface tension value of $1\,\mathrm{mmol \cdot L^{-1}}$ SDS is shown. It was found to agree very well with the experimental values from this study (Solution SDS-NaCl-1).[169] To check the purity of the used glassware, also the surface tension of water was measured and confirmed to be close to its literature value.

2.2 Sum Frequency Generation Vibrational Spectroscopy

Sum frequency generation (SFG) vibrational spectra of the studied solutions in the spectral range from 2800 to 3000 cm^{-1} are compared in Figure IV.8.

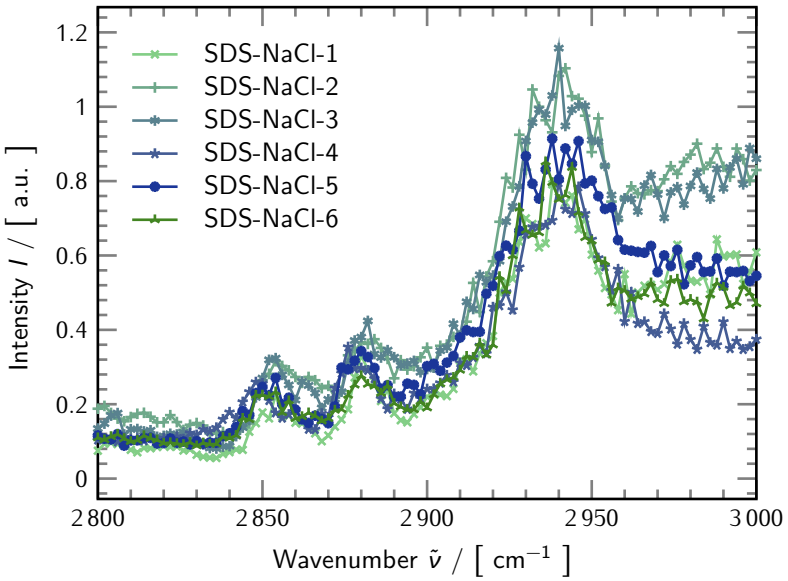

Figure IV.8: SFG-spectra of the studied solutions as specified in Table III.1 measured under *ssp*-polarization.

Despite the rather pronounced noise, they were found to agree especially below 2900 cm^{-1}. At higher wavenumbers, the differences between the samples become more distinct. However, they were found to follow a non-monotonous course within the series of specimens considered upon approaching the 3000 cm^{-1} border. This unusual behavior also holds within the spectral region characteristic of the interfacially confined water (spectral region from 3200 to 3700 cm^{-1}, not shown in Figure IV.8).

2.3 Infrared Reflection Absorption Spectroscopy

In contrast to the previously shown data from SFG-experiments, the surface specific information obtained from IRRAS under *s*-polarization shows a more pronounced trend across the series of samples as depicted in Figure IV.9.

Upon increasing the relative amount of salt in the mixtures characterized by a constant equilibrium surface tension γ_e around 65 $mN \cdot m^{-1}$, a clear decrease in reflectance-absorbance (RA) around 3600 cm^{-1} was observable. As IRRAS is to be understood as another special type of infra-red (IR)-spectroscopy, this domain is characteristic of the interactions between water molecules, *i.e.,* the hydrogen bonding network. Therefore, information on its disturbance in the presence of surface active compounds can be inferred.

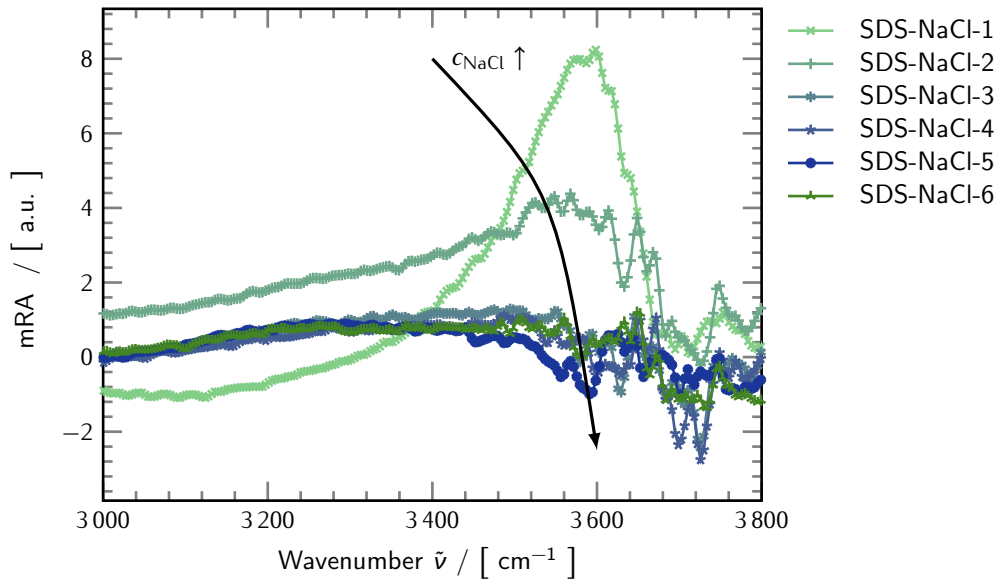

Figure IV.9: IRRAS-spectra of the studied solutions as specified in Table III.1 measured with *s*-polarization.

2.4 Foam Stability

The results on stability of foam columns and single foam lamellae are represented in Figure IV.10. A general trend is clearly visible. Upon increasing the relative amount of salt with respect to the surfactant, the stability of both foam columns and individual foam lamellae decreased. For foam columns this is represented by reduced values of the half-life time $t_{1/2}$, *i.e.*, the time required for half of the foam height to decay and the R5-value. This is the characteristic parameter representing the relative remaining foam height five minutes after the foaming process has ceased. Single foam lamella stabilities measured in repeated experiments confirm these findings. Exemplarily, the characteristic time $\tau_{\text{Lamella}90\,\%}$ is given. It represents the time required for 90 % of the individual foam lamellae to rupture. The asymmetry in the error bars arises due to the fact that this parameter is given with an error of ±5 %. A larger error bar towards longer times is the consequence of the elongated time required for 95 % than for 85 % of the lamellae to collapse.

For solutions SDS-NaCl-1 to SDS-NaCl-4, a clear decrease in foam and lamella stability was observed, which is visible from the course of the three studied parameters. Solutions SDS-NaCl-5 and SDS-NaCl-6, however, do not lead to the formation of stable foams.

2.5 Oscillating Bubble

The surface dilatational characteristics of solutions SDS-NaCl-1 to SDS-NaCl-6 are given in Figure IV.11 for the amplitude and in Figure IV.12 for the phase angle ϕ, respectively. Whereas the magnitude

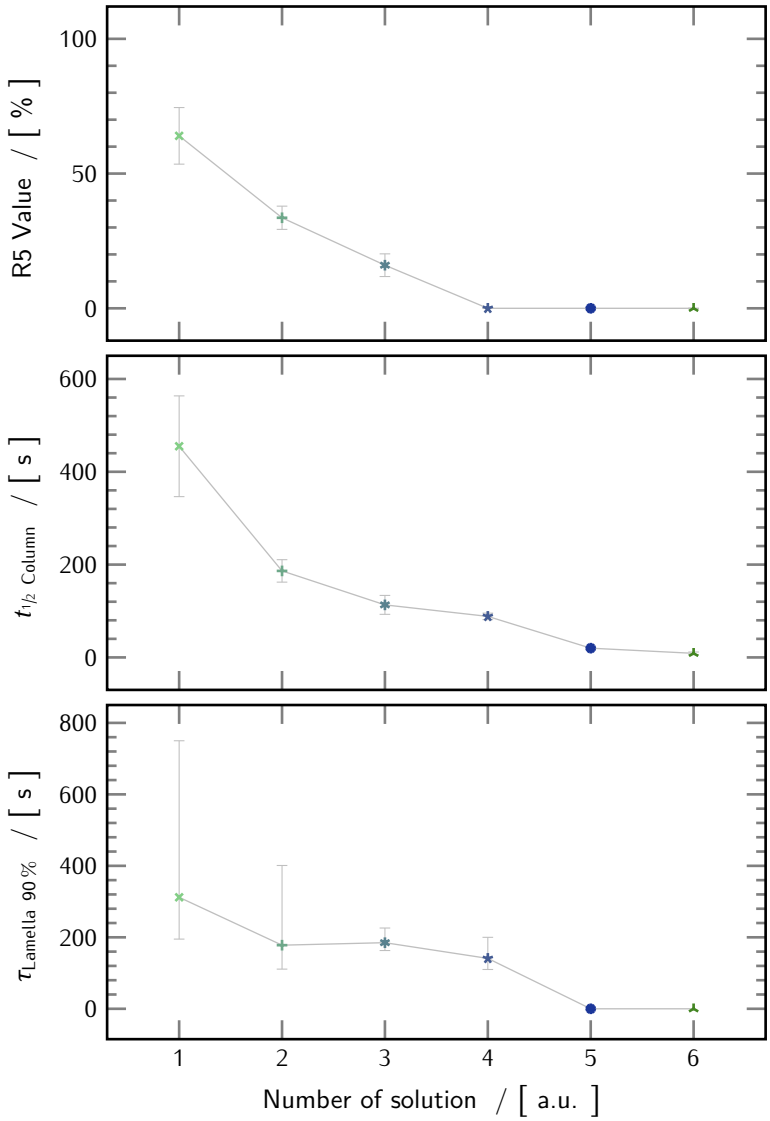

Figure IV.10: Characteristic parameters of foam column and single foam lamella stability of the studied solutions as specified in Table III.1. Top: R5-value. Middle: Half-life time of a foam column. Bottom: Time required for 90 % of individually studied foam lamellae to rupture. (Solid line as guide to the eye).

of the surface dilatational modulus E remained within a range between 40 and 60 $mN \cdot m^{-1}$, larger differences were observed for the phase angles of the studied solutions. Upon increasing the relative salt content, they were found to pass through a maximum before approaching zero at frequencies above 100 Hz.

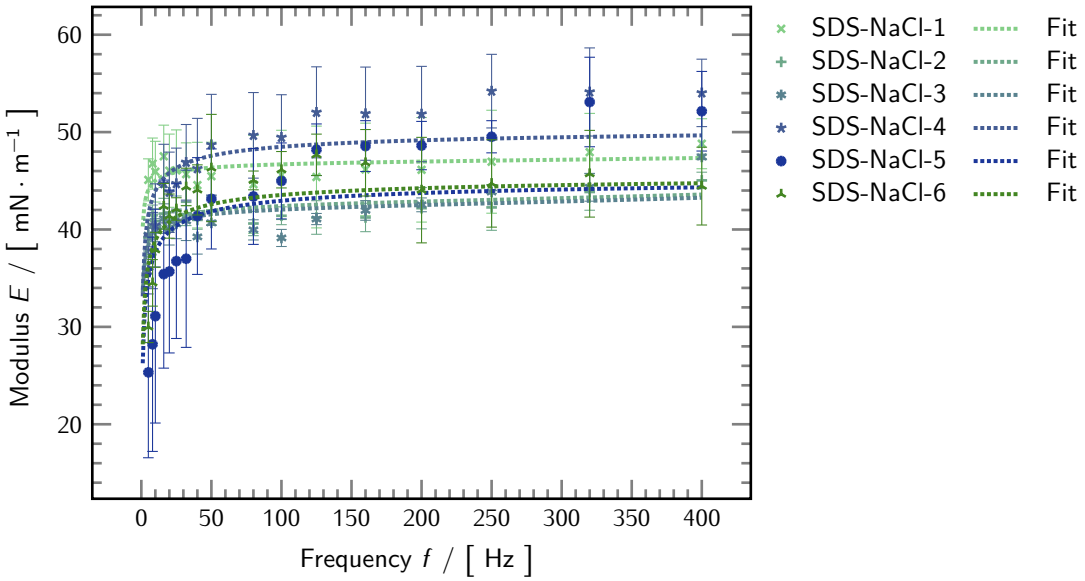

Figure IV.11: Magnitude of the surface dilatational modulus E of aqueous mixtures of SDS and NaCl as specified in Table III.1 and the respective fits as dotted lines.

2.6 Electrocapillary Wave Experiments

The surface dilatational characteristics of the SDS-NaCl mixtures obtained from ECW-experiments are compared in their representation as amplitude and phase angle in Figures IV.13 and IV.14, respectively.

The most apparent observation at a first glance is, that this set of data is subject to larger scatter as compared to the oscillating bubble results gathered in a comparable frequency range. Due to the wider accessible spectrum of this method, a logarithmic scaling of the frequency axis was chosen for the ECW-data. Nevertheless, a trend within the series was observable. Upon increasing the relative amount of salt contained in the respective solution, both the amplitude and the phase angle of the surface dilatational modulus E were found to decrease over the vast majority of sampled frequencies.

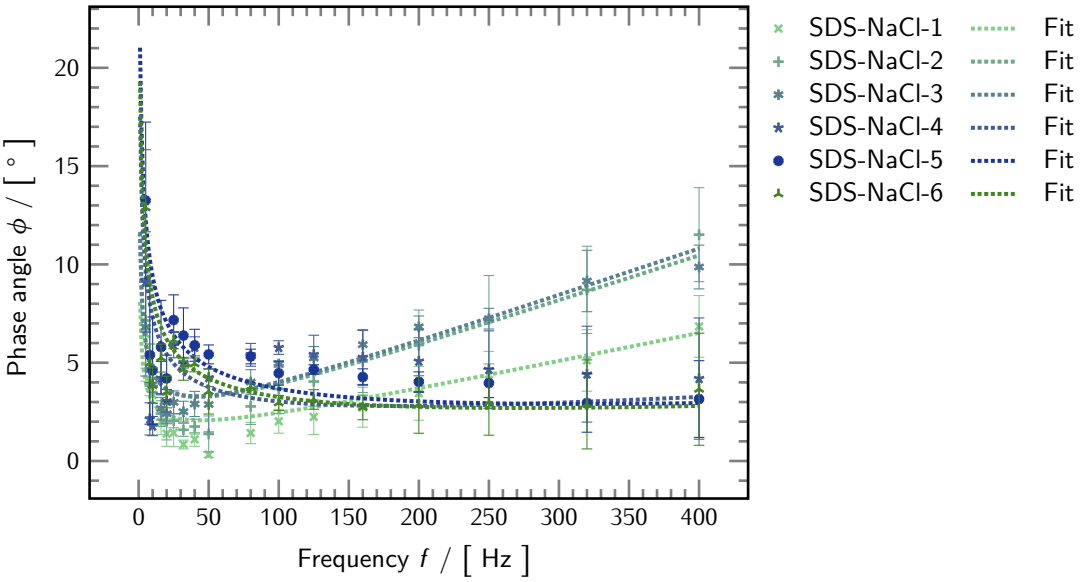

Figure IV.12: Phase angle of the surface dilatational modulus E of aqueous mixtures of SDS and NaCl as specified in Table III.1 and the respective fits as dotted lines.

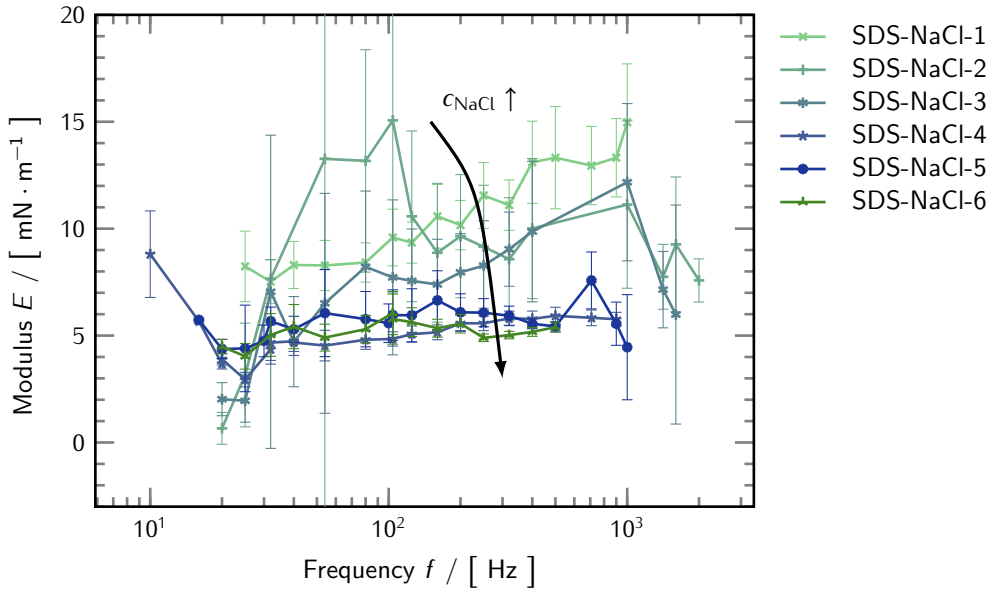

Figure IV.13: Magnitude of the surface dilatational modulus E of aqueous mixtures of SDS and NaCl as specified in Table III.1 obtained from ECW.

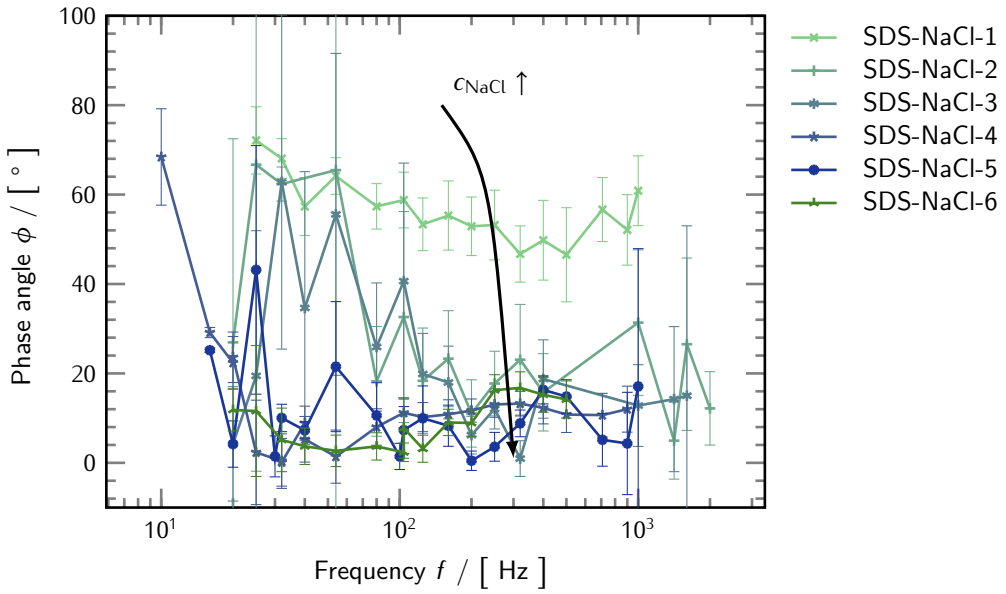

Figure IV.14: Phase angle of the surface dilatational modulus E of aqueous mixtures of SDS and NaCl as specified in Table III.1 obtained from ECW.

3 Ion Specific Effects in Alkali Decyl Sulfates

Physico-chemical properties of solvents, solutes, dispersed and biological systems are known to be influenced in a specific manner by the mere presence of electrolytes.[174] This includes influences on the „inner friction“, *i.e.,* viscosity,[213] vapor pressure of water,[214] freezing point depression,[215] molecular diffusion against water,[216] osmotic coefficients,[217] and surface tension.[218] The most prominent effects of ion specificity, however, have been observed in systems containing more components than just water and the electrolyte. Following up contemporary research, Hofmeister *et al.* demonstrated the ability of salts to precipitate proteins from blood serum and egg white in a systematic study. Depending on the nature of the electrolyte, the precipitation was found to occur at a specific concentration.[219,220] The strength of these effects depends both on the anion and the cation used in the course of the experiment, but the influence of the anion generally is assumed to be stronger. For simple, monovalent cations, which will be used in the following, this *Hofmeister series* of cation influence is given by

$$Li^+ < Na^+ < K^+ < Rb^+ < Cs^+ < NH_4^+ < NMe_4^+.$$

Next to the ion specific effects of electrolyte on biological systems, the same consequences for the stability of aqueous suspensions of isinglass, colloidal ferric oxide and sodium oleate could be confirmed. In more recent contributions, Hofmeister effects on coalescence of surfactant free bubbles have been studied.[221,222]

Generally, stabilization of foam lamellae and bubbles is more effective with amphiphilic molecules present at the interface. Counterion effects on the thermodynamics of the micellation behavior in studies of purified surfactant solutions have been evidenced. Ropers *et al.* described ion specificity in temperature dependent determination of critical micellar concentration (cmc) and the associated enthalpy by means of isothermal titration calorimetry (ITC) for both decyl sulfate (DeS) and dodecyl sulfate (DS) with counterions Li, Na, K and Cs.[223] At elevated concentrations high above the cmc, solutions of potassium alkyl sulfates are not entirely soluble. Consequently, the solutions contain hydrated crystals dispersed in a micellar phase. The phenomenon of a solubility gap for potassium alkyl sulfates has been reported[224–226] and might be associated to the higher foam stability of this kind of solutions studied in the following. Analytical chemistry sets the stage for applications of ion specific effects in separation processes. The efficiency and resolution in micellar electrokinetic chromatography could be tuned successfully by replacing the sodium counterion of the typically used pseudostationary phase sodium dodecyl sulfate (SDS) by other monovalent ions. Also on this occasion, potassium DS stood out due to its high Krafft temperature.[227] Furthermore, the addition of baryte solution caused an ion specific flocculation behavior dependent on the temperature. Maximum flocculation with formation of larger aggregates was observed in case of lower solubility of the used surfactant, *i.e.,* especially below its Krafft point.[228] This characteristic is equally reported to depend on the counterion in more complex mixtures containing a certain amount of foam booster.[229] The Krafft temperature describes the temperature above which micelle formation is possible.

In the context of foam and lamella stability, the type of counterion was shown to significantly influence the disjoining pressure in foam lamellae.[230] Furthermore, pronounced anion specific effects on the equilibrium adsorption properties of cationic surfactants were reported and ascribed to deviating excess polarizabilities of the respective ions.[231,232] This is in agreement with the recently emerging picture of the air-water interface characterized by specific affinity for „soft“ ions and non-monotonous ion concentration profiles perpendicular to the interface.[233,234]

In the following, ion specific effects in pure surfactant solutions of alkali decyl sulfates (XDeSs) with counterions Li, Na, K and Cs will be studied both under equilibrium and dynamic conditions using the oscillating bubble method. A possible rationale for the experimentally acquired foam stabilities taking into account the unified information on the adsorption layer characteristics will be given.

3.1 Equilibrium Surface Tension Isotherms

All of the studied surfactant solutions were characterized by decreasing surface tension upon increasing bulk concentration. As evident from Figure IV.15, the surface tension increased from cesium decyl sulfate (CsDeS) over sodium decyl sulfate (NaDeS) and potassium decyl sulfate (KDeS) to lithium decyl sulfate (LiDeS) comparing identical amphiphile concentrations. An ordering in the sense of an ion specific series was obeyed.

An alternative representation of the surface tension data obtained for the studied XDeSs applying

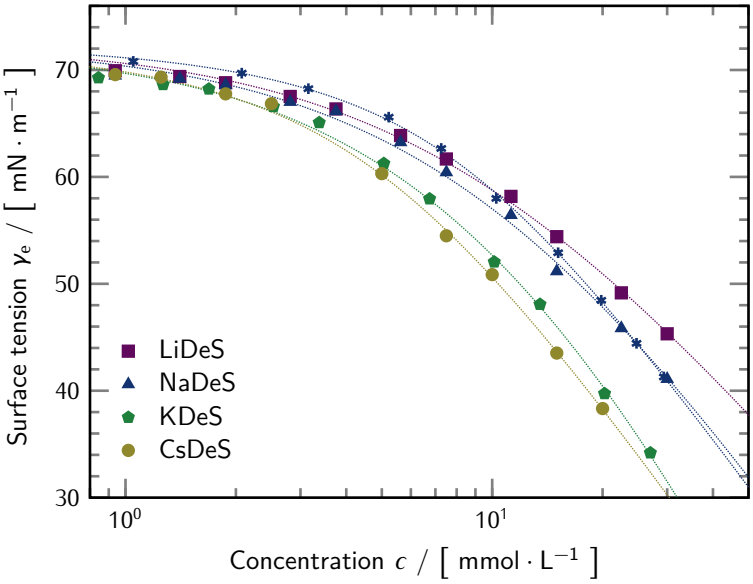

Figure IV.15: Equilibrium surface tension isotherms of aqueous solutions of XDeS measured at room temperature.

another scaling of the concentration axis is given in Figure IV.16. Therein, the distinction between the studied solutions in terms of surface specificity introduced by the presence of different counterions appears in a more pronounced manner. The trend of decreasing equilibrium surface tension γ_e observed upon going from lithium to cesium as the monovalent alkali counterion for DeS necessarily remains unchanged.

3.2 Time Dependent Surface Tension

The pendant drop tensiometer described previously was used to collect values of time dependent surface tension for durations up to 300 s after the formation of a droplet. As shown in Figure IV.17, the solutions were characterized by a rather low decrease within the experimental time frame. The respective concentrations of the studied XDeSs were chosen according to the experimental equilibrium surface tension isotherms (see Figure IV.15) in order to arrive at equilibrium surface tension γ_e values of approximately 45, 55 and 65 mN · m^{-1}.

Despite the slight decrease, the respective target value of equilibrium surface tension γ_e could be achieved within the accuracy required for the further characterization of the solutions by means of surface dilatational rheology and measurements of foam stability.

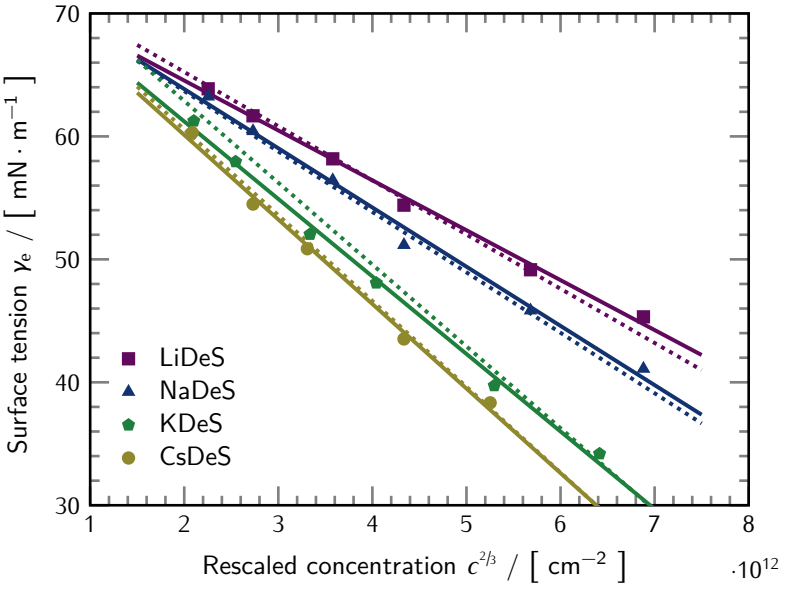

Figure IV.16: Equilibrium surface tension isotherms of aqueous solutions of XDeSs measured at room temperature in a representation leading to linearization of the acquired surface values of equilibrium surface tension γ_e.

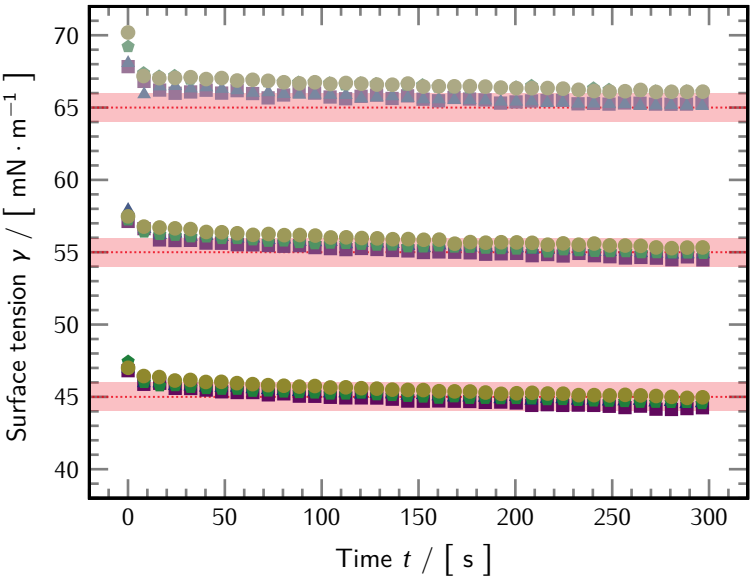

Figure IV.17: Time dependent values of surface tension of the studied solutions of XDeSs with the aim of reaching value of equilibrium surface tension γ_e around 45, 55 and 65 mN · m^{-1} measured at room temperature. The shaded areas indicate the surface tension range of ±1 mN · m^{-1} around the target value.

3.3 Foam Stability

The decay of foam column height with time for the studied solutions of XDeSs is compared in Figure IV.18. For the experiments conducted with these short alkyl chain surfactants, slightly different parameters compared to the previously described protocol were applied during the foaming phase. The solution volume was reduced to 30 ml at a simultaneous increase of the gas flow rate to $0.5\,\mathrm{L}\cdot\mathrm{min}^{-1}$.

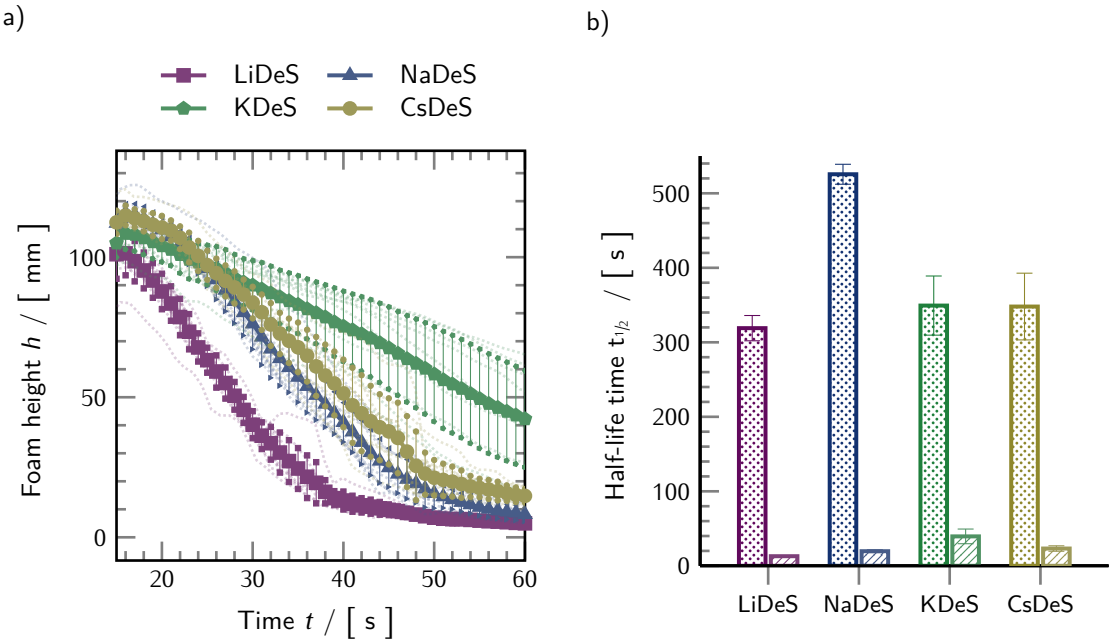

Figure IV.18: a) Time dependence of foam column heights of aqueous solutions of the studied XDeSs for solutions of constant equilibrium surface tension γ_e of $55\,\mathrm{mN}\cdot\mathrm{m}^{-1}$. Dotted lines represent the heights of individual runs. b) The characteristic half-life times of the XDeSs are compared for solutions of $45\,\mathrm{mN}\cdot\mathrm{m}^{-1}$ (dotted bars) and $55\,\mathrm{mN}\cdot\mathrm{m}^{-1}$ (striped bars).

The conducted foam stability experiments equally allowed for a distinction between the individual XDeSs for solutions studied at the same nominal equilibrium surface tension γ_e. However, a clear trend of increasing or decreasing foam column stability along the range from lithium to cesium was not evident.

3.4 Oscillating Bubble

The characteristic trends obtained from oscillating bubble experiments in this counterion- and concentration dependent study are summarized in Figures IV.19 to IV.22. To avoid an overcrowding of the respective plots, Figures IV.19 and IV.20 show the amplitude and phase angles of the surface

dilatational modulus E, respectively, as obtained for solutions with different counterion at a fixed value of equilibrium surface tension γ_e. The influence of surfactant concentration for a given counterion (here K) is shown in Figures IV.21 and IV.22. It is to be noted that the trends described in the following equally hold for the other measured solutions with their respective variations in equilibrium surface tension γ_e and type of counterion.

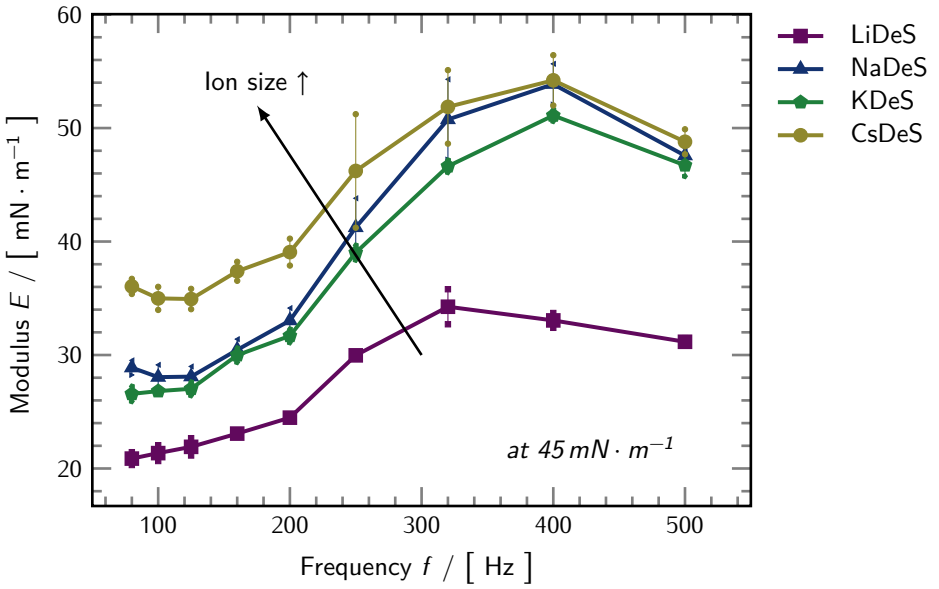

Figure IV.19: Trends of the amplitude of the surface dilatational modulus E for the studied XDeSs. At the same value of equilibrium surface tension ($45\,\mathrm{mN \cdot m^{-1}}$), the amplitudes tend to increase with size of the counterion in the order Li $<$ (Na $<$) K $<$ Cs over almost the entire frequency range covered.

Considering the solutions of anionic DeS surfactant ions in the presence of different counterions at a fixed value of equilibrium surface tension (here $45\,\mathrm{mN \cdot m^{-1}}$), a clear trend – except for NaDeS – is evident from both amplitude and phase angle data. Over almost the entire frequency range covered with the oscillating bubble device, a monotonous transition from lithium to cesium as observed for the equilibrium surface tension data, was confirmed. Whereas the amplitude increases from counterions Li via Na and K to Cs, this type of behavior is more or less recovered for the phase angle data. The difference lies in the observation, that for the latter kind of data, the discrimination between Na, K and Cs is less pronounced compared to the amplitude information and that the solution of NaDeS disobeys its established ordering in the series. Especially concerning the amplitude, solutions of NaDeS and KDeS behave similarly.

The concentration dependent, *i.e.*, equilibrium surface tension dependent results for the three studied samples of each XDeS are characterized by a similar and consistent progression. Exemplarily, the results for amplitudes and phase angles of the surface dilatational modulus E collected for KDeS are considered. Just as in the case of the remaining XDeS, increasing the surfactant concentration, *i.e.*,

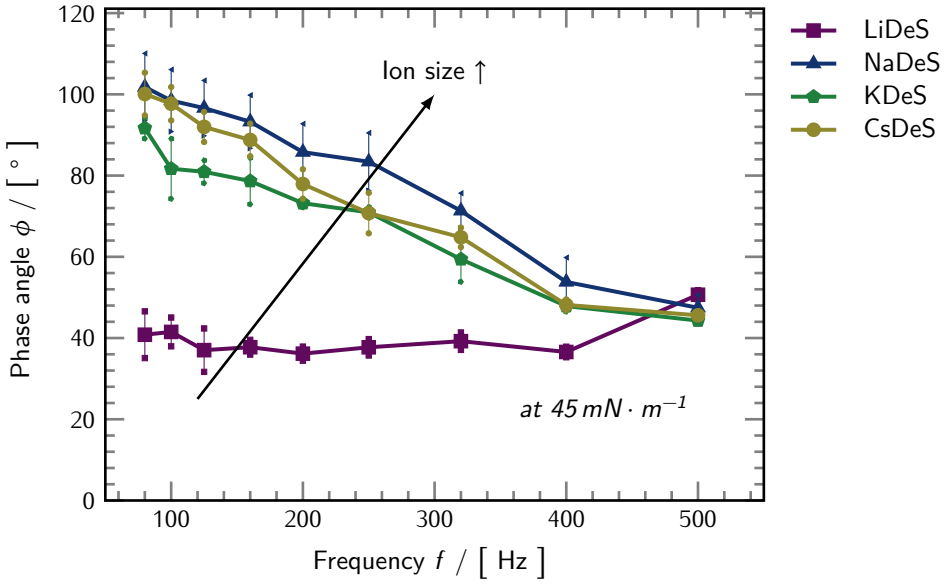

Figure IV.20: Trends in the phase angle of the surface dilatational modulus E for the studied XDeSs. At the same value of equilibrium surface tension ($45\,\mathrm{mN \cdot m^{-1}}$), the phase angles tend to increase with size of the counterion in the order Li $<$ (Na $<$) K $<$ Cs over almost the entire frequency range covered.

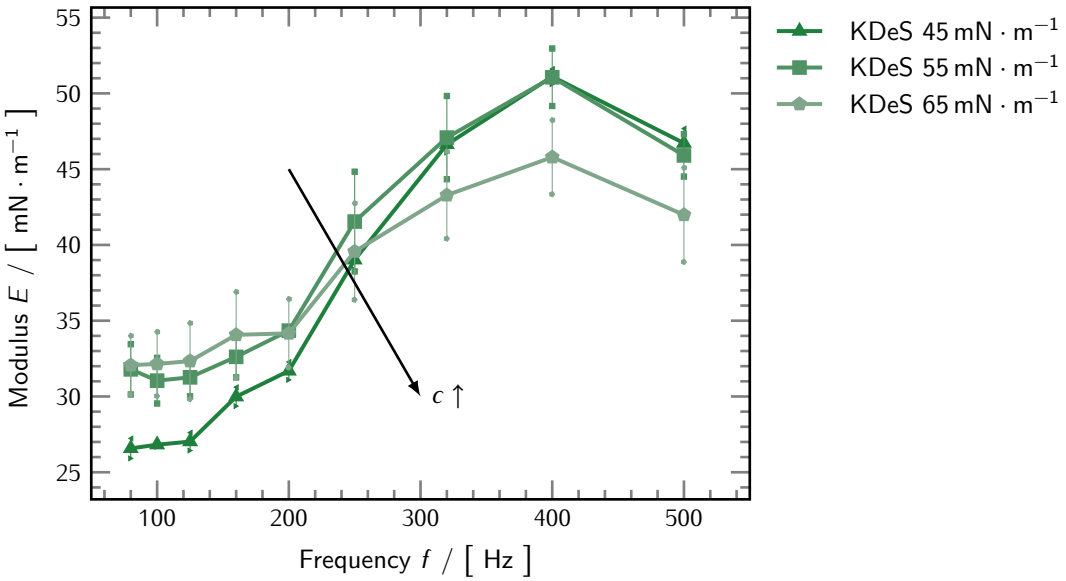

Figure IV.21: Exemplary concentration dependence of the amplitude of the surface dilatational modulus E for solutions of KDeS. An increase in surfactant bulk concentration tends to lead to a reduction in the amplitude.

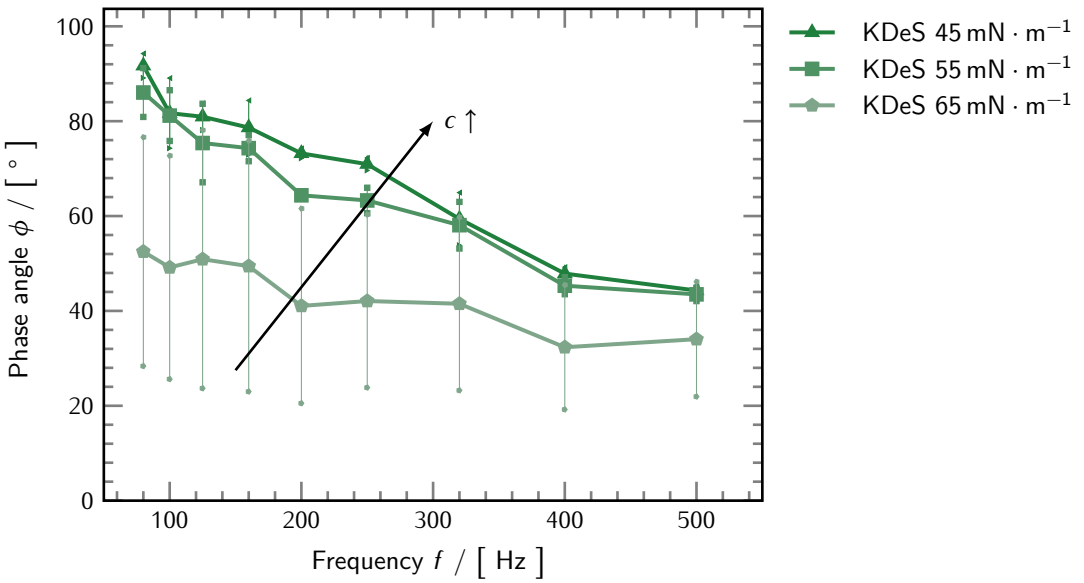

Figure IV.22: Exemplary concentration dependence of the phase angle of the surface dilatational modulus E for solutions of KDeS. An increase in surfactant bulk concentration tends to lead to an elevated phase shift.

transition to lower values of equilibrium surface tension γ_e causes the amplitude to decrease and the phase angle to increase over most of the frequency range covered.

4 Ion Specificity in Adsorption Layers of *n*-Dodecylphosphinecholine

The common denominator of modern and desirable technology is „going green“ due to the increasing awareness of environmental threats in most parts of the developed western world. Windmill-powered plants deliver sustainable energy devoid of primary greenhouse gas emissions during operation. The implementation of this technology is far advanced and some countries such as Denmark aim to supply a considerable amount of the required electricity demand from renewable sources with a large share of wind power.[235]

Also, consciousness of the limited oil resources and the impact on climate caused by fossil fuel combustion is rising. An alternative form of individual transport is offered by e-mobility moving away from the traditional vehicle design powered by gasoline. One of its key elements is the need for strong permanent magnets, comprising rare earth metals, which are characterized by a significantly stronger magnetic field than other known materials. This superiority of rare earth metals is a consequence of their electron configuration in the *f*-shell and the crystalline structure of the corresponding metals and alloys that preferentially magnetizes along a specific crystal axis.[236]

Lanthanides also play an important role in the nuclear industry. They possess a high neutron absorption cross section and are used in nuclear power plants, where they are implemented inside control rods for the regulation of the neutron flux. Furthermore, they are utilized as shielding materials around reactors. In short, lanthanides are a key ingredient to high-end state-of-the-art and trend-setting technologies. Originally, lanthanides were referred to as „rare earth elements“. Chemists once thought that these elements only occur in small amounts in the earth's crust. This assumption turned out to be incorrect. Rather than their sparsity, the main challenge with lanthanides for chemist is their similarity. Due to their ionic radii differing by as little as 0.15 Å from lanthanum to lutetium, they appear together in numerous naturally available minerals for the reason of isomorphic permutability.[237] Therefore, they are extremely difficult to separate from each other. The deeper reason is related to the electronic structure introduced by the filling of inner $4f$-electron shells with little impact on the resulting chemistry, which is dominated by the valence electrons. The separation of lanthanides at industrial scale continues to remain a significant technical challenge. Valuable ions should be recovered and recycled from waste. In a typical separation process, the ions to be recovered are dissolved in a small quantity of water and subsequently complexed into an organic phase by an oil-soluble ligand. Separation methods based on this kind of selective binding-process rely on ion specific effects. Lanthanide cations bind strongly to phospholipids, but less to sulfobetaines and weakly to malonamides, which are used for lanthanide extraction in the nuclear industry.[238] Generally, ion specificity is a subject of great importance for the separation of lanthanides.

Besides, effects of ion specificity in different fields ranging from biology to colloidal chemistry have been of interest to several generations of researchers starting with the early experiments of Hofmeister.[219] Fostered by advances in instrumentation and theory, a new picture of ion specificity deviating from

previous concepts are emerging.[239–242] Especially the importance of dispersion forces was found to be enlightening for several surface specific phenomena.[26,232,239,243–250] Methods and systems of various degrees of complexity have been used to study Hofmeister-effects to this very day.

A rather simplistic determination of cloud points allowed proving a Hofmeister type series of molecular cations in presence of sodium dodecyl sulfate (SDS) and sodium dodecylbenzenesulfonate.[251] The same holds for a more complex systems comprising block copolymers, surfactants and salts studied with tensiometric methods, conductivity and dynamic light scattering (DLS) with respect to its critical aggregation concentration.[252] The binding strength between the metal ions provided by a salt and the surfactant headgroup of a monomer or dimer have been studied in the gas phase via mass spectroscopy.[253] Further and more intricate heterodyne sum frequency generation vibrational spectroscopy (SFGVS) yielded insight into the deviating mechanisms governing the effects for cationic and anionic salts.[254] Generally, cation specific effects tend to be less pronounced compared to their anionic analogues. Another spectroscopic study by Guo *et al.* focusing on the OH-stretching mode of water coordinated to Gd^{3+}-ions led to another rationale for the emerging of Hofmeister-effects: the disruption of hydrogen bonding *within* the hydration shells of the respective cation but not in the bulk.[255] Moreover, phase transitions of lyotropic liquid crystalline mesophases formed by non-ionic surfactants upon the addition of salt could be arranged in a systematical order.[256]

However, the theoretical description of ion partitioning at interfaces leading to specific effects remains challenging. Langmuir monolayers, *i.e.,* layers formed by insoluble surfactants have proven to be valuable model systems to study ion specific effects at soft interfaces.[257–265] Leontidis *et al.* were able to recover the established Hofmeister series of anions in compression isotherms of Langmuir layers formed from the zwitter-ionic model lipid dipalmitoylphosphatidylcholine (DPPC) in presence of various sodium salts.[244,266] A further study aiming to investigate the effect of (non-lanthanide) trivalent counterions on the bulk and surface properties of an anionic surfactant has been carried out by Xu *et al.* using neutron reflectivity (NR) and small angle X-ray scattering. From these experiments, the type of counterion and its hydration were identified as the main influencing factors.[267]

Here, adsorption layers of the soluble analogue of the membrane-building phospholipid DPPC, the zwitter-ionic surfactant *n*-dodecylphosphinecholine (DPC), are characterized with respect to their equilibrium and dynamic surface properties. They are used as a probe to study the ion specific effects caused by their interaction with electrolyte sub-phases containing the lanthanide salts $Ce(NO_3)_3$ and $Yb(NO_3)_3$. Next to their surface rheological properties subject to dilatational deformation using the oscillating bubble technique, further experimental information on the bulk characteristics of the aqueous solutions is obtained using isothermal titration calorimetry (ITC) and dielectric relaxation spectroscopy (DRS). Additionally, densities, viscosities and electrical conductivities of the samples studied by means of DRS experiments are determined. From the combined experimental findings, a possible mechanism causing the deviating surface dilatational modulus E in terms of ion specificity is suggested.

4.1 Density, Viscosity and Electrical Conductivity

Measurements of density, viscosity and electrical conductivity of the pure electrolyte solutions without DPC as specified in Table III.2 were performed as auxiliary characterization for the conducted DRS experiments. The respective results are compared in Figures IV.23 to IV.25.

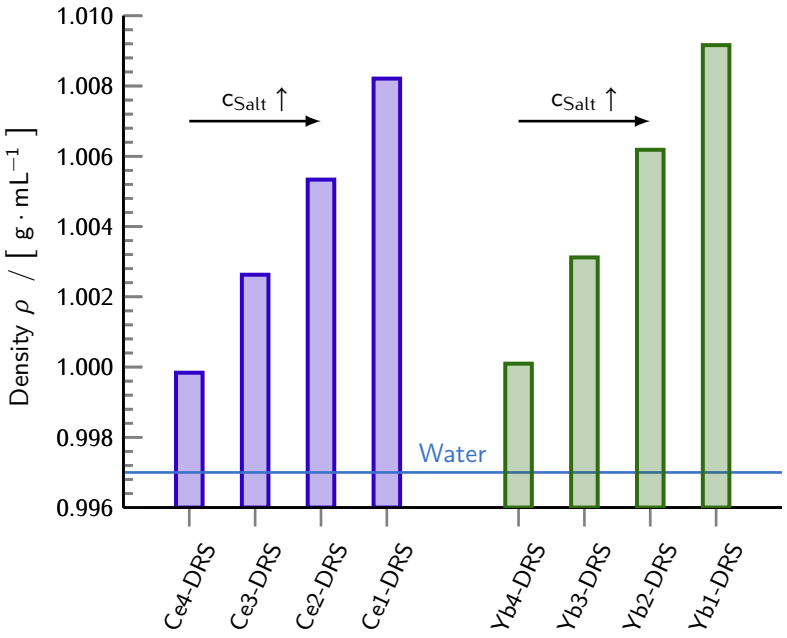

Figure IV.23: Densities of the studied solutions of $Ce(NO_3)_3$ and $Yb(NO_3)_3$ as specified in Table III.2 at 25 °C. The published value of pure water is shown for comparison.[268,269]

Upon increasing salt concentration, density, viscosity and electric conductivity were found to gradually increase. This holds true for aqueous solutions of both $Ce(NO_3)_3$ and $Yb(NO_3)_3$.

Additionally, the best fitting values of the electrical conductivity for the respective solutions as obtained from the procedure outlined in subsection 11.2 of chapter II are shown in Figure IV.25. Therein, the experimentally gained results and the fitting parameters for the two probes, *i.e.*, $\kappa_{el}^{20\,GHz}$ and $\kappa_{el}^{50\,GHz}$ are compared. The respective values showed the same trend along the studied concentration series. However, for one and the same solution, the electrical conductivities were found to decrease from the experimental value over best fitting value of the 20 GHz probe to the result obtained from the 50 GHz probe.

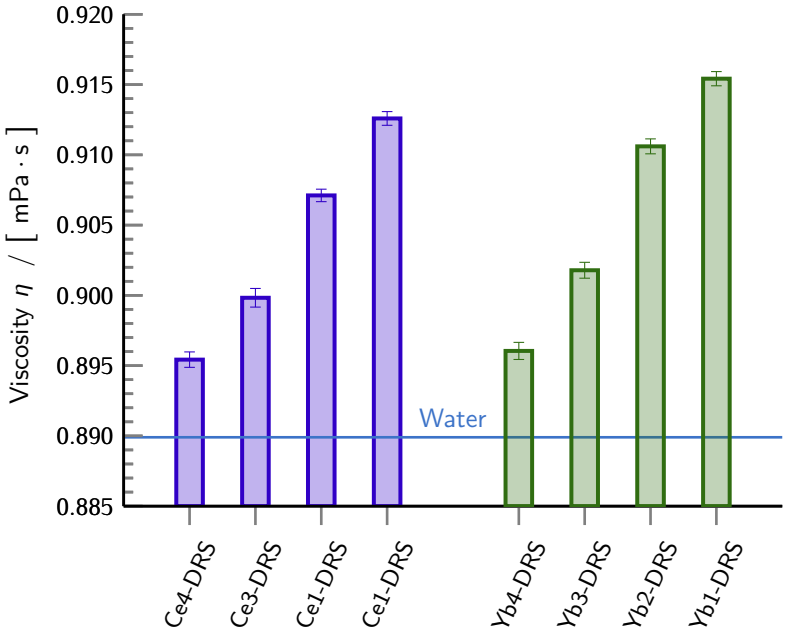

Figure IV.24: Viscosities of the studied solutions of $Ce(NO_3)_3$ and $Yb(NO_3)_3$ as specified in Table III.2 at 25 °C. The published value of pure water is shown for comparison. [269]

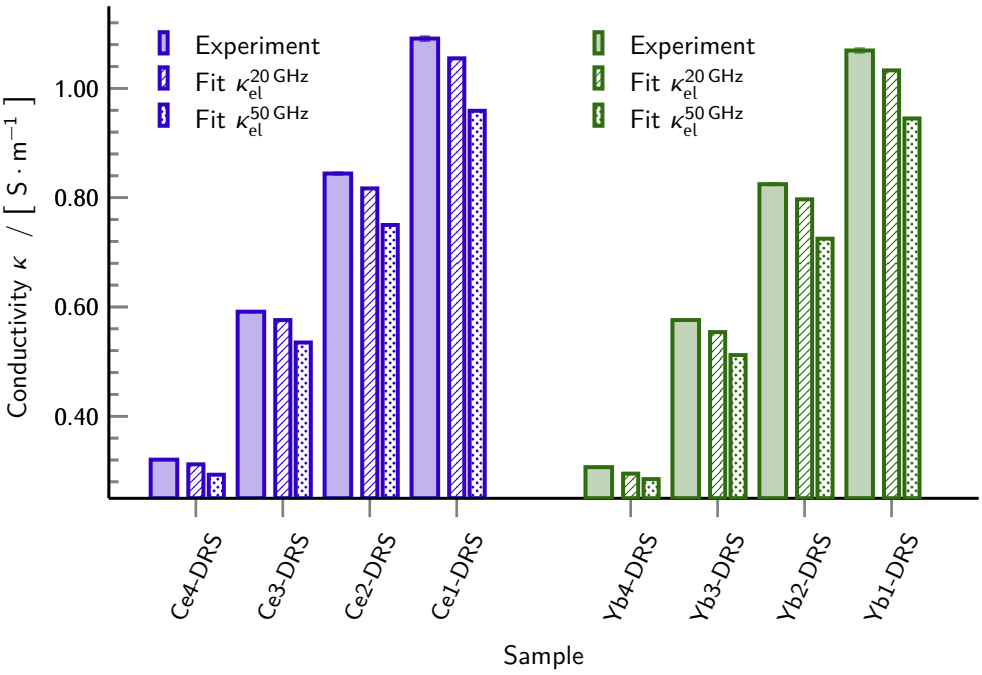

Figure IV.25: Electric conductivities of the studied solutions of $Ce(NO_3)_3$ and $Yb(NO_3)_3$ as specified in Table III.2 at 25 °C.

4.2 Isothermal Titration Calorimetry

An estimation of the solvation energies upon dissolving the studied salts in water was obtained from ITC-measurements. Therefore, a solution of the respective electrolyte was added to pure water in aliquots. The differential power required to compensate the heat of reaction upon addition of the respective volume of 10 mmol · L^{-1} $Ce(NO_3)_3$ and $Yb(NO_3)_3$ are compared in Figure IV.26.

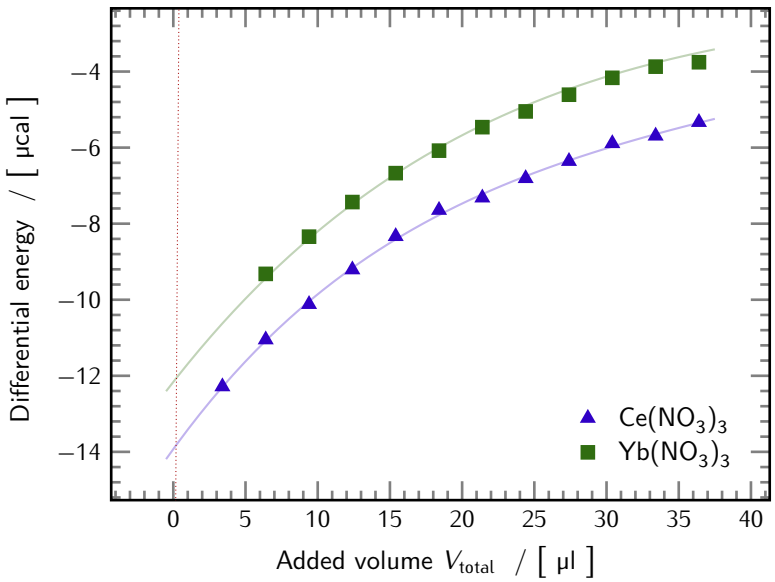

Figure IV.26: Energy turnover upon dissolution of $Ce(NO_3)_3$ and $Yb(NO_3)_3$ in initially pure water as a function of added volume. The solid lines correspond to an empiric polynomial fit.

For all the aliquots of electrolyte solution added to the initially pure water in the course of the experiment, larger absolute amounts of heat were turned over for the solutions of $Ce(NO_3)_3$ as compared to $Yb(NO_3)_3$. It is to be noted that the negative sign corresponds to an exothermic process, *i.e.*, the temperature in the sample cell is elevated with respect to the reference cell of the device.

4.3 Surface Tension

The equilibrium surface tension isotherm of DPC is given in Figure IV.27.

Decreasing values of equilibrium surface tension γ_e upon increasing surfactant bulk concentration were observed until the cmc. It occurred in the range between 1 and 2 mmol · L^{-1}. Above, the equilibrium surface tension γ_e remained at a relatively constant value.

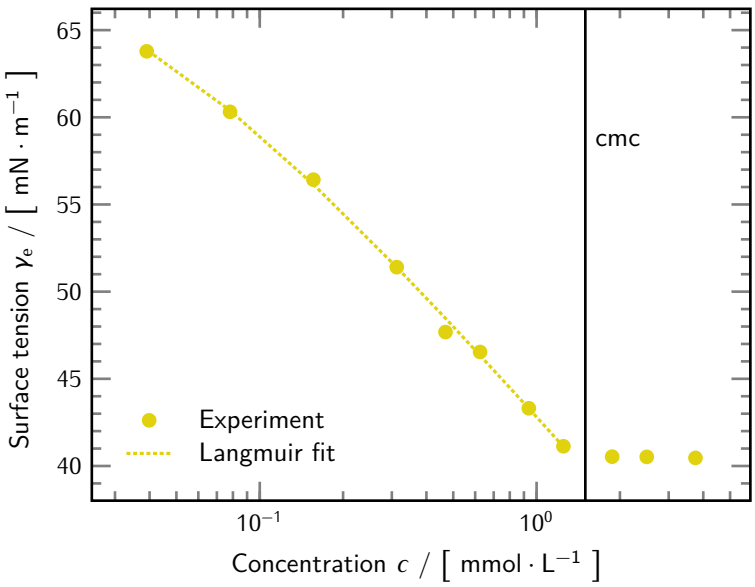

Figure IV.27: Equilibrium surface tension isotherm of DPC. Experimental data and best fit according to the Langmuir adsorption isotherm taking into account only data points below the cmc. It is assumed to occur in the range between 1 and 2 mmol · L^{-1} as indicated by the vertical line.

4.4 Foam Stability

The foam column stabilities of aqueous solutions containing 1 mmol · L^{-1} DPC without salt and in the presence of 30 mmol · L^{-1} $Ce(NO_3)_3$ and $Yb(NO_3)_3$ are compared in Figure IV.27.

Whereas the height of the foam column remained more or less constant after an initially fast decrease for the pure 1 mmol · L^{-1} DPC surfactant solution, the decay was more uniform in the presence of the studied salts. Furthermore, the disintegration started immediately after the foaming has ceased in this case. Despite the electrolytes being used at the same concentration, a pronounced difference between the solutions with added $Ce(NO_3)_3$ and $Yb(NO_3)_3$ was evident. Foams containing $Yb(NO_3)_3$ were found to collapse remarkably slower.

4.5 Oscillating Bubble

In the course of oscillating bubble studies, DPC solutions containing $Ce(NO_3)_3$ and $Yb(NO_3)_3$ were compared to the pure surfactant solution (for details see Table III.2). The amplitudes and phase angles of the studied solutions are given in Figures IV.29 and IV.30, respectively. Therein, the averaged data obtained from three independent measurements for each solution were found to differ strongly.

A clear distinction between all of the three studied solutions was observable in terms of the amplitudes. In the presence of the studied electrolytes, the amplitudes were elevated with respect to adsorption

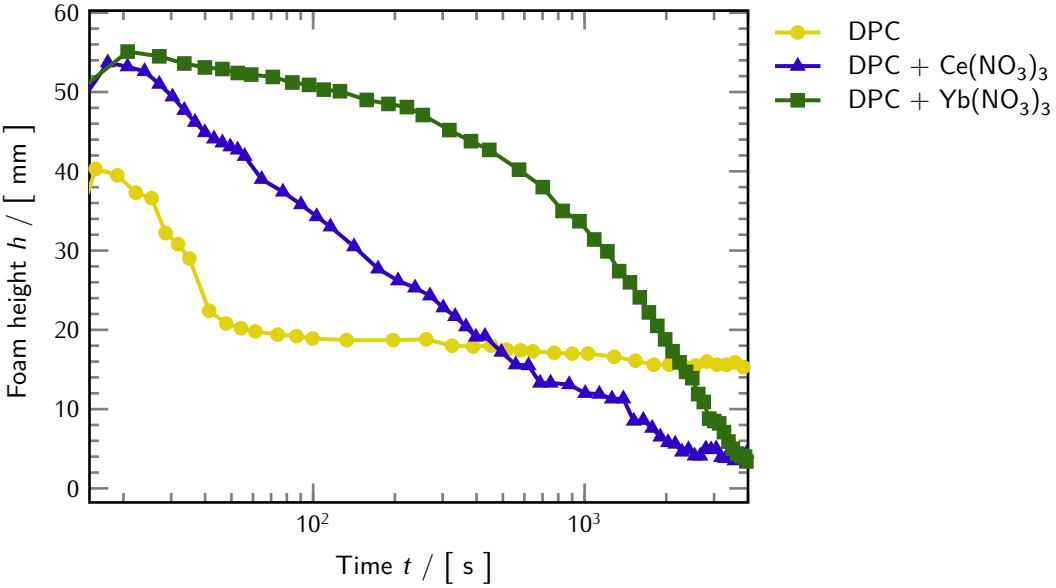

Figure IV.28: Time dependence of foam column heights of $1\,\text{mmol} \cdot \text{L}^{-1}$ DPC aqueous solutions without salt and in the presence of $30\,\text{mmol} \cdot \text{L}^{-1}$ $Ce(NO_3)_3$ and $Yb(NO_3)_3$.

layers of pure DPC. Moreover, the layers formed in the presence of $Yb(NO_3)_3$ were found to lead to higher values of the amplitude of the modulus as compared to $Ce(NO_3)_3$.

Regarding the phase angle, the responses of the DPC-layers with both types of electrolyte present in the sublayer could not be discerned. The values were found to vastly agree within experimental error over the entire frequency range covered. They decreases monotonously at frequencies exceeding 10 Hz. A generically similar behavior of the phase angle was observed for the pure DPC layers. In this case the monotonous descent was found starting at frequencies higher than 20 Hz. Furthermore, the phase angle values of this solution were elevated by around 20° compared to the solutions containing electrolyte.

It is to be noted that no description of the results in terms of the Lucassen-van den Tempel (LvdT)-model was possible. An agreement could be achieved only for adsorption layers with $Ce(NO_3)_3$ and $Yb(NO_3)_3$ in the subphase, if data below 10 Hz were discarded. The experimental results for pure DPC-layers are out of range for modeling with this theory.

4.6 Dielectric Relaxation Spectroscopy

The experimentally obtained spectra of the aqueous $Ce(NO_3)_3$ and $Yb(NO_3)_3$ solutions without the presence of DPC are shown in Figures IV.31 and IV.32, respectively. In all of them, the relative permittivity $\epsilon'(\nu)$ remains more or less unaltered compared to the results for pure water at first sight. For both types of electrolyte solutions, however, the directly accessible total loss $\eta''(\nu)$ was found to

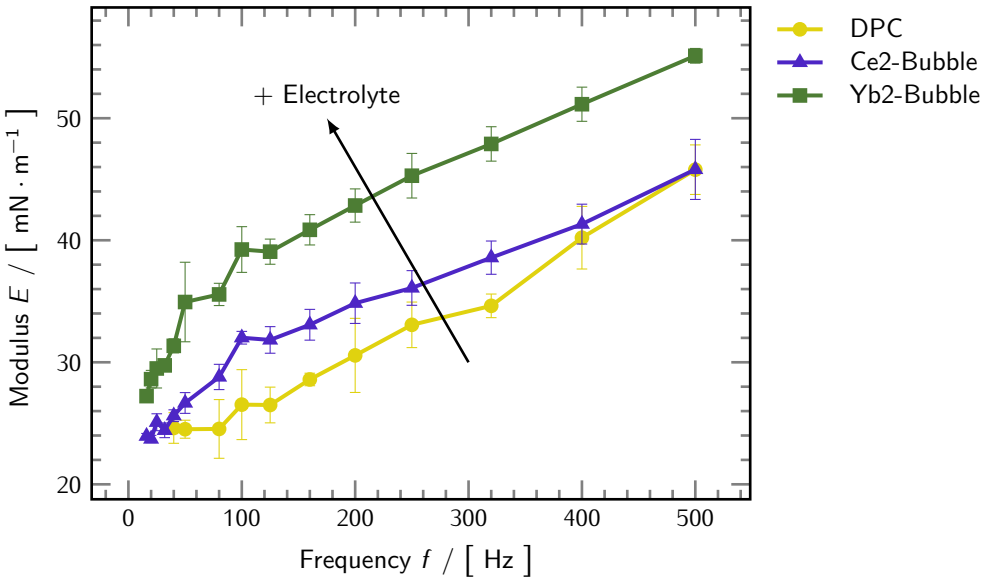

Figure IV.29: Amplitudes of the surface dilatational modulus E of adsorption layers formed by DPC without salt and with the presence of $Ce(NO_3)_3$ and $Yb(NO_3)_3$.

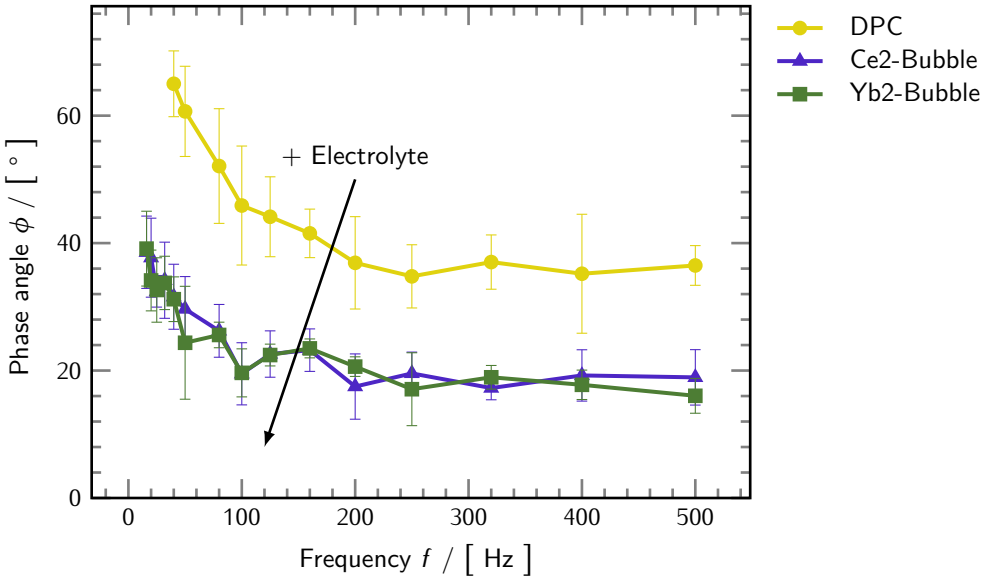

Figure IV.30: Phase angles of the surface dilatational modulus E of adsorption layers formed by DPC without salt and with the presence of $Ce(NO_3)_3$ and $Yb(NO_3)_3$.

clearly increase with salt concentrations (see Table III.2) especially at low frequencies. The same holds for the dielectric loss $\epsilon''(\nu)$, which is obtained from the experimental data by virtue of correction for the electrical conductivity κ_{el}.

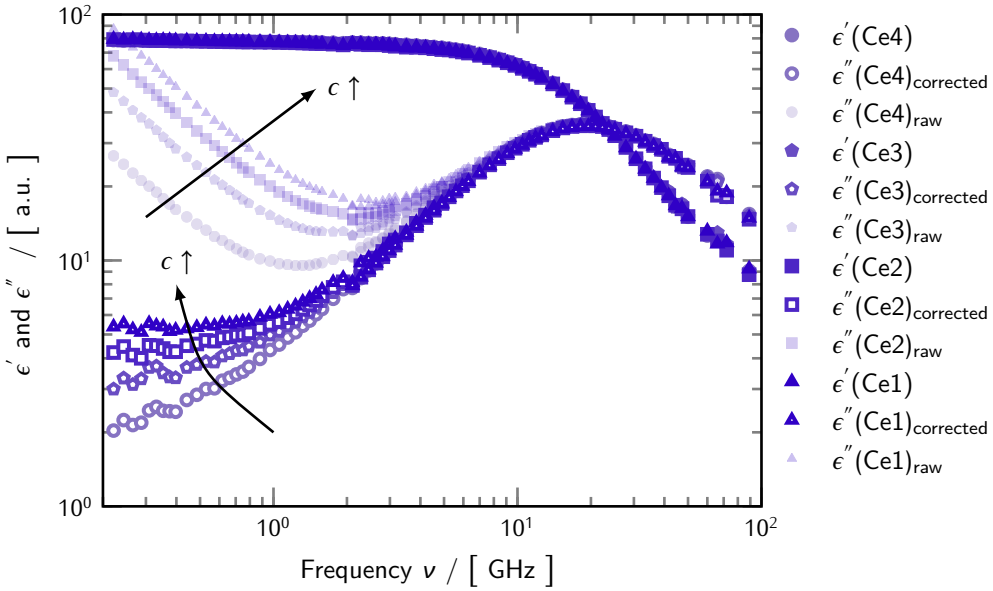

Figure IV.31: Experimentally obtained values of relative permittivity $\epsilon'(\nu)$, total loss $\eta''(\nu)$ and dielectric loss $\epsilon''(\nu)$ subject to conductivity correction for $Ce(NO_3)_3$. The extension „-DRS“ given in Table III.2 is omitted for clarity of the legend.

The subtlety of these results points out the importance of using proper fitting tools in order to obtain quantitative information from carefully conducted experiments. Exemplarily, this decomposition into the contributions giving rise to the experimentally observed spectrum according to the fitting procedure outlined in subsection 11.2 of chapter II is given in Figure IV.33 for sample „Ce1-DRS“. The measurable quantities are recovered from adding the components arising from cooperative relaxation processes, high frequency limiting permittivity ϵ_∞ and the electrical conductivity κ_{el}. Fitting was performed for all of the studied solutions in the same manner without limitations of the accessible parameter range.

A total of seven adjustable model constants was used to adequately describe the experimentally observed set of complex data within the applied model. This set of parameters comprises two relaxation modes (characterized by an amplitude S_j and a relaxation time τ_j each), the high frequency limiting permittivity ϵ_∞ and the two values of the electrical conductivities $\kappa_{el}^{20\,GHz}$ and $\kappa_{el}^{50\,GHz}$ as perceived by the two probes. The conductivity corresponding to the data obtained from the interferometric frequency range is fixed to zero. Table IV.2 summarizes the best fit parameters obtained for the studied solutions.

Within the concentration series of $Ce(NO_3)_3$ and $Yb(NO_3)_3$ similar trends could be observed. Upon

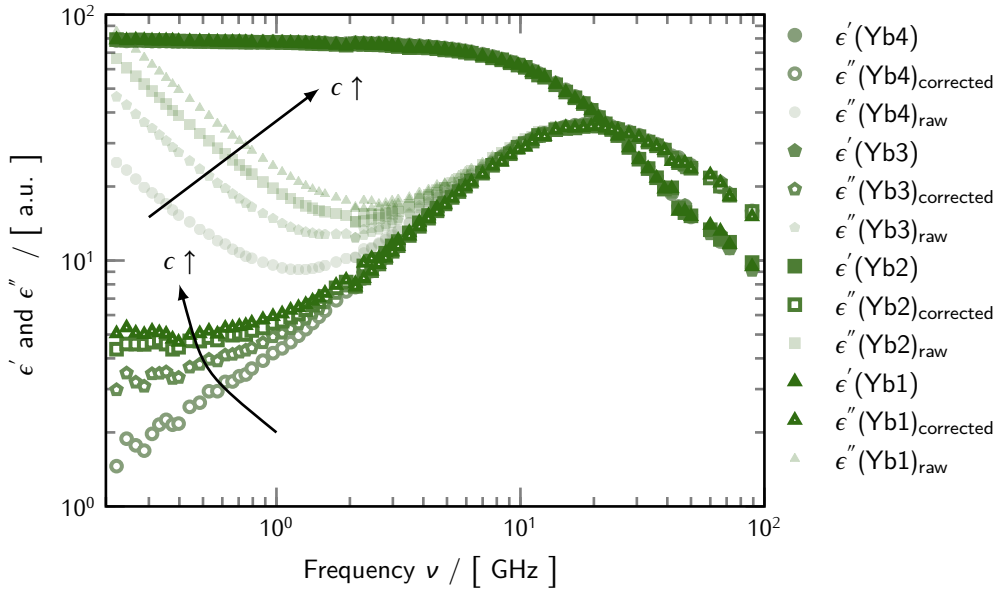

Figure IV.32: Experimentally obtained values of relative permittivity $\epsilon'(\nu)$, total loss $\eta''(\nu)$ and dielectric loss $\epsilon''(\nu)$ subject to conductivity correction for $Yb(NO_3)_3$. The extension „-DRS“ given in Table III.2 is omitted for clarity of the legend.

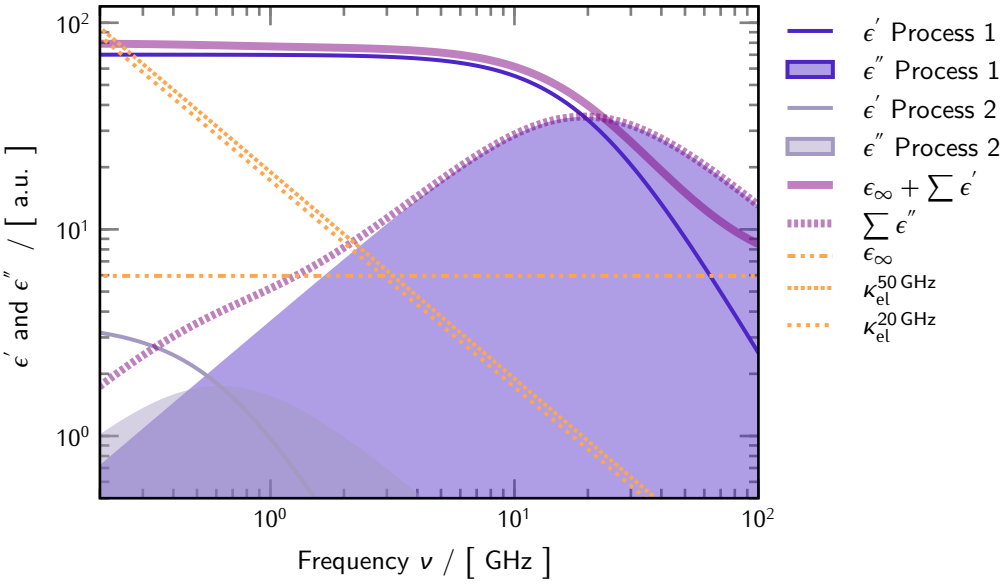

Figure IV.33: Exemplary decomposition of DRS data for Sample Ce1. The spectrum is considered the sum of contributions arising from collective relaxation, the high frequency limiting permittivity ϵ_∞ and the respective values of electrical conductivity κ_{el} as obtained from the utilized probes, *i.e.*, $\kappa_{el}^{20\,GHz}$ and $\kappa_{el}^{50\,GHz}$.

Table IV.2: Parameters corresponding the respective best fit assuming a relaxation process with two Debye-peaks obtained from least-squares fitting of the experimentally obtained spectra.

Sample	S_1 [a.u.]	τ_1 [ps]	S_2 [a.u.]	τ_2 [ps]	ϵ_∞ [a.u.]	$\kappa_{el}^{20\,GHz}$ [$S \cdot m^{-1}$]	$\kappa_{el}^{50\,GHz}$ [$S \cdot m^{-1}$]
Ce1	70.083	8.233	3.495	256.616	5.956	1.055	0.959
Ce2	70.602	8.256	2.920	293.533	5.887	0.817	0.750
Ce3	71.016	8.270	2.319	338.495	5.988	0.576	0.535
Ce4	71.685	8.290	1.350	407.767	5.874	0.312	0.293
Yb1	69.843	8.221	3.293	268.804	6.044	1.033	0.945
Yb2	70.379	8.267	2.978	310.870	6.071	0.797	0.725
Yb3	70.946	8.246	2.218	327.582	5.901	0.554	0.512
Yb4	71.532	8.279	1.203	408.689	5.885	0.295	0.285

increasing electrolyte concentration, the amplitude S_1 associated with collective water dynamics decreased slightly, whereas the corresponding relaxation time τ_1 remained virtually constant. The characteristics of the second relaxation process describing the behavior of the dipolar species introduced by the presence of salt differ significantly. A more than 2.5-fold increase in its amplitude S_2 and almost a bisection in the relaxation time τ_2 was observable over the studied concentration range. Increasing electrical conductivity κ_{el} with salt concentration was confirmed for both $Ce(NO_3)_3$ and $Yb(NO_3)_3$ also from the fitting results. It is to be noted that the electrical conductivity parameter $\kappa_{el}^{50\,GHz}$ corresponding to the 50 GHz coaxial probe is generally about 10 % lower compared to the value of $\kappa_{el}^{20\,GHz}$ associated with the 20 GHz probe. In comparison to the experimental electrical conductivity κ_{el} collected from measurements of impedance, the values of $\kappa_{el}^{20\,GHz}$ were found to be smaller by 3.324 ± 0.441 % on average.

5 Photo-Responsive Azo-surfactant

In 2016, the work of Jean-Pierre Sauvage, Sir James Fraser Stoddart and Bernard L. Feringa was awarded with the Nobel Prize in chemistry for the rational design and synthesis of molecular machines.[270] Just as machines from the macroscopic world, also the molecular sized counterparts envisioned by these pioneers are characterized by machine-like movements as the consequence of an externally induced stimulus under the consumption of energy, which is typically provided via irradiation with light.[271] The two main approaches for the construction of machines at molecular scale are based on topological entanglements or isomerisable unsaturated bonds. Catenanes and rotaxanes operating on the entanglement principle are readily available from template synthesis.[272] Access to externally controlled translational motion, however, is provided only by introduction of asymmetric moieties within the structure.[273,274] Equally, an asymmetry is at the heart of molecular structures providing controlled unidirectional motion in overcrowded alkenes by application of irradiation with light and thermal relaxation. This principle finally led to the well-known „nanocar“.[275]

But not only since then, switchable or responsive molecules have been of interest to the community.[276] Next to photochromic compounds able to reversibly switch between open and closed forms (spiropyrans and diarylethene) or undergoing reversible dimerization (anthracene and coumarin derivatives), molecular switches operating on a *cis-trans*-isomerization (azobenzene, stilbene and hemithioindigo) are still widely used.[277] When covalently attached towards chromophores, they can act as molecular photonic analogues of electronic transistors eventually enabling digital logic on a molecular level in the wide range of data and signal processing.[278] Furthermore, azo-based fluorogenic probes are of high relevance for biosensing and bioimaging as fluorescence can be tuned by the non-fluorescent relaxation pathways provided by the azo-moiety.[279]

So called „smart foams“ are to be mentioned as another field, in which photo-responsive compounds play a significant role.[280,281] Chevallier *et al.* demonstrated the destabilization of foam columns generated from a cationic azo-surfactant upon irradiation with ultraviolet (UV)-light.[282] In a systematic study considering a series of cationic azo-surfactants, Hayashita *et al.* were able to point out the influence of molecular structure on basic characteristics such as critical micellar concentration (cmc) and electrical conductivity of the respective *cis*- and *trans*-conformation-isomers.[283] Equally, the induced change in polarity upon illumination was shown to be beneficial for light-controlled separation of a catalytic polyoxometalate complex from the reaction medium.[284] Moreover, bulk rheological properties were found to be determined and reversibly switchable for photoresponsive amphiphiles leading to so-called photorheological fluids.[285] This is based on the concept of the isomers aggregating to distinct units depending on the molecular shape. It is to be noted that both self-assembly and the change in behavior to be expected upon illumination is highly sensitive towards the position of the azo-moiety within the molecular structure.[286]

In this section, the equilibrium and dynamic surface properties of the photosensitive azo-surfactant T226 subject to illumination with UV- and visible (Vis)-light inducing a transition between the

geometric *cis*- and *trans*-isomeric form are studied. A characterization of the adsorption layers formed from this soluble surfactant was carried out relying on axis symmetric drop shape analysis (ADSA) using a pendant drop tensiometer and surface rheological experiments with the oscillating bubble to cover the frequency range from 10 to 500 Hz.

5.1 Ultraviolet-Visible-Spectroscopy

The ultraviolet-visible (UV-Vis)-spectra of the azo-surfactant T226 subject to UV and Vis-illumination are given in Figure IV.34. Both geometric isomers of the surfactant are characterized by negligible absorption at wavelengths above 550 nm and a maximum in absorption around 480 nm. The spectra of the respective *cis*- and *trans*-geometric isomers differ most remarkably in the range from 320 to 380 nm

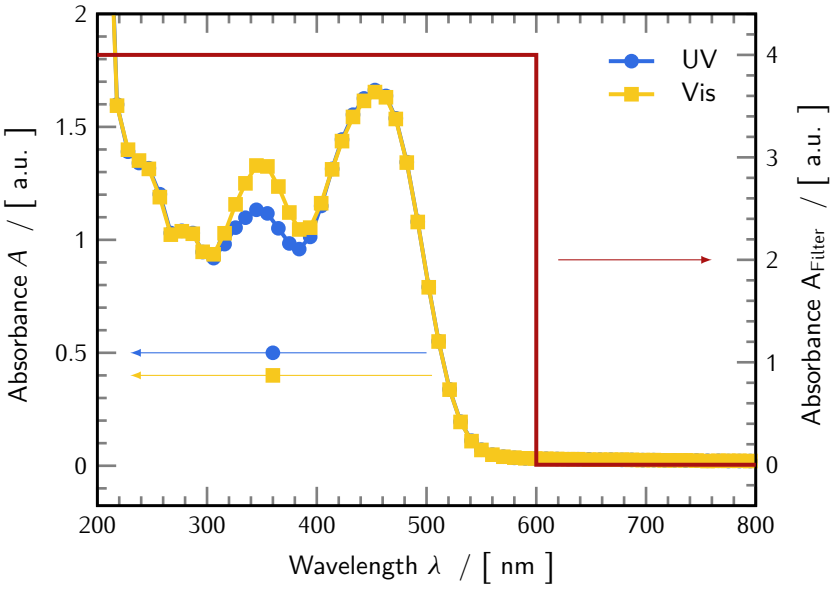

Figure IV.34: Absorption spectra of the used azo-surfactant T226 subject to UV and Vis illumination (Left hand scale for the absorption of the surfactant, right hand scale for the absorption of the filter).

In this region, the Vis-illuminated solution features more pronounced absorption. In order to describe the action of the spectral filter used for the modification of both the pendant drop and oscillating bubble devices, its schematic absorption spectrum is shown for comparison on the right hand axis of Figure IV.34. For wavelengths shorter than 600 nm the absorbance is very high, *i.e.*, the corresponding light is absorbed almost entirely. The consequence of the use of this filter is that no further light-induced transition between the *cis*- and *trans*-isomers will take place, as „it is always dark for this molecule“. In other words, no light overlapping with an absorption band of the studied azo-surfactant will interact with the amphiphile. Accordingly, a relaxation can take place only via a thermally induced

process.

Additionally, measurements of UV-Vis-absorption spectra of the UV-illuminated azo-surfactant T226 after defined temporal intervals *with* protection by the cut-off filter were carried out. The unaltered state of the *cis*-state on the time-scale of the pendant drop and oscillating bubble experiments could be ensured from this.

5.2 Surface Tension

Measurements of dynamic surface tension were carried out using a modified pendant drop tensiometer. In order to allow for unaltered determination of the surface properties of the UV-illuminated form of the surfactant, the apparatus was equipped with an additional optical cut-off filter characterized by an absorbance above 3 for spectral wavelengths below 600 nm. This filter was placed before the sample and served to protect the UV-illuminated azo-surfactant from relaxing back to its *trans*-conformation due to a light-induced process. Additionally, the sample vials, syringes and tubing of the device were covered in aluminum foil to further hinder this process.

A sub-cmc excerpt of the equilibrium surface tension isotherms of the respective geometric isomers is shown in Figure IV.35. Therein, the assumed respective equilibrium surface tension γ_e is plotted versus the azo-surfactant's bulk concentration.

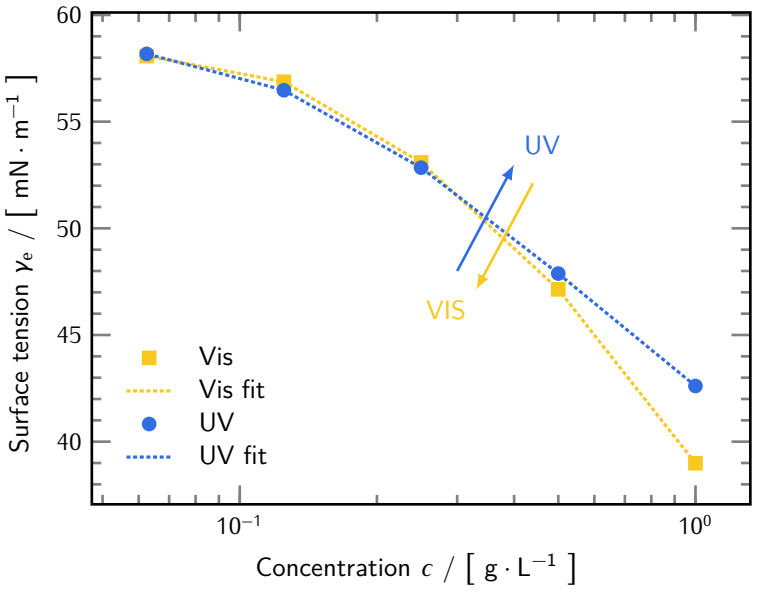

Figure IV.35: Comparison of the equilibrium surface tension isotherm of T226 in the Vis and UV illuminated limiting cases at $T = 25\,°C$.

The values of equilibrium surface tension γ_e were obtained from extrapolating the dynamic surface tension data collected for the respective sample solution by the pendant drop device against the

inverse square root of the experimental time t. The value of interest was determined as the intercept of a linear fit, when plotting the instantaneous surface tension γ against $\sqrt{t}^{-1}$ for surface tension values obtained in the temporal range from 200 to 300 s subsequent to drop formation. This concept was suggested by Joos is based on a limiting solution of the Ward-Tordai-equation as described in subsection 3.2 of chapter II.[287,288]

At concentrations exceeding $0.5\,g \cdot L^{-1}$, the isotherms of the respective geometric isomers start to differ significantly. The aqueous solutions of UV-illuminated samples gradually led to higher values of equilibrium surface tension γ_e compared to the Vis-form upon increasing surfactant bulk concentration. After illumination with Vis-light, a pronounced drop in equilibrium surface tension could be observed. As mentioned previously, a steady state of the ratio between the *cis*- and *trans*-conformation was ensured on the time scale of the conducted surface tension experiments.

5.3 Oscillating Bubble

Analogously to the modifications of the pendant drop device described in the previous subsection, also the oscillating bubble setup was adjusted to meet the requirements of the experiment. Besides the mentioned optical cut-off filter positioned between the illumination source and the sample chamber, all sample containers, syringes and tubing of the device were covered in aluminum foil. Furthermore, additional blackened lockable pipes were mounted to the measurement chamber to avoid exposure to daylight within the entire course of the procedure.

The surface dilatational moduli of T226 for its both geometric isomers are given in Figures IV.36 and IV.37 in the representation as amplitude and phase, respectively.

Within experimental error, the adsorption layers of the UV- and Vis-illuminated forms could be distinguished clearly. All over the entire frequency range covered by the oscillating bubble technique, the interfacial region of the Vis-illuminated form was characterized by lower values of the amplitude and elevated phase angles compared to the UV-illuminated sample.

5.4 Foam Stability

A first rough estimation of foam stability was obtained from shaking the UV- and Vis-illuminated samples in glass vials. Furthermore, quantitative measurements in the foam column analyzer should be possible as the within device, red light emitting diodes (LEDs) in conjunction with a sensitive photo-detector array is used to measure the foam height. According to the UV-Vis-absorption spectrum, illumination with light at wavelengths above roughly 550 nm is expected to leave the isomerization state of azo-surfactant T226 unaltered. Therefore, the relevant parts of the apparatus were wrapped into aluminum foil to avoid exposure of the sample to daylight in the course of the measurement. The surfactant was filled into the darkened glass column subsequent to illumination. A total of ten foam columns were generated from the only once illuminated samples in consecutive runs. The respective

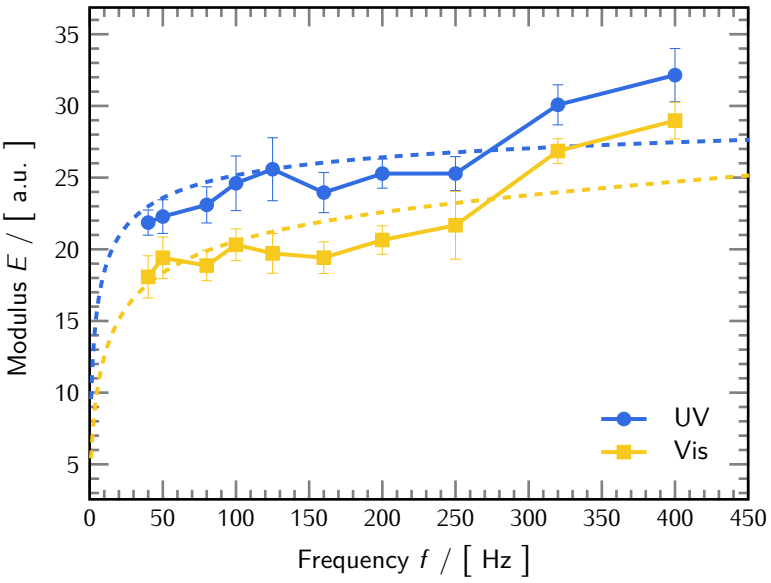

Figure IV.36: Amplitude of the surface dilatational modulus E as measured for the Vis- and UV-isomers of azo-surfactant T226 by the oscillating bubble device. Dashed lines correspond to best fits according to the extended LvdT-model.

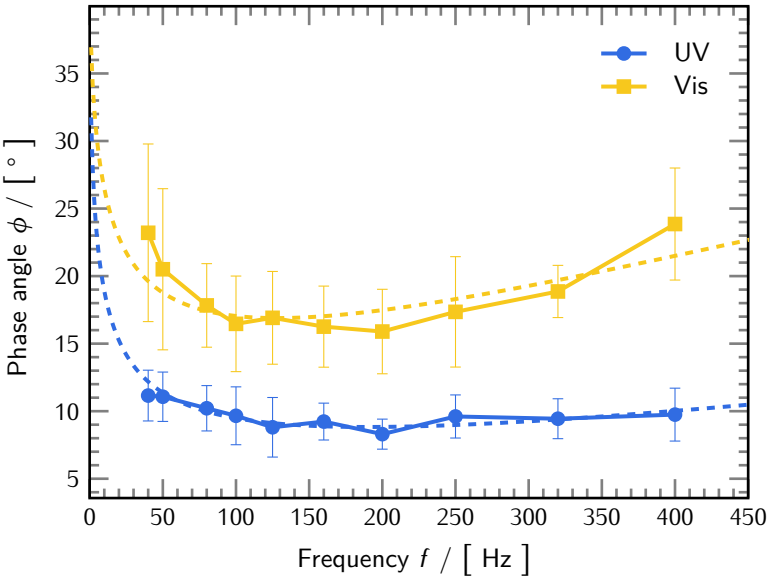

Figure IV.37: Phase angle of the surface dilatational modulus E as measured for the Vis- and UV-isomers of azo-surfactant T226 by the oscillating bubble device. Dashed lines correspond to best fits according to the extended LvdT-model.

individual and averaged decay curves together with an image of the UV- and Vis-illuminated samples are shown in Figure IV.38.

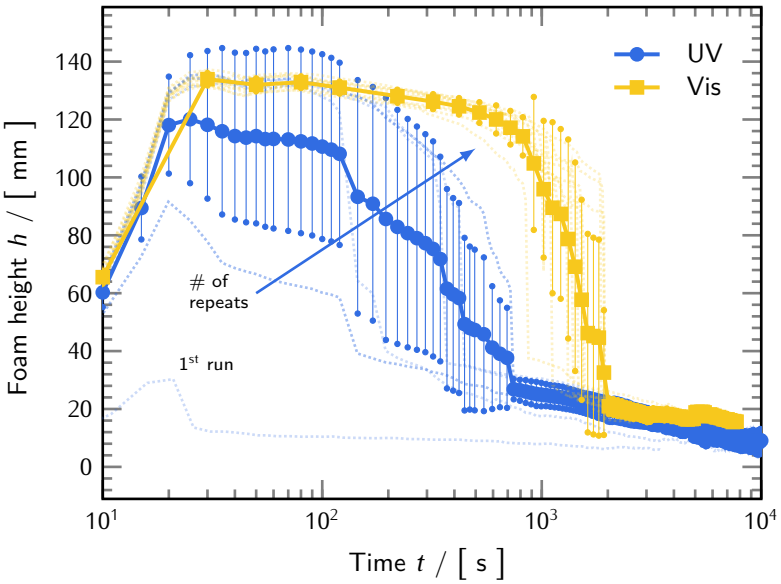

Sample	$t_{1/2}$ [s]
UV	317 ± 226
VIS	1455 ± 363

Figure IV.38: Time dependence of foam columns heights of T226 subject to UV- and Vis-illumination. The thin dotted lines correspond to the individual repeats of foam column decay.

The foam stabilities of the samples illuminated with the different types of light were found to differ significantly. Whereas the solution irradiated with Vis-light was characterized by a rather reproducible decay behavior and a prolonged stability, foams generated by agitating the UV-sample was less stable. Furthermore, the scatter between the individual subsequent measurements *without* meanwhile UV-irradiation is much more pronounced. The initially low foamability and fast decay gradually transformed into characteristics of both increased foamability and stability with ongoing duration of the experiment.

V Discussion

In the following sections, the experimental results given in chapter IV will be discussed individually. At the end of each respective part, a corresponding conclusion will be drawn.

The material presented in this chapter has been (partially) published or is currently under revision for publication in peer reviewed journals. A list of respective publications is given in Appendix A.

1 Surface Effects in the Escape Mechanism of the Stenus Beetle

1.1 Surface Tension

The deviating surface affinity of stenusine and norstenusine seems reasonable considering that norstenusine bears one methylene group less. This results in a lower hydrophobicity of norstenusine in comparison to stenusine. A Frumkin type adsorption isotherm was chosen in order to fit the experimentally obtained set of concentration dependent values of equilibrium surface tension γ_e.

For compounds of the *N*-alkyl piperidine type, pK_A-values values around 10 are reported.[289] Therefore, quantitative protonation of the alkaloids in the present case of pH 7 can safely be assumed. Gedig *et al.* performed similar experiments in buffer solutions of pH 6.[167] Since the difference in pH is rather small, in particular considering the pK_A, a comparison of the latter with the presented data (see Figure IV.1) is justified due to a similar protonation state. However, some discrepancies were observable. The isotherm extracted from data by Gedig *et al.* is characterized by significantly reduced values of surface tension, especially for the alkaloid solutions at lower concentrations. These differences to the previous work are ascribed to the presence of trace impurities originating from the synthesis. They come more into effect at lower bulk concentrations due to higher surface activity of the contaminants. By applying the outlined purification procedure, surface tension values are typically shifted upwards with an increasing number of cycles until the state of surface chemical purity is accomplished.[290]

1.2 Oscillating Bubble and Pendant Drop Rheology

The values of the high frequency limiting elasticity ϵ^{∞} as obtained from the fitting procedure to the Lucassen-van den Tempel (LvdT)-model agree within experimental (see Table IV.1) error for the studied solutions. Interestingly enough, the frequency dependent values of the amplitude are not indicative for this behavior judging from the respective plots in Figure IV.2. However, the deviating best fit parameters (see Equation II.118) for the characteristic diffusion frequency f_{diff} can be rationalized in terms of the polarity of the alkaloids. A higher degree of hydrophobicity due to the additional methylene group in stenusine as compared to norstenusine manifests as an increased characteristic diffusion frequency f_{diff}. The widely differing values of intrinsic surface dilatational viscosity κ are hard to be interpreted based on their molecular structures, as the increased energetic loss upon dilatational deformation at higher frequencies is apparently not associated with the larger number of degrees of conformational freedom in stenusine.

In order to assure the validity of the previously discussed oscillating bubble data, which have been assessed on a standalone basis, its connection towards the surface dilatational results at slower perturbation rates accessible via the oscillating pendant drop technique has been checked. Partially neglecting the values gathered at the lower frequencies accessible by the oscillating bubble device, a more or less smooth transition for both the amplitude and the phase angle of the studied solutions is apparent from Figures IV.4 and IV.5, respectively. To strengthen this notion of a proper match between the results obtained from the two instruments, the theoretical approach utilized by Ravera *et al.* accounting for additional relaxation processes has been taken up.[156] Disregarding the evident outliers in the connecting frequency region, the theory leads to a decent agreement with the experimentally determined values of the complex surface dilatational modulus E over roughly five orders of magnitude.

1.3 Conclusion

For both natural spreading alkaloids, stenusine and norstenusine, the induced surface pressure is rather low as compared to classical long-chain surfactants at comparable concentrations. This moderate reduction of surface tension of pure water is sufficient, however, to induce a surface pressure driving the beetle towards its preferred terrestrial habitat. At the same time it is sufficiently low to avoid a drowning of the *stenus comma* beetle. The Baudoin number is especially important for skimming of beetles, since a reduction of equilibrium surface tension γ_e below a critical value would cause the animal to sink immediately. The spreading alkaloids modify the dynamics of the respective adsorption layers as evidenced by the data from both the oscillating pendant drop and the oscillating bubble device. In both cases, shifts towards surface viscoelastic behavior characterized by an increasing value of the amplitude of the surface dilatational modulus E and a non-zero phase angle ϕ at perturbation frequencies above 100 Hz were observed. The experimental values of amplitude and phase angle obtained from the oscillating bubble device could be described successfully by the extended LvdT-model. Adsorption layers of stenusine and norstenusine are characterized by a non-zero value of the intrinsic surface

dilatational viscosity κ. This means that the expansion-compression deformation-type is associated with a loss in energy, which makes it increasingly difficult for other water walking arthropods to follow the *stenus comma* beetle. Furthermore, the validity of the latter findings has been corroborated by two approaches. Firstly, a smooth transition between oscillating bubble and the complementary oscillating pendant drop data was observable. Secondly, the combined results from both methods were found to be in approximate agreement with a theoretical model allowing for a description of surface dilatational characteristics of the studied system over a frequency range covering almost six orders of magnitude.

To conclude, the spreading alkaloids excreted by the *stenus comma* beetle in the course of escaping from a water surface have a twofold purpose in terms of their physico-chemical properties at concentrations close to the solubility limit at room temperature: inducing a surface pressure driving the beetle to the water's edge and rendering the adsorption layer surface viscoelastic, which additionally favors the beetle's escape. Semiaquatic bugs are supported by surface tension to keep them from drowning. The locomotion of water walking arthropods leads to deformations of the water surface and the formation of capillary waves. The decisive frequency range for the oscillating bubble studies is from 50 to 500 Hz as it matches the characteristic time of the surface deformations caused by the legs of predatory water striders and spiders.[291]

2 Mixed Surfactant-Electrolyte System

2.1 Surface Tension

Commercially available sodium dodecyl sulfate (SDS) is typically known to be contaminated by *n*-dodecanol which possesses a higher surface activity than the main component. The applied surface purification protocol successfully removed surface active trace impurities. Therefore, the experimentally obtained surface tension isotherm and literature data for surface chemically purified SDS are in good agreement, which is indicative for the absence of impurities to a large extent. Equally, this is manifested in the negligible decrease in surface tension with time. Each point in the measured surface tension isotherm (see Figure IV.6) represents the average value of repeated measurements by a ring tensiometer. The change in surface tension over the time span of measurement was found to be below $0.1\,\mathrm{mN \cdot m^{-1}}$ and therefore assumed to be the respective equilibrium value. Additionally, the surface tension of $40\,\mathrm{mN \cdot m^{-1}}$ measured for the purified $6\,\mathrm{mmol \cdot L^{-1}}$ stock solution of SDS given by Lunkenheimer *et al.*[169] could be confirmed in this study. The same holds for the value of $65\,\mathrm{mN \cdot m^{-1}}$ for a $1\,\mathrm{mmol \cdot L^{-1}}$ solution.

The absence of dynamics in surface tension equally holds for the studied mixtures of SDS and NaCl shown in Figure IV.7. As discussed by Fainerman *et al.*,[212] a reduced amount of an ionic surfactant can be compensated by the addition of electrolyte, *i.e.*, the surface tension of solutions from this class of amphiphiles is mainly determined by the mean ionic strength rather than the surfactant concentration. Here, the differences in foam stability are attributed to differences in surfactant dynamics. Therefore, comparable values of equilibrium surface tension have to be assured for the studied solutions. For solutions 1 to 5 as specified in Table III.1, the constancy of equilibrium surface tension for constant mean ionic strength I_{mean} is fulfilled. This allows for interpretation of foam and foam lamella stabilities in terms of non-equilibrium properties obtained from surface rheological characterization.

2.2 Sum Frequency Generation Spectroscopy

An estimation of the combined information on orientation and surface propensity of SDS in the presence of NaCl was achieved by the „leveling“ approach described in subsection 7.1 of chapter II. The ratios of the effective second order resonant non-linear susceptibility $\tilde{\chi}^{(2)}_{\mathrm{eff,R}}$ of the solutions containing salt to salt-free reference solution are shown in Figure V.1.

These results indicate that the adsorbed amount of SDS contained in the interfacial layer remains more or less constant within experimental error for the solutions containing salt. This is in agreement with surface tension measurements assuming that a constant surface coverage leads to the same value of equilibrium surface tension γ_{e}.

Besides the insensitivity of adsorption layers formed by a non-ionic bulky alcohol model substance upon addition of salt up to $2\,\mathrm{mol \cdot L^{-1}}$, further confirmation has been provided for the hypothesis of

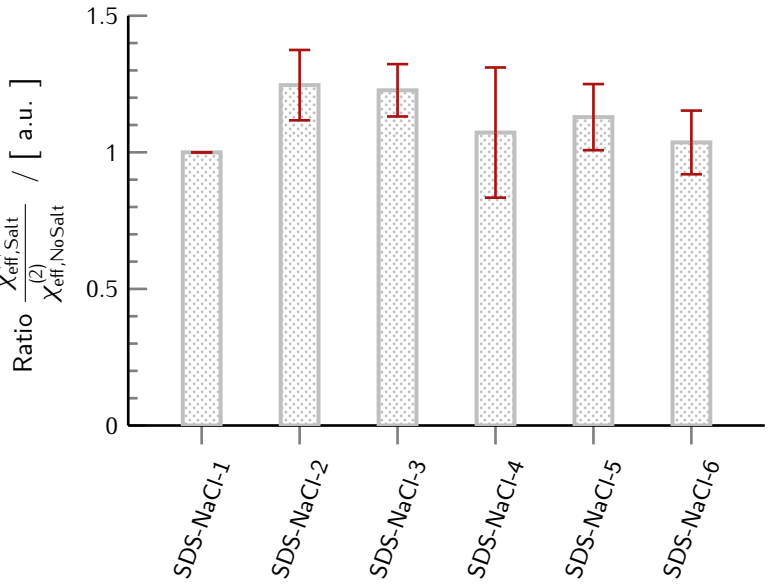

Figure V.1: Ratios of $\chi^{(2)}_{\text{eff,Salt}}/\chi^{(2)}_{\text{eff,NoSalt}}$ in the alkyl region for mixed solutions of SDS and NaCl.

a constant orientation of interfacially active soluble molecules.[6] Johnson *et al.* published a similar outcome for the same SDS-NaCl system in an extensive sum frequency generation (SFG)-study.[292] The change in molecular surface area was found to remain constant within 10 % up to concentrations of 300 mmol $\cdot$ L^{-1} and below 5 % up to 30 mmol $\cdot$ L^{-1} NaCl. As the influence of added salt is anticipated to cause the most pronounced effects at high surface coverage, *i.e.*, highest bulk concentration, it is assumed, that the addition of salt will not lead to a pronounced difference in terms of interfacial orientation of the adsorbed dodecyl sulfate (DS)-ions. Changes in effective resonant second order susceptibility should therefore be ascribable to changes in the number density of adsorbed material. As the relative intensities of the respective vibrational modes remain constant, an experimental scatter-corrected ratio of $\tilde{\chi}^{(2)}_{\text{eff,R}}$ of sample to reference solutions should be obtainable from averaging the ratio over the entire alkyl spectral region.

2.3 Infrared Reflection Absorption Spectroscopy

Similar to the surface specific infra-red (IR)-spectra obtained from sum frequency generation vibrational spectroscopy (SFGVS), also infrared reflection absorption spectroscopy (IRRAS) serves to deliver vibrational spectra originating from the interfacial region. Instead of having foundations in non-linear optics, it is based on the intensity of light reflected from an interface and its comparison with the signal detected from a reference system holding the pure solvent. Interpretation is conducted in terms of the reflectance-absorbance (RA) specifying the differences between a sample and the reference system.

The observable decrease in RA in the region around 3600 cm^{-1} upon addition of salt as shown in Figure IV.9 is indicative for an increasing amount of vibrational excitation of water in the samples. As discussed in subsection 7.2, a positive value of RA is associated with an elevated amount of vibrational oscillators in the reference trough of the setup as compared to the container of the sample. Consequently, this suggests that the presence of the pure surfactant solution dramatically reduces the experimentally „visible“ amount of surface water leading to the most prominent RA-peak. Increasing the relative amount of electrolyte NaCl causes this peak to decrease in intensity and finally to cross over to negative RA-values of water. This is to be interpreted as higher presence of interfacial water molecules in solutions containing both SDS and a rather high amount of salt.

This finding or trend, however, could not be confirmed from the presented SFG-experiments, which should in principle lead to the same conclusion. A possible reason for this might be the more intricate experimental requirements for conducting this kind of (semi-) quantitative SFG-spectra as compared to the IRRAS-method operating at high sampling frequencies and therefore allowing for faster data acquisition.

2.4 Foam Stability

Upon increasing the relative salt content, the stability of foam columns and lamellae was found to decrease. Foam lamella stability is frequently discussed in terms of both headgroup [293–295] and hydrophobic interaction [295–298] between the surfactant chains. Further reasons associated with the stability of films are the repulsion between the equally charged adsorption layers [36,299,300] and the presence of an osmotic pressure due to counter-ion concentration. [301] For the studied solutions, the decrease in surfactant and simultaneous increase in salt concentration lead to opposing effects. A reduced surfactant concentration and therefore decreased chain interaction is compensated by a reduction of headgroup repulsion due to the screening of electrostatic charges according to the Debye-Hückel (DH)-theory. This so-called compression of the electric double layer leads to a thinning of the foam films which ultimately causes them to rupture faster. For the studied solutions, the Debye screening length κ_D^{-1} decreases from approximately 100 to 20 Å upon increasing salt concentration. Effects of ion specificity on solutions of SDS in terms of adding alkali chlorides have been found to be highly dependent on the used concentrations. [302] Moreover, there have been interesting recent developments in the theory of drainage processes in surfactant-electrolyte mixtures. [303]

2.5 Oscillating Bubble

The surface dilatational characteristics obtained from the oscillating bubble technique can be described theoretically by the Lucassen-van den Tempel (LvdT)-model outlined in subsection 11.1 of chapter II.

Dissipative processes occurring within the surface region are parametrized by the value of the intrinsic surface dilatational viscosity κ. Its best fit values were found to decrease from solution 1 to 6, whereas

the high frequency limiting elasticity ϵ^{m} slightly increased and the characteristic diffusion frequency f_{diff} remained constant within the studied series. The experimental surface dilatational data of SDS-NaCl-1 (pure, $1\,mmol \cdot L^{-1}$) are not in full agreement with published literature data.[121] Even though a viscoelastic character of this solution could be confirmed in the present study, the absolute values differ considerably. This might be due to different states of surfactant purity (here: surface chemically pure; Wantke *et al.*: used as received), although this possibility has been discussed and argued *not* to be the case.[121] An influence of the hydrolysis product *n*-dodecanol on solutions of SDS has been subject to various studies.[121,138,304] The observed deviations may be due to the differences in the used experimental setup. A certain degree of uncertainty in the presented measurements of $1\,mmol \cdot L^{-1}$ SDS is to be assumed based on the slight deviations to the best fit parameters in contributions from Fruhner *et al.*[138] and Wantke and coworkers.[121] This points out the challenges in the use of the oscillating bubble method.

2.6 Electrocapillary Wave Studies

Electrocapillary wave (ECW) studies served as the second class of experiments to determine surface dilatational characteristics in an elevated frequency range comparable to the operating area of the oscillating bubble.

The data were found to show a rather pronounced scatter and extraction of valid surface visco-elasticity data was possible only at deformation frequencies exceeding around 20 to 25 Hz. The exact value was chosen depending on the respective sample in order to meet the criteria ensuring validity of results obtained from ECW-experiments.[305] Despite the noise in the amplitude and phase angle data, a similar, yet less pronounced trend as from the oscillating bubble experiments could be found. It does, however, not hold exactly for each solution in the series according to the specifications in Table III.1. Upon increasing the relative amount of salt, the amplitudes were found to decrease, whereas the phase angles gradually were shifted to lower values over the entire accessible frequency range. This behavior describes the transition of an initially visco-elastic adsorption layer to a more elastic state. Processes associated with a dissipation of energy are less pronounced for the solutions characterized by a high content of salt.

2.7 Correlation of Oscillating Bubble Results to Foam Stability Data

The mechanisms governing foam stability are very complex and several key parameters have been claimed to be found.[136,306] Depending on the method of foam generation, even opposite behavior concerning the amount of generated foam has been observed.[295] Here, a new parameter Λ showing a good correlation to all of the studied foam and lamella stability parameters (R5, $t_{1/2}$ and $\tau_{Lamella\ 90\,\%}$, see Figure IV.10) is introduced. It is derived from the parameters of the extended LvdT-model and defined as

$$\Lambda = \frac{\kappa \cdot \epsilon^{m}}{f_{diff}}. \tag{V.1}$$

This new parameter is a dimensional quantity given by the product of intrinsic surface dilatational viscosity κ and high frequency limiting elasticity ϵ^{m} normalized to the characteristic diffusion frequency f_{diff}. A rationale for this definition of the parameter is as follows: The elasticity modulus was frequently claimed to be responsible for the stability of foams.[307] The same holds for the intrinsic surface viscosity.[120] It is therefore a natural idea to mutually scale these quantities. The normalization with respect to the diffusion frequency was chosen in order to eliminate this parameter, *i.e.*, to compare the mutually scaled modulus and viscosity as if the diffusion frequency was constant. Therefore, a higher value of the parameter Λ is assumed to correlate with increased foam and lamella stability. Exemplarily, the half-life time of foam columns of the mixtures containing SDS and NaCl were plotted against the newly introduced parameter Λ in Figure V.2.

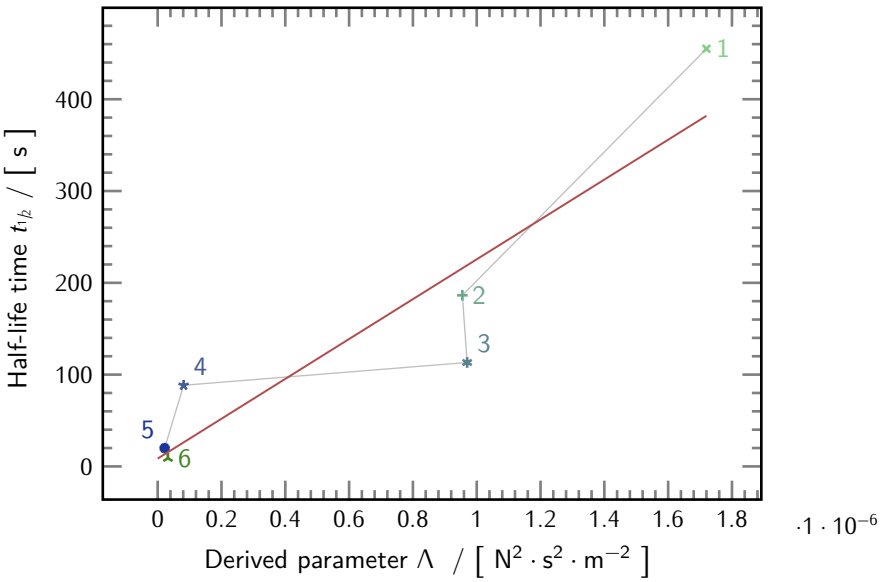

Figure V.2: Half-life time of foam columns of the mixtures of SDS and NaCl as specified in Table III.1 plotted against the newly introduced parameter Λ. It is derived from the LvdT fitting parameters of surface dilatational experiments (Symbols as in Figure IV.10).

The correlation of this parameter leads to an $R^2 > 0.8$ with all of the studied foam column and foam lamella stability parameters discussed previously.

2.8 Comparison of Bubble and ECW Data

Oscillating bubble experiments and ECW-studies allow accessing dilatational properties in roughly the same frequency range.[67] Whereas the perturbations in oscillating bubble experiments are bound

to take place due to mechanical interaction of the device with the volume phase of the sample, the surface deformations introduced by the non-invasive ECW-technique are determined by the system itself. Experiments conducted with the same solutions therefore – ideally – should yield the very same results.

Plotting the experimental results of amplitude and phase angle of the surface dilatational modulus E obtained from ECW and oscillating bubble experiments against one another clearly leads to a different picture as shown in Figures V.3 and V.4, respectively.

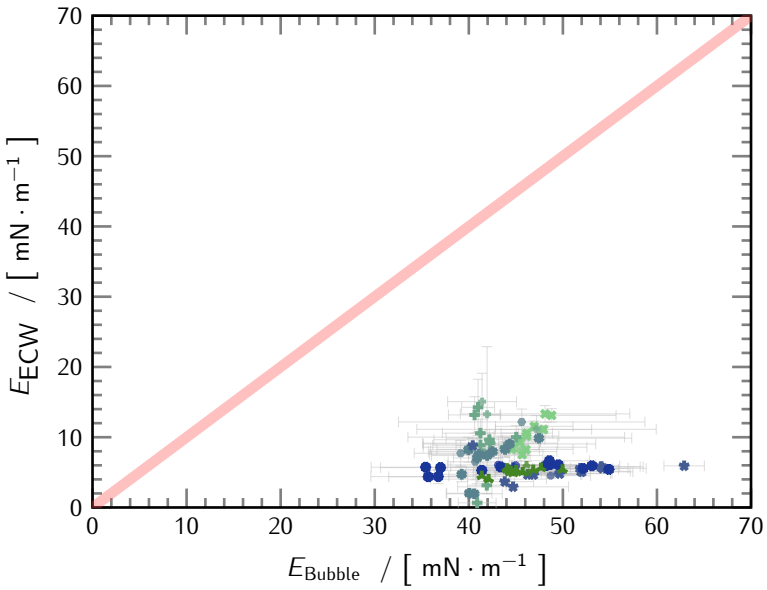

Figure V.3: Comparison of the absolute value of the surface dilatational modulus E obtained from ECWs and the oscillating bubble. One point corresponds to an experiment conducted at the same defined frequency with both the oscillating bubble and via ECWs. The color-code corresponds to the previous graphs of this section.

Not only, that both amplitude and phase values distinctly differ in their absolute values obtained from both methods, there is also no easy „offset"-behavior. Furthermore, the scatter is quite pronounced in each of the dimensions of the representation. Judging from comparison with the ideally equal result from both techniques as represented by the thicker red diagonal line, a very general and simplified observation can be made. Amplitudes collected by the ECW-technique are too low and phase angles are too high as compared to the oscillating bubble data. Not knowing which type of experiment yields the more valid results, the previous claim could also be stated inversely: The amplitudes from oscillating bubble experiments are too high and the phase angles it delivers are too low.

So far, there has been only scarce literature on the combination of these kinds of methods. Rather other combinations of surface rheological devices are applied when targeting to cover a possible broad frequency range.[308,309] As the notion of mutual validation of surface dilatational data from ECW

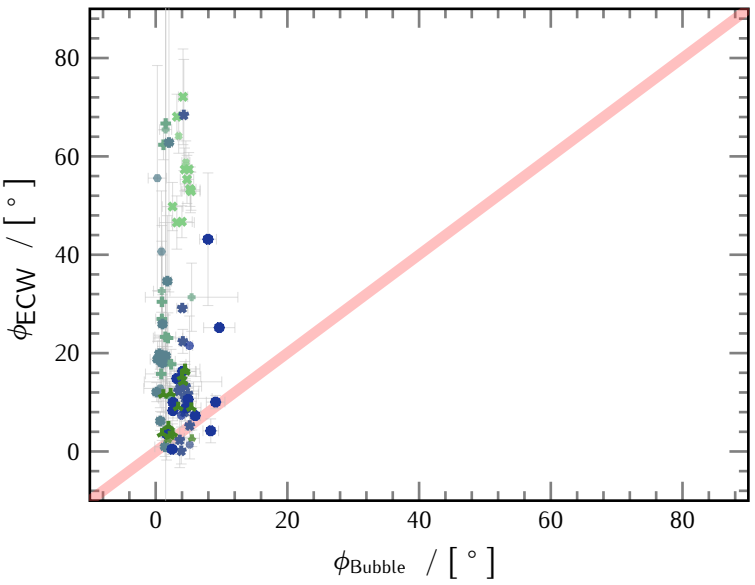

Figure V.4: Comparison of the phase angles of the surface dilatational modulus E obtained from ECWs and the oscillating bubble. One point corresponds to an experiment conducted at the same defined frequency with both the oscillating bubble and via ECWs. The color-code corresponds to the previous graphs of this section.

and oscillating bubble experiments in this specific frequency range did not lead to a fully satisfactory outcome, additional experiments aiming to check connectivity to lower frequency data were carried out. This will be discussed in the following.

2.9 Surface Dilatational Characteristics

Whereas both ECW and oscillating bubble setups serve to assess surface dilatational characteristics at frequencies above 1 to 10 Hz, oscillating pendant drop experiments target the adjoining lower frequencies down to the mHz-regime.

Exemplarily, the combined surface dilatational characteristics obtained from the applied experimental techniques (oscillating pendant drop, oscillating bubble and ECW) are compared for the limiting cases of the SDS-NaCl series containing pure surfactant and the highest salt concentration in Figures V.5 and V.6, respectively.

Here, the representation of the surface dilatational modulus E in terms of its constituting real and imaginary parts, rather than the previously used amplitude and phase picture was chosen. For the considered solutions, both the real and imaginary part of the surface dilatational modulus E as obtained from oscillating pendant drop experiments were found to increase upon elevated perturbation frequencies. The solution containing salt (see Figure V.6), however, is characterized by a much less

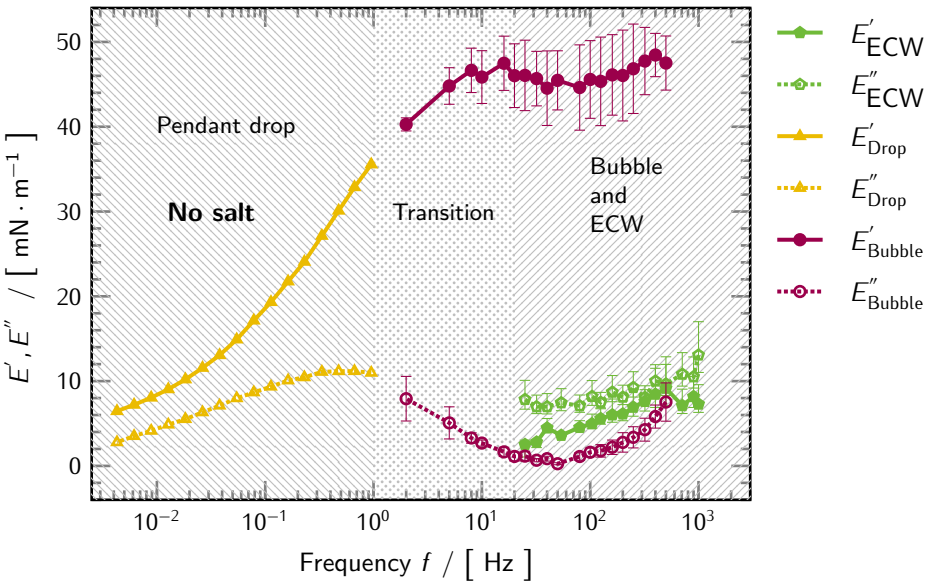

Figure V.5: Comparison of experimental surface rheological data obtained from oscillating pendant drop, oscillating bubble and ECW for the salt-free solution SDS-NaCl-1. The data at elevated perturbation rates from both high frequency methods are indicative for the formation of a stable foam.

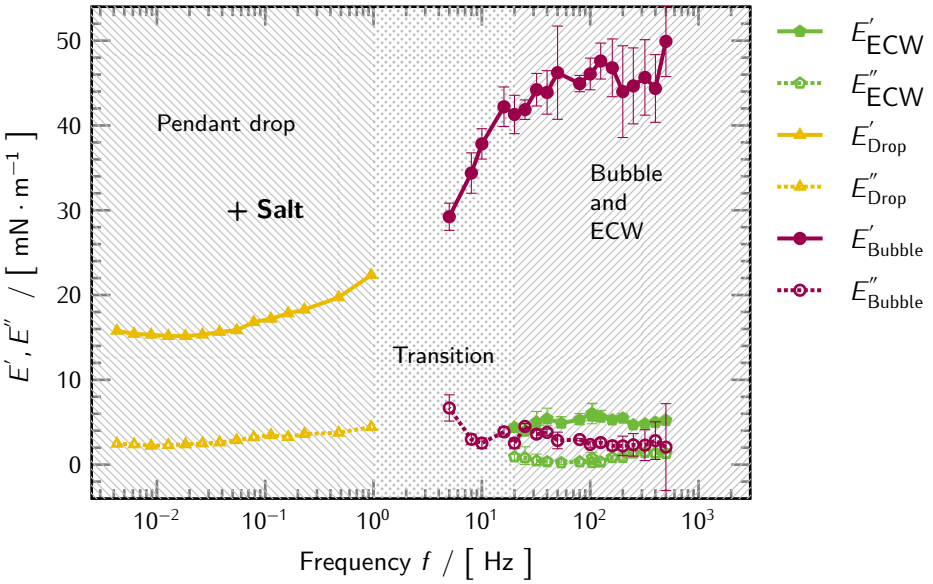

Figure V.6: Comparison of experimental surface rheological data obtained from oscillating pendant drop, oscillating bubble and ECW for solution SDS-NaCl-6. The data at elevated perturbation rates from both high frequency methods are indicative for the formation of a foam of poor stability.

pronounced frequency dependence in both its real and imaginary parts. Next to the rather low values of the loss modulus, also the storage modulus increases only slightly starting from a rather elevated amount upon rising frequencies.

The measurement of the surface dilatational modulus E requires several techniques to cover a sufficiently broad frequency range. Unfortunately, there is still a gap, where all known techniques are at their respective limits. Disregarding this transition zone, a more or less smooth connection between oscillating pendent drop and the high frequency methods was observed regarding the loss modulus for both solutions. Also the trend of increasing loss modulus for the salt free and the rather constant values of the loss modulus for the solution containing salt could be confirmed in the high frequency range. The situation turns out to be entirely different considering the real part of the surface dilatational modulus E. Values gathered by ECW tend to be lower by a factor of 5 to 10 as compared to the oscillating bubble results. A further difficulty hindering a full frequency range comparison is due to the fact, that capillary waves could be excited only at frequencies exceeding roughly 20 Hz. This leaves open a rather broad frequency range, where both the respective techniques approach their limits.

Nevertheless, it seems reasonable to assume that the connection of oscillating pendant drop and oscillating bubble data is sound also for the real part of the surface dilatational modulus E, which is not the case for the association of low frequency to ECW-data. Additionally, real and imaginary parts could be – more or less successfully – fitted simultaneously to the model presented in subsection 11.1 of chapter II. This potentially provides further evidence for the validity of the shown oscillating bubble data assuming that the model function was appropriate. Furthermore, this step-type behavior of surface dilatational characteristics is in agreement with published results aiming to study surfactant-particle interactions at liquid-liquid interfaces. [126]

2.10 Conclusion

A remarkably decreasing foam stability of aqueous solutions of SDS upon increasing the NaCl content has been confirmed for both foam columns and single foam lamellae. It is to be concluded, that both headgroup and hydrophobic chain interactions influence foam stability. Within the studied series of mixtures, headgroup repulsion decreases upon increasing salt concentration due to the more pronounced screening of the charged surfactant. This also allows for stronger inter-chain forces due to closer approach. These counteracting effects lead to comparable equilibrium surface tension values corresponding to similar values of adsorption, *i.e.,* surface coverage. At the same time, it is to be noted that the non-equilibrium properties of adsorption layers of these surfactant electrolyte mixtures differ significantly. This is especially pronounced at higher frequencies. By combination of the most adequate model constants of the surface dilatational data described in terms of the extended LvdT-model, a new derived parameter Λ has been defined. For the studied solutions, a high correlation of Λ to characteristic measures of foam column and lamella stability determined by different methods could

be established.

Concerning the comparability of ECW and oscillating bubble results, it is to be noted that no full agreement of the respective surface dilatational data could be confirmed. In this very case, the differences in absolute values were too large to allow for a quantitative comparison. Nevertheless, the general trend of a transition from surface viscoelastic to surface elastic adsorption layers upon addition of salt was recovered from both data sets. Issues that need to be pointed out are the major drawbacks of the methods. Whereas ECW-studies heavily depend on the underlying hydrodynamic theory for the extraction of surface rheological parameters, oscillating bubble experiments are – in the current version of the experimental setup – limited by the precision and validity of the applied calibration substance and algorithm. Despite these not yet entirely clarified concerns, both methods can serve as valuable tools for, *e.g.,* relating foam stabilities to physico-chemical properties of adsorbed interfacial layers. The appearance of a clearly non-zero value of the loss-modulus especially at elevated frequencies was found to be the decisive factor determining foam stability in this admittedly simple surfactant-electrolyte system. Interestingly enough, this feature could be confirmed by both of the high frequency surface dilatational techniques applied.

3 Ion Specific Effects in Alkali Decyl Sulfates

3.1 Surface Tension

The experimentally observed trend of decreasing surface tension upon increasing mass of the counterion coincides reasonably with the earlier observations published by Warszyński *et al.* on this subject.[26] Equally, this holds for the absolute values. The consistency of these results approves a proper state of the studied alkali decyl sulfates (XDeSs).

A fit of the experimental data using the theoretical model accounting for both surfactant and counterion adsorption (see Section 3 of chapter II) within the Stern-layer allows for a precise description of the equilibrium surface tension results below the respective critical micellar concentrations (cmcs). Furthermore, a decomposition of the overall adsorption into contributions arising from the decyl sulfate (DeS) surfactant ion and the respective counterion could be achieved. The agreement of measured equilibrium surface tension γ_e as a function of bulk surfactant concentration with the corresponding theoretical curve as shown in Figure V.7 is remarkably increased compared to the conventional surface equation of state (SEOS)-based Frumkin-fit in Figure IV.15.

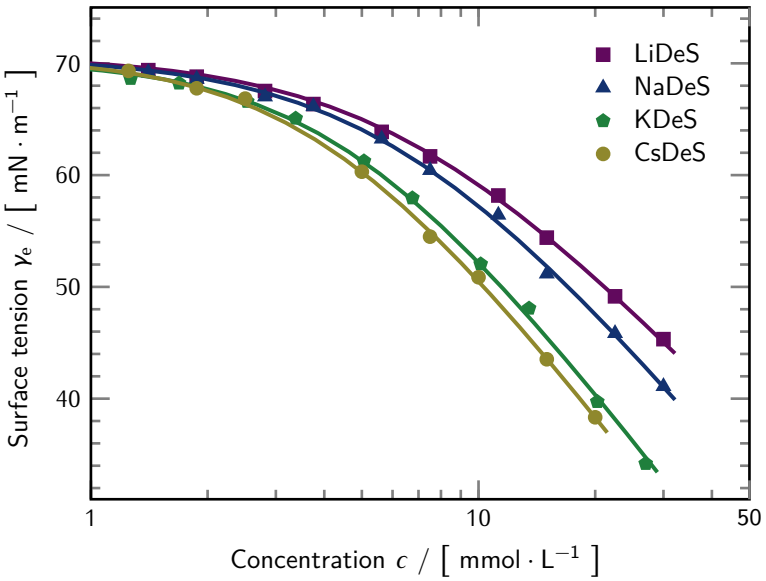

Figure V.7: Experimental surface tension isotherms of aqueous solutions of LiDeS, NaDeS, KDeS and CsDeS with the respective best fits according to the theory outlined by Warszyński and coworkers (solid lines of the respective color).

According to the individual surface concentrations, *i.e.*, values of adsorption Γ of surfactant ion and counterion as shown in Figure V.8, the specificity effect is recovered for both of the species. The surface concentration of the counterion – model-intrinsically – remains below the value of the surfactant ion. Nevertheless, this implies that an increased adsorption of a counterion is accompanied

by a higher surface activity of the surfactant ion DeS. As the nature of DeS certainly does not differ for the studied XDeSs, it is noteworthy to point out this tunability of DeS surface affinity via the counterions' tendency for adsorption.

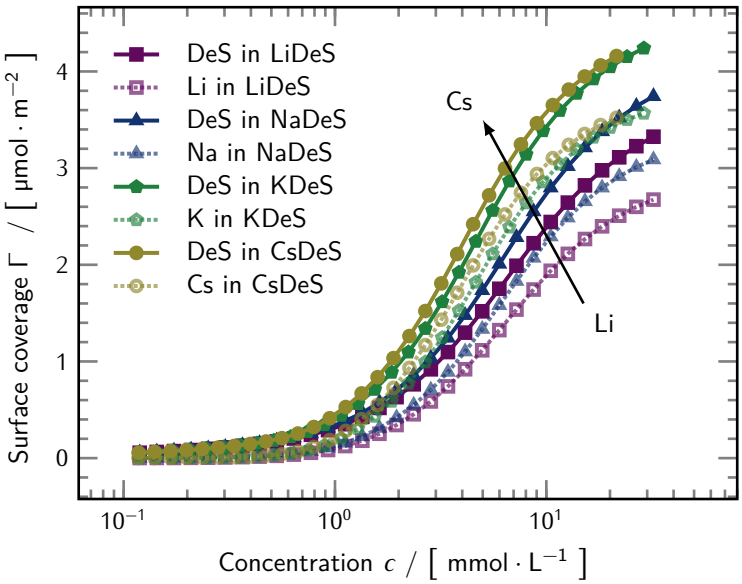

Figure V.8: Calculated adsorption of surfactant ions and the respective counter-ions for LiDeS, NaDeS, KDeS and CsDeS. The counterion adsorption is lower than the corresponding DeS adsorption for all the studied XDeSs. An increasing adsorption for both of the comprising ionic species from LiDeS to CsDeS is evident.

The surface concentration of both the surfactant ion and counterion was confirmed to be higher for smaller, weakly hydrated CsDeS. Lower values were observed for the strongly hydrated and therefore in bulk solution larger LiDeS.[26] Interestingly enough, the series of increasing *atomic* radii from Li to Cs is reversed for the monovalent *hydrated* cations.[310] Consequently, the values of adsorption calculated from the experimentally determined equilibrium surface tension isotherms imply a closer packing within the interfacial layer in the presence of smaller hydrated Cs-ions. Warszyński *et al.* argued that according to the decomposed surface concentration for the considered types of ions, more than 80 % of the charge inside the Stern-layer is compensated.[26] Under the static conditions of the conducted equilibrium surface tension experiments, counterions which are smaller in their hydrated state will therefore lead to the formation of more compact adsorption layers.

As discussed and derived by Ivanov *et al.*, concentration dependent equilibrium surface tension γ_e of ionic surfactants can be described by a linearized dependence on a concentration-proportional quantity (see Figure IV.16).[230,311] By means of this approach, surfactant solutions with and without added electrolyte are treated equally. Next to „collapsing" equilibrium surface tension isotherms of ionic surfactants dissolved in electrolyte solutions of varying concentration, Ivanov's version of the surface tension isotherm is highly valuable for pointing out the effects of ion specificity in the latter class of

amphiphiles. They showed the surface tension γ_e and surface concentration Γ to linearly depend on $c^{2/3}$ for comparable surfactants at low coverage and suggested an extraction of a dimensionless adsorption constant K from a linear fit of equilibrium surface tension γ_e against the rescaled concentration axis in analogy to the Henry isotherm via

$$\Gamma = K \cdot c^{2/3}. \tag{V.2}$$

The corresponding SEOS allows for an extraction of the adsorption constant K with an additional parameter a_1, which is close to the equilibrium surface tension of the pure solvent. It is given by

$$\gamma_e = a_1 - 3k_B T \cdot K \cdot c^{2/3}. \tag{V.3}$$

In order to relate the experimentally accessible adsorption constant K to properties on the molecular scale, the calculation of the non-electrostatic adsorption energies of the counterions from the solution u_0 is crucial. Theoretical considerations demand, that the logarithm of the adsorption constant K has to be related to the negative of the adsorption energy u_0 via a linear relationship with slope $1/2$. In order to obey this relation, critical parameters such as radii of hydrated ions have to be selected appropriately from literature. The adsorption energy u_0 can be obtained from a geometrical interaction model taking into account the London expression for the intermolecular potential.[230] A comparison of the experimentally gained slopes plotted against the calculated negative Boltzmann-scaled adsorption energies of the respective counterions to literature data is given in Figure V.9. Next to the results from the previously mentioned study by Warszyński *et al.* on XDeSs, also sodium dodecyl sulfate (SDS) in presence of alkali chlorides M^IX was shown to obey the relationship between adsorption energy and adsorption constant K. The extracted values of K are summarized in Table V.1.

Table V.1: Dimensionless adsorption constant K as obtained from the linear fit of surface tension as a function of the rescaled concentration $\gamma_e(c^{2/3})$ according to Equation V.3. The values obtained for the studied XDeSs as shown in Figure IV.16, solutions of XDeSs studied by Warszyński *et al.*[26] and mixtures of 0.5 mmol · L^{-1} SDS with alkali-chlorides M^IX of varying concentration studied by Ivanov *et al.*[230] are compared.

Counterion	K_{XDeS} [1]	K_{XDeS} [26]† [1]	K_{SDS} [230]‡ [1]
Li	33.43	36.29	105
Na	39.66	40.47	123
K	51.92	54.80	166
Cs	56.62	57.47	166

The increased adsorption constant K observed for longer chain dodecyl sulfate (DS) compared to DeS

†extracted from the provided experimental data according to the outlined procedure.
‡use of values tabulated in the respective publication.

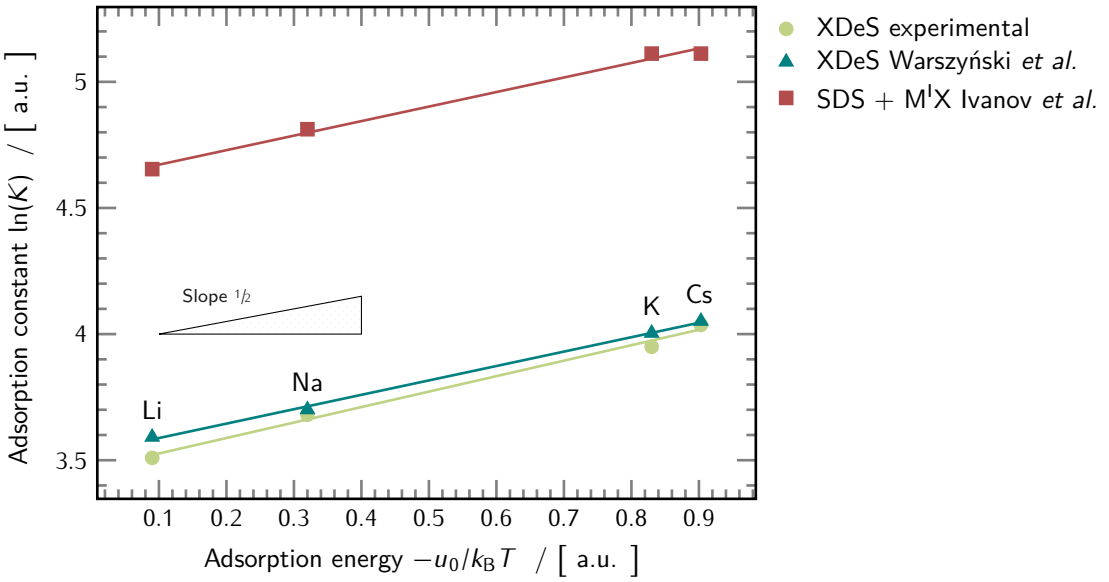

Figure V.9: Natural logarithm of the adsorption constant K plotted against the dimensionless adsorption energy of the respective alkali ion for decyl sulfate from this study, decyl sulfate from Warszyński *et al.*[26] and SDS in the presence of the respective alkali chlorides $M^{I}X$ from Ivanov and coworkers.[230] The solid lines represent the best linear fits with a slope close to the theoretical value of 0.5.

is to be understood as a consequence of the higher solubility of DeS.[230] Good agreement between the experimental results and the values derived from the data provided by Warszyński *et al.* for the adsorption constant were found.[26]

3.2 Time Dependent Surface Tension

The absence of a temporal dependence in surface tension is considered one of the criteria to judge the state of surface chemical purity in a surfactant solution.[169,172] As evident from Figure IV.17, there is still a slight decrease in the experimental value, which is indicative for trace amounts of amphiphiles competing for adsorption towards the surface. The fact that the equilibrium surface tension isotherms published by Warszyński *et al.* could be recovered both in their trends and roughly in terms of absolute values was assumed to be adequate for the main purpose of the study conducted here.[26] Additionally, there was only a subtle change in surface tension over the studied time frame. Surface dilatational rheology of aqueous solutions of XDeSs at specified values of equilibrium surface tension γ_e and its relation to foam stability was the major aim of this investigation. The solutions eventually studied at their respective concentrations did not differ by more than $\pm 1\,\mathrm{mN \cdot m^{-1}}$ in surface tension, which was expected to be sufficient for the purpose of the study.

3.3 Foam Stability

As pointed out previously, a smooth transition from low stability to high stability foams along the ion specific series established from equilibrium surface tension measurements was *not* clearly evident in the conducted foam stability experiments. For each of the studied solutions with non-negligible foaming behavior (45 and $55\,\mathrm{mN \cdot m^{-1}}$) there is one counterion causing an outlier in the trend of foam column decay (see Figure IV.18). This is additionally complicated by the fact, that the non-monotonous course of foam stability parameters varies with equilibrium surface tension γ_e. Whereas for the $45\,\mathrm{mN \cdot m^{-1}}$ solutions, NaDeS was found to generate „too stable“ foams, the same holds true for KDeS at $55\,\mathrm{mN \cdot m^{-1}}$. In this case, the typical ordering is hampered by a „too low“ stability of CsDeS or „too high“ stability for the solution of KDeS. As in other experiments, NaDeS and KDeS were found to behave similarly and NaDeS maintained its position in the series, the role of the outlier is ascribed to KDeS for the $55\,\mathrm{mN \cdot m^{-1}}$ samples.

Due to repeated difficulty in collecting valuable assessments of stability from analysis of foam columns possibly caused by non-uniform rupture or other artifacts, a more simplistic approach was chosen. A rough approximate estimation of foam stability was obtained by manually shaking defined volumes of aqueous solutions at constant equilibrium surface tension γ_e of $55\,\mathrm{mN \cdot m^{-1}}$ for a certain time. The picture in Figure V.10 was taken a few seconds after the foam generation process. Interestingly enough, a trend of increasing stability along the series from LiDeS over NaDeS and KDeS to CsDeS could be confirmed from this – admittedly not highly scientific – method.

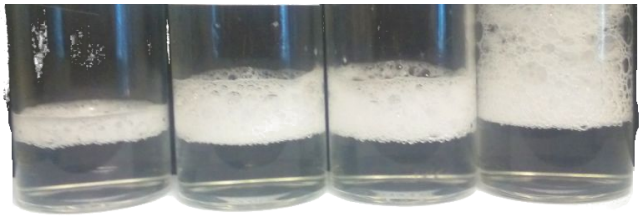

LiDeS NaDeS KDeS CsDeS

Figure V.10: Photograph of manually foamed XDeSs columns from solutions with an equilibrium surface tension γ_e of 55 mN · m^{-1}.

It is to be noted, however, that this observation was to be expected solely from the oscillating bubble results gathered for the aqueous solutions of XDeSs making use of experience from previous projects. The corresponding surface rheological data will be discussed in the following.

Even though literature on the effects on ion specificity is not abundant, there have been some interesting findings.[174] Pandey *et al.* demonstrated increasing foam stability of the closely related DS in the series of counterions from Li over Na and Cs to Mg at sub-cmc concentrations in a similar experiment.[312] Besides these cation-related effects, also the ion specificity in foaming behavior introduced by different anions has been subject to investigations. Whereas protein isolates from *Lablab purpureus* were found to be stabilized by the presence of chaotropic, soft counterions, the opposite holds true for whey protein isolate.[313,314]

3.4 Oscillating Bubble

A trend of ion specificity was equally observable under the dynamic conditions of the conducted surface rheological measurements applying dilatational deformation by means of the oscillating bubble technique. As previously discussed in subsection 3.1, the deviating behavior of the investigated DeS surfactant ions accompanied by various alkali counterions may be accounted for by the different hydrated sizes of the latter in solution. In a highly recognized contribution, Collins chose to classify ions according to their ability for „structure-breaking“ and „structure-making“ in aqueous solutions, whereas the interaction strength between two water molecules is considered the reference of this ordering scheme.[315] Small, hardly polarizable ions are characterized by a stronger attraction to water than other water molecules. They are referred to as cosmotropic, *i.e.*, order-inducing. Larger and therefore more polarizable ions having less affinity to water are called chaotropic. For alkali-metal ions the dividing line between these two types of behavior is situated between K and Na. In principle, the Collins-concept is to be understood as an evolution of the hard and soft acids and bases-approach suggested by Pearson more than 40 years earlier.[316–318]

Going back to the relation between the size of the hydrated ion and the experimentally assessed

surface dilatational rheological characteristics, it is to be noted that the presence of smaller hydrated ions is associated with elevated values of the amplitude and the phase angle of the surface dilatational modulus E. Exemplarily, the amplitude is higher by a factor of roughly two and also the phase angle is significantly increased for the small hydrated Cs-ion in CsDeS as compared to the highly solvated and therefore large Li-ions in LiDeS. These characteristics of CsDeS are associated with a larger force counteracting an induced deformation of the surface area and simultaneously an increased viscous loss in the course of this procedure. Adsorption layers of CsDeS were found to exhibit more pronounced surface viscoelastic behavior with higher values of the amplitude of the surface dilatational modulus E compared to LiDeS. The picture of a closer packing within the equilibrium adsorption layers in the presence of smaller hydrated counterions therefore is in agreement with the findings under dynamic conditions. A higher adsorption density of adsorbed surfactant requires more energy for perturbation of the respective layer. This manifests in an elevated amplitude of the surface dilatational modulus E. Furthermore, the combination of larger values of the amplitude of the complex modulus with elevated phase angles suggests the formation of stable foams.

A possible reason for the deviation of NaDeS under dynamic conditions could be identified from subsequently collected dynamic light scattering (DLS) data. In contrast to the correlograms obtained from the other solutions, an onset of a bimodal distribution at the concentration of the used stock solutions was observable. Complementary measurements above cmc of – not surface chemically purified – samples confirmed the non-monomodal aggregation exclusively for solutions of NaDeS. The deviations of NaDeS under dynamic conditions therefore suggest a not entirely successfully conducted surface chemical purification procedure. Nevertheless, an effect of ion specificity on the dynamic interfacial properties of aqueous solutions of alkali DeSs was demonstrated.

3.5 Conclusion

Despite the study of ion specific effects representing a field of active interest to colloid and interface science, corresponding studies of foam stability have attracted little attention so far. Aqueous sub-cmc solutions of XDeSs have been characterized with respect to their adsorption behavior at the air-water interface and analyzed in terms of their deviating surface affinity by the theory of simultaneous surfactant and counterion adsorption outlined by Warszyński.

Even though a clear Hofmeister series was not evident from measurements of foam column stability, a rough estimate trend in agreement with published literature results for structurally related alkali-DS could be obtained. Accordingly, foam stability should increase with the chaotropic nature of the cationic counterion. This evolution is in agreement with surface dilatational properties assessed by the oscillating bubble technique. Solutions of both elevated values of the amplitude of the surface dilatational modulus E and phase angle ϕ were found to lead to the formation of more stable foams. Additionally, these findings under non-equilibrium conditions could be related successfully to the information obtained from conventional measurements of equilibrium surface tension γ_e. Higher

adsorption of smaller *hydrated* ions equally favors a transfer of the oppositely charged DeSs. Due to the smaller extension of the cation, the surfactant molecules can approach each other more intimately. This results from the reduced steric repulsion introduced by the cation and stronger dispersive interactions between the hydrophobic moieties of interfacial DeSs. The dilatational probing of this „more dense“ DeS layer strengthened by the presence of small counterions manifests as an increased amplitude of the surface dilatational modulus E with the consequence of more pronounced foam stability on a macroscopic level.

In order to further quantify the validity of this concept, an extended version of this experiment using surfactants of different chain lengths and counterions on the extreme ends of the Hofmeister series, also taking into account differently charged ions, would be desirable. The resulting clarification of the relative importance of electrostatic surfactant-counterion interactions, headgroup-headgroup-repulsion and dispersive chain attraction is expected to contribute to the understanding of ion specificity in foams.

4 Ion Specificity in Adsorption Layers of *n*-Dodecylphosphinecholine

4.1 Density, Viscosity and Electrical Conductivity

By virtue of their sufficiently high solubility dissolution of both $Ce(NO_3)_3$ and $Yb(NO_3)_3$ increases the number of charge carriers within the solution. Besides elevated densities as compared to the „empty" solvent, this comes along with increased values of electrical conductivity and viscosity. Whereas the relation between the respective property and the concentration is roughly linear in the highly dilute regime, more or less pronounced deviations from this behavior can be observed at higher concentrations.[190]

The experimentally observed increasing viscosity upon rising salt concentration is in agreement with previous, long-standing findings. For strong electrolytes at low concentrations, Jones and Dole suggested a relation between viscosity η and solute concentration c given by[319,320]

$$\eta_{\text{normalized}} = 1 + A\sqrt{c} + Bc. \tag{V.4}$$

The parameters A and B extracted from a concentration dependent fit of the viscosities normalized to the pure solvent viscosity, *i.e.*, $\eta_{\text{normalized}} = \eta/\eta_{\text{solvent}}$ can be traced back to interactions within the solution. Whereas A takes into account the interaction between ions, the coefficient B serves to describe interactions between solvent and solute. It has been used as one of the first measures of ion specificity.[321–323]

4.2 Isothermal Titration Calorimetry

Hydration enthalpies of $Ce(NO_3)_3$ and $Yb(NO_3)_3$ were intended to be derived from isothermal titration calorimetry (ITC) measurements via extrapolation to infinite dilution of the data shown in Figure IV.26. It is to be noted that here only the heat coloring upon further dilution of an electrolyte solution was measured. An extrapolation using an empirical expression yields a more negative value for $Ce(NO_3)_3$ as compared to $Yb(NO_3)_3$. This means, that the further dilution of $10\,\text{mmol}\cdot\text{L}^{-1}$ $Ce(NO_3)_3$ with pure water is more exothermic compared to the same process for $Yb(NO_3)_3$.

Keeping in mind, that the differences are bound to originate exclusively from the nature of the cation, this finding is rather surprising judging from the hydration enthalpies and ionic radii tabulated for the respective ions.[237,324,325] Even though the absolute values of the trivalent ionic radii differ depending on the source, they are reported to decrease with increasing atom number due to the effect of lanthanide contraction, *i.e.*, Ce^{3+}-ions are larger than Yb^{3+}-ions. From an exclusively electrostatic point of view, the closer approach between cation and coordinating species is expected to lead to a

more exothermic binding under the assumption that the same number of water ligands can interact. From the experimental ITC-data, however, a stronger binding, *i.e.,* association of water was suggested for the larger $Ce(NO_3)_3$. This finding could be rationalized by the presence of *more* rather than *stronger* binding of water towards the larger $Ce(NO_3)_3$ as compared to smaller $Yb(NO_3)_3$. It is to be noted that the terms „smaller“ and „larger“ used in this context refer to the crystallographic radii.

4.3 Surface Tension

The equilibrium surface tension isotherm of *n*-dodecylphosphinecholine (DPC) features the typical behavior of an aggregating surfactant characterized by decreasing values up to the critical micellar concentration (cmc), after which the value remained constant within experimental error. Even though the hydrophobic part of the studied DPC does not differ from the anionic standard surfactant sodium dodecyl sulfate (SDS), the cmc is greatly reduced from $8\,\mathrm{mmol}\cdot\mathrm{L}^{-1}$ to the range from 1 to $2\,\mathrm{mmol}\cdot\mathrm{L}^{-1}$.[326] This finding is indicative for a reduced solubility of the zwitter-ionic phosphocholine headgroup compared to the negatively charged and therefore more hydrophilic alkyl sulfate in SDS. Nevertheless, the sub-cmc part of the equilibrium surface tension isotherm can be described satisfactorily relying on the Langmuir adsorption isotherm

$$\gamma_e = \gamma_0 - RT\Gamma_\infty \cdot \ln(1 + K_L c) \tag{V.5}$$

with the maximum surface coverage Γ_∞ and the Langmuir adsorption constant K_L as adjustable model parameters. The equilibrium surface tension of the solvent is represented by γ_0 and the constants R and T have their usual meanings.

Furthermore, the absence of aggregates in $1\,\mathrm{mmol}\cdot\mathrm{L}^{-1}$ DPC solutions in presence of $30\,\mathrm{mmol}\cdot\mathrm{L}^{-1}$ $Ce(NO_3)_3$ and $Yb(NO_3)_3$, which have been studied in more detail in further surface rheological and foam stability investigations, was confirmed by vanishing magnitudes of the autocorrelation function in dynamic light scattering (DLS) measurements. The concept of inducing aggregation in ionic surfactant solutions upon addition of salt, *i.e.,* shifting the isotherm further towards lower concentrations is reported.[327] The zwitter-ionic surfactant DPC appeared to be unsusceptible to this effect in case of adding $Ce(NO_3)_3$ or $Yb(NO_3)_3$ at the specified concentrations.

4.4 Foam Stability

Mixtures containing the soluble surfactant DPC and two types of lanthanide electrolytes confirmed a similar trend of foam stability as discussed in section 2 for the SDS-NaCl system. The addition of salt was equally found to bring along a reduced foam stability of the respective aqueous solutions for the zwitter-ionic amphiphile. As this charge distribution within the headgroup demands an electrostatic interaction with both the cation and the anion of the respective added salt, the deviating foam

stabilities have to be accounted for by the nature of the cation.

The most prominent feature of a spherical ion is its radius. Foams generated in presence of the larger Ce-ions ($r = 1.01\,\text{Å}$) as compared to the smaller Yb-ions ($r = 0.86\,\text{Å}$) were characterized by a reduced lifetime.[328] This implies, that larger charge carriers either have an intrinsic destabilizing mechanism or that they counteract the usually operative stabilizing mechanisms more effectively than ions with smaller radii. The latter effect might be the weakening of hydrophobic interactions between the alkyl chains of the surfactant adsorbed towards the interface. A cation-intrinsic destabilization might be due to the preferred interfacial adsorption of the „softer“ Ce-ions.

Interestingly enough, also the initial foam volumes generated under the same conditions almost coincided for the respective surfactant solutions containing electrolyte. In both cases they were remarkably higher than for the pure surfactant. A non-negligible deviation of initial foam volumes between the studied samples could be identified, nevertheless. This observation is indicative for foamability, *i.e.,* the foam volume obtained under certain constraints being related to equilibrium surface tension γ_e as well. A lower value will allow for the creation of larger surface areas upon the same energy input. The equilibrium surface tension γ_e of salt-free $1\,\text{mmol} \cdot \text{L}^{-1}$ DPC was found to decrease from roughly $44\,\text{mN} \cdot \text{m}^{-1}$ in presence of the studied lanthanide-(III)-nitrates to reduced values. Approximate reductions by 4 and $8\,\text{mN} \cdot \text{m}^{-1}$ manifested in 1.3 and 1.5-fold initial foam volumes for $30\,\text{mmol} \cdot \text{L}^{-1}$ $Ce(NO_3)_3$ and $Yb(NO_3)_3$, respectively.

4.5 Oscillating Bubble

As pointed out in subsection 4.5 of chapter II, a clear distinction between the three studied solutions was possible in terms of the amplitudes of the surface dilatational modulus E, whereas the phase angles agreed within experimental error in presence of the electrolyte. The characteristics of an increasing modulus and decreasing phase angle are indicative for a transition from a surface viscous towards a more surface elastic behavior upon addition of an electrolyte. This could be confirmed for both studied mixtures of DPC with the respective lanthanide-(III)-nitrate. The extent of this effect on the modulus is assumed to be due to ion specificity as the system was varied only with respect to the type of the cation.

These findings are in agreement with a previous study on a mixed surfactant-electrolyte system comprising SDS and $Ce(SO_4)_2$. It served as a proof of principle, that a transition from surface viscous to surface elastic behavior could be induced by addition of a highly charged electrolyte to an ionic surfactant.[329] Here, the effects are more subtle but still follow the same trend. This is the case for several reasons. First, the concentration of the DPC probe molecule was reduced as compared to the previous study. Second, the strength of the generally strong electrostatic interaction between the surfactant headgroup and the electrolyte ions was reduced by using a zwitter-ionic instead of an anionic headgroup and three-fold positively charged cations rather than the Ce(IV)-ions.

Interestingly enough, even at this rather low surfactant concentration, the ion specific influence of the respective salt solution on the dynamic properties of the DPC adsorption layer serving as a probe for these effects can be clearly discerned. The differences in the surface dilatational modulus E are assumed to be due to deviating interaction strengths between the zwitter-ionic surfactant headgroups and the ions formed from the dissolved salt. Especially the solvation behavior of the electrolyte is expected to be decisive.

4.6 Dielectric Relaxation Spectroscopy

The importance of a valid and robust fitting procedure is crucial for the extraction of meaningful parameters and thus a sound quantitative interpretation of dielectric relaxation spectroscopy (DRS) data. Generally, small-amplitude modes peaking at the edges of the covered frequency range tend to be over-estimated in terms of their amplitudes.[165] Here, especially the mode due to the dipolar species formed in presence of the respective electrolyte is located rather closely to the lower border of the accessible frequency range and characterized by a low amplitude. This is anticipated from the almost indistinguishable relative permittivity $\epsilon'(\nu)$ in the raw data. The values found with the approach described in subsection 11.2 of chapter II tend to be lower as compared to the formerly used IGOR-script.[159,163,330] Furthermore, no restriction of any of the model constants was required to reach a stable solution.

From analysis of the best fit amplitude of the relaxation modes reported in Table IV.2, solvation numbers of the corresponding dielectric species can be inferred.[165] Therefore, the analytical water concentration c_{H_2O} is compared to the apparent water concentration $c^{app}_{H_2O}$ and normalized with respect to the concentration of the dipolar species introduced due to the presence of the electrolyte c_{IP} to yield the effective solvation number Z_{eff} via

$$Z_{eff} = \frac{c_{H_2O} - c^{app}_{H_2O}}{c_{IP}}. \tag{V.6}$$

The latter two concentrations, *i.e.*, $c^{app}_{H_2O}$ and c_{IP} are calculated from the respective peak amplitudes via the Cavell-equation assuming slip boundary condition for kinetic depolarization.[331] The concentration dependent results for the electrolyte solutions of $Ce(NO_3)_3$ and $Yb(NO_3)_3$ are summarized in Figure V.11.

As evident from this plot of solvation numbers against the electrolyte concentration present in the sample, the dielectric species formed from $Yb(NO_3)_3$ are generally characterized by a higher degree of solvation. Typically, *the* solvation number of an electrolyte solution refers to the extrapolation of this value against zero, *i.e.*, the idealistic case of infinite dilution. Here solvation numbers of 58.4 ± 7.5 and 46.1 ± 3.6 were identified for $Yb(NO_3)_3$ and $Ce(NO_3)_3$, respectively.

The apparent lower solvation number in case of $Ce(NO_3)_3$ compared to $Yb(NO_3)_3$ further complicates

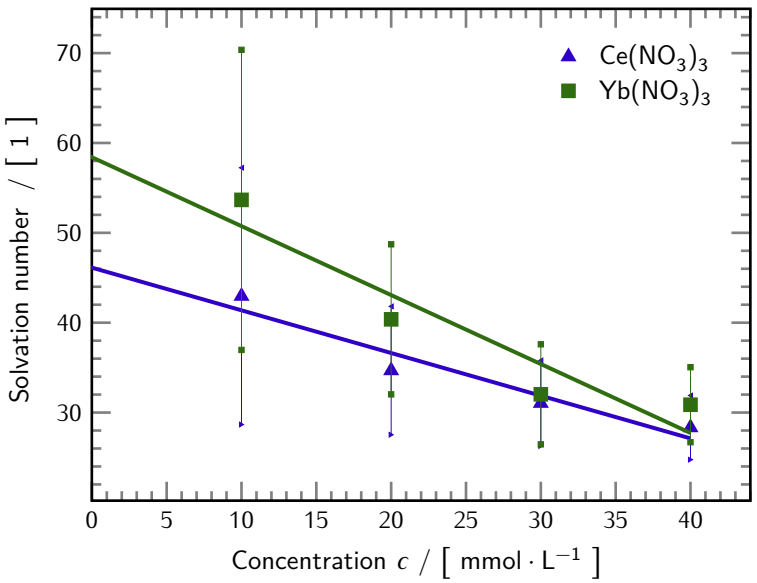

Figure V.11: Solvation numbers of the dipolar species inferred from analyzing the respective peak amplitude and salt concentrations of $Ce(NO_3)_3$ and $Yb(NO_3)_3$. Solid lines correspond to the respective linear regressions.

the interpretation of the previously discussed ITC data. As the more exothermic dissolution of $Ce(NO_3)_3$ could be rationalized neither in terms of a stronger individual electrostatic interaction nor an increased number of ion-water contacts via the solvation number, additional forces have to be operating in order to explain the findings from ITC. These forces could be related to the existence of more pronounced dispersion forces in Ce^{3+}-ions compared to Yb^{3+}-ions. Despite the higher number of electrons in Yb, the ions are „harder“ and possibly less polarizable due to the contraction effect, which supports the concept of relevant dispersion forces in $Ce(NO_3)_3$.

4.7 Relating Surface and Bulk Properties

In order to get further insight into the effects of ion specificity for the studied system, all of the experimental evidence from the different types of measurements will be taken into account. The main finding is that a higher bulk solvation number of the respective pure electrolyte solution as inferred from the DRS study comes along with an increased value of the surface dilatational modulus E and *vice versa*. In the following, a rationale for this behavior is suggested.

The oscillating bubble technique serves to characterize the exchange processes between bulk and interface upon varying surface area. During a surface area expansion, this comprises – on a molecular level – the desolvation and transfer of surfactant and ions towards the interface. In case of $Yb(NO_3)_3$ present in the solution, a larger number of water molecules will have to be forced away from the dipolar species assessed by DRS and accordingly also the cation. In the oscillating bubble experiments,

this results in an increased surface dilatational modulus E.

Going back to the molecular level picture, a concept unifying the experimental results can be developed. It is assumed, that the interaction strength between the zwitter-ionic surfactant headgroup and the dipolar species probed via DRS is the determining factor for the amplitude of the surface dilatational modulus E. A strong interaction is anticipated to be related to higher values of the surface dilatational modulus E. As schematically shown in Figure V.12, the combined information from DRS- and ITC-experiments suggests the presence of a larger and simultaneously less strongly bound water shell around the dipolar species formed from $Yb(NO_3)_3$ as compared to $Ce(NO_3)_3$. Consequently, this „softer“ shell around $Yb(NO_3)_3$ at only slightly differing ionic radii should be easier to be stripped off upon approaching the interfacially adsorbed DPC to form quadrupole-type interactions. As this mechanism is associated with a higher energy barrier in case of the more tightly bound and smaller shell in $Ce(NO_3)_3$, also the interaction strength between dipolar electrolyte species and the headgroup is reduced.

4.8 Conclusion

A combination of surface rheological measurements and DRS in conjunction with ITC was used in order to identify possible origins of ion specific effects in aqueous mixtures of the soluble phospholipid model substance DPC and the lanthanide-(III)-electrolytes $Ce(NO_3)_3$ and $Yb(NO_3)_3$. The transition towards a more surface elastic behavior of surfactant adsorption layers upon addition of highly charged salts found in a previous study could be – to a less pronounced extent – confirmed. Additionally, an ion specificity of the used salt having an influence on the amplitude of the surface dilatational modulus E was detected. This finding is suggested to be caused by the deviating solvation behavior of the respective dipolar species in the bulk and its consequences for the interaction with the zwitter-ionic headgroups of DPC. The need to overcome this solvent association with the dipolar electrolyte species to achieve a transfer towards the interface is associated with a certain energy manifesting in the surface dilatational modulus E. Further experiments using additional lanthanide salts and will be required to clarify the suggested relation between DRS and oscillating bubble data, *i.e.,* bulk solvation behavior and surface dilatational modulus E. Furthermore, an in-depth study of mixed DPC electrolyte solutions is expected to contribute significantly to the understanding of the governing processes. A first set of preliminary DRS data (not shown) obtained for mixed DPC-electrolyte solutions suggests that in this case ion specificity is a purely interfacial effect, as the spectra were almost indistinguishable to the results given in the previous sections.

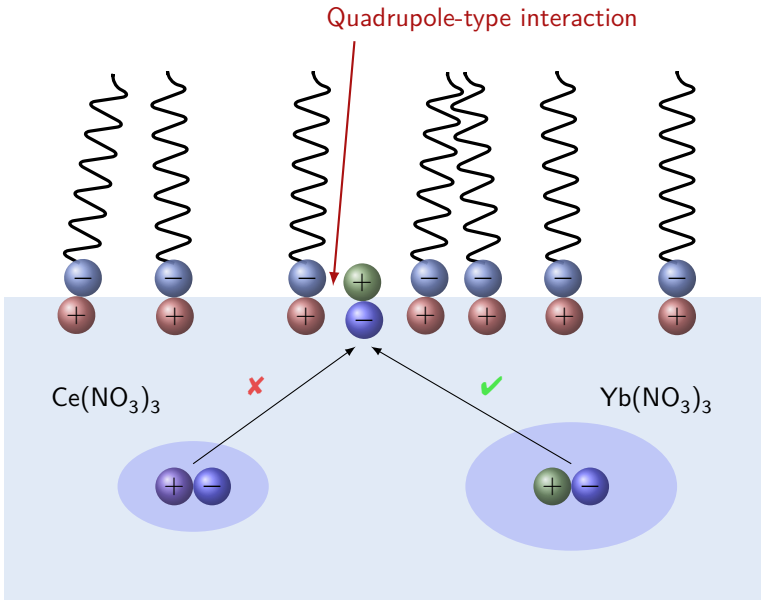

Figure V.12: Interaction scheme in mixed DPC-lanthanide-(III)-nitrate layers.

5 Photo-Responsive Azo-surfactant

5.1 Ultraviolet-Visible-Spectroscopy

As described previously, the spectra of T226's *cis*- and *trans*-isomers differ most significantly in the spectral range around 350 nm. The absorption in this region is characteristic for the composition of the solution in terms of relative amounts. Upon continued illumination with ultraviolet (UV) or visible (Vis) light, the absorption spectrum is modified accordingly. On a molecular scale, the transition towards lower absorption upon irradiation with UV light is connected to a switch to the *cis*-state.[277,332]

Illumination with light outside the range of non-vanishing absorption leaves the azo-surfactant – photochemically – unaltered with respect to its *cis*-*trans*-mixture. This principle is at the heart of the „protection scheme“ introduced by the use of the described cut-off filter.

5.2 Surface Tension

The deviations in equilibrium surface tension γ_e of the azo-surfactant subject to different types of illumination as shown in the surface tension isotherms in Figure IV.35 can be interpreted in terms of diverging surface activity of the respective dominating geometric isomers. According to the Gibbs adsorption isotherm (GAI) given by

$$\Gamma = -\frac{1}{RT}\frac{\mathrm{d}\,\gamma_e}{\mathrm{d}\ln c}, \tag{V.7}$$

the surface coverage Γ can be related to the slope of the equilibrium surface tension isotherm. In the latter equation, R and T have their usual meanings. The higher absolute value of the slope in the isotherm of the Vis-illuminated solution, *i.e.,* the sample dominated by the *trans*-isomer, can therefore be interpreted in term of increased surface activity of the *trans*-form compared to the *cis*-isomer obtained from UV-illumination.

Moreover, this adsorption behavior can be related to the dipole moment of the *cis*- and *trans*-species. The measured equilibrium surface tension isotherm is in agreement with Hartley's conclusion of higher water solubility of the *cis*-isomer due to a significant increase in the dipole moment to values on the order of 3 D.[332] This increased polarity allows for a better interaction with the polar solvent water. It is characterized by a dipole moment of about 1.85 D, which can be obtained from a simplified consideration of the valence shell electron pair repulsion-model. The value has been confirmed by an extensive experimental study taking into account vibrational excitation.[333] Consequently, the more soluble *cis*-isomer is present preferentially in the bulk with a lower affinity towards the surface. This manifests as both a lower slope and higher absolute values in the equilibrium surface tension isotherms.

5.3 Oscillating Bubble

The experimental results for the UV- and Vis-illuminated adsorption layers of the studied azo-surfactant T226 were found to be clearly distinguishable. Additionally, the respective experimental amplitude and phase values of the surface dilatational modulus E varying with the applied perturbation frequency could satisfactorily be described in terms of the extended Lucassen-van den Tempel (LvdT)-model in a frequency range from 40 to 400 Hz. The best-fit values of model parameters are summarized in Table V.2.

Table V.2: Best fit parameters of the extended LvdT-model to match the experimentally obtained surface dilatational modulus gathered by means of the oscillating bubble device.

Sample	ϵ^{m} $[\ \mathrm{mN \cdot m^{-1}}\ ]$	f_{diff} $[\ \mathrm{s^{-1}}\ ]$	κ $[\ \mathrm{N \cdot s \cdot m^{-1}}\ ]$
UV	29.4 ± 2.8	5.2 ± 0.4	$1.1 \pm 0.2 \cdot 10^{-6}$
Vis	26.9 ± 6.3	17.7 ± 2.7	$2.4 \pm 0.7 \cdot 10^{-6}$

The parameter values of the high frequency limiting elasticity ϵ^{m} are in agreement with what could be expected from the experimental data shown in Figure IV.36: only slight differences. In terms of the remaining model parameters of characteristic diffusion frequency f_{diff} and intrinsic surface dilatational viscosity κ, a more pronounced distinction is obvious. The respective values are increased by factors between 2.5 and 3 for the Vis-form in comparison to the UV-isomer. Both findings can be interpreted as the emerging of more pronounced dissipative loss processes in adsorption layers formed by the less soluble *trans*-isomer in comparison to the more polar and therefore readily water-soluble *cis*-form of the azo-surfactant T226.

5.4 Placement of Oscillating Bubble Results on Previous Studies

In a conceptually related work, Chevallier *et al.* utilized the photoresponsive cationic trimethyl-ammonium azo-surfactant AzoTMA to generate „photofoams“.[282] They showed critical micellar concentration (cmc), equilibrium surface tension γ_{e} and interfacial composition to be dependent on the illumination state of the solution, but pointed out that their results on foam stability of the respective isomers „do not correlate with effects of light on surface tension, nor with total surfactant concentration“. The importance of competitive adsorption of the isomers was deemed to be crucial. As the major finding of their contribution, the photo-controlled foam could be switched from a stable to an unstable state subject to irradiation with UV-light. Due to the structural similarity of surfactant used by Chevallier *et al.* and T226, it is assumed that conclusions drawn from the T226-system similarly hold for AzoTMA. The elevated phase angles of T226 after Vis-illumination are indicative for the action of energy-dissipative processes in the interfacially adsorbed layer. Foams corresponding to this state were found to feature higher stability. Reversely, decreasing foam stability upon irradiation

with UV-light was associated with lower values of the phase angle, *i.e.*, less pronounced processes involving a dissipation of energy.

This highlights the finding that the photo-controlled stability of the studied azo-surfactant could be anticipated judging solely the data obtained from the oscillating bubble device *before* actually testing the foam stability of the respective solutions.

5.5 Conclusion

Adsorption layers formed from the *cis*- and *trans*-isomers of the photosensitive azo-surfactant T226 were found to be distinguishable with respect to both their equilibrium and dynamic interfacial properties. In the higher frequency range from 40 to 400 Hz covered by the oscillating bubble technique, the Vis light irradiated sample with the predominant *trans*-isomer was found to be subject to more pronounced dissipative losses. This manifested in both higher values of the phase angle and increased foam stability. Just as for the UV-irradiated solution, a quantitative description relying on the extended LvdT-model was found to deliver adequate agreement between model and experimental data. These findings are in agreement with previously published results on structurally related photofoams. It is to be pointed out, that the relative stabilities of the foams generated from the solutions dominated by the *cis*- and *trans*-isomers could successfully be predicted judging from the results of oscillating bubble experiments.

An attempt to model the surface dilatational properties in the overall frequency range covered by combining both low frequency oscillating pendant drop and high frequency oscillating bubble experimental data did not lead to a satisfactory agreement between a two-process relaxation model and the measured results. Next to the possibility of failing experimental techniques, the used model might not be valid. To exclude the effects of experimental shortcomings of the devices, an overlap of the respective accessible frequency ranges would be desirable. So far, valid oscillating pendant drop data can be obtained until an upper frequency around 0.5 Hz, the oscillating bubble is limited to frequencies exceeding 3 Hz leaving the range of interest uncovered. Further developments on the instrumental side will be required to confirm the validity of the experimental data and only then discuss the potential deficiencies of the model.

VI Conclusion

By virtue of the presented highlights focusing on different aspects of interfacial behavior, the importance and relevance of surface dilatational rheology could be demonstrated successfully. The thesis' goal of establishing a clearer relation between microscopic properties and macroscopic observables was accomplished. Very subtle effects such as differences in molecular structure, ionic strength and nature of counterions on the characteristics of adsorbed surfactant layers were found to be distinguishable with the presented state of the further developed oscillating bubble device. This allowed for contributing to the elucidation of the relation between surface dilatational properties and foam stability.

It has to be noted that the presented oscillating bubble results have been measured with differently developed states of the apparatus. Even though there have been deviations in terms of absolute values using distinct evolution stages, interesting conclusions could be drawn from measurements conducted with the same setup. The main findings of the presented projects will be pointed out in the following.

i) A remarkable property of the secretion of the *stenus comma* beetle upon its escape from predatory insects was confirmed. Next to propelling the beetle towards the edges of ponds and lakes, it renders the interfacial region visco-elastic. Consequently, it is more cumbersome for predators to follow its prey, the *stenus comma*. Only the access to elevated perturbation frequencies provided by the oscillating bubble device allowed for identification of this unusual feature.

ii) The extensive study of mixed sodium dodecyl sulfate (SDS)-NaCl solutions led to the development of a new parameter relating foam stability to characteristics obtained from surface dilatational experiments at elevated frequencies. Furthermore, the importance of a multi-technique approach for the assessment of rheological characteristics with the purpose of mutual validation was pointed out. A first criterion to judge the validity of high frequency data is the connectivity to low frequency data collected by established techniques such as the oscillating pendant drop. A challenge for the future is to „close“ the transition zone between low and high frequency techniques, at which the respective devices reach their limits. The use of adequately sized capillaries in appropriately adjusted sample cells is suggested as a remedy.

Whereas ion specificity has been a subject of long-standing interest in biology, only the advent of new developments in theory and instrumentation brought it to a revived focus of physical chemists' investigations.

iii) Oscillating bubble data suggested the eventually apparent series of alkali decyl sulfate (XDeS) foam stability with varying counterions devoid of previous knowledge on the foaming behavior. The

results were found to be in agreement with an ordering according to the Hofmeister series of cations. Furthermore, they are to be understood as an example for the predictive power of surface dilatational characteristics on foam properties.

iv) Ion specificity was equally confirmed for mixtures of the zwitter-ionic model surfactant *n*-dodecylphosphinecholine (DPC) with highly charged lanthanide-(III)-nitrates. The combination of methods sensitive to the surface and the bulk allowed for an unexpected interpretation: ion specificity in this system is of interfacial origin, *i.e.,* the bulk properties as evidenced from dielectric relaxation spectroscopy (DRS) of the salt solutions did not differ in presence of the surfactant, whereas the surface characteristics did. The specificity of the studied types of cations was ascribed to the deviating interaction of the apparent dipolar species with its surrounding water shell and the adsorbed zwitter-ionic surfactant.

v) The capability of distinguishing the geometrical isomers of an azo-surfactant subject to different types of illumination by means of surface rheological measurements at elevated frequencies is another showcase example of the oscillating bubble experiment. Due to the fast data acquisition time on the order of 10 min for the entire accessible frequency range, the system could safely be assumed to be unmodified at the time scale of the experiment. A comparison of the obtained results to electrocapillary wave (ECW)-data for the sake of confirmation is unfortunately expected to be unlikely due to the elevated demand for sample and the need for a time-consuming preparation.

Whereas the focus of this work was on the investigation of ionic surfactants and their susceptibility to modifications introduced by the presence of counterions of different nature, it is to be noted that also non-ionic amphiphiles represent an intriguing field of research. The incidence of ion specificity in non-ionic surfactant solutions is probably one of the most compelling pieces of evidence for the importance of Hofmeister-effects. For instance, experimental findings on disjoining pressure isotherms cannot be accounted for by the Derjaguin Landau Verwey Overbeek-theory. Conversely, it even suggests foam stabilities opposite to the actual observations in these systems. This is indicative for the importance of interactions between ions and water at interfaces, which appears not to be described appropriately in the present state of theory. Surface rheological data has the potential to contribute to modeling of dynamic processes at interfaces.

The presented oscillating bubble device enables to address further challenging questions of interest for both academia and industry in the near future.

From an academical point of view, further questions are emerging from the availability of accelerated surface dilatational data acquisition in an extended frequency range. This includes the existence of surface-specific analogs of time-dependent rheological behaviors well established in the bulk phase such as thixotropy or rheopexy. Moreover, in-depth studies of the rheological characteristics subsequent to external stimuli span a further field of interest. Studying adsorption layers consisting of adequate switchable surfactant model systems under dynamic conditions is expected to contribute to a better understanding of interfaces. Next to photo-switchable amphiphiles, also molecules featuring other

kinds of phase transitions, *e.g.,* induced by a change in temperature, could serve as model substances. A probably very pronounced effect and time dependence is to be expected from azo-bolaamphiphiles. In this case, illumination with ultraviolet (UV) or visible (Vis) light should allow for a precise reversible tuning from a one-headgroup to a two-headgroup surfactant characterized by – presumably – largely discriminable surface rheological behavior.

Considering the „practical“ use of the device from an application point of view, scanning of a broader range of surfactants from various classes to further deepen the relation between surface dilatational properties at elevated frequencies and foam stability or foam quality is required. As bulk rheology has been applied in food industry for a long time to assess quantities such as texture, it is possible to find some rather unconventional correlations of surface dilatational characteristics to parameters associated with human perception of a product such as the „feel“ of a surface.

A rather pessimistic notion by Eugene C. Bingham, one of the scientists shaping modern rheology, points out the challenges of measuring the respective quantities and the long way rheology has gone from the first half of the 20th century.

> „*The properties are ill defined and they are imperfectly measured if at all and they are in no way organized into a systematic body of knowledge which can be called a science.*“[†]

Ever since then, rheology nevertheless managed to grow into a mature discipline with vast applications in numerous fields. Not least due to the observations by Zell *et al.*, who pointed out that the predominant part of surface shear measurements of surfactant solutions typically overestimates the surface moduli by three to four orders of magnitude, Bingham's view is not yet entirely outdated. It still holds true for certain areas of *interfacial* rheology but at the same time illustrates its potentially promising trail upon further developments in equipment and theory.

For the next step of the oscillating bubble development, a highly precise fabrication of the required steel components taking into account all of the gained knowledge and experience is crucial. Only then, the expected further advances in reproducibility and ease of handling will be effective. Furthermore, a theoretical description of the flow profiles inside the sampling chamber of the oscillating bubble device upon perturbation would be greatly appreciated. Despite the challenges in daily work with the apparatus, it holds promise to serve as a highly valuable and – more or less – unrivaled tool for the assessment of surface dilatational characteristics at elevated frequencies over an extended range in the upcoming version.

[†]from **E. C. Bingham**. “Some Fundamental Definitions of Rheology.” *In J. Rheol.*, *1*(5) 507–516. **1930**

Appendix A

Published Research Results

The following contributions have been published in the course of preparing this thesis.

- **D. Stadler, M. J. Hofmann, H. Motschmann and M. Shamonin**. "Automated System for Measuring the Surface Dilational Modulus of Liquid–Air Interfaces." *In Meas. Sci. Technol.*, *27*(6) 65 301. **2016**
- **M. J. Hofmann and H. Motschmann**. "Measurement of the Lifetime of Individual Foam Lamellae." *In Rev. Sci. Instrum.*, *87* 94 101. **2016**
- **R. Weikl, M. J. Hofmann and H. Motschmann**. "The Influence of Highly Charged Ce^{4+}-Cations on Aqueous Solutions of SDS." *In Colloids Surf. A*, *505* 93–97. **2016**
- **A. A. Dietz, M. J. Hofmann and H. Motschmann**. "The Role of Surface Viscosity in the Escape Mechanism of the Stenus Beetle." *In J. Phys. Chem. B*, *120*(29) 7143–7147. **2016**
- **M. J. Hofmann and H. Motschmann**. "Surface Rheology and Its Relation to Foam Stability in Solutions of Sodium Decyl Sulfate." *In Colloids Surf. A*, *532* 472–475. **2017**
- **M. J. Hofmann and H. Motschmann**. "A Parameter Predicting the Foam Stability of Mixtures of Aqueous Ionic Amphiphile Solutions With Indifferent Electrolyte." *In Colloids Surf. A*, *529* 1024–1029. **2017**

Further publications from previous stages of studies are listed in the following.

- **M. J. Hofmann, R. Weikl, H. Motschmann and G. J. M. Koper**. "Impact of the Imaginary Part of the Surface Dilatational Modulus on the Splashing Behavior of Drops." *In Langmuir*, *31*(6) 1874–1878. **2015**
- **M. J. Hofmann and P. Koelsch**. "Retrieval of Complex $\chi^{(2)}$ Parts for Quantitative Analysis of Sum-Frequency Generation Intensity Spectra." *In J. Chem. Phys.*, *143*(13) 134 112. **2015**
- **M. J. Hofmann and P. Koelsch**. "Introduction to Quantitative Data Analysis in Vibrational Sum-Frequency Generation Spectroscopy." *In Soft Matter at Aqueous Interfaces* (Edited by **P. R. Lang and Y. Liu**), *Lecture Notes in Physics*, volume 917, 491–513 (Springer, New York, London). **2016**

Declaration

Ich, Matthias Hofmann, erkläre hiermit an Eides statt, dass ich die vorliegende Arbeit ohne unzulässige Hilfe Dritter und ohne Benutzung anderer als der angegebenen Hilfsmittel angefertigt habe; die aus anderen Quellen direkt oder indirekt übernommenen Daten und Konzepte sind unter Angabe des Literaturzitats gekennzeichnet. Die Arbeit wurde bisher weder im In- noch im Ausland in gleicher oder ähnlicher Form einer anderen Prüfungsbehörde vorgelegt. Von den vorgesehenen Rechtsfolgen habe ich Kenntnis genommen.

Matthias Hofmann

Ort, Datum

List of Figures

List of Tables

Bibliography

[1] **D. Stadler, M. J. Hofmann, H. Motschmann and M. Shamonin**. "Automated System for Measuring the Surface Dilational Modulus of Liquid–Air Interfaces." *In Meas. Sci. Technol.*, *27*(6) 65 301. **2016**.

[2] **M. J. Hofmann and H. Motschmann**. "Measurement of the Lifetime of Individual Foam Lamellae." *In Rev. Sci. Instrum.*, *87* 94 101. **2016**.

[3] **A. A. Dietz, M. J. Hofmann and H. Motschmann**. "The Role of Surface Viscosity in the Escape Mechanism of the Stenus Beetle." *In J. Phys. Chem. B*, *120*(29) 7143–7147. **2016**.

[4] **M. J. Hofmann and H. Motschmann**. "A Parameter Predicting the Foam Stability of Mixtures of Aqueous Ionic Amphiphile Solutions With Indifferent Electrolyte." *In Colloids Surf. A*, *529* 1024–1029. **2017**.

[5] **A. A. Shahir, K. T. Nguyen and A. V. Nguyen**. "A Sum-Frequency Generation Spectroscopic Study of the Gibbs Analysis Paradox: Monolayer or Sub-Monolayer Adsorption?" *In PCCP*, *18*(13) 8794–8805. **2016**.

[6] **A. Asadzadeh Shahir, D. Arabadzhieva, H. Petkova, S. I. Karakashev, A. V. Nguyen and E. Mileva**. "Effect of Under-monolayer Adsorption on Foamability, Rheological Characteristics and Dynamic Behaviour of Fluid Interfaces: Experimental Evidence for the Guggenheim Extended Interface Model." *In J. Phys. Chem. C*, *121*(21) 11 472–11 487. **2017**.

[7] **F. M. Menger, S. A. A. Rizvi and L. Shi**. "Reply to "Should the Gibbs Analysis Be Revised? "." *In Langmuir*, *27*(12) 7963–7965. **2011**.

[8] **J. Laven and G. de With**. "Should the Gibbs Analysis Be Revised?" *In Langmuir*, *27*(12) 7958–7962. **2011**.

[9] **C. Bermudez-Salguero and J. Gracia-Fadrique**. "Analysis of Gibbs Adsorption Equation and Thermodynamic Relation Between Gibbs Standard Energies of Adsorption and Micellization Through a Surface Equation of State." *In J. Colloid Interface Sci.*, *355*(2) 518–519. **2011**.

[10] **I. Mukherjee, S. P. Moulik and A. K. Rakshit**. "Tensiometric Determination of Gibbs Surface Excess and Micelle Point: A Critical Revisit." *In J. Colloid Interface Sci.*, *394* 329–336. **2013**.

[11] **J. Eastoe, S. Nave, A. Downer, A. Paul, A. Rankin, K. Tribe and J. Penfold**. "Adsorption of Ionic Surfactants at the Air–Solution Interface." *In Langmuir*, *16*(10) 4511–4518. **2000**.

[12] **R. Humphry-Baker, M. Gratzel and Y. Moroi**. "Pyrene Fluorescence at Air/sodium Dodecyl Sulfate Solution Interface." *In Langmuir*, *22*(26) 11 205–11 207. **2006**.

[13] **R. Parsons**. "Gibbs' Method, Guggenheim's Method and the Surface Excess as Measured by Thermodynamic Methods and Radiotracer Methods." *In J. Electroanal. Chem.*, *484*(1) 97–98. **2000**.

[14] **E. A. Simister, E. M. Lee, R. K. Thomas and J. Penfold**. "Structure of a Tetradecyltrimethylammonium Bromide Layer at the Air/water Interface Determined by Neutron Reflection." *In J. Phys. Chem.*, *96*(3) 1373–1382. **1992**.

[15] **S. Bae, K. Haage, K. Wantke and H. Motschmann**. "On the Factor in Gibbs Equation for Ionic Surfactants." *In J. Phys. Chem. B*, *103*(7) 1045–1050. **1999**.

[16] **N. Matubayasi**. *Surface Tension and Related Thermodynamic Quantities of Aqueous Electrolyte Solutions* (Taylor & Francis). **2013**.

[17] **E. A. Guggenheim**. "The Thermodynamics of Interfaces in Systems of Several Components." *In J. Chem. Soc. Faraday Trans.*, *35* 397. **1940**.

[18] **E. A. Guggenheim and N. K. Adam**. "The Thermodynamics of Adsorption at the Surface of Solutions." *In Proc. Royal Soc. A*, *139*(837) 218–236. **1933**.

[19] **A. Couper**. "Thermodynamics of Surfactants Solutions." *In Surfactants* (Edited by **T. F. Tadros**) (Academic Press, London). **1983**.

[20] **R. Parsons**. "The Specific Adsorption of Ions at the Metal-Electrolyte Interphase." *In J. Chem. Soc. Faraday Trans.*, *51* 1518. **1955**.

[21] **I. Langmuir**. "The Adsorption of Gases on Plane Surfaces of Glass, Mica and Platinum." *In J. Am. Chem. Soc.*, *40* 1361–1402. **1918**.

[22] **A. Frumkin**. "Surface Tension Curves of the Higher Fatty Acids and the Equation of Condition of the Surface Layer." *In Z. Phys. Chem.*, *116* 466–484. **1925**.

[23] **R. Miller, E. V. Aksenenko and V. B. Fainerman**. "Dynamic Interfacial Tension of Surfactant Solutions." *In Adv. Colloid Interface Sci.*, *247* 115–129. **2017**.

[24] **R. Miller, V. B. Fainerman, M. E. Leser and M. Michel**. "Kinetics of Adsorption of Proteins and Surfactants." *In Curr. Opin. Colloid Interface Sci.*, *9*(5) 350–356. **2004**.

[25] **P. Warszyński, W. Barzyk, K. Lunkenheimer and H. Fruhner**. "Surface Tension and Surface Potential of Na *n*-Dodecyl Sulfate at the Air-Solution Interface: Model and Experiment." *In J. Phys. Chem. B*, *102*(52) 10 948–10 957. **1998**.

[26] **P. Warszyński, K. Lunkenheimer and G. Czichocki**. "Effect of Counterions on the Adsorption of Ionic Surfactants at Fluid−Fluid Interfaces." *In Langmuir*, *18*(7) 2506–2514. **2002**.

[27] **R. J. Pugh**. "Foams and Foaming." *In Handbook of Applied Surface and Colloid Chemistry* (Edited by **K. Holmberg**), 23–43 (Wiley, New York). **2001**.

[28] **R. J. Pugh**. *Bubble and Foam Chemistry* (Cambridge University Press, Cambridge, United Kingdom). **2016**.

[29] **S. I. Karakashev and M. V. Grozdanova**. "Foams and Antifoams." *In Adv. Colloid Interface Sci.*, *176-177* 1–17. **2012**.

[30] **P. Ball**. *Shapes: Nature's Patterns: A Tapestry in Three Parts* (Oxford Univ. Press, Oxford). **2011**.

[31] **B. Vincent**. "Emulsions ans Foams." *In Surfactants* (Edited by **T. F. Tadros**) (Academic Press, London). **1983**.

[32] **K. Osei-Bonsu, N. Shokri and P. Grassia**. "Fundamental Investigation of Foam Flow in a Liquid-Filled Hele-Shaw Cell." *In Adv. Colloid Interface Sci.*, *462* 288–296. **2016**.

[33] **R. E. Beddoe and R. Lippok**. "Hygral Stress in Hardened Cement Paste." *In Mater. Struct.*, *32*(9) 627–634. **1999**.

[34] **R. J. Pugh**. "Foaming, Foam Films, Antifoaming and Defoaming." *In Adv. Colloid Interface Sci.*, *64* 67–142. **1996**.

[35] **M. J. Rosen and J. T. Kunjappu**. *Surfactants and Interfacial Phenomena* (Wiley, Hoboken, N.J.), 4th edition. **2012**.

[36] **V. Bergeron and C. J. Radke**. "Equilibrium Measurements of Oscillatory Disjoining Pressures in Aqueous Foam Films." *In Langmuir*, *8*(12) 3020–3026. **1992**.

[37] **V. Bergeron**. "Disjoining Pressures and Film Stability of Alkyltrimethylammonium Bromide Foam Films." *In Langmuir*, *13*(13) 3474–3482. **1997**.

[38] **J. L. Joye, G. J. Hirasaki and C. A. Miller**. "Dimple Formation and Behavior During Axisymmetrical Foam Film Drainage." *In Langmuir*, *8*(12) 3083–3092. **1992**.

[39] **T. Kolarov, R. Cohen and D. Exerowa**. "Direct Measurement of Disjoining Pressure in Black Foam Films II. Films From Nonionic Surfactants." *In Colloids Surf.*, *42*(1) 49–57. **1989**.

[40] **J. Schulze-Schlarmann, N. Buchavzov and C. Stubenrauch**. "A Disjoining Pressure Study of Foam Films Stabilized by Tetradecyl Trimethyl Ammonium Bromide C14TAB." *In Soft Matter*, *2*(7) 584. **2006**.

[41] **S. Sett, R. P. Sahu, D. D. Pelot and A. L. Yarin**. "Enhanced Foamability of Sodium Dodecyl Sulfate Surfactant Mixed with Superspreader Trisiloxane-(poly)ethoxylate." *In Langmuir*, *30*(49) 14 765–14 775. **2014**.

[42] **C. Stubenrauch, J. Schlarmann and R. Strey**. "A Disjoining Pressure Study of *n*-Dodecyl-β-D-Maltoside Foam Films." *In PCCP*, *4*(18) 4504–4513. **2002**.

[43] **Marangoni, C. G. M.** "Ueber die Ausbreitung der Tropfen einer Flüssigkeit auf der Oberfläche einer anderen." *In Ann. Phys. Chem. (Poggendorff)*, *143* 337–354. **1871**.

[44] **C. D. Bain**. "The Overflowing Cylinder Sixty Years On." *In Adv. Colloid Interface Sci.*, *144*(1-2) 4–12. **2008**.

[45] **K. A. Erk, J. D. Martin, J. T. Schwalbe, Phelan Jr. , Frederick R. and S. D. Hudson**. "Shear and Dilational Interfacial Rheology of Surfactant-Stabilized Droplets." *In J. Colloid Interface Sci.*, *377*(1) 442–449. **2012**.

[46] **D. Langevin and F. Monroy**. "Marangoni Stresses and Surface Compression Rheology of Surfactant Solutions. Achievements and Problems." *In Adv. Colloid Interface Sci.*, *206* 141–149. **2014**.

[47] **W.-f. Pu, P. Wei, L. Sun, F.-y. Jin and S. Wang**. "Experimental investigation of viscoelastic polymers for stabilizing foam." *In Journal of Industrial and Engineering Chemistry*, *47* 360–367. **2017**.

[48] **J. Lee, A. Nikolov and D. Wasan**. "Foam stability: The Importance of Film Size and the Micellar Structuring Phenomenon." *In Can. J. Chem. Eng.*, *92*(12) 2039–2045. **2014**.

[49] **Z. A. Zell, A. Nowbahar, V. Mansard, L. G. Leal, S. S. Deshmukh, J. M. Mecca, C. J. Tucker and T. M. Squires**. "Surface Shear Inviscidity of Soluble Surfactants." *In Proc. Natl. Acad. Sci. U.S.A.*, *111*(10) 3677–3682. **2014**.

[50] **A. Bureiko, A. Trybala, J. Huang, N. Kovalchuk and V. Starov**. "Effects of Additives on the Foaming Properties of Aculyn 22 and Aculyn 33 Polymeric Solutions." *In Colloids Surf., A*, *460* 265–271. **2014**.

[51] **R. Petkova, S. Tcholakova and N. D. Denkov**. "Foaming and Foam Stability for Mixed Polymer-Surfactant Solutions: Effects of Surfactant Type and Polymer Charge." *In Langmuir*, *28*(11) 4996–5009. **2012**.

[52] **R. Gmoser, R. Bordes, G. Nilsson, A. Altskär, M. Stading, N. Lorén and M. Berta**. "Effect of Dispersed Particles on Instant Coffee Foam Stability and Rheological Properties." *In Eur. Food Res. Technol.*, *243*(1) 115—-121. **2016**.

[53] **E. Guzmán, L. Liggieri, E. Santini, M. Ferrari and F. Ravera**. "Influence of Silica Nanoparticles on Dilational Rheology of DPPC-Palmitic Acid Langmuir Monolayers." *In Soft Matter*, *8*(14) 3938–3948. **2012**.

[54] **E. Guzmán, E. Santini, D. Zabiegaj, M. Ferrari, L. Liggieri and F. Ravera**. "Interaction of Carbon Black Particles and Dipalmitoylphosphatidylcholine at the Water/Air Interface: Thermodynamics and Rheology." *In J. Phys. Chem. C*, *119*(48) 26 937–26 947. **2015**.

[55] **M. Hasanzadeh, V. Mottaghitalab and M. Rezaei**. "Rheological and Viscoelastic Behavior of Concentrated Colloidal Suspensions of Silica Nanoparticles: A Response Surface Methodology Approach." *In Adv. Powder Technol.*, *26*(6) 1570–1577. **2015**.

[56] **I. Kim, A. J. Worthen, K. P. Johnston, D. A. DiCarlo and C. Huh**. "Size-Dependent Properties of Silica Nanoparticles for Pickering Stabilization of Emulsions and Foams." *In J. Nanopart. Res.*, *18*(4). **2016**.

[57] **H. A. Wege, S. Kim, V. N. Paunov, Q. Zhong and O. D. Velev**. "Long-Term Stabilization of Foams and Emulsions With In-Situ Formed Microparticles From Hydrophobic Cellulose." *In Langmuir*, *24*(17) 9245–9253. **2008**.

[58] **A.-L. Fameau, A. Saint-Jalmes, F. Cousin, B. H. Hossou, B. Novales, L. Navailles, F. Nallet, C. Gaillard, F. Boué and J.-P. Douliez**. "Smart Foams: Switching Reversibly between Ultrastable and Unstable Foams." *In Angew. Chem. Int. Ed.*, *123* 8414–8419. **2011**.

[59] **A.-L. Fameau and A. Saint-Jalmes**. "Non-Aqueous Foams: Current Understanding on the Formation and Stability Mechanisms." *In Adv. Colloid Interface Sci.*, *247* 454–464. **2017**.

[60] **R. A. Robinson, R. H. Stokes and R. G. Bates**. "Electrolyte Solutions: The Measurement and Interpretation of Conductance, Chemical Potential and Diffusion in Solutions of Simple Electrolytes (Second Edition)." *In J. Electrochem. Soc.*, *107*(8) 205C. **1960**.

[61] **P. Debye and E. Hückel**. "The Theory of Electrolytes. I. Lowering of Freezing Point and Related Phenomena." *In Phys. Z.*, *24* 185–206. **1923**.

[62] **N. Bjerrum**. "Ionic Association. I. Influence of Ionic Association on the Activity of Ions at Moderate Degrees of Association." *In Kgl. Danske Videnskab. Selskab. Math.-fys. Medd.*, *9*(7) 1–48. **1926**.

[63] **L. Onsager**. "The Theory of Electrolytes. II." *In Phys. Z.*, *28* 277–298. **1927**.

[64] **H. Falkenhagen, M. Leist and G. Kelbg**. "Theory of the Conductivity of Strong, Nonassociative Electrolytes at Higher Concentrations." *In Ann. Phys. (Berl.)*, *11* 51–59. **1952**.

[65] **P. L. Du Noüy**. "An Interfacial Tensiometer for Universal Use." *In J. Gen. Physiol.*, *7(5)* 625–633–625–633. **1925**.

[66] **Sinterface Technologies**. "Profile Analysis Tensiometer: PAT-1M: Version 1.02."

[67] **B. A. Noskov**. "Dilational Surface Rheology of Polymer and Polymer/Surfactant Solutions." *In Curr. Opin. Colloid Interface Sci.*, *15*(4) 229–236. **2010**.

[68] **F. Monroy, F. Ortega, R. G. Rubio and M. G. Velarde**. "Surface Rheology, Equilibrium and Dynamic Features at Interfaces, With Emphasis on Efficient Tools for Probing Polymer Dynamics at Interfaces." *In Adv. Colloid Interface Sci.*, *134-135* 175–189. **2007**.

[69] **Y. Takajo, M. Yamanaka, R. G. Rubio, T. Takiue, H. Matsubara and M. Aratono**. "Synergistic Interaction of Short-Chain Phospholipids in the Adsorbed Film and Micelles: Study by Surface Tension and Dilational Viscoelasticity Measurements." *In J. Phys. Chem. C*, *117*(2) 1097–1104. **2013**.

[70] **R. Miller and K. H. Schano**. "Adsorption Kinetics of Nonionic Surfactants Using the Drop Volume Method." *In Colloid Polym. Sci.*, *264*(3) 277–281. **1986**.

[71] **U. Teipel and N. Aksel**. "Adsorption Behavior of Nonionic Surfactants Studied by Drop Volume Technique." *In Chem. Eng. Technol.*, *24*(4) 393–400. **2001**.

[72] **A. Javadi, V. B. Fainerman and R. Miller**. "Drop Volume Tensiometry." *In Progress in Colloid and Interface Science*, *2* 119–141. **2011**.

[73] **D. Wu and V. Hornof**. "Influence of Phase Orientation of Dynamic Interfacial Tension Measured by Drop Volume Tensiometry." *In Can. J. Chem. Eng.*, *75*(5) 969–974. **1997**.

[74] **Z. H. Asadov, R. A. Rahimov, S. M. Nasibova and G. A. Ahmadova**. "Surface Activity, Thermodynamics of Micellization and Adsorption Properties of Quaternary Salts Based on Ethanolamines and Decyl Bromide." *In J. Surfactants Deterg.*, *13*(4) 459–464. **2010**.

[75] **A. Javadi, D. Bastani, J. Kraegel and R. Miller**. "Interfacial Instability of Growing Drop. Experimental Study and Conceptual Analysis." *In Colloids Surf., A*, *347*(1-3) 167–174. **2009**.

[76] **I. L. Metcalfe, G. Enhorning and F. Possmayer**. "Pulmonary Surfactant-Associated Proteins: Their Role in the Expression of Surface Activity." *In J. Appl. Physiol.*, *49*(1) 34–41. **1980**.

[77] **G. Enhorning**. "Pulsating Bubble Technique for Evaluating Pulmonary Surfactant." *In J. Appl. Physiol.*, *43*(2) 198–203. **1977**.

[78] **S. H. Yu and F. Possmayer**. "Comparative Studies on the Biophysical Activities of the Low-Molecular-Weight Hydrophobic Proteins Purified from Bovine Pulmonary Surfactant." *In Biochim. Biophys. Acta*, *961*(3) 337–350. **1988**.

[79] **S. B. Hall, M. S. Bermel, Y. T. Ko, H. J. Palmer, G. Enhorning and R. H. Notter**. "Approximations in the Measurement of Surface Tension on the Oscillating Bubble Surfactometer." *In J. Appl. Physiol.*, *75*(1) 468–477. **1993**.

[80] **C. H. Chang and E. I. Franses**. "An Analysis of the Factors Affecting Dynamic Tension Measurements with the Pulsating Bubble Surfactometer." *In J. Colloid Interface Sci.*, *164*(1) 107–113. **1994**.

[81] **C. H. Chang and E. I. Franses**. "Dynamic Tension Behavior of Aqueous Octanol Solutions Under Constant-Area and Pulsating-Area Conditions." *In Chem. Eng. Sci.*, *49*(3) 313–325. **1994**.

[82] **S. Y. Park, C. H. Chang, D. J. Ahn and E. I. Franses**. "Dynamic Surface Tension Behavior of Hexadecanol Spread and Adsorbed Monolayers." *In Langmuir*, *9*(12) 3640–3648. **1993**.

[83] **K. D. Wantke, R. Miller and K. Lunkenheimer**. "Theory of Radially Oscillating Bubbles in Interfacial-Active Solutions." *In Z. Phys. Chem.*, *261*(6) 1177–1190. **1980**.

[84] **K. Lunkenheimer and R. Miller**. "Investigations on the Radially Oscillating Bubble for the Determination of the Surface Dilational Elasticity. Considerations of an Optimization of the Experimental Procedure." *In Z. Phys. Chem.*, *265*(1) 71–80. **1984**.

[85] **K. Lunkenheimer, C. Hartenstein, R. Miller and K. D. Wantke**. "Investigations on the Method of the Radially Oscillating Bubble." *In Colloids Surf.*, *8*(3) 271–288. **1984**.

[86] **K. D. Wantke, K. Lunkenheimer and C. Hempt**. "Calculation of the Elasticity of Fluid Boundary Phases with the Oscillating Bubble Method." *In J. Colloid Interface Sci.*, *159*(1) 28–36. **1993**.

[87] **J. Lucassen**. "Hydrolysis and Precipitates in Carboxylate Soap Solutions." *In J. Phys. Chem.*, *70*(6) 1824–1830. **1966**.

[88] **Y. Tian, R. G. Holt and R. E. Apfel**. "Investigations of Liquid Surface Rheology of Surfactant Solutions by Droplet Shape Oscillations: Theory." *In Phys. Fluids*, *7*(12) 2938–2949. **1995**.

[89] **H. L. Lu and R. E. Apfel**. "Quadrupole Oscillations of Drops for Studying Interfacial Properties." *In J. Colloid Interface Sci.*, *134*(1) 245–255. **1990**.

[90] **C. J. Hsu and R. E. Apfel**. "A Technique for Measuring Interfacial Tension by Quadrupole Oscillation of Drops." *In J. Colloid Interface Sci.*, *107*(2) 467–476. **1985**.

[91] **D. O. Johnson and K. J. Stebe**. "An Oscillating Bubble Technique to Determine Surfactant Mass Transfer Kinetics." *In Colloids Surf., A*, *114* 41–52. **1996**.

[92] **N. J. Alvarez, L. M. Walker and S. L. Anna**. "A Microtensiometer To Probe the Effect of Radius of Curvature on Surfactant Transport to a Spherical Interface." *In Langmuir*, *26*(16) 13 310–13 319. **2010**.

[93] **A. P. Kotula and S. L. Anna**. "Insoluble Layer Deposition and Dilatational Rheology at a Microscale Spherical Cap Interface." *In Soft matter*, *12*(33) 7038–7055. **2016**.

[94] **M. Corti, M. Bonomo and A. Raudino**. "New Interferometric Technique to Evaluate the Electric Charge of Gas Bubbles in Liquids." *In Langmuir*, *28*(14) 6060–6066. **2012**.

[95] **A. Raudino, D. Raciti, A. Grassi, M. Pannuzzo and M. Corti**. "Oscillations of Bubble Shape Cause Anomalous Surfactant Diffusion: Experiments, Theory, and Simulations." *In Langmuir*, *32*(34) 8574–8582. **2016**.

[96] **R. P. Valle, T. Wu and Y. Y. Zuo**. "Biophysical Influence of Airborne Carbon Nanomaterials on Natural Pulmonary Surfactant." *In ACS Nano*, *9*(5) 5413–5421. **2015**.

[97] **R. P. Valle, C. L. Huang, Loo, Joachim S. C. and Y. Y. Zuo**. "Increasing Hydrophobicity of Nanoparticles Intensifies Lung Surfactant Film Inhibition and Particle Retention." *In ACS Sustainable Chem. Eng.*, *2*(7) 1574–1580. **2014**.

[98] **E. S. Goetzman, J. F. Alcorn, S. S. Bharathi, R. Uppala, K. J. McHugh, B. Kosmider, R. Chen, Y. Y. Zuo, M. E. Beck, R. W. McKinney, H. Skilling, K. R. Suhrie, A. Karunanidhi, R. Yeasted, C. Otsubo, B. Ellis, Y. Y. Tyurina, V. E. Kagan, R. K. Mallampalli and J. Vockley**. "Long-Chain Acyl-CoA Dehydrogenase Deficiency as a Cause of Pulmonary Surfactant Dysfunction." *In J. Biol. Chem.*, *289*(15) 10 668–10 679. **2014**.

[99] **S. I. Karakashev, R. Tsekov, E. D. Manev and A. V. Nguyen**. "Soap Bubble Elasticity: Analysis and Correlation with Foam Stability." *In Plovdiv University Scientific Papers*, *37* 109–116. **2010**.

[100] **R. Mendelsohn and C. R. Flach**. "Infrared Reflection–Absorption Spectrometry of Monolayer Films at the Air–Water Interface." **2002**.

[101] **F. Zernike and J. E. Midwinter**. *Applied Nonlinear Optics* (Wiley). **1973**.

[102] **Y. R. Shen**. *The Principles of Nonlinear Optics* (Wiley-Interscience). **2003**.

[103] **V. Ostroverkhov, G. A. Waychunas and Y. R. Shen**. "New Information on Water Interfacial Structure Revealed by Phase-Sensitive Surface Spectroscopy." *In Phys. Rev. Lett.*, *94*(4) 046 102/1–046 102/4. **2005**.

[104] **R. E. Pool, J. Versluis, Backus, Ellen H. G. and M. Bonn**. "Comparative Study of Direct and Phase-Specific Vibrational Sum-Frequency Generation Spectroscopy: Advantages and Limitations." *In J. Phys. Chem. B*, *115*(51) 15 362–15 369. **2011**.

[105] **I. V. Stiopkin, C. Weeraman, P. A. Pieniazek, F. Y. Shalhout, J. L. Skinner and A. V. Benderskii**. "Hydrogen Bonding at the Water Surface Revealed by Isotopic Dilution Spectroscopy." *In Nature*, *474*(7350) 192–195. **2011**.

[106] **I. V. Stiopkin, H. D. Jayathilake, A. N. Bordenyuk and A. V. Benderskii**. "Heterodyne-Detected Vibrational Sum Frequency Generation Spectroscopy." *In J. Am. Chem. Soc.*, *130*(7) 2271–2275. **2008**.

[107] **D. Blaudez, T. Buffeteau, J. C. Cornut, B. Desbat, N. Escafre, M. Pezolet and J. M. Turlet**. "Polarization Modulation FTIR Spectroscopy at the Air-Water Interface." *In Thin Solid Films*, *242*(1-2) 146–150. **1994**.

[108] **C. R. Flach, J. W. Brauner, J. W. Taylor, R. C. Baldwin and R. Mendelsohn**. "External Reflection FTIR of Peptide Monolayer Films in Situ at the Air/water Interface: Experimental Design, Spectra-Structure Correlations, and Effects of Hydrogen-Deuterium Exchange." *In Biophys. J .*, *67*(1) 402–410. **1994**.

[109] **A. H. Pfund**. "A New Method of Producing Ripples. Optical Analogies." *In Phys. Rev.*, *32*(3) 324–327. **1911**.

[110] **F. Monroy, F. Ortega and R. G. Rubio**. "Rheology of a Miscible Polymer Blend at the Air-Water Interface. Quasielastic Surface Light Scattering Study and Analysis in Terms of Static and Dynamic Scaling Laws." *In J. Phys. Chem. B*, *103*(12) 2061–2071. **1999**.

[111] **H. Fruhner and K. D. Wantke**. "A New Instrument for Measuring the Viscoelastic Properties of Dilute Polymer Solutions." *In Colloid Polym. Sci.*, *274*(6) 576–581. **1996**.

[112] **K.-D. Wantke and H. Fruhner**. "The Oscillating Bubble Method." *In General Review*, *6* 327–365. **1998**.

[113] **I. Lesov, S. Tcholakova and N. Denkov**. "Factors Controlling the Formation and Stability of Foams Used as Precursors of Porous Materials." *In J. Colloid Interface Sci.*, *426* 9–21. **2014**.

[114] **E. Rio, W. Drenckhan, A. Salonen and D. Langevin**. "Unusually Stable Liquid Foams." *In Adv. Colloid Interface Sci.*, *205* 74–86. **2014**.

[115] **T. B. J. Blijdenstein, R. A. Ganzevles, de Groot, P. W. N. and S. D. Stoyanov**. "On the Link Between Surface Rheology and Foam Disproportionation in Mixed Hydrophobin HFBII and Whey Protein Systems." *In Colloids Surf., A*, *438* 13–20. **2013**.

[116] **Matthias Hofmann**. *An Oscillating Bubble Technique as a Tool for the Study of Intrinsic Surface Dilatational Viscosity and Dissipative Processes in Aqueous Surfactant Solutions*. M.Sc. thesis, Universität Regensburg. **2015**.

[117] **D. Langevin**. "Influence of Interfacial Rheology on Foam and Emulsion Properties." *In Avdvances in Colloid and Interface Science*, *88* 209–222. **2000**.

[118] **P. Joos and E. Rillaerts**. "Theory on the Determination of the Dynamic Surface Tension with the Drop Volume and Maximum Bubble Pressure Methods." *In J. Colloid Interface Sci.*, *79*(1) 96–100. **1981**.

[119] **R. L. Bendure**. "Dynamic Surface Tension Determination with the Maximum Bubble Pressure Method." *In J. Colloid Interface Sci.*, *35*(2) 238–248. **1971**.

[120] **P. Koelsch and H. Motschmann**. "Relating Foam Lamella Stability and Surface Dilational Rheology." *In Langmuir*, *21*(14) 6265–6269. **2005**.

[121] **K.-D. Wantke, H. Fruhner and J. Ortegren**. "Surface Dilatational Properties of Mixed Sodium Dodecyl Sulfate/Dodecanol Solutions." *In Colloids Surf., A*, *221*(1-3) 185–195. **2003**.

[122] **F. Ravera, G. Loglio and V. I. Kovalchuk**. "Interfacial Dilational Rheology by Oscillating Bubble/Drop Methods." *In Curr. Opin. Colloid Interface Sci.*, *15*(4) 217–228. **2010**.

[123] **L. Liggieri, M. Ferrari, D. Mondelli and F. Ravera**. "Surface Rheology as a Tool for the Investigation of Processes Internal to Surfactant Adsorption Layers." *In Faraday Discuss.*, *129* 125–140. **2005**.

[124] **V. I. Kovalchuk, J. Krägel, A. V. Makievski, G. Loglio, F. Ravera, L. Liggieri and R. Miller**. "Frequency Characteristics of Amplitude and Phase of Oscillating Bubble Systems in a Closed Measuring Cell." *In J. Colloid Interface Sci.*, *252*(2) 433–442. **2002**.

[125] **L. Liggieri, V. Attolini, M. Ferrari and F. Ravera**. "Measurement of the Surface Dilational Viscoelasticity of Adsorbed Layers With a Capillary Pressure Tensiometer." *In J. Colloid Interface Sci.*, *255*(2) 225–235. **2002**.

[126] **F. Ravera, M. Ferrari, L. Liggieri, G. Loglio, E. Santini and A. Zanobini**. "Liquid-Liquid Interfacial Properties of Mixed Nanoparticle-Surfactant Systems." *In Colloids Surf., A*, *323*(1-3) 99–108. **2008**.

[127] **J. Oertegren, K.-D. Wantke, H. Motschmann and H. Moehwald**. "A Study of Kinetic Molecular Exchange Processes in the Medium Frequency Range by Surface SHG on an Oscillating Bubble." *In J. Colloid Interface Sci.*, *279*(1) 266–276. **2004**.

[128] **J. Lucassen and M. van den Tempel**. "Dynamic Measurements of Dilational Properties of a Liquid Interface." *In Chem. Eng. Sci.*, *27*(6) 1283–1291. **1972**.

[129] **J. Lucassen and G. T. Barnes**. "Propagation of Surface Tension Changes Over a Surface With Limited Area." *In J. Chem. Soc. Faraday Trans.*, *68*(11) 2129–2138. **1972**.

[130] **K.-D. Wantke and H. Fruhner**. "Determination of Surface Dilational Viscosity Using the Oscillating Bubble Method." *In J. Colloid Interface Sci.*, *237*(2) 185–199. **2001**.

[131] **F. Pásztor-Rozzo**. "Modifizierter Ross-Miles-Test zur Messung des Schaumes von Detergentien-Lösungen bei erhöhter Temperatur." *In Fett. Wiss. Technol.*, *67*(9) 688–689. **1965**.

[132] **J. Ross and G. D. Miles**. "An Apparatus for Comparison of Foaming Properties of Soaps and Detergents." *In Oil Soap*, *18*(5) 99–102. **1941**.

[133] **J. R. Kanicky, A. F. Poniatowski, N. R. Mehta and D. O. Shah**. "Cooperativity Among Molecules at Interfaces in Relation to Various Technological Processes: Effect of Chain Length on the pKa of Fatty Acid Salt Solutions." *In Langmuir*, *16*(1) 172–177. **2000**.

[134] **A. Fains, D. Bertrand, A. Baniel and Y. Popineau**. "Stability and Texture of Protein Foams: A Study by Video Image Analysis." *In Food Hydrocoll.*, *11*(1) 63–69. **1997**.

[135] **K. Lunkenheimer and K. Malysa**. "Simple and Generally Applicable Method of Determination and Evaluation of Foam Properties." *In J. Surfactants Deterg.*, *6*(1) 69–74. **2003**.

[136] **K. Lunkenheimer, K. Malysa, K. Winsel, K. Geggel and St. Siegel**. "Novel Method and Parameters for Testing and Characterization of Foam Stability." *In Langmuir*, *26*(6) 3883–3888. **2010**.

[137] **K. J. Mysels and M. N. Jones**. "Direct Measurement of the Variation of Double-Layer Repulsion With Distance." *In Disc. Faraday Soc.*, *42* 42. **1966**.

[138] **H. Fruhner, K.-D. Wantke and K. Lunkenheimer**. "Relationship Between Surface Dilational Properties and Foam Stability." *In Colloids Surf., A*, *162*(1-3) 193–202. **2000**.

[139] **T. Gilanyi, C. Stergiopoulos and E. Wolfram**. "Equilibrium Surface Tension of Aqueous Surfactant Solutions." *In Colloid. Polym. Sci.*, *254*(11) 1018–1023. **1976**.

[140] **K. Lunkenheimer, K. Malysa and K.-D. Wantke**. "A Remark on the Dependence of Foam Lamella Stability on the Geometric Structure of Ohosphine Oxide Surfactants." *In Colloids Surf., A*, *143*(2-3) 403–411. **1998**.

[141] **D. Exerowa and P. M. Krugljakov** (Editors). *Foam and Foam Films: Theory, Experiment, Application*, *Studies in Interface Science*, volume 5 (Elsevier, Amsterdam). **1998**.

[142] **S. Schrödle**. *Effects of non-ionic surfactants and related compounds on the cooperative and molecular dynamics of their aqueous solutions*. Ph.D. thesis, Universität Regensburg, Regensburg. **2005**.

[143] **H.-F. Eicke, S. Geiger, F. A. Sauer and H. Thomas**. "Dielectric Study of Fractal Clusters Formed by Aqueous Nanodroplets in Apolar Media." *In Ber. Bunsenges. Phys. Chem.*, *90*(10) 872–876. **1986**.

[144] **M.-C. Justice, J.-C. Justice and R. L. Kay**. "A Comparison of Ion-Solvent Interactions Evaluated From Both Emf and Conductance Data for HCl in Aqueous Solvent Mixtures." *In J. Solution Chem.*, *23*(6) 703–709. **1994**.

[145] **A. Ponton, T. K. Bose and G. Delbos**. "Dielectric Study of Percolation in an Oil–continuous Microemulsion." *In J. Chem. Phys.*, *94*(10) 6879–6886. **1991**.

[146] **E. A. S. Cavell, P. C. Knight and M. A. Sheikh**. "Dielectric Relaxation in Non Aqueous Solutions. Part 2.—Solutions of Tri(n-Butyl)ammonium Picrate and Iodide in Polar Solvents." *In Trans. Faraday Soc.*, *67*(0) 2225–2233. **1971**.

[147] **X. Du, Y. Li, Y.-L. Xia, S.-M. Ai, J. Liang, P. Sang, X.-L. Ji and S.-Q. Liu**. "Insights into Protein-Ligand Interactions: Mechanisms, Models, and Methods." *In Int. J. Mol. Sci.*, *17*(2). **2016**.

[148] **M. W. Freyer and E. A. Lewis**. "Isothermal Titration Calorimetry: Experimental Design, Data Analysis, and Probing Macromolecule/Ligand Binding and Kinetic Interactions." *In Biophysical Tools for Biologists* (Edited by **H. W. Detrich and J. J. Correia**), *Methods in Cell Biology*, volume 84, 79–113 (Elsevier, Amsterdam and s.l.). **2008**.

[149] **C. S. Johnson and D. A. Gabriel**. *Laser Light Scattering*. Dover books on physics (Dover, New York, NY). **1994**.

[150] **L. Ogendal**. "Light Scattering: A Brief Introduction."

[151] **H. Dubbel, W. Beitz and K.-H. Grote** (Editors). *Taschenbuch für den Maschinenbau* (Springer, Berlin), 19th edition. **1997**.

[152] **D. M. Sztukowski and H. W. Yarranton**. "Rheology of Asphaltene-Toluene/Water Interfaces." *In Langmuir*, *21*(25) 11 651–11 658. **2005**.

[153] **The MathWorks, Natick, MA, USA**. "MATLAB Optimization Toolbox."

[154] **M. Newville, T. Stensitzki, D. B. Allen and A. Ingargiola**. "LMFIT: Non-Linear Least-Square Minimization and Curve-Fitting for Python." **2014**.

[155] **F. Ravera, M. Ferrari, E. Santini and L. Liggieri**. "Influence of Surface Processes on the Dilational Viscoelasticity of Surfactant Solutions." *In Adv. Colloid Interface Sci.*, *117*(1-3) 75–100. **2005**.

[156] **F. Ravera, M. Ferrari and L. Liggieri**. "Modelling of Dilational Visco-Elasticity of Adsorbed Layers With Multiple Kinetic Processes." *In Colloids Surf., A*, *282–283* 210–216. **2006**.

[157] **V. I. Kovalchuk, G. Loglio, V. B. Fainerman and R. Miller**. "Interpretation of Surface Dilational Elasticity Data Based on an Intrinsic Two-Dimensional Interfacial Compressibility Model." *In J. Colloid Interface Sci.*, *270*(2) 475–482. **2004**.

[158] **J. Hunger, A. Stoppa, S. Schrödle, G. Hefter and R. Buchner**. "Temperature Dependence of the Dielectric Properties and Dynamics of Ionic Liquids." *In ChemPhysChem*, *10*(4) 723–733. **2009**.

[159] **A. Stoppa, A. Nazet, R. Buchner, A. Thoman and M. Walther**. "Dielectric Response and Collective Dynamics of Acetonitrile." *In J. Mol. Liq.*, *212* 963–968. **2015**.

[160] **P. Fernandez**. *Dielectric Relaxation Spectroscopy of Ionic Micelles and Microemulsions*. Ph.D. thesis, Universität Regensburg. **2002**.

[161] **S. Fernandez**. *Dielectric Relaxation Study of the Cellulose Solvent System LiCl/N,N-Dimethylacetamide*. Ph.D. thesis, Universität Regensburg. **2003**.

[162] **A. Stoppa**. *Chemical Speciation in Mixtures of Ionic Liquids and Polar Compounds*. Ph.D. thesis, Universität Regensburg. **2010**.

[163] **T. Sonnleitner**. *Dielectric Properties and Cooperative Dynamics of Protic and Aprotic Room-Temperature Ionic Liquids*. Ph.D. thesis, Universität Regensburg, Regensburg. **2014**.

[164] **J. Hunger, A. Stoppa, R. Buchner and G. Hefter**. "Dipole Correlations in the Ionic Liquid 1-*N*-Ethyl-3-*N*-Methylimidazolium Ethylsulfate and Its Binary Mixtures With Dichloromethane." *In J. Phys. Chem. B*, *113*(28) 9527–9537. **2009**.

[165] **R. Buchner**. "Evaluation of Relaxation Amplitudes Arising From Dipole Relaxation." **2015**.

[166] **P. R. Bevington and D. K. Robinson**. *Data Reduction and Error Analysis for the Physical Sciences* (McGraw-Hill, Boston, Mass.), 3rd edition. **2003**.

[167] **T. Gedig, K. Dettner and K. Seifert**. "Short Synthesis of Stenusine and Norstenusine, Two Spreading Alkaloids From Stenus Beetles (Coleoptera: Staphylinidae)." *In Tetrahedron*, *63*(12) 2670–2674. **2007**.

[168] **K. Lunkenheimer, K. Haage and R. Miller**. "On the Adsorption Properties of Surface-Chemically Pure Aqueous Solutions of *n*-Alkyl-Dimethyl and *n*-Alkyl-Diethyl Phosphine Oxides." *In Colloids Surf.*, *22*(2-4) 215–224. **1987**.

[169] **K. Lunkenheimer, H. J. Pergande and H. Krueger**. "Apparatus for Programmed High-Performance Purification of Surfactant Solutions." *In Rev. Sci. Instrum.*, *58*(12) 2313–2316. **1987**.

[170] **D. Vollhardt and G. Emrich**. "Coadsorption of Sodium Dodecyl Sulfate and Medium-Chain Alcohols at the Air-Water Interface." *In Colloids Surf., A*, *161*(1) 173–182. **2000**.

[171] **K. Lunkenheimer, K. Haage and R. Hirte**. "Novel Results on the Adsorption Properties of *n*-Alkyldimethylphosphine Oxides at the Air/Water Interface." *In Langmuir*, *15*(4) 1052–1058. **1999**.

[172] **K. Lunkenheimer and R. Miller**. "A Criterion for Judging the Purity of Adsorbed Surfactant Layers." *In J. Colloid Interface Sci.*, *120*(1) 176–183. **1987**.

[173] **R. Miller and K. Lunkenheimer**. "Adsorption Kinetics Measurements of Some Nonionic Surfactants." *In Colloid Polym. Sci.*, *264*(4) 357–361. **1986**.

[174] **S. Sett, S. I. Karakashev, S. K. Smoukov and A. L. Yarin**. "Ion-Specific Effects in Foams." *In Adv. Colloid Interface Sci.*, *225* 98–113. **2015**.

[175] **P. Karageorgiev, J. G. Petrov, H. Motschmann and H. Moehwald**. "Why Fluorination of the Polar Heads Reverses the Positive Sign of the Dipole Potential of Langmuir Monolayers: A Vibrational Sum Frequency Spectroscopic Study." *In Langmuir*, *29*(15) 4726–4736. **2013**.

[176] **A. M. Díez-Pascual, A. Compostizo, A. Crespo-Colín, R. G. Rubio and R. Miller**. "Adsorption of Water-Soluble Polymers With Surfactant Character. Adsorption Kinetics and Equilibrium Properties." *In J. Colloid Interface Sci.*, *307*(2) 398–404. **2007**.

[177] **A. F. H. Ward and L. Tordai**. "Time–Dependence of Boundary Tensions of Solutions I. The Role of Diffusion in Time–Effects." *In J. Chem. Phys.*, *14*(7) 453–461. **1946**.

[178] **V. B. Fainerman** (Editor). *Surfactants: Chemistry, Interfacial Properties, Applications*, *Studies in Interface Science*, volume 13 (Elsevier Science, Amsterdam), 1st edition. **2001**.

[179] **S. S. Dukhin, G. Kretzschmar and R. Miller**. *Dynamics of Adsorption at Liquid Interfaces. (Studies in Interface Science, Vol. 1)* (Elsevier). **1995**.

[180] **C. H. Sohl, K. Miyano and J. B. Ketterson**. "Novel Technique for Dynamic Surface Tension and Viscosity Measurements at Liquid-Gas Interfaces." *In Rev. Sci. Instrum.*, *49*(10) 1464. **1978**.

[181] **R. Weikl**. *Dynamische Grenzflächeneigenschaften Wässriger Tensidlösungen*. Ph.D. thesis, Universität Regensburg. **2013**.

[182] **A. Ruhland**. *Project Omega - Reengineering der Software eines Messinstruments zur Bestimmung des Grenzflächendilatationsmoduls*. M.Sc. thesis, Universität Regensburg. **2017**.

[183] **Jäger Computergesteuerte Messtechnik GmbH**. "ADwin-light-16: Handbuch." **2009**.

[184] **Keysight Technologies Inc.** "Understanding the Fundamental Principles of Vector Network Analysis." **2017**.

[185] **G. A. Reider**. *Photonik: Eine Einführung in Die Grundlagen* (Springer, Vienna), 3rd edition. **2012**.

[186] **S. Schrödle, G. Hefter, W. Kunz and R. Buchner**. "Effects of Nonionic Surfactant C12E5 on the Cooperative Dynamics of Water." *In Langmuir*, *22*(3) 924–932. **2006**.

[187] **J. Barthel, K. Bachhuber, R. Buchner, H. Hetzenauer and M. Kleebauer**. "A Computer-Controlled System of Transmission Lines for the Determination of the Complex Permittivity of Lossy Liquids Between 8.5 and 90 GHz." *In Ber. Bunsenges. Phys. Chem.*, *95*(8) 853–859. **1991**.

[188] **A. R. H. Goodwin, K. N. Marsh and W. A. Wakeham**. *Measurement of the Thermodynamic Properties of Single Phases: Experimental Thermodynamics* (Elsevier), 6th edition. **2003**.

[189] **E. Pehl**. *Mikrowellentechnik: Grundlagen, Leitungen, Antennen, Anwendungen* (VDE-Verl., Berlin), 3rd edition. **2012**.

[190] **S. Shaukat and R. Buchner**. "Densities, Viscosities [from (278.15 to 318.15) K], and Electrical Conductivities (at 298.15 K) of Aqueous Solutions of Choline Chloride and Chloro-Choline Chloride." *In J. Chem. Eng. Data*, *56*(12) 4944–4949. **2011**.

[191] **J. Barthel, H. Graml, R. Neueder, P. Turq and O. Bernard**. "Electrolyte Conductivity From Infinite Dilution to Saturation." *In Curr. Top. Solution Chem.*, 223–239. **1994**.

[192] **J. Barthel, R. Wachter and H.-J. Gores**. "Temperature Dependence of Conductance of Electrolytes in Nonaqueous Solutions." *In Modern Aspects of Electrochemistry* (Edited by **B. E. Conway and J. O. Bockris**), 1–79 (Springer US, Boston, MA). **1979**.

[193] **A. Stoppa, J. Hunger and R. Buchner**. "Conductivities of Binary Mixtures of Ionic Liquids with Polar Solvents." *In J. Chem. Eng. Data*, *54*(2) 472–479. **2009**.

[194] **A. Stoppa**. *Chemical Speciation in Mixtures of Ionic Liquids and Polar Compounds*. Ph.D. thesis, Universität Regensburg, Regensburg. **2010**.

[195] **J. Barthel, F. Feuerlein, R. Neueder and R. Wachter**. "Calibration of Conductance Cells at Various Temperatures." *In J. Solution Chem.*, *9*(3) 209–219. **1980**.

[196] **M. F. Jenkins**. "On the Method by Which Stenus And Dianous (Coleoptera: Staphylinidae) Return to the Banks of a Pool." *In Trans. Entomol. Soc. Lond.*, *112*(1) 1–14. **1960**.

[197] **H. Schildknecht, D. Krauß, J. Connert, H. Essenbreis and N. Orfanides**. "Das Spreitungsalkaloid Stenusin aus dem Kurzflügler *Stenus Comma* (Coleoptera: Staphylinidae)." *In Angew. Chem.*, *87*(11) 421–422. **1975**.

[198] **C. Lang, K. Seifert and K. Dettner**. "Skimming Behaviour and Spreading Potential of Stenus Species and Dianous Coerulescens (Coleoptera: Staphylinidae)." *In Naturwissenschaften*, *99*(11) 937–947. **2012**.

[199] **N. Møller Andersen**. *The Semiaquatic Bugs (Hemiptera, Gerromorpha): Phylogeny, Adaptations, Biogeography and Classification*, *Entomonograph*, volume 3 (Scandinavian Science Press, Klampenborg). **1982**.

[200] **K. E. Linsenmair and R. Jander**. "Das Entspannungsschwimmen von Velia und Stenus." *In Naturwissenschaften*, *50*(6) 231. **1963**.

[201] **J. M. Bush and D. L. Hu**. "Walking on Water: Biolocomotion at the Interface." *In Annu. Rev. Fluid. Mech*, *38* 339–369. **2006**.

[202] **H. Schildknecht, D. Berger, D. Krauss, J. Connert, J. Gehlhaus and H. Essenbreis**. "Defense Chemistry of *Stenus Comma* (Coleoptera: Staphylinidae)." *In J. Chem. Ecol.*, *2*(1) 1–11. **1976**.

[203] **P. Kohler**. *Die Absolute Konfiguration des Stenusins und die Aufklärung Weiterer Inhaltsstoffe des Spreitungsschwimmers Stenus Comma*. **1979**.

[204] **R. P. A. Baudoin**. *La Physico-Chimie Des Surfaces Dans La Vie Des Arthropodes Aériens, Des Miroirs D'eau Des Rivages Marins Et Lacustres De La Zone Intercotidale* (Paris). **1955**.

[205] **L. E. Scriven**. "Dynamics of a Fluid Interface. Equation of Motion for Newtonian Surface Fluids." *In Chem. Eng. Sci.*, *12* 98–108. **1960**.

[206] **S. R. Gallagher**. "Electrophoresis of Proteins and Nucleic Acids." *In Encyclopedia of Industrial Biotechnology: Bioprocess, Bioseparation, and Cell Technology* (Edited by **M. C. Flickinger**) (Wiley, Hoboken, NJ). **2010**.

[207] **M. C. Flickinger** (Editor). *Encyclopedia of Industrial Biotechnology: Bioprocess, Bioseparation, and Cell Technology* (Wiley, Hoboken, NJ). **2010**.

[208] **S. Chen, Y. Zhou, G. Wang, W. Li, Y. Zhu and J. Zhang**. "Influence of Foam Apparent Viscosity and Viscoelasticity of Liquid Films on Foam Stability." *In J. Dispersion Sci. Technol.*, *37*(4) 479–485. **2015**.

[209] **Y. Zhu, X. Pei, J. Jiang, Z. Cui and B. P. Binks**. "Responsive Aqueous Foams Stabilized by Silica Nanoparticles Hydrophobized in Situ with a Conventional Surfactant." *In Langmuir*, *31*(47) 12 937–12 943. **2015**.

[210] **L. Zhang, A. Mikhailovskaya, P. Yazhgur, F. Muller, F. Cousin, D. Langevin, N. Wang and A. Salonen**. "Precipitating Sodium Dodecyl Sulfate to Create Ultrastable and Stimulable Foams." *In Angew. Chem. Int. Ed.*, *54*(33) 9533–9536. **2015**.

[211] **J. Wang, A. V. Nguyen and S. Farrokhpay**. "A Critical Review of the Growth, Drainage and Collapse of Foams." *In Adv. Colloid Interface Sci.*, *228* 55–70. **2016**.

[212] **V. B. Fainerman, S. V. Lylyk, E. V. Aksenenko, J. T. Petkov, J. Yorke and R. Miller**. "Surface Tension Isotherms, Adsorption Dynamics and Dilational Visco-Elasticity of Sodium Dodecyl Sulphate Solutions." *In Colloids Surf., A*, *354*(1-3) 8–15. **2010**.

[213] **W. Kunz, J. Henle and B. W. Ninham**. "'Zur Lehre Von Der Wirkung Der Salze' (About the Science of the Effect of Salts): Franz Hofmeister's Historical Papers." *In Curr. Opin. Colloid Interface Sci.*, *9*(1-2) 19–37. **2004**.

[214] **W. Ostwald**. *Lehrbuch der Allgemeinen Chemie* (W. Engelmann, Leipzig). **1887**.

[215] **F. M. Raoult**. "Sur La Tension De Vapeur Et Sur Le Point De Congélation Des Solutions Salines." *In C. R. Chim.*, *87* 167–169. **1878**.

[216] **J. H. Long**. "Ueber Diffusion von Salzen in Wässriger Lösung." *In Wiedemann'sche Annalen*, *242*(6) 613–641. **1880**.

[217] **K. S. Pitzer and G. Mayorga**. "Thermodynamics of Electrolytes. II. Activity and Osmotic Coefficients for Strong Electrolytes With One or Both Ions Univalent." *In J. Phys. Chem.*, *77*(19) 2300–2308. **1973**.

[218] **A. Heydweiler**. "Über physikalische Eigenschaften von Lösungen un ihrem Zusammenhang. II. Oberflächenspannung Und Elektrisches Leitvermögen Wässriger Salzlösungen." *In Ann. Phys. (Berl.)*, *33* 145–185. **1910**.

[219] **F. Hofmeister**. "Zur Lehre von der Wirkung der Salze." *In Archiv für Experimentelle Pathologie und Pharmakologie*, *24*(4) 247–260. **1888**.

[220] **F. Hofmeister**. "Zur Lehre von der Wirkung der Salze." *In Archiv für Experimentelle Pathologie und Pharmakologie*, *25*(1) 1–30. **1888**.

[221] **Craig, Vincent S. J., B. W. Ninham and R. M. Pashley**. "The Effect of Electrolytes on Bubble Coalescence in Water." *In J. Phys. Chem.*, *97*(39) 10 192–10 197. **1993**.

[222] **S. I. Karakashev, P. T. Nguyen, R. Tsekov, M. A. Hampton and A. V. Nguyen**. "Anomalous Ion Effects on Rupture and Lifetime of Aqueous Foam Films Formed From Monovalent Salt Solutions Up to Saturation Concentration." *In Langmuir*, *24*(20) 11 587–11 591. **2008**.

[223] **M. H. Ropers, G. Czichocki and G. Brezesinski**. "Counterion Effect on the Thermodynamics of Micellization of Alkyl Sulfates." *In J. Phys. Chem. B*, *107*(22) 5281–5288. **2003**.

[224] **L. S. Romsted and C. O. Yoon**. "Counterion Affinity Orders in Aqueous Micellar Solutions of Sodium Decyl Phosphate and Sodium Dodecyl Sulfate Determined by Changes in Sodium-23 NMR Relaxation Rates: A Surprising Dependence on Head Group Charge." *In J. Am. Chem. Soc.*, *115*(3) 989–994. **1993**.

[225] **P. J. Missel, N. A. Mazer, M. C. Carey and G. B. Benedek**. "Influence of alkali-metal counterion identity on the sphere-to-rod transition in alkyl sulfate micelles." *In The Journal of Physical Chemistry*, *93*(26) 8354–8366. **1989**.

[226] **P. Mukerjee, K. Mysels and P. Kapauan**. "Counterion Specificity in the Formation of Ionic Micelles - Size, Hydration, and Hydrophobic Bonding Effects." *In J. Phys. Chem.*, *71*(13) 4166–4175. **1967**.

[227] **E. S. Ahuja and J. P. Foley**. "Influence of Dodecyl Sulfate Counterion On Efficiency, Selectivity, Retention, Elution Range, and Resolution in Micellar Electrokinetic Chromatography." *In Anal. Chem.*, *67*(14) 2315–2324. **1995**.

[228] **Z. Sadowski and R. W. Smith**. "Effect of Alkyl Sulfate Chain Length on Flocculation and Flotation of Barite Suspensions." *In Colloids Surf.*, *33* 239–248. **1988**.

[229] **R. R. Prajapati and S. S. Bhagwat**. "Effect of Foam Boosters on Krafft Temperature." *In J. Chem. Eng. Data*, *57*(3) 869–874. **2012**.

[230] **I. B. Ivanov, K. G. Marinova, K. D. Danov, D. Dimitrova, K. P. Ananthapadmanabhan and A. Lips**. "Role of the Counterions on the Adsorption of Ionic Surfactants." *In Adv. Colloid Interface Sci.*, *134-135* 105–124. **2007**.

[231] **G. Para, E. Jarek and P. Warszynski**. "The Surface Tension of Aqueous Solutions of Cetyltrimethylammonium Cationic Surfactants in Presence of Bromide and Chloride Counterions." *In Colloids Surf., A*, *261*(1-3) 65–73. **2005**.

[232] **G. Para, E. Jarek and P. Warszynski**. "The Hofmeister Series Effect in Adsorption of Cationic Surfactants–Theoretical Description and Experimental Results." *In Adv. Colloid Interface Sci.*, *122*(1-3) 39–55. **2006**.

[233] **D. J. Tobias and J. C. Hemminger**. "Chemistry. Getting Specific About Specific Ion Effects." *In Science*, *319*(5867) 1197–1198. **2008**.

[234] **P. Jungwirth and D. J. Tobias**. "Specific Ion Effects at the Air/water Interface." *In Chem. Rev.*, *106*(4) 1259–1281. **2006**.

[235] "Denmark aims to get 50% of all electricity from wind power." *In The Guardian*, *2012*. **March 26**.

[236] **J. Lucas, P. Lucas, T. Le Mercier, A. Rollat and W. G. Davenport**. *Rare Earths: Science, Technology, Production and Use*. Chemical engineering (Elsevier, Amsterdam). **2015**.

[237] **A. F. Holleman, E. Wiberg and N. Wiberg**. *Lehrbuch der Anorganischen Chemie* (de Gruyter, Berlin), 102nd edition. **2007**.

[238] **C. Musikas, N. Condamines and C. Cuillerdier**. "Sepration Chemistry for the Nuclear Industry." *In Anal. Sci.*, *7* 11–16. **1991**.

[239] **T. P. Pollard and T. L. Beck**. "Toward a Quantitative Theory of Hofmeister Phenomena: From Quantum Effects to Thermodynamics." *In Curr. Opin. Colloid Interface Sci.*, *23* 110–118. **2016**.

[240] **H. I. Okur, J. Hladílková, K. B. Rembert, Y. Cho, J. Heyda, J. Dzubiella, P. S. Cremer and P. Jungwirth**. "Beyond the Hofmeister Series: Ion-Specific Effects on Proteins and Their Biological Functions." *In J. Phys. Chem. B*, *121*(9) 1997–2014. **2017**.

[241] **B. W. Ninham, K. Larsson and P. Lo Nostro**. "Two Sides of the Coin. Part 1. Lipid and Surfactant Self-Assembly Revisited." *In Colloids Surf., B*, *152* 326–338. **2017**.

[242] **T. T. Duignan, D. F. Parsons and B. W. Ninham**. "A Continuum Solvent Model of the Partial Molar Volumes and Entropies of Ionic Solvation." *In J. Phys. Chem. B*, *118*(11) 3122–3132. **2014**.

[243] **B. Lukanov and A. Firoozabadi**. "Specific Ion Effects on the Self-Assembly of Ionic Surfactants: A Molecular Thermodynamic Theory of Micellization With Dispersion Forces." *In Langmuir*, *30*(22) 6373–6383. **2014**.

[244] **E. Leontidis and A. Aroti**. "Liquid Expanded Monolayers of Lipids as Model Systems to Understand the Anionic Hofmeister Series: 2. Ion Partitioning Is Mostly a Matter of Size." *In J. Phys. Chem. B*, *113*(5) 1460–1467. **2009**.

[245] **D. F. Parsons, M. Boström, T. J. Maceina, A. Salis and B. W. Ninham**. "Why Direct or Reversed Hofmeister Series? Interplay of Hydration, Non-Electrostatic Potentials, and Ion Size." *In Langmuir*, *26*(5) 3323–3328. **2010**.

[246] **B. W. Ninham, T. T. Duignan and D. F. Parsons**. "Approaches to Hydration, Old and New: Insights Through Hofmeister Effects." *In Curr. Opin. Colloid Interface Sci.*, *16*(6) 612–617. **2011**.

[247] **A. Salis, F. Cugia, D. F. Parsons, B. W. Ninham and M. Monduzzi**. "Hofmeister Series Reversal for Lysozyme by Change in pH and Salt Concentration: Insights From Electrophoretic Mobility Measurements." *In PCCP*, *14*(13) 4343–4346. **2012**.

[248] **T. T. Duignan, D. F. Parsons and B. W. Ninham**. "Collins's Rule, Hofmeister Effects and Ionic Dispersion Interactions." *In Chem. Phys. Lett.*, *608* 55–59. **2014**.

[249] **A. Salis and B. W. Ninham**. "Models and Mechanisms of Hofmeister Effects in Electrolyte Solutions, and Colloid and Protein Systems Revisited." *In Chem. Soc. Rev.*, *43*(21) 7358–7377. **2014**.

[250] **B. W. Ninham, R. M. Pashley and P. Lo Nostro**. "Surface forces: Changing Concepts and Complexity With Dissolved Gas, Bubbles, Salt and Heat." *In Curr. Opin. Colloid Interface Sci.*, *27* 25–32. **2017**.

[251] **S. K. Yadav and S. Kumar**. "Counterion-Specific Clouding in Aqueous Anionic Surfactant: A Case of Hofmeister-Like Series." *In Colloid Polym. Sci.*, *295*(5) 869–876. **2017**.

[252] **Q. Jadoon, I. Bibi, K. Mehmood, S. Sajjad, M. Nawaz, F. Ali, S. Bibi, W. ur Rehman, S. Bano and M. Usman**. "Interaction of Surfactants With Block-Copolymer Systems in the Presence of Hofmeister Anions." *In Mater. Res. Express*, *4*(3) 035 307. **2017**.

[253] **A. Jakubowska**. "Interactions of Univalent Counterions With Headgroups of Monomers and Dimers of an Anionic Surfactant." *In Langmuir*, *31*(11) 3293–3300. **2015**.

[254] **S. Nihonyanagi, S. Yamaguchi and T. Tahara**. "Counterion Effect on Interfacial Water at Charged Interfaces and Its Relevance to the Hofmeister Series." *In J. Am. Chem. Soc.*, *136*(17) 6155–6158. **2014**.

[255] **F. Guo and J. M. Friedman**. "Charge Density-Dependent Modifications of Hydration Shell Waters by Hofmeister Ions." *In J. Am. Chem. Soc.*, *131*(31) 11 010–11 018. **2009**.

[256] **C. Albayrak, G. Barım and Ö. Dag**. "Effect of Hygroscopicity of the Metal Salt on the Formation and Air Stability of Lyotropic Liquid Crystalline Mesophases in Hydrated Salt–surfactant Systems." *In J. Colloid Interface Sci.*, *433* 26–33. **2014**.

[257] **P. B. Petersen, J. C. Johnson, K. P. Knutsen and R. J. Saykally**. "Direct Experimental Validation of the Jones–Ray Effect." *In Chem. Phys. Lett.*, *397*(1-3) 46–50. **2004**.

[258] **W.-K. Zhang, D.-S. Zheng, Y.-Y. Xu, H.-T. Bian, Y. Guo and H.-F. Wang**. "Reconsideration of Second-Harmonic Generation From Isotropic Liquid Interface: Broken Kleinman Symmetry of Neat Air/water Interface From Dipolar Contribution." *In J. Chem. Phys.*, *123*(22) 224 713/1–224 713/11. **2005**.

[259] **H. Schollmeyer, P. Guenoun, J. Daillant, D. V. Novikov and R. V. Klitzing**. "Ion Distribution in Polyelectrolyte Multilayers With Standing-Wave X-Ray Fluorescence." *In J. Phys. Chem. B*, *111*(16) 4036–4042. **2007**.

[260] **J. Pignat, J. Daillant, L. Leiserowitz and F. Perrot**. "Grazing Incidence X-Ray Diffraction on Langmuir Films: Toward Atomic Resolution." *In J. Phys. Chem. B*, *110*(44) 22 178–22 184. **2006**.

[261] **J. Daillant, E. Bellet-Amalric, A. Braslau, T. Charitat, G. Fragneto, F. Graner, S. Mora, F. Rieutord and B. Stidder**. "Structure and Fluctuations of a Single Floating Lipid Bilayer." *In Proc. Natl. Acad. Sci. U.S.A.*, *102*(33) 11 639–11 644. **2005**.

[262] **M. Hishida, Y. Kaneko, M. Okuno, Y. Yamamura, T.-a. Ishibashi and K. Saito**. "Salt-Induced Water Orientation at a Surface of Non-Ionic Surfactant in Relation to a Mechanism of Hofmeister Effect." *In J. Chem. Phys.*, *142*(17) 171 101. **2015**.

[263] **T. Alejo, M. D. Merchán and M. M. Velázquez**. "Specific Ion Effects on the Properties of Cationic Gemini Surfactant Monolayers." *In Thin Solid Films*, *519*(16) 5689–5695. **2011**.

[264] **B. Lonetti, P. Lo Nostro, B. W. Ninham and P. Baglioni**. "Anion Effects on Calixarene Monolayers: A Hofmeister Series Study." *In Langmuir*, *21*(6) 2242–2249. **2005**.

[265] **M. Lakshmanan, R. Parthasarathi and A. Dhathathreyan**. "Do Properties of Bovine Serum Albumin at Fluid/electrolyte Interface Follow the Hofmeister Series?–an Analysis Using Langmuir and Langmuir-Blodgett Films." *In Biochim. Biophys. Acta*, *1764*(11) 1767–1774. **2006**.

[266] **E. Leontidis, A. Aroti and L. Belloni**. "Liquid Expanded Monolayers of Lipids as Model Systems to Understand the Anionic Hofmeister Series: 1. a Tale of Models." *In J. Phys. Chem. B*, *113*(5) 1447–1459. **2009**.

[267] **H. Xu, J. Penfold, R. K. Thomas, J. T. Petkov, I. Tucker, J. R. P. Webster, I. Grillo and A. Terry**. "Ion Specific Effects in Trivalent Counterion Induced Surface and Solution Self-Assembly of the Anionic Surfactant Sodium Polyethylene Glycol Monododecyl Ether Sulfate." *In Langmuir*, *30*(16) 4694–4702. **2014**.

[268] **R. C. Weast**. *Handbook of Chemistry & Physics* (CRC Press), 53rd edition. **1971**.

[269] **J. Kestin, M. Sokolov and W. A. Wakeham**. "Viscosity of Liquid Water in the Range −8 °C to 150 °C." *In J. Phys. Chem. Ref. Data*, *7*(3) 941–948. **1978**.

[270] **Royal Swedish Academy of Sciences**. "Scientific Background on the Nobel Prize in Chemistry 2016: Molecular Machines." **2016**.

[271] **V. Balzani, A. Credi, F. M. Raymo and J. F. Stoddart**. "Artificial Molecular Machines." *In Angew. Chem. Int. Ed.*, *39*(19) 3348–3391. **2000**.

[272] **C. Dietrich-Buchecker, J. Sauvage and J. Kintzinger**. "Une Nouvelle Famille De Molecules: Les Metallo-Catenanes." *In Tetrahedron Lett.*, *24*(46) 5095–5098. **1983**.

[273] **A. Livoreil, C. O. Dietrich-Buchecker and J.-P. Sauvage**. "Electrochemically Triggered Swinging of a 2-Catenate." *In J. Am. Chem. Soc.*, *116*(20) 9399–9400. **1994**.

[274] **R. A. Bissell, E. Córdova, A. E. Kaifer and J. F. Stoddart**. "A Chemically and Electrochemically Switchable Molecular Shuttle." *In Nature*, *369*(6476) 133–137. **1994**.

[275] **T. Kudernac, N. Ruangsupapichat, M. Parschau, B. Maciá, N. Katsonis, S. R. Harutyunyan, K.-H. Ernst and B. L. Feringa**. "Electrically Driven Directional Motion of a Four-Wheeled Molecule on a Metal Surface." *In Nature*, *479*(7372) 208–211. **2011**.

[276] **A. Bafana, S. S. Devi and T. Chakrabarti**. "Azo Dyes: Past, Present and the Future." *In Environ. Rev.*, *19*(NA) 350–371. **2011**.

[277] **X. Yao, T. Li, J. Wang, X. Ma and H. Tian**. "Recent Progress in Photoswitchable Supramolecular Self-Assembling Systems." *In Adv. Opt. Mater.*, *4*(9) 1322–1349. **2016**.

[278] **D. Gust, J. Andréasson, U. Pischel, T. A. Moore and A. L. Moore**. "Data and Signal Processing Using Photochromic Molecules." *In Chemical communications (Cambridge, England)*, *48*(14) 1947–1957. **2012**.

[279] **A. Chevalier, P.-Y. Renard and A. Romieu**. "Azo-Based Fluorogenic Probes for Biosensing and Bioimaging: Recent Advances and Upcoming Challenges." *In Chem. Asian J.*, *12*(16) 2008–2028. **2017**.

[280] **A.-L. Fameau, A. Saint-Jalmes, F. Cousin, B. H. Houssou, F. Boue, B. Novales, L. Navailles, F. Nallet, C. Gaillard and J.-P. Douliez**. "Smart Foams: Switching Reversibly Between Ultrastable and Unstable Foams." *In Angew. Chem. Int. Ed.*, *123*(36) 8414–8419. **2012**.

[281] **A.-L. Fameau, A. Carl, A. Saint-Jalmes and R. v. Klitzing**. "Responsive Aqueous Foams." *In ChemPhysChem*, *16*(1) 66–75. **2015**.

[282] **E. Chevallier, C. Monteux, F. Lequeux and C. Tribet**. "Photofoams: Remote Control of Foam Destabilization by Exposure to Light Using an Azobenzene Surfactant." *In Langmuir*, *28*(5) 2308–2312. **2012**.

[283] **T. Hayashita, T. Kurosawa, T. Miyata, K. Tanaka and M. Igawa**. "Effect of Structural Variation Within Cationic Azo-Surfactant Upon Photoresponsive Function in Aqueous Solution." *In Colloid Polym. Sci.*, *272*(12) 1611–1619. **1994**.

[284] **Y. Yang, B. Zhang, Y. Wang, L. Yue, W. Li and L. Wu**. "A Photo-Driven Polyoxometalate Complex Shuttle and Its Homogeneous Catalysis and Heterogeneous Separation." *In J. Am. Chem. Soc.*, *135*(39) 14 500–14 503. **2013**.

[285] **S. Peng, Q. Guo, T. C. Hughes and P. G. Hartley**. "Reversible Photorheological Lyotropic Liquid Crystals." *In Langmuir*, *30*(3) 866–872. **2014**.

[286] **S. Peng, Q. Guo, P. G. Hartley and T. C. Hughes**. "Azobenzene Moiety Variation Directing Self-Assembly and Photoresponsive Behavior of Azo-Surfactants." *In J. Mater. Chem. C*, *2*(39) 8303–8312. **2014**.

[287] **G. Serrien and P. Joos**. "Dynamic Surface Properties of Aqueous Sodium Dioctyl Sulfosuccinate Solutions." *In J. Colloid Interface Sci.*, *139*(1) 149–159. **1990**.

[288] **G. Serrien, G. Geeraerts, L. Ghosh and P. Joos**. "Dynamic Surface Properties of Adsorbed Protein Solutions: BSA, Casein and Buttermilk." *In Colloids Surf.*, *68*(4) 219–233. **1992**.

[289] **I. Juranić**. "Simple Method for the Estimation of pKa of Amines." *In Croat. Chem. Acta*, *87*(4) 343–347. **2014**.

[290] **T. Priester, Bartoszek. Michael and K. Lunkenheimer**. "Influence of Surface-Active Trace Impurities on the Surface Properties of Aqueous Solutions of Oligoethylene Glycol Monooctyl Ethers." *In J. Colloid Interface Sci.*, *208*(1) 6–13. **1998**.

[291] **R. B. Suter**. "Spider Locomotion on the Water Surface: Biomechanics and Diversity." *In J. Arachnol.*, *41*(2) 93–101. **2013**.

[292] **C. M. Johnson and E. Tyrode**. "Study of the adsorption of sodium dodecyl sulfate (SDS) at the air/water interface: targeting the sulfate headgroup using vibrational sum frequency spectroscopy." *In Physical chemistry chemical physics : PCCP*, *7*(13) 2635–2640. **2005**.

[293] **K. Schellmann, N. Preisig, P. Claesson and C. Stubenrauch**. "Effects of Protonation on Foaming Properties of Dodecyldimethylamine Oxide Solutions: A pH-Study." *In Soft Matter*, *11*(3) 561–571. **2015**.

[294] **A. Patist, P. D. T. Huibers, B. Deneka and D. O. Shah**. "Effect of Tetraalkylammonium Chlorides on Foaming Properties of Sodium Dodecyl Sulfate Solutions." *In Langmuir : the ACS journal of surfaces and colloids*, *14*(16) 4471–4474. **1998**.

[295] **A. Patist, Huibers, P. D. T., B. Deneka and D. O. Shah**. "Effect of Tetraalkylammonium Chlorides on Foaming Properties of Sodium Dodecyl Sulfate Solutions." *In Langmuir*, *14*(16) 4471–4474. **1998**.

[296] **N. Kristen-Hochrein, N. Schelero and R. v. Klitzing**. "Effects of Oppositely Charged Surfactants on the Stability of Foam Films." *In Colloids Surf., A*, *382*(1-3) 165–173. **2011**.

[297] **I. Blute, M. Jansson, S. G. Oh and D. O. Shah**. "The Molecular Mechanism for Destabilization of Foams by Organic Ions." *In Journal of the American Oil Chemists' Society*, *71*(1) 41–46. **1994**.

[298] **L. Wang and R. H. Yoon**. "Hydrophobic Forces in the Foam Films Stabilized by Sodium Dodecyl Sulfate: Effect of Electrolyte." *In Langmuir : the ACS journal of surfaces and colloids*, *20*(26) 11 457–11 464. **2004**.

[299] **P. A. Kralchevsky, K. D. Danov and E. S. Basheva**. "Hydration Force Due to the Reduced Screening of the Electrostatic Repulsion in Few-Nanometer-Thick Films." *In Current Opinion in Colloid & Interface Science*, *16*(6) 517–524. **2011**.

[300] **H. D. Yaros, J. Newman and C. J. Radke**. "Evaluation of DLVO Theory With Disjoining-Pressure and Film-Conductance Measurements of Common-Black Films Stabilized With Sodium Dodecyl Sulfate." *In Journal of Colloid and Interface Science*, *262*(2) 442–455. **2003**.

[301] **M. J. Rosen and J. T. Kunjappu**. "Foaming and Antifoaming by Aqueous Solutions of Surfactants." **2012/01/25**.

[302] **S. Sett, S. I. Karakashev, S. K. Smoukov and A. L. Yarin**. "Ion-Specific Effects in Foams." *In Adv. Colloid Interface Sci.*, *225* 98–113. **2015**.

[303] **S. I. Karakashev, R. Tsekov and D. S. Ivanova**. "Dynamic Effects in Thin Liquid Films Containing Ionic Surfactants." *In Colloids and Surfaces A: Physicochemical and Engineering Aspects*, *356*(1-3) 40–45. **2010**.

[304] **J. Wang and A. V. Nguyen**. "Foam drainage in the presence of solid particles." *In Soft Matter*, *12*(12) 3004–3012. **2016**.

[305] **M. G. Muñoz, L. Luna, F. Monroy, R. G. Rubio and F. Ortega**. "Viscoelastic Behavior of 1-Dodecanol Monolayers Undergoing a Liquid−Solid Phase Transition. A Surface Quasielastic Light Scattering Study." *In Langmuir*, *16*(16) 6657–6666. **2000**.

[306] **C. Stubenrauch and R. Miller**. "Stability of Foam Films and Surface Rheology: An Oscillating Bubble Study at Low Frequencies." *In J. Phys. Chem. B*, *108*(20) 6412–6421. **2004**.

[307] **D. Grigoriev and C. Stubenrauch**. "Surface elasticities of aqueous Î²-dodecyl-D-maltoside solutions: A capillary wave study." *In Colloids Surf., A*, *296*(1-3) 67–75. **2007**.

[308] **S. Rivillon, F. Monroy, F. Ortega and R. G. Rubio**. "Dilational rheology of monolayers of a miscible polymer blend: from good- to poor-solvent conditions." *In The European physical journal. E, Soft matter*, *9*(4) 375–385. **2002**.

[309] **R. Miller, V. B. Fainerman, V. I. Kovalchuk, L. Liggieri, G. Loglio, B. A. Noskov, F. Ravera and E. V. Aksenenko**. "Surface Dilational Rheology." *In Encyclopedia of Surface and Colloid Science* (Edited by **P. Somasundaran**) (CRC Press, Boca Raton, Fla.). **2016**.

[310] **J. Koryta, J. Dvořák and V. Boháčková**. *Lehrbuch der Elektrochemie* (Springer Vienna, Vienna). **1975**.

[311] **I. B. Ivanov, K. P. Ananthapadmanabhan and A. Lips**. "Adsorption and structure of the adsorbed layer of ionic surfactants." *In Advances in Colloid and Interface Science*, *123-126* 189–212. **2006**.

[312] **S. Pandey, R. P. Bagwe and D. O. Shah**. "Effect of counterions on surface and foaming properties of dodecyl sulfate." *In Journal of colloid and interface science*, *267*(1) 160–166. **2003**.

[313] **L. G. Phillips, S. Yang and J. E. Kinsella**. "Neutral Salt Effects on Stability of Whey Protein Isolate Foams." *In Journal of Food Science*, *56*(2) 588–589. **1991**.

[314] **O. S. Lawal, T. A. Afolabi, K. O. Adebowale, B. M. Ogunsanwo and S. A. Bankole**. "Effect of selected Hofmeister anions on functional properties of protein isolate prepared from lablab seeds (Lablab purpureus)." *In Journal of the Science of Food and Agriculture*, *85*(15) 2655–2659. **2005**.

[315] **K. D. Collins**. "Charge Density-Dependent Strength of Hydration and Biological Structure." *In Biophys. J.*, *72*(1) 65–76. **1997**.

[316] **R. G. Pearson**. "Hard and Soft Acids and Bases." *In Journal of the American Chemical Society*, *85*(22) 3533–3539. **1963**.

[317] **R. G. Pearson**. "Hard and soft acids and bases, HSAB, part 1: Fundamental principles." *In Journal of Chemical Education*, *45*(9) 581. **1968**.

[318] **R. G. Pearson**. "Hard and soft acids and bases, HSAB, part II: Underlying theories." *In Journal of Chemical Education*, *45*(10) 643. **1968**.

[319] **G. Jones and M. Dole**. "The Viscosity of Aqueous Solutions of Strong Electrolytes With Special Reference to Barium Chloride." *In Journal of the American Chemical Society*, *51*(10) 2950–2964. **1929**.

[320] **W. E. Waghorne**. "Viscosities of electrolyte solutions." *In Philosophical Transactions of the Royal Society of London, Series A: Mathematical, Physical and Engineering Sciences*, *359* 1529–1543. **2001**.

[321] **Y. Marcus**. "Effect of ions on the structure of water: structure making and breaking." *In Chemical reviews*, *109*(3) 1346–1370. **2009**.

[322] **H. D. B. Jenkins and Y. Marcus**. "Viscosity B-Coefficients of Ions in Solution." *In Chemical Reviews*, *95*(8) 2695–2724. **1995**.

[323] **P. Lo Nostro and B. W. Ninham**. "Hofmeister phenomena: an update on ion specificity in biology." *In Chemical reviews*, *112*(4) 2286–2322. **2012**.

[324] **N. N. Greenwood and A. Earnshaw**. *Chemistry of the elements* (Elsevier, [Place of publication not identified]), 2nd edition. **1997**.

[325] **D. G. Karraker**. "Coordination of trivalent lanthanide ions." *In Journal of Chemical Education*, *47*(6) 424. **1970**.

[326] **K. Lunkenheimer, G. Czichocki, R. Hirte and W. Barzyk**. "Novel results on the adsorption of ionic surfactants at the air/water interface — sodium-n-alkyl sulphates." *In Colloids and Surfaces A: Physicochemical and Engineering Aspects*, *101*(2-3) 187–197. **1995**.

[327] **G. Para, E. Jarek, P. Warszyński and Z. Adamczyk**. "Effect of electrolytes on surface tension of ionic surfactant solutions." *In Colloids and Surfaces A: Physicochemical and Engineering Aspects*, *222*(1-3) 213–222. **2003**.

[328] **Y. Marcus**. *Ion properties: Volume 1* (CRC Press, New York). **1997**.

[329] **R. Weikl, M. J. Hofmann and H. Motschmann**. "The Influence of Highly Charged Ce^{4+}-Cations on Aqueous Solutions of SDS." *In Colloids Surf. A*, *505* 93–97. **2016**.

[330] **A. Nazet, L. Weiß and R. Buchner**. "Dielectric relaxation of nitromethane and its mixtures with ethylammonium nitrate: Evidence for strong ion association induced by hydrogen bonding." *In Journal of Molecular Liquids*, *228* 81–90. **2017**.

[331] **H. M. A. Rahman, G. Hefter and R. Buchner**. "Hydration of formate and acetate ions by dielectric relaxation spectroscopy." *In The Journal of Physical Chemistry B*, *116*(1) 314–323. **2012**.

[332] **G. S. Hartley**. "The Cis-form of Azobenzene." *In Nature*, *140*(3537) 281. **1937**.

[333] **S. L. Shostak, W. L. Ebenstein and J. S. Muenter**. "The dipole moment of water. I. Dipole moments and hyperfine properties of H 2 O and HDO in the ground and excited vibrational states." *In The Journal of chemical physics*, *94*(9) 5875–5882. **1991**.

[334] **E. C. Bingham**. "Some Fundamental Definitions of Rheology." *In J. Rheol.*, *1*(5) 507–516. **1930**.

[335] **M. J. Hofmann and H. Motschmann**. "Surface Rheology and Its Relation to Foam Stability in Solutions of Sodium Decyl Sulfate." *In Colloids Surf. A*, *532* 472–475. **2017**.

[336] **M. J. Hofmann, R. Weikl, H. Motschmann and G. J. M. Koper**. "Impact of the Imaginary Part of the Surface Dilatational Modulus on the Splashing Behavior of Drops." *In Langmuir*, *31*(6) 1874–1878. **2015**.

[337] **M. J. Hofmann and P. Koelsch**. "Retrieval of Complex $\chi^{(2)}$ Parts for Quantitative Analysis of Sum-Frequency Generation Intensity Spectra." *In J. Chem. Phys.*, *143*(13) 134 112. **2015**.

[338] **M. J. Hofmann and P. Koelsch**. "Introduction to Quantitative Data Analysis in Vibrational Sum-Frequency Generation Spectroscopy." *In Soft Matter at Aqueous Interfaces* (Edited by **P. R. Lang and Y. Liu**), *Lecture Notes in Physics*, volume 917, 491–513 (Springer, New York, London). **2016**.